Sintering and microstructure property relationships of porous hydroxyapatite

Zakaria, Fadzil Ayad

Award date:
2000

Awarding institution:
University of Bath

SINTERING AND MICROSTRUCTURE PROPERTY RELATIONSHIPS OF POROUS HYDROXYAPATITE

submitted by

Fadzil Ayad Zakaria

for the degree of Doctor of Philosophy

of the University of Bath

2000

ProQuest LLC
789 East Eisenhower Parkway
P.O. Box 1346
Ann Arbor, MI 48106-1346

ACKNOWLEDGEMENTS

I would like to take this opportunity to thank everyone who has helped me with their expertise in this field of study especially Dr Alpagut Kara, Dr Jie Luo, and my supervisors, Professor Ron Stevens and Dr Irene Turner. Special acknowledgement to Kartini Noorsal for her help in the thermogravimetric analysis study. I would also like to thank all my friends, especially Jose Fernando Mikan-Venegas, for their encouragement to help me to get through the difficult times occurred during this study. Also, I would like to thank SIRIM Berhad for their financial support which made this study possible.

I would like to dedicate this work to my family especially my mom, Umi and dad, Zakaria and thank them for their emotional support and encouragement. Without their support, I would never have finished writing my thesis.

Abstract

The use of ceramics inside the body, as implant materials, is a relatively new technology, the first instance having been reported just 20 years ago. The ceramics used for the repair and reconstruction of diseased, damaged or 'worn out' parts of the body are referred to as bioceramics, and such a material is hydroxyapatite. The use of calcium phosphate to repair bone defects has been based on the rationale that calcium phosphate resembles vertebrate tooth and bone mineral, and is biologically compatible with these and surrounding tissues.

The concept of preparing porous hydroxyapatite was developed to prevent loosening of implants by enhancing the ingrowth of tissue into the pores (biological fixation). A structural limitation of this type of implant is the requirement to have a minimal pore size between 80-100 μm in diameter to allow bone to grow into the pores. The presence of such porosity would lead to a lower strength of the bioceramic component, but this is offset by the advantages of biocompatibility.

It is well known that hydroxyapatite is a brittle material and making it porous would reduce the existing mechanical properties. This study was carried out to optimise the mechanical properties by investigating the processing conditions and methods of preparation. The effect of forming method, pore geometry, pore size, sintering cycle, sintering atmosphere and types of spherical polymers on the microstructure and mechanical properties were studied.

As a consequence of the experiments, it was observed that porous hydroxyapatite is formed using an isostatic pressing technique, with 53 vol. % of HMWPVC as the porosifier. Sintering in air, with a heating rate of 50°C/h, held for 1h at 600°C in the first stage, and a heating rate of 100°C/h, held for 4h at between 1200 and 1250°C, generated a spherical pore geometry which gave the best combination of properties. This fabrication route resulted in an interconnected porous hydroxyapatite with a pore size ~90 μm, the volume fraction of porosity ~35%, relative density of ~60%, a grain size ~1.7-2 μm, a compressive strength between 14-18 MPa and a tensile strength of 4-5 MPa.

Table of Contents

Acknowledgements.....i
Abstract.....ii
Table of Contents.....iii
List of Tables.....iv
List of Figures.....v

Chapter 1 Introduction..... 1

1.1 Bone..... 2
1.1.1 Bone shapes..... 2
1.1.2 Bone structure..... 5
1.1.2.1 Macroscopic anatomy..... 5
1.1.2.2 Microscopic structure of bone..... 7
1.1.2.3 Chemical structure of bone..... 9
1.1.3 Bone cells..... 12
1.1.3.1 Osteogenic cells..... 12
1.1.3.2 Osteoblasts..... 12
1.1.3.3 Osteocytes..... 13
1.1.3.4 Osteoclasts..... 13
1.1.3.5 Bone-lining cells..... 13
1.1.4 Mechanical properties of bone..... 14
1.1.5 Summary..... 15

1.2 Bioceramics..... 16
1.2.1 Types of tissue attachment to bioceramics..... 16
1.2.2 Bone formation in calcium phosphate ceramics..... 18

1.2.3 Hydroxyapatite..... 19
1.2.3.1 Structure of hydroxyapatite..... 20
1.2.3.2 Phases of calcium phosphate..... 22
1.2.3.3 Decomposition of hydroxyapatite..... 25
1.2.3.4 Powder preparation of hydroxyapatite..... 28
1.2.3.5 Porous hydroxyapatite..... 31
1.2.3.6 Fabrication of porous hydroxyapatite..... 33
1.2.3.7 Mechanical properties of porous hydroxyapatite..... 34
1.2.3.8 Summary..... 37

1.3 Polymer..... 38
1.3.1 Polymer degradation..... 38
1.3.2 Poly (vinyl chloride)..... 39
1.3.3 Poly (vinyl alcohol)..... 41
1.3.4 Polymer degradation in ceramics..... 42
1.3.5 Summary..... 44

1.4 Processing and Mechanical Behaviour of Ceramics..... 44
1.4.1 Ceramic processing technology..... 44
1.4.1.1 Powder synthesis..... 45
1.4.1.2 Forming method..... 46
1.4.1.3 Sintering processes..... 49
1.4.2 Effect of porosity on the strength of the ceramics..... 51
1.4.3 Effect of grain size on the mechanical properties of ceramics..... 52
1.4.4 Summary..... 53

Chapter 2 Experimental Procedures..... 54

2.1 Fabrication and Processing Technique..... 54
2.1.1 Starting materials..... 54
2.1.2 Powder preparation..... 54
2.1.2.1 Sieving..... 54
2.1.2.2 Mixing..... 55
2.1.3 Pellet formation..... 55
2.1.3.1 Uniaxial die pressing..... 55
2.1.3.2 Cold isostatic pressing..... 56
2.1.4 Sample preparation 57
2.1.4.1 Sintering regime..... 57
2.1.4.2 Surface preparation..... 58

2.2 Characterisation Procedures..... 59
2.2.1 Powder characterisation..... 59
2.2.1.1 Sintering dilatometer..... 59
2.2.1.2 Specific surface area..... 60
2.2.1.3 Particle size distribution..... 60
2.2.1.4 Measurement of calcium to phosphorus ratio. 61
2.2.2 Microstructural characterisation..... 61
2.2.2.1 X-ray diffraction phase analysis..... 61
2.2.2.2 Scanning electron microscopy..... 62
2.2.2.3 Density and porosity..... 62
2.2.2.4 Grain size measurement..... 63
2.2.2.5 Thermogravimetric and infrared spectroscopy analysis..... 64
2.2.3 Mechanical properties evaluation..... 64
2.2.3.1 Compressive strength..... 64
2.2.3.2 Tensile strength..... 65

2.3 Sol-gel Technique..... 66
2.3.1 Synthesis of amorphous calcium phosphate gel..... 66
2.3.2 Freeze casting..... 67

Chapter 3 Sintering and Decomposition of Hydroxyapatite..... 70

3.1 Introduction..... 70

3.2 Powder Characteristics..... 71

3.3 The study of the hydroxyapatite and poly vinyl chloride and the mixture of both with temperature..... 74
3.3.1 Thermogravimetric analysis..... 74
3.3.2 Linear shrinkage..... 75
3.3.3 Porosity and density..... 76
3.3.4 X-ray diffraction..... 77
3.3.5 Scanning electron microscope..... 78
3.3.6 Discussion..... 78
3.3.7 Summary..... 80

3.4 Effect of sintering cycle on the porous hydroxyapatite behaviour..... 86
3.4.1 Heating rate..... 86
3.4.1.1 Optical microscope photographs..... 86
3.4.1.2 Porosity, density and grain size..... 87
3.4.1.3 X-ray diffraction..... 87
3.4.2 Holding time..... 88

3.4.2.1 Porosity, density and grain size..... 88
3.4.2.2 Scanning electron microscope..... 89
3.4.2.3 X-ray diffraction..... 89
3.4.3 Discussion..... 90
3.4.4 Summary..... 91

3.5 Effect of Sintering Atmosphere..... 103
3.5.1 Microstructural analysis..... 103
3.5.1.1 Linear shrinkage..... 103
3.5.1.2 Thermal gravimetric analysis..... 105
3.5.1.3 Porosity and density..... 106
3.5.1.4 Grain size..... 106
3.5.1.5 Scanning electron microscope..... 107
3.5.1.6 X-ray diffraction..... 107
3.5.2 Mechanical property analysis..... 107
3.5.3 Discussion..... 108
3.5.4 Summary..... 110

3.6 Study of the Effect of Different Types Of Polymer..... 123
3.6.1 Effect of different polymer content..... 123
3.6.2.1 Microstructural analysis..... 123
3.6.1.1.1 Porosity..... 123
3.6.1.1.2 Density..... 124
3.6.2.2 Mechanical property analysis..... 124
3.6.2 Effect of different sintering temperatures..... 126
3.6.2.1 Microstructural analysis..... 126
3.6.2.1.1 Porosity..... 126
3.6.2.1.2 Density..... 127
3.6.2.1.3 Grain size..... 127
3.6.2.1.4 SEM micrographs..... 128

3.6.2.1.5 X-ray diffraction..... 128
3.6.2.2 Mechanical property analysis..... 129
3.6.3 Discussion..... 129
3.6.4 Summary..... 131

Chapter 4 Study on the Optimisation of Porosity..... 145

4.1 Introduction..... 145
4.2 Effect of using different forming techniques on porosity..... 145
4.3 Effect of pore size on strength..... 149
4.4 Effect of pore geometry on strength..... 151
4.5 Summary..... 155

Chapter 5 Sol-Gel Technique..... 156

5.1 Introduction..... 156

5.2 Synthesis of calcium phosphate gel..... 156
5.2.1 Aging effect on the Ca/P ratio..... 156
5.2.2 Freeze drying and freeze casting..... 157

5.3 Summary..... 159

Chapter 6 General Discussion..... 160

6.1 General discussion..... 160
6.2 Summary..... 165
6.3 Conclusions..... 167
6.4 Suggestions for future work..... 167

References

List Of Tables

Table 1.1	Typical composition of the mineral phases of human femoral bone	12
Table 1.2	Mechanical properties of human femur and bioactive ceramics	14
Table 1.3	Phases in calcium phosphate	23
Table 1.4	Biomechanical properties of HA200	36
Table 1.5	Stages of microstructural characteristics during solid state sintering of powder compacts	50
Table 2.1	Materials used in the study	54
Table 2.2	Sample size and weight used for different types of experiments	56
Table 2.3	Sintering regime used to study the effect of sintering cycle on the HA	58
Table 2.4	Surface preparation procedure for SEM samples	58
Table 3.1	The properties of the hydroxyapatite powder	71
Table 5.1	Result of the ageing effect on the Ca/P ratio of the precipitated hydroxyapatite	158

List Of Figures

Figure 1.1	Bone shapes.....	3
Figure 1.2	Longitudinal section of a long bone.....	6
Figure 1.3	Structure of a flat bone.....	8
Figure 1.4	Photomicrograph from human tibia; **A**. cortical bone; **B**. cancellous bone.....	8
Figure 1.5	Fine structure of bone without inner marrow.....	10
Figure 1.6	Clinical uses of bioceramics.....	17
Figure 1.7	Hydroxyapatite structure projected down to the c-axis onto the basal plane.....	21
Figure 1.8A	X-ray diffraction pattern of hydroxyapatite powder showing the presence of only hydroxyapatite phase.....	21
Figure 1.8B	Infra-red absorption spectrum of hydroxyapatite powder showing the characteristic absorption bands of O-H and P-O reflecting the vibrations of the OH and PO_4 groups in the calcium hydroxyapatite, $Ca_{10}(PO_4)_6(OH)_2$.....	21
Figure 1.9	Phase diagram of system CaO/P_2O_5 at high temperatures (^oC). No water present.....	24
Figure 1.10	Phase diagram of CaO/P_2O_5 at high temperature (^oC). Water pressure = 500mm Hg.....	24
Figure 1.11	Influence of ambient water vapour pressure on phase composition.....	24
Figure 1.12	Enlarged part of Figure 1.9. $T_1 = 1360^oC$ and $T_2 = 1475^oC$.....	24
Figure 1.13	Influence of Ca/P ratio on the flexural strength.....	27
Figure 1.14	Powder synthesis method.....	27
Figure 2.1	Stages of sintering of the green compacts.....	57
Figure 2.2	Schematic diagram of the diametral compression test.....	65

Figure 2.3	Schematic diagram showing the sintering of calcium phosphate gel.....	67
Figure 2.4	Schematic diagram of sample preparation by freeze drying.....	68
Figure 3.1	X-ray diffraction pattern of hydroxyapatite powder as received ..	72
Figure 3.2	EDAX analysis of the hydroxyapatite powder as received.....	72
Figure 3.3	FTIR diagram of hydroxyapatite powder as received.....	73
Figure 3.4	SEM micrographs of (a) hydroxyapatite powder, and (b) PVC powder as received.....	73
Figure 3.5	TGA plot of hydroxyapatite powder heated in air at 20°C/min with a holding temperature at 500°C for 1/2h.....	81
Figure 3.6	TGA plot of poly (vinyl chloride) powder heated in air at 20°C/min with a holding temperature at 500°C for 1/2h.....	81
Figure 3.7	TGA plot of 64wt% of hydroxyapatite mixed with 36 wt% of poly (vinyl chloride) compact, heated in air at 20°C/min with a holding temperature at 600°C for 1h.....	82
Figure 3.8	Linear shrinkage plot of HA and HA+PVC compact heated at 5°C/min.....	82
Figure 3.9	Porosity of dense and porous hydroxyapatite.....	83
Figure 3.10	Porosity of porous hydroxyapatite at different PVC content sintered at different temperatures.....	83
Figure 3.11	Density of porous hydroxyapatite achieved after sintering at 1200°C for 1h.....	84
Figure 3.12	XRD result of HA powder after sintering at different temperature for 4h.....	84
Figure 3.13	XRD result of HA powder sintered as 1150°C at different holding time.....	85
Figure 3.14	SEM micrographs of porous hydroxyapatite with interconnected porosity (a) broken pieces of porous hydroxyapatite (b) porous hydroxyapatite impregnated with resin.....	85

Figure 3.15	Optical micrographs of dense hydroxyapatite and porous hydroxyapatite sintered at different first stage heating rate. (1). Dense hydroxyapatite at heating rate of (a) 30°C/h and (b) 50°C/h; (2). Porous hydroxyapatite at heating rate of (a) 30°C/h and (b) 50°C/h.....	93
Figure 3.16	Volume fraction of porosity of porous hydroxyapatite sintered at a different temperature with different first stage heating rate.....	94
Figure 3.17	Relative density of porous hydroxyapatite sintered at a different temperature with different first stage heating rate.....	94
Figure 3.18	Grain size of porous hydroxyapatite sintered at a different temperature with different first stage heating rate.....	95
Figure 3.19 (a)	The XRD result of porous hydroxyapatite sintered at a different temperature with a heating rate of 30°C/h.....	95
Figure 3.19 (b)	The XRD result of porous hydroxyapatite sintered at a different temperature with a heating rate of 50°C/h.....	96
Figure 3.20	The volume fraction of porosity of porous hydroxyapatite at different holding time.....	96
Figure 3.21	The relative density of porous hydroxyapatite at different holding time.....	97
Figure 3.22	The grain size of the porous hydroxyapatite at different holding time.....	97
Figure 3.23 (a)	The microstructure of porous hydroxyapatite at a different temperatures and holding time of 1h.....	98
Figure 3.23 (b)	The microstructure of porous hydroxyapatite at a different temperatures and holding time of 4h.....	99
Figure 3.23 (c)	The microstructure of porous hydroxyapatite at a different temperatures and holding time of 12h.....	100
Figure 3.23 (d)	The microstructure of porous hydroxyapatite at a different temperatures and holding time of 36h.....	101

Figure 3.24	The XRD plot of porous hydroxyapatite sintered at first stage of heating rate of 50°C/h, holding temperature of 400°C for 1h and a second stage of holding temperature at 1150°C with a different holding time.....	102
Figure 3.25	The XRD plot of porous hydroxyapatite sintered at a first stage of sintering of heating rate at 30°C/h, holding temperature of 600°C for 1h and a second stage of sintering with different temperatures and holding time of 4h.....	102
Figure 3.26	Linear shrinkage of hydroxyapatite and PVC mixture compact sintered in different environment, air and argon.....	112
Figure 3.27	TGA result of PVC fired in argon at 20°C/min, (a) from 50°C to 500°C, and (b) 500°C to 900°C.....	113
Figure 3.28	TGA result of HA fired in argon at 20°C/min, (a) from 50°C to 500°C, and (b) 500°C to 900°C.....	114
Figure 3.29	TGA result of hydroxyapatite (64wt%) mixed with PVC (36wt%) fired in argon at 20°C/min, (a) from 50°C to 500°C, and (b) 500°C to 900°C.....	115
Figure 3.30	TGA and DTA result of PVC fired in air at 20°C/min.....	116
Figure 3.31	TGA and DTA result of HA fired in air at 20°C/min.....	116
Figure 3.32	TGA and DTA result of HA (64wt%) mixed with PVC (36wt%) fired in air at 20°C/min.....	117
Figure 3.33	Volume fraction of porosity of porous hydroxyapatite sintered in air and argon.....	117
Figure 3.34	Relative density of porous hydroxyapatite sintered in air and argon.....	118
Figure 3.35	Grain size of porous hydroxyapatite sintered in air and argon.....	118
Figure 3.36	SEM micrographs of porous hydroxyapatite sintered in air.....	119
Figure 3.37	SEM micrographs of porous hydroxyapatite sintered in argon at different temperatures.....	120

Figure 3.38	XRD pattern of porous hydroxyapatite ceramic sintered at different temperature with 53vol% of PVC in (a) air (b) argon...	121
Figure 3.39	Compressive strength of porous hydroxyapatite ceramics sintered for 4h in air and argon.....	122
Figure 3.40	Tensile strength of porous hydroxyapatite ceramics sintered in air and argon for 4h.....	122
Figure 3.41	SEM micrographs of polymers powder used as porosifier in producing porous hydroxyapatite ceramic: (a) PVC, and (b) PVA.....	132
Figure 3.42	Volume fraction of porosity of porous hydroxyapatite after sintering for 4h at 1200°C at different percentage of polymer content.....	132
Figure 3.43	Relative density of porous hydroxyapatite at different polymer content after sintering at 1200°C for 4h.....	133
Figure 3.44	Compressive strength of porous hydroxyapatite after sintering for 4h at 1200°C using three types of polymer as a porosifier, HMWPVC, LMWPVC and PVA.....	133
Figure 3.45	Compressive strength if porous hydroxyapatite sintered for 4h using different volume % of polymer content.....	134
Figure 3.46	Volume fraction of porosity of porous hydroxyapatite after sintering at different temperatures.....	134
Figure 3.47	Size of macropores after sintering at different temperatures for 4h using different types of polymers with starting size of 125μm-180μm.....	135
Figure 3.48	Relative density of porous hydroxyapatite using different types of polymers at different sintering temperatures.....	135
Figure 3.49	Grain size of porous hydroxyapatite sintered for 4h at different temperatures using different polymers.....	136

Figure 3.50	EDAX result of samples prepared using (a) HMWPVC and (b) LMWPVC as a porosifier.....	136
Figure 3.51	(a) TEM micrograph and (b) EDAX result from porous hydroxyapatite prepared using poly (vinyl chloride) as a porosifier.....	137
Figure 3.52	EDAX result of porous hydroxyapatite prepared using PVA as a porosifier.....	137
Figure 3.53	SEM micrographs of porous hydroxyapatite prepared using LMWPVC as a porosifier at different sintering temperatures.....	138
Figure 3.54	SEM micrographs of porous hydroxyapatite prepared using PVA as a porosifier at different sintering temperatures.....	139
Figure 3.55	SEM micrographs of porous hydroxyapatite prepared using PVA as porosifier. (a) macropores (~120μm), (b) medium pores (~10μm) and micropores (~1μm).....	140
Figure 3.56	SEM micrographs of porous hydroxyapatite prepared using PVA as porosifier. (a) macropores (~90μm) and (b) micropores (~1μm).....	141
Figure 3.57	XRD result of porous hydroxyapatite after sintering for 4h using LMWPVC as a porosifier.....	142
Figure 3.58	XRD result of porous hydroxyapatite after sintering for 4h using PVA as a porosifier.....	142
Figure 3.59	Compressive strength of porous hydroxyapatite sintered for 4h using three different polymers at different sintering temperatures.....	143
Figure 3.60	Tensile strength of porous hydroxyapatite sintered for 4h using two different polymers at different sintering temperatures.....	143
Figure 3.61	SEM micrographs of porous hydroxyapatite using different types of polymers: (a) PVA, (b) LMWPVC and (c) HMWPVC.....	144

Figure 3.62	SEM micrographs of pore agglomeration occurred in porous hydroxyapatite prepared using LMWPVC.....	144
Figure 4.1	Compaction behaviour of hydroxyapatite powder at different pressure using the isostatic pressing technique.....	146
Figure 4.2	Compressive strength of porous hydroxyapatite using different forming techniques.....	146
Figure 4.3	SEM micrographs of porous hydroxyapatite formed using (a) uniaxial and (b) isostatic pressing technique.....	148
Figure 4.4	SEM micrographs of porous hydroxyapatite using PVC with particle size of 125μm.....	150
Figure 4.5	The compressive strength-porosity behaviour of the porous hydroxyapatite in terms of different sizes of starting PVC particles.....	150
Figure 4.6	SEM micrograph of porous hydroxyapatite prepared at 80 MPa showing ellipsoid shape.....	152
Figure 4.7	The pore geometry (pore axis ratio c/a) plotted against the effect of punch pressure.....	152
Figure 4.8	The compressive strength-porosity behaviour of porous hydroxyapatite plotted against different types of pore geometry.....	153
Figure 5.1	XRD analysis of the hydroxyapatite powders produced at 48h...	158

Chapter 1 Introduction

A successful application of calcium phosphate (β-tricalcium phosphate, β-$Ca_3(PO_4)_2$) to repair bone defect has been reported as early as 1920 [94]. The studies on calcium phosphates later accelerated in the mid-seventies, by three groups: Jarcho et al in USA, De Groot et al and Denissen, in Europe and Aoki et al in Japan who worked simultaneously but independently towards the development and commercialisation of hydroxyapatite ($Ca_{10}(PO_4)_6(OH)_2$) for bone repair and substitution [25]. This was based on the rationale that the hydroxyapatite resembles vertebrate tooth and bone mineral, and is biologically compatible with these tissues [14].

Since the studies by Klawitter and Hulbert in 1971 [95] established that a minimum pore size of 100μm is important for bone ingrowth into ceramic structures, more studies on developing porous materials with porosity >100μm have been pursued. However, several researches also showed that a 80-100 μm is the minimal pore size for osteoconduction [21, 53]. White et al [61] developed a technique known as replamineform, successfully copied the interconnected structure of a coral, genus *Porites*, for pores with size range of 140-160μm and genus *Goniopora,* for pore sizes between 200-1000μm. The technique used by Ryshkewitch [63], where porous ceramic developed by using H_2O_2, has also been used to develop porous hydroxyapatite.

The interest in the biocompatibility of hydroxyapatite and the importance of porosities have lead to this study. The objective of my study is to develop a porous hydroxyapatite with porosities more than 80μm, study the microstructure after sintering and the characteristic of porosity in order to optimise the strength of the porous material.

1.1 Bone

Bone tissue is a specialised connective tissue that has the strength of cast iron and the lightness of pine wood. The bone tissue, comprising the skeleton, not only supports and protects our internal organs but also acts as the storehouse and main supply of a reserve of calcium and phosphate; the bone marrow serves as the site for the manufacture of red blood cells and some white blood cells. Bone structures aid movement by providing a point of attachment for muscles and transmitting the forces of muscular contraction from one part of the body to another during movement.

Formation of bone is a biphasic process. During the first phase, the osteoblasts secrete an organic matrix called preosseous matrix or osteoid, made up of collagen and ground substance (proteoglycans, glycoproteins, non collagenous protein). During the second phase, mineralisation occurs, transforming the osteoid into bone tissue [1].

1.1.1 Bone shapes

Bones make up the skeleton and provide the rigid framework that supports the body. They protect the vulnerable internal organs such as the brain, heart, lungs and organs of the pelvis by forming the sturdy walls of body cavities. They also make body movement possible by providing anchoring points for muscles and by acting as lever arms at the joints. Bones are usually classified by shape as flat, irregular, long, sesamoid or short (Figure 1.1) [2].

A bone is classified as a long bone when its length is greater than its width as is the case for the femurs, fingers and toes. Long bones act as lever arms that are pulled by

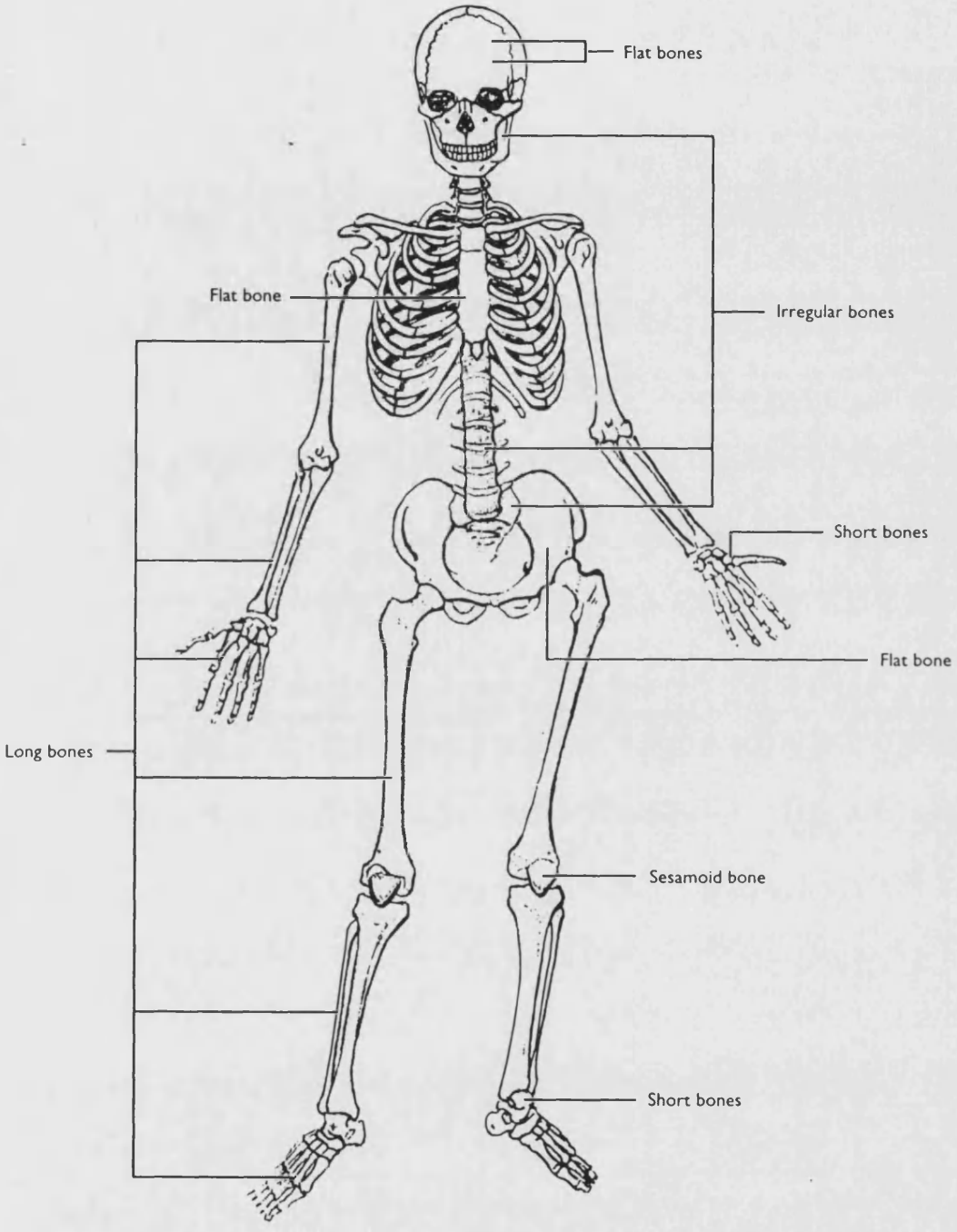

Figure 1.1: Bone shapes [3]

contracting muscles. It is this lever action that makes it possible for the body to move effectively [2].

The short bones have similar dimensions of length, width and thickness, but they are shaped irregularly. They occur only in the wrist (carpal bones) and ankles (tarsal bones), where only limited movement is required. Short bones are almost completely covered with articular surfaces, where one bone moves against another in a joint. However, there are some non-articular areas on short bones where nutrient blood vessels enter, where tendons attach bones to muscles, and where ligaments connect bones [2].

The flat bones are actually thin or curved more often than they are flat. Flat bones include the ribs, scapulae (shoulder blades), sternum (breastbone) and cranium (skull). The shape of the flat bones usually facilitates muscle attachment and the gently curved bones of the skull form a protective enclosure for the brain [2].

Irregular bone does not fit neatly into any of the other categories, as for instance, vertebrae, many facial bones and the hipbones. The vertebrae have extensions that protrude from their many bony elements and serve as sites for muscle attachment. These bones support the spinal cord and protect it against compression forces. Pneumatic bones, such as the maxillary bone of the skull, have air-filled cavities that help warm and humidify the air in the sinuses [2].

The sesamoid bones are the small bones embedded within certain tendons, the fibrous cords that connect muscle to bones. Sesamoid bones usually occur where tendons pass over the joint of a long bone, as in the wrist or knee. The patella, or kneecap, within the tendon of the one of the thigh muscle (quadriceps femoris) and the pisiform carpal bone within the tendon of a wrist muscle (flexor carpi ulnaris) are typical sesamoid bones. Besides helping to protect the tendon, the sesamoid bones help the tendon to overcome compression forces , thus increasing the mechanical efficiency of joints [2].

Accessory bones, also called supernumerary bones, are most commonly found in the feet. They usually occur when developing bones do not fused completely. Sutural (Wormian) bones are small bone clusters that occur between the joints of the flat bones of the skull. The number of sutural bones in an individual varies. In general, the accessory bones add slight support and protection to the area of the skeleton where they are found [2].

1.1.2 Bone structure

Bone structure can be considered at three levels: the macroscopic, microscopic, and the chemical.

1.1.2.1 Macroscopic anatomy

Structure of typical long bone

With a few exceptions, all long bones have the same general structure (Figure 1.2) [3]. Most adult long bones have a tubular shaft, called the diaphysis. It is constructed of a relatively thick collar of compact bone that surrounds a central medullary cavity or marrow cavity. The wall of the medullary cavity is called the endosteum. In adults, the medullary cavity containing fat (yellow marrow) is called the yellow bone marrow cavity.

The epiphyses, which are usually wider than the shaft, are present at the bone ends. Compact bone forms the exterior of epiphyses and the interior contains spongy bone. Red bone marrow is found within the porous chambers of spongy bone. The joint surface of each epiphyses is covered with a thin layer of articular (hyaline) cartilage which cushions the opposing bone ends during joint movement and absorbs stress. Between the diaphysis and each epiphyses of an adult long bone, is an epiphyseal line. This line is the remnant of

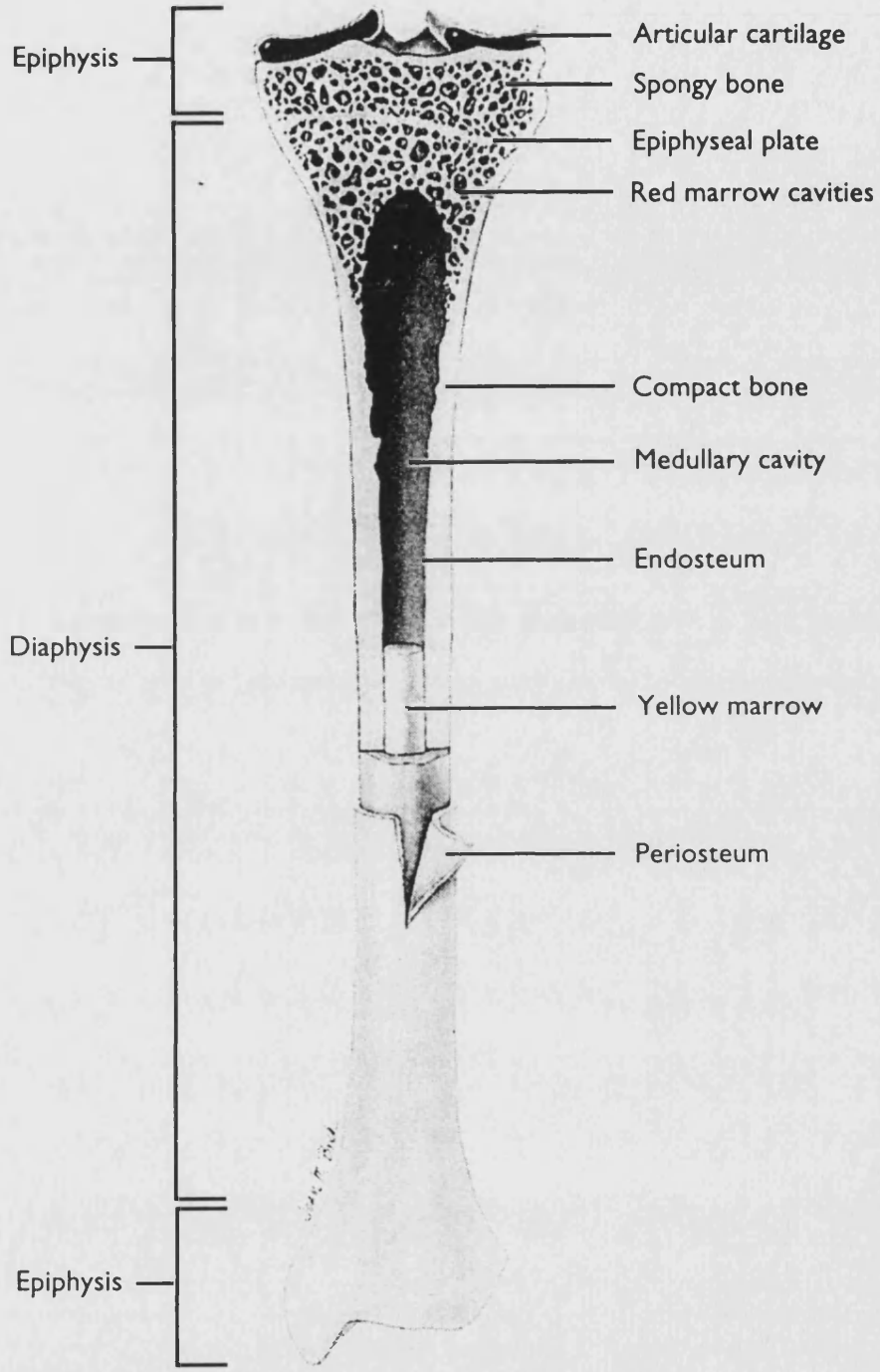

Figure 1.2: Longitudinal section of a long bone [3]

the epiphyseal plate, a disc-like region of hyaline cartilage that grows during childhood to lengthen the bone [3,4,5].

Covering the outer surface of the diaphysis is the periosteum, a fibrous membrane that has the potential to form bone during growth periods and in fracture healing. The periosteum contains nerves, lymphatic vessels, and many capillaries that provide nutrients to the bone and which gives the distinctive pink colour to living bone. Nutrients reach the marrow and spongy bone tissue by arteries that penetrate the compact bone tissue through small openings called the nutrient foramen. At the epiphyses, there is no periosteum present. There, it is replaced by articular cartilage, which provides a smooth, low friction surface that allows the articulate to work smoothly [2].

Structure of short, irregular and flat bones

Short, irregular and flat bones consist of thin plates of periosteum-covered compact bone on the outside and endosteum-covered spongy bone within. These bones have no shaft or epiphyses. They contain bone marrow between the trabeculae but no marrow cavity is present as shown in Figure 1.3 [4]. In flat bones, the whole arrangement resembles a stiffened sandwich.

1.1.2.2 Microscopic structure of bone

There are two basic histological types of bone which are easily distinguishable with the naked eye: compact bone and cancellous (spongy) bone (Figure 1.4). Each bone type has different properties that contribute to the specific needs of the body with respect to its location and abundance. The porosity of bone ranges from 5 to 30% in cortical bone and from 30 to 90% in cancellous bone [6].

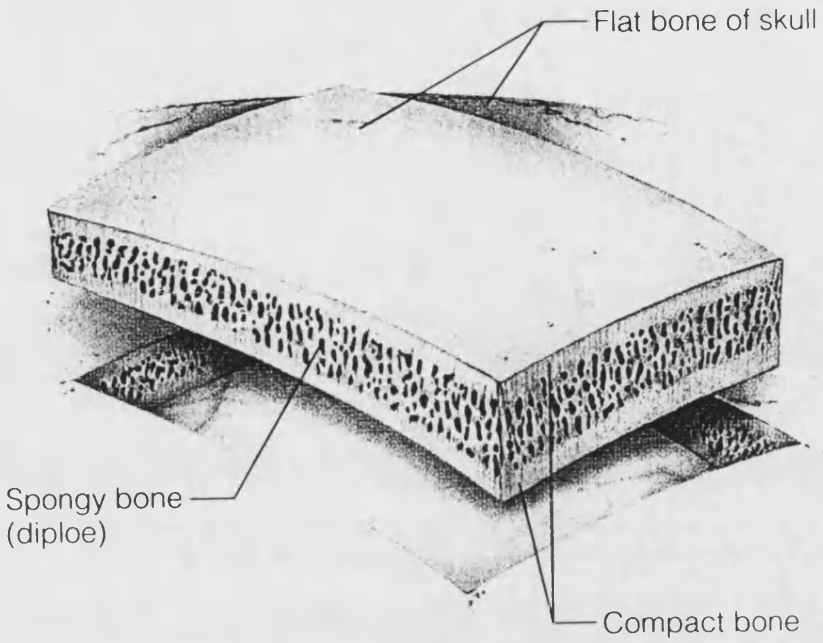

Figure 1.3: Structure of a flat bone [4]

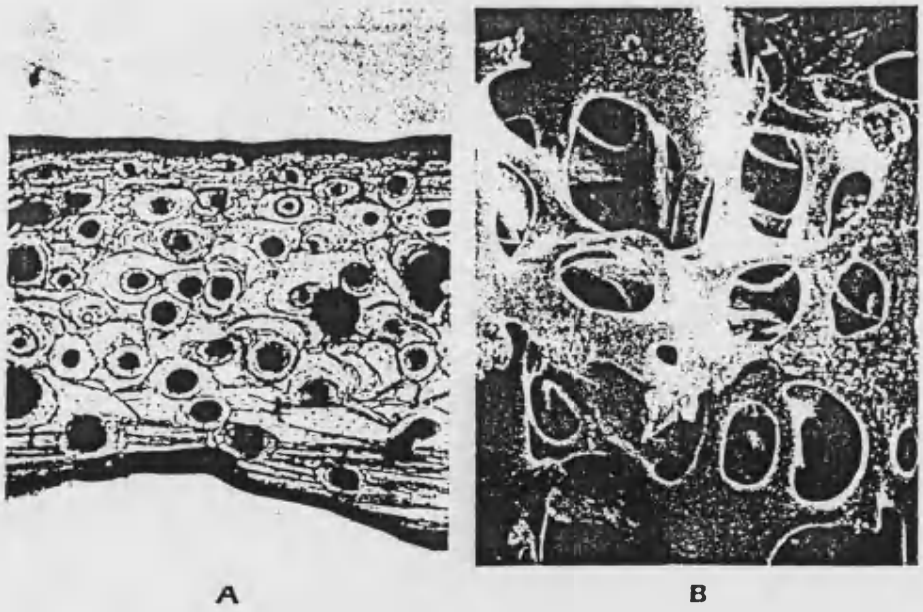

Figure 1.4: Photomicrograph from human tibia; **A.** cortical bone; **B.** cancellous bone [6]

Compact (cortical) bone

Observed by eye, the compact bone, which forms the external portion of the bone, appears to be very dense. However, at a microscope level, it is revealed to comprise canals and passageways that serve as a conduit for nerves, blood vessels and lymphatic vessels. It consists of precise arrangements of microscopic cylindrical structures oriented parallel to the long axis of the bone. The fundamental column-like structure unit of compact bone is the osteon or Haversian system [6] (Figure 1.5). At the centre of each osteon is a small channel called the Haversian canal that allows passage of blood vessels and nerve fibres. The osteon consists of layers (lamellae) of mineralised matrix surrounding the central canal. Along each boundary layer of lamellae are lacunae which are small cavities containing a bone cell, or osteocyte. Radiating from each lacuna are small channels called canaliculi, which connect to the lacunae of adjacent lamellae, ultimately reaching the Haversian canal. Cell processes extend from the osteocytes into the canaliculi allowing nutrients from blood vessels in the Haversian canal to reach the osteocytes. The osteon or Haversian canal has a diameter of ~200μm and is located no more than 100μm from the blood supply.

Spongy (cancellous) bone

In contrast to compact bone, spongy bone which is located deep in the compact bone tissue, is in the form of a loose mesh structure and composed of thin plates or trabeculae. The interstices between the trabeculae are filled with red marrow. Cancellous bone does not contain Haversian canals.

1.1.2.3 Chemical composition of bone

Bone is a living organism composed of inorganic salts and an organic matrix [7]. Properties of bone vary from one point to another according to the different part of the skeleton, but average compact bone contains by weight approximately 30 percent organic

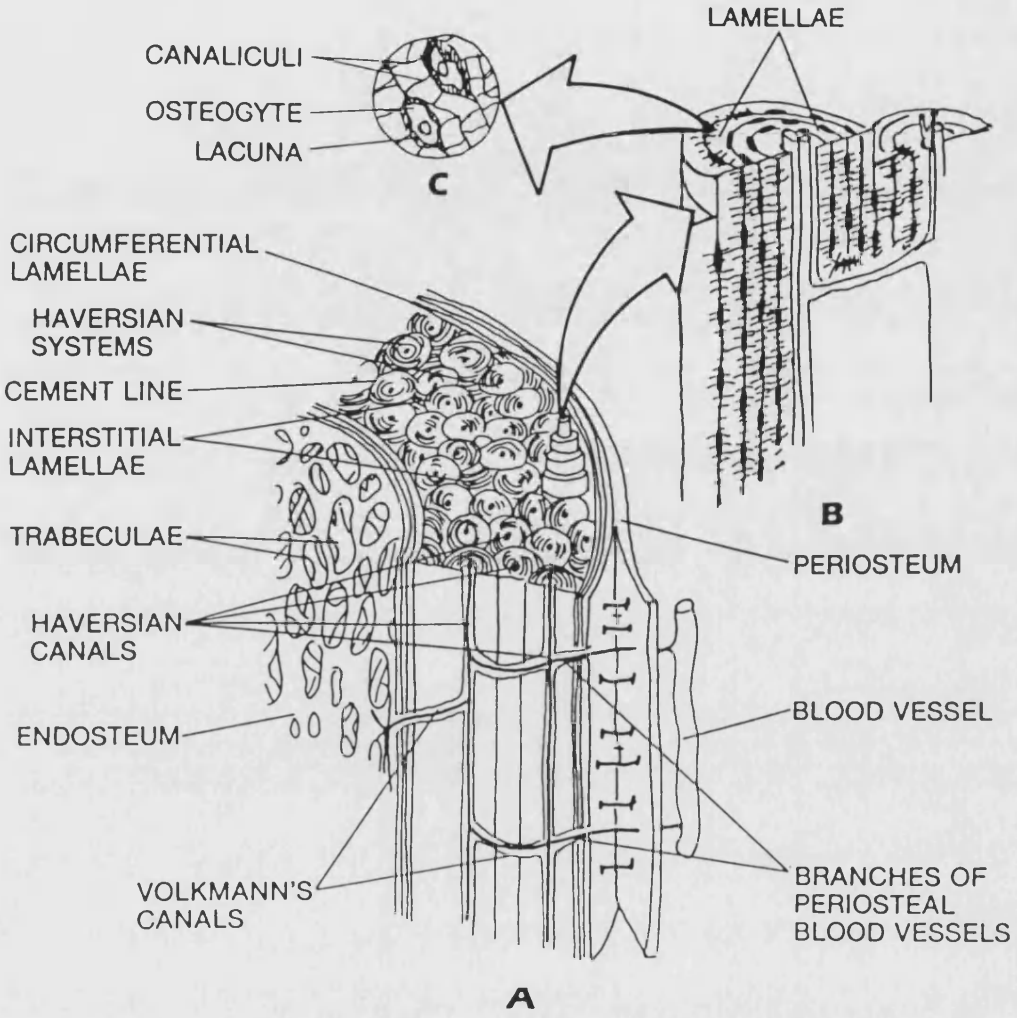

Figure 1.5: Fine structure of bone without inner marrow [6]

matrix and 70 percent inorganic salts. However, newly formed bone may have a considerably higher percentage of matrix relative to mineral content.

The organic components in a bone include the cells osteoblasts, osteocytes, osteoclasts and osteiods. Osteoid, which makes up approximately one-third of the matrix, includes proteoglycans, glycoproteins and collagen fibres, all of which are made and secreted by the osteoblasts. These organic substances, particularly collagen, not only contribute to a bone's structure but are also responsible for the flexibility and great tensile strength that allow the bone to resist stretch and twisting [4].

The organic matrix of bone is 90 to 95 percent collagen fibres and the remainder consists of a homogeneous medium termed 'ground substance'. The collagen fibres extend primarily along the lines of tensional force. These fibres give bone its good tensile properties. The ground substance is composed of extracellular fluid plus proteoglycans, especially chondroitin sulphate and hyaluronic acid. The precise function of these is not known, though perhaps they control the deposition of calcium salts.

The inorganic part of bone consists of an amorphous and crystalline phase. The amorphous phase, which is composed of tricalcium phosphate (TCP), predominates in younger bones and is partially transformed into crystalline phase with age [8]. The crystalline inorganic bone salts deposited in the organic matrix of bone are composed principally of calcium and phosphate, known as hydroxyapatite with a formula of $Ca_{10}(PO_4)_6(OH)_2$. Each crystal, about 400Å long, 10 to 30 Å thick, and 100 Å wide, is shaped like a long, flat plate. The relative ratio of calcium to phosphorus can vary markedly under different nutritional conditions, the Ca/P ratio on a weight basis varying between 1.3 and 2.0. Magnesium, sodium, potassium and carbonate ions are also present among bone salts [9]. In geographical regions where drinking water has been treated with fluoride, it is common to find hydroxyl groups in the hydroxyapatite crystals replaced by fluoride ion [7]. Chloride ion is also present in bone but in a small quantity. The typical

composition of the mineral phases of human femoral bone is given in Table 1.1 below [10].

Table 1.1: Typical composition of the mineral phases of human femoral bone[a] [10].

CaO	P_2O_5	Na_2O	CO_2	H_2O	MgO	K_2O	F	Cl
51.31	36.65	1.04	5.86	3.78	0.77	0.32	0.23	0.01

[a]Weight percentage after removal of organic fraction by glycerine per 6% KOH

1.1.3 Bone cells

Bone contains five types of cells that are capable of changing their roles as the needs of the body change in the growing and adults' skeletons.

1.1.3.1 Osteogenic cells

They are found mostly in the deep layers of the periosteum and in bone marrow. These cells are capable of being transformed into bone-forming cells (osteoblasts) or bone destroying cells (osteoclasts) during times of stress and healing [2].

1.1.3.2 Osteoblasts

These cells synthesise and secrete unmineralised ground substances, called osteoid. The primary role of osteoblasts is the production of collagen and ultimately bone [7]. When calcium salts are deposited in the fibrous osteoid, it becomes hardened, or calcifies, into bone matrix. Osteoblasts act as pump cells to move calcium and phosphate into and out of

bone tissue, thereby calcifying or decalcifying it. Osteoblasts are usually found in the growing portions of bones including the periosteum [2].

1.1.3.3 Osteocytes

Osteocytes are the main cells of fully developed bones. As bone grows and osteoblasts deposit collagen and ground substances (organic matrix of bones prior to calcification) around themselves, they become entrapped within spaces termed lacunae. Calcification of the matrix occurs and the cells within the lacunae are referred to as osteocytes. Each of the osteocytes is in contact with nearby osteocytes through minute canals termed canaliculi. Osteocytes play an important role in the regulation of blood calcium levels in body fluids, helping to release calcium from bone tissue into the blood. Their presence also seems to keep the matrix stable and healthy by secreting enzymes and maintaining its mineral content [2].

1.1.3.4 Osteoclasts

Osteoclasts are very large, multinucleated cells that function in the resorption (removal) of bone. Their formation with subsequent bone resorption is stimulated when parathyroid hormone levels in the blood remain elevated for a long period of time.

1.1.3.5 Bone-lining cells

These cells are found on the surface of most bones in the adult skeleton and they are derived from osteoblasts that cease their physiological activity and flatten out on the bone surface. These cells serve as osteogenic cells that can divide and differentiate into osteoblasts. They also serves as ion barrier around bone tissue which contribute to the mineral homeostasis by regulating the movement of calcium and phosphate into and out of the bone matrix, which in turn helps control the deposition of hydroxyapatite in the bone tissue [2].

1.1.4 Mechanical properties of bone

Each collagen fibre of compact bone is composed of repeating periodic segments every 640 Å, along its length; hydroxyapatite crystals lie adjacent to each segments of the fibre, bound tightly to it. This intimate bonding prevents shear in the bone, that is, it prevents the crystals and collagen fibres from slipping out of place, which is essential in providing strength to the bone. In addition, the segments of adjacent collagen fibres overlap each other, also causing hydroxyapatite crystals to be overlapped like bricks keyed to each other in a brick wall [9].

Table 1.2: Mechanical properties of human femur and bioactive ceramics

Properties	Human Femur [11]	Bioglass 45S5 [12]	Glass-Ceramic Cerabone A-W [13]	Sintered Hydroxyapatite [14]	Sintered β-Tricalcium Phosphate [15]
Density (g/cm^3)		2.6572	3.07	3.16	3.07
Hardness (Vickers) (HV)		458	680	600	
Tensile Strength (MPa)	89 - 118	42			
Bending Strength (MPa)	76		215	115-200	140-154
Compression Strength (MPa)	125-166		1080	500-1000	460-687
Young's Modulus (GPa)	19.5-20.5	35	218	80-110	33-90

The collagen fibres of bone, like those of tendons, have a high tensile strength, while calcium salts, which have similar physical properties to marble, have a high compressional strength. These combined properties, plus the degree of bonding between the collagen

fibres and the crystals, provide a bony structure that have both high tensile and compressional strengths [9]. The combination of organic and inorganic matrix elements allows bones to be exceedingly durable and strong without being brittle [4].

The mechanical properties of human femurs and bioactive ceramics have been compared and are listed in the Table 1.2 above.

1.1.5 Summary

1. Bones are usually classified by shape as flat, irregular , long, sesamoid or short.
2. Most adult long bones have a tubular shaft, the diaphysis, constructed from compact bone and covered at the outer surface by periosteum, and the epiphyses, the bone end, containing spongy bone in the interior.
3. The basic structural unit of the bone is the Haversian system.
4. The centre of each Haversian system has a small channel called the Haversian canal that contains blood vessels which provide the nutrient and blood for the ingrowth of the bone tissue.
5. The total volume of porosity in a bone is between 5 and 90%.
6. Bone is composed of 70 wt% of inorganic salts, which primarily consists of calcium phosphate, and 30wt% of organic matrix, of which 90-95% is collagen fibres.
7. The combined properties of the collagen fibres and the calcium phosphate crystals result in the good tensile and compressive strength properties of the bone.

1.2 Bioceramics

Ceramics have been used for external body applications in the health industry for a long time. However the use of ceramics inside the body, as implants, is relatively new, the first instance reported just 20 years ago [16]. The ceramics used for the repair and reconstruction of diseased, damaged or 'worn out' parts of the body are referred to as bioceramics which can be used in the form of bulk materials of a specific shape, as a space filler while the natural repair processes restore function, or, as a coating on a substrate. Bioceramics can be polycrystalline (alumina, zirconia or hydroxyapatite), bioactive glass, bioactive glass-ceramic or bioactive composite (polyethylene - hydroxyapatite). The clinical uses of bioceramics are summarised in Figure 1.6 [1].

1.2.1 Types of Tissue Attachment to Bioceramics

The tissue attachment mechanism to implant materials is related directly to the tissue response towards the implant interface. Bioceramics can be divided into four types of implants, according to the tissue attachment; nearly inert, porous, resorbable and bioactive implant. For nearly inert implant materials, such as alumina and zirconia, only mechanical interlock or morphological fixation would occur, where the fibrous tissue would capsulate the implant without any bonding. The implant would loosen very quickly, which could lead to clinical failure. Porous bioceramics such as hydroxyapatite, and hydroxyapatite coatings on porous metals, were developed to prevent loosening of implants by the ingrowth of tissues into the pores (biological fixation). The limitation of this implant is the requirement to have pores of at least 80-100 μm in diameter to allow bone to grow into the pores and this would lead to a lower strength of the bioceramic [17]. Resorbable implants such as tricalcium phosphate, are designed to degrade gradually with time and be replaced with tissue. The limitation of this type of material is the difficulty in

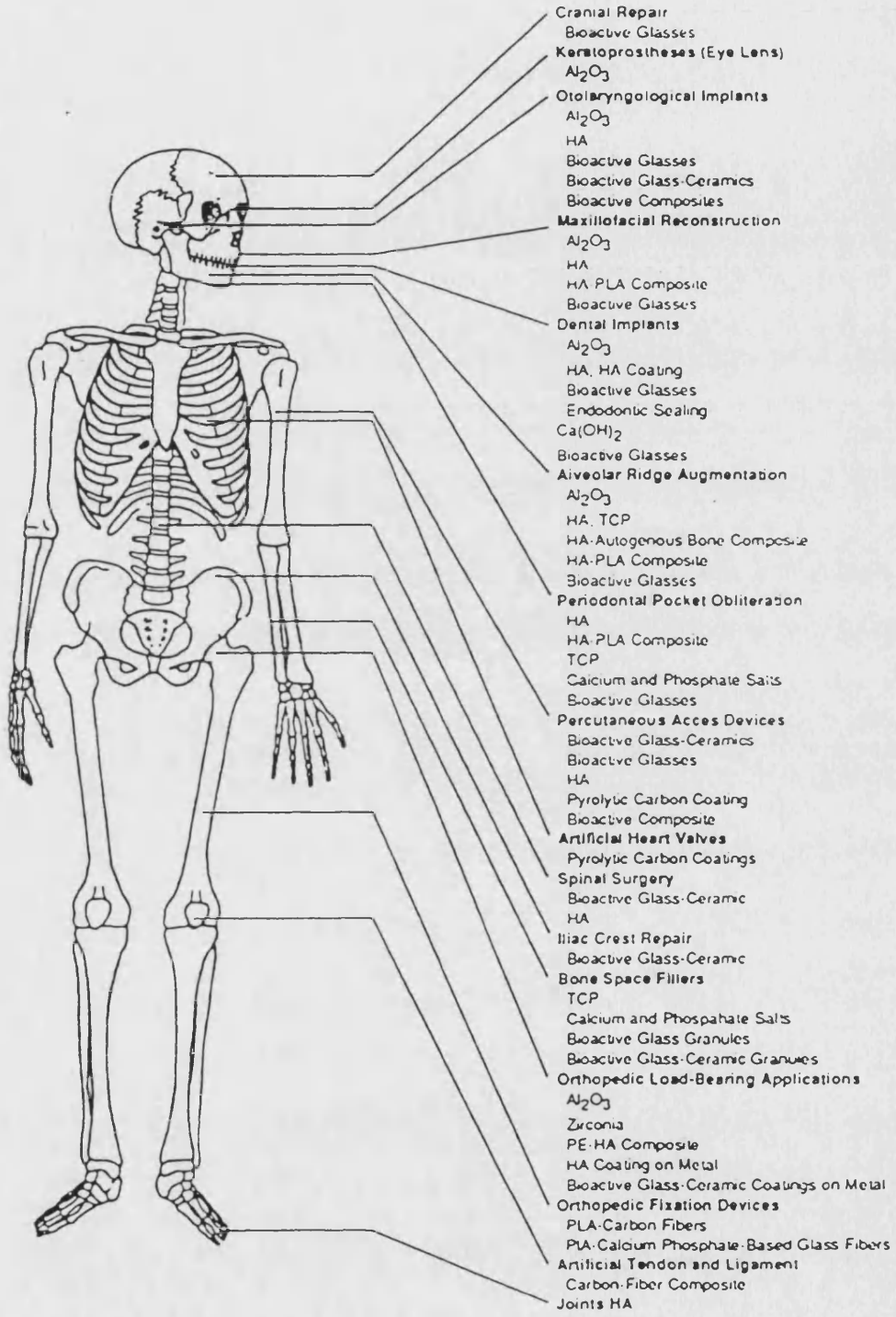

Figure 1.6: Clinical uses of bioceramics [1].

sustaining the strength of the implant while regeneration of tissue occurs. The resorption rate of the material must match the repair rate of the body tissue and this differs greatly depending on the age of the patient and type of tissue replaced. Another type of implant is the bioactive implant, such as hydroxyapatite and the bioactive glasses, where the behaviour falls between inert and resorbable material. A biological response would take place at the interface of the material, resulting in a formation of a bond between the tissues and the material. However the time taken for the bond to form, strengthen, thicken and which mechanism of bonding take place, differs according to the materials used [17].

1.2.2 Bone formation in calcium phosphate ceramics

Insertion of a biomaterial into living tissue creates an artificial interface between the living tissue and the biomaterial. Calcium phosphate ceramics, especially hydroxyapatite have been extensively studied for biocompatibility as an implant material because they have shown a lack of toxicity, inflammation and foreign body response towards the living tissue. Many investigators have demonstrated direct development of a new bone when implanted in bony tissue. New bone formation begins both at the edge of a defect and the ceramic surface. It occurs along the HA, forming a bridge between host bone and HA, and eventually the immature bone is remodelled [18].

The importance of having a sufficient pore size to allow bone growth has been identified and studied. Daculsi's study [19] showed that macropores up to 100μm are large enough to allow bone ingrowth, however during the first months of implantation, larger macropore sizes are more suitable for bone ingrowth. The optimum pore size for HA to permit bone growth is between 300 and 600μm [20]. However, Eggli et al [21] found that HA with small pores was totally infiltrated by bone or bone marrow after 4 months, whereas in the larger-pored HA implants, tissue did not penetrate all pores after 6 months and the amount of bone within the implant was small.

Osseo-integration of calcium phosphate depends not only on the pore size but also the chemical composition of the ceramic. The most frequently used orthopaedic bioceramics are HA and β-TCP. The addition of β-TCP to the HA used for implantation increases the solubility of the porous ceramic and dramatically increases the bone ingrowth in the ceramic pores [22].

In a study of ceramic/bone interfaces of calcium phosphate ceramics with different calcium/phosphorus molar ratios, β-calcium pyrophosphate, CPP, ($Ca_2P_2O_7$), β-tricalcium phosphate, TCP, ($Ca_3(PO_4)_2$), hydroxyapatite, HA, ($Ca_{10}(PO_4)_6(OH)_2$) and tetracalcium phosphate, TTCP, ($Ca_4(PO_4)_2O$), with a molar ratio of 1, 1.5, 1.67 and 2 respectively, it was shown that the bone-bonding behaviour of calcium phosphate ceramics at the interface with bone did not vary with the calcium/phosphate molar ratio. The ceramics showed direct continuity of formation of amorphous-needle like microcrystals even after 6 months of implantation but no collagen fibres were observed at the bone/ceramic interface, the ceramics getting smaller with time [23]. However, according to Bauer et al [24] there is direct contact between implants and the surrounding bone for samples with a Ca/P ratio 1.6 or higher (70-90% covered with bone), while TCP implants showed hardly any direct bony contact (<25%). Below a ratio of 1.4, only limited contact is found, and a thick fibrous tissue is developed.

1.2.3 Hydroxyapatite

Apatite is the name given by Werner in 1788 to a group of crystals with a general formula of $M_{10}(RO_4)_6X_2$, where M could be one of several metals, although it is usually calcium, R is commonly phosphorus and X is commonly hydroxide or a halogen such as fluorine or chlorine. The first x-ray diffraction study of bone by DeJong (1926) identified the resemblance of the inorganic phase of bone to the mineral structure of apatite [10].

Hydroxyapatite ($Ca_{10}(PO_4)_6(OH)_2$) is an attractive material for human hard tissue implantation. The crystallography and chemical composition of hydroxyapatite closely resemble those of bone and tooth mineral. Natural bone contains approximately 70% of hydroxyapatite by weight and 50% by volume.

1.2.3.1 Structure of hydroxyapatite

Hydroxyapatite belongs to the hexagonal system with a space group $P6_3/m$. This group is characterised by a six fold c-axis perpendicular to three equivalent a-axes (a_1, a_2, a_3) at angles 120° to each other. The unit cell, containing a complete representation of the apatite crystal consists of Ca, PO_4 and OH groups closely packed together; shown in Figure 1.7 [25].

The isomorphous substitution of the apatite, is the replacement of one ion by another in the crystal lattice without disrupting its crystal structure. The substitution can be classified as iso-ionic and hetero-ionic. The former can be defined as the exchange of ions from solution phase with identical ions a of solid phase that are in contact, and the composition of the two phases are not being altered. This type of substitution occurs during skeletal fixation of calcium and phosphorus and also during bone resorption, which is the process of bone being dissolved during growth and returned to the blood stream. The hetero-ionic substitution occurs when ions of a solid phase are being replaced by different ions from the solution in contact with it, thereby altering the composition of both phases. Hydroxyapatite can have both iso-ionic and hetero-ionic substitution, involving both anions and cations that have similarity in charge and size. Among the significant ones are cation substitution of Ca^{2+} by Ba^{2+}, Pb^{2+} and Cd^{2+} with ionic radii of 0.099, 0.113, 0.135 and 0.097 nm respectively. Among the important anionic substitutions are, the replacement of OH^- by F^-, Cl^- and I^-, and PO_4^{3-} by AsO_4^{3-} and VO_4^{3-} with the ionic radii of these being 0.168, 0.132, 0.181, 0.216, 0.110, 0.118 and 0.122nm respectively [8]. The

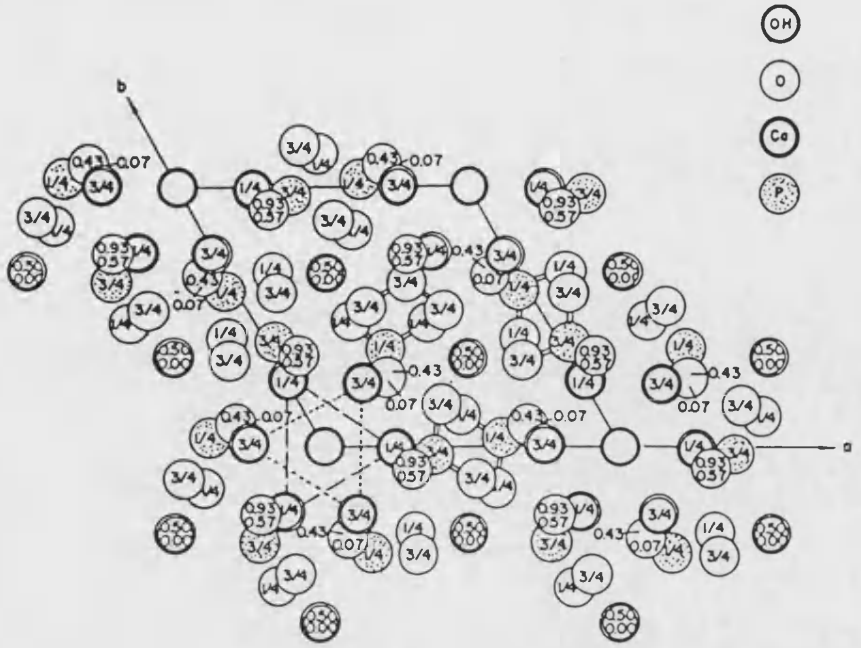

Figure 1.7: Hydroxyapatite structure projected down to the c-axis onto the basal plane [25]

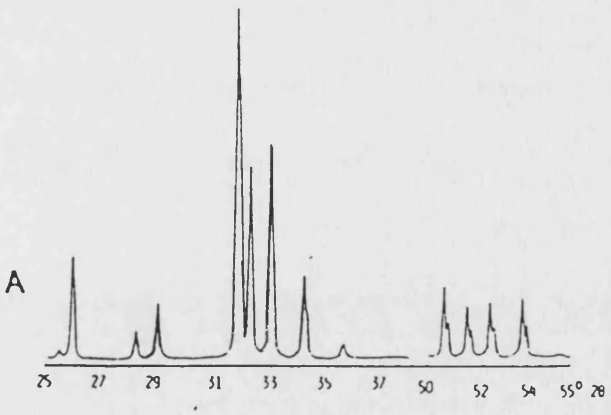

Figure 1.8A: X-ray diffraction pattern of hydroxyapatite powder showing the presence of only hydroxyapatite phase [25]

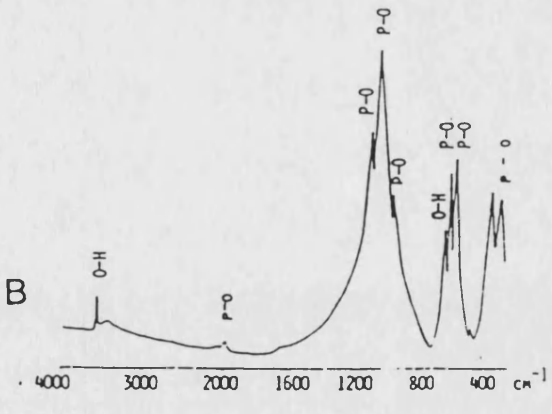

Figure 1.8B: Infra red absorption spectrum of hydroxyapatite powder showing the characteristic absorption bands of O-H and P-O reflecting the vibrations of the OH and PO_4 groups in the calcium hydroxyapatite, $Ca_{10}(PO_4)_6(OH)_2$ [25]

most common substitution of HA occurs in the OH^- ion position, yielding fluorapatite and chlorapatite. The chemical stability of these compounds varies due to the presence of these substitutions with flourapatite the most chemically stable, followed by hydroxyapatite and chlorapatite.

1.2.3.2 Phases of calcium phosphate

Pure hydroxyapatite has the theoretical density of 3.156 gcm^{-3} [26], a theoretical composition of 39.68 wt % Ca; 18.45 wt % P; Ca/P wt ratio 3.151 and Ca/P molar ratio of 1.667 [27]. Variations in the Ca/P ratio reflect the β-tricalcium phosphate/ hydroxyapatite (β-TCP/HA) ratios in the sintered material which in turn reflect the purity (whether consisting of only the apatite phase or mixed with other Ca/P phases); and/or composition or calcium deficiency of the apatite preparation before sintering. If the Ca/P ratio is 1.67, only hydroxyapatite will be observed in the X-ray diffraction (Figure 1.8A) and infrared spectrum (Figure 1.8B). If the Ca/P ratio is lower than 1.67, β-TCP, and other phases such as tetracalcium phosphate, TTCP, $Ca_4P_2O_9$ or $Ca_4(PO_4)_2O$ will be present with the HA phase in the sintered material, treatment depending on the temperature and conditions of sintering. If the Ca/P ratio is higher than 1.67, CaO will be present with the hydroxyapatite phase [28]. The phases that can be present in calcium phosphate are summarised in Table 1.3 below.

The purity, composition and particle size of the apatite preparation before sintering also affect the type and amount of other calcium phosphate and/or calcium compounds which will be present with the hydroxyapatite phase. According to ASTM F1185-88 [29], the acceptable composition for commercial HA contains a minimum of 95% hydroxyapatite, as established by x-ray diffraction analyses, and the acceptable concentration of trace elements is limited (maximum ppm) as follows: As = 3; Cd = 5; Hg = 5; Pb = 30, total heavy metals (as lead) = 50.

Table 1.3: Phases of calcium phosphate [15].

	Mineral	Empirical Formulas	Ca/P
Dicalcium phosphate dihydrate	Brushite	$CaHPO_4.2H_2O$	1.00
Dicalcium phosphate	Monetite	$CaHPO_4$	1.00
β-Tricalcium phosphate	Whitlockite	β-$Ca_3(PO_4)_2$	1.50
Hydroxyapatite		$Ca_{10}(PO_4)_6(OH)_2$	1.67
Tetra calcium phosphate		$Ca_4P_2O_9$	2.0

The thermodynamical stability of calcium phosphate powders obtained either commercially or produced in the laboratory are described by the phase diagrams (Figures 1.9 - 1.12) of de Groot et al [24, 30].

For commercial and non commercial hydroxyapatite, in the temperature range from 950 - 1500°C the following calcium phosphates can form with or without the additional calcium oxide phase: β-TCP, α-TCP (resulting from the transformation of β-TCP at temperatures above 1300°C), TTCP and oxyapatite according to the reaction outlined below. In a recent paper, Wang and Chaki [31] have shown that dissociation of hydroxyapatite is very much influenced by the atmosphere, no dissociation being observed at 1300°C when sintering took place in a moist atmosphere.

'Apatite' preparation (AP) / Ca-deficient AP $\xrightarrow[>900°C]{}$ $Ca_{10}(PO_4)_6(OH)_2$ HA + $Ca_3(PO_4)_2$ β-TCP

β-TCP $\xrightarrow[>1100°C]{}$ α-TCP

$Ca_{10}(PO_4)_6(OH)_2$ HA $\xrightarrow[\geq 1300°C]{}$ 2 $Ca_3(PO_4)_2$ α-TCP + $Ca_4(PO_4)_2O + H_2O$ TTCP

$Ca_3(PO_4)_2 + CaO$ β-TCP $\xrightarrow[>1400°C]{}$ $Ca_4(PO_4)_2O$ TTCP

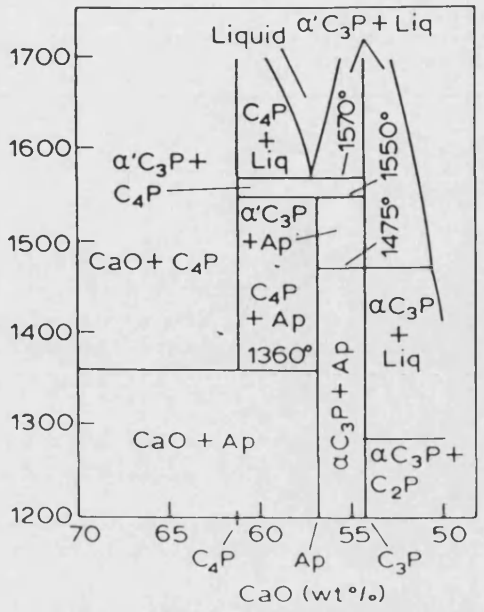

Figure 1.9: Phase diagram of system CaO/P_2O_5 at high temperatures (°C). No water present [30].

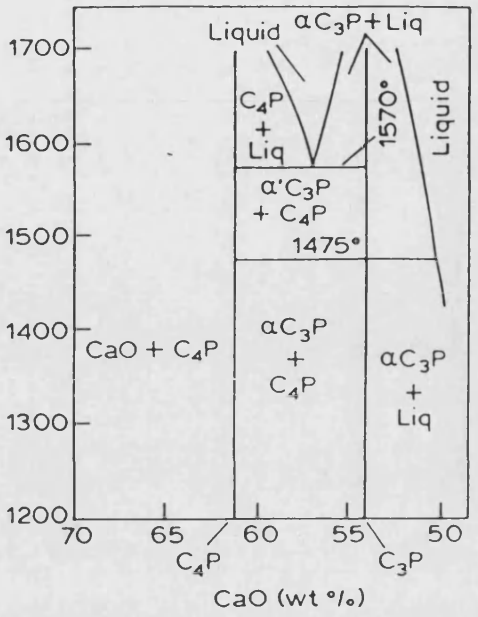

Figure 1.10: Phase diagram of CaO/P_2O_5 at high temperature (°C). Water pressure = 500mm Hg [30].

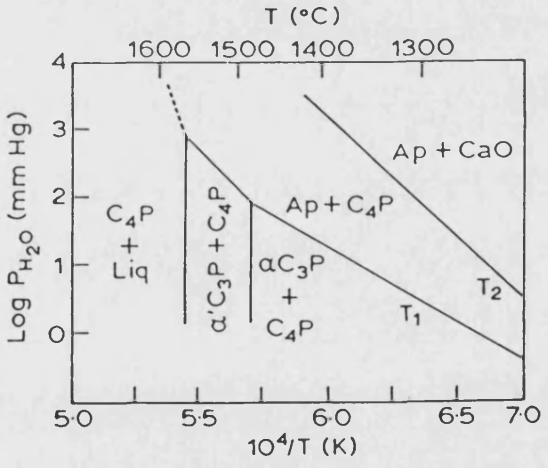

Figure 1.11: Influence of ambient water vapour pressure on phase composition [30]

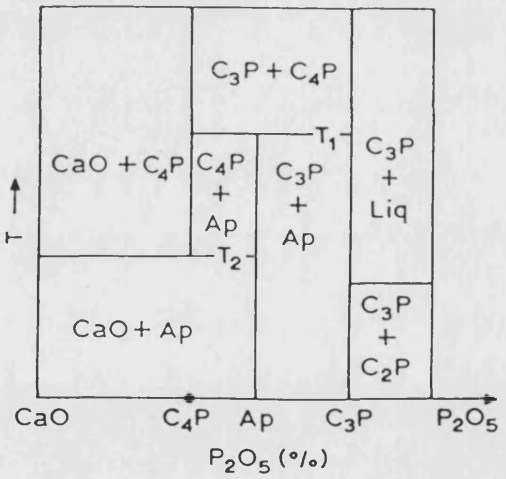

Figure 1.12: Enlarged part of Figure 1.9. T_1 = 1360°C and T_2 = 1475°C [30]

Apatite prepared from highly alkaline solution in the presence of air may often contain CO_3^{2-} and can form CaO and hydroxyapatite upon sintering above 900°C. TTCP can also result from the reaction between β-TCP and CaO.

Another calcium phosphate compound reported to form with hydroxyapatite, after sintering the apatite preparation above 900°C, is anhydrous dicalcium phosphate, DCP, $CaHPO_4$. However, DCP is not stable at these temperatures, transforming instead to β-TCP and calcium pyrophosphate, $Ca_2P_2O_7$. If sintering take place with a water vapour pressure of about 500mm Hg, the formation of the other Ca/P phases (α and β-TCP, TTCP) will be minimised and hydroxyapatite will be the more stable phase [24,32]. Thus the Ca/P molar ratio of the apatite preparation, the sintering temperature and processing conditions determine the final composition of the dense hydroxyapatite.

1.2.3.3 Decomposition of hydroxyapatite

The properties of hydroxyapatite at elevated temperatures are important for the design of experiments to obtain the ceramic by sintering. Hydroxyapatite sintered at a temperature lower than 800°C does not show any phase transformation, only increased crystallinity of the as-received hydroxyapatite powder. At temperatures above 800°C, significant reversible dehydroxylation can occur; up to 70 - 80% of the total hydroxyl group can be lost reversibly [33]. Hydroxyapatite starts decomposing to anhydrous calcium phosphate, such as TCP, around 1200°C when heat treated in O_2 for 6h [34] or in dry air for 4h [31]. Van Landuyt et al [35] reported, stoichiometric hydroxyapatite sintered in air decomposes only slightly when heat treated at 1300°C for 8h. Between 1250°C and 1450°C is the critical temperature range and if it is exceeded, complete and irreversible dehydroxylation occurs resulting in collapse of the hydroxyapatite structure and decomposition [33].

The atmosphere used also influences the sintering behaviour of hydroxyapatite. Dehydroxylation of hydroxyapatite sintered in air and vacuum occurs in the temperature range 850 - 900°C but it does not obstruct the densification process. At higher

temperatures, ~1150°C, decomposition of hydroxyapatite in air and vacuum causes a decrease in the density, flexural strength and Knoop hardness. Hydroxyapatite sintered in moisture however does not show any dehydroxylation or decomposition even at the highest sintering temperature ~1350°C. However at temperatures <1200°C, the density, flexural strength and Knoop hardness of the HA compact sintered in moisture are lower than those sintered in air, indicating that sinterability of hydroxylated hydroxyapatite is poorer than that of oxyhydroxyapatite ($Ca_{10}(PO_4)_6(OH)_{2-2x}O_x\square_x$) [31, 36].

Decomposition must be avoided since it results in enhanced in-vitro dissolution [24]. For temperatures below the critical point, the hydroxyapatite crystal structure is retained despite dehydroxylation and the hydroxyapatite rehydrates on cooling [37].

The strength of dense hydroxyapatite sintered in air, starts to decrease when the density reached ~ 95% (~1200°C) and more severely at ~ 1350°C, due to the dehydroxylation effect. At ~95% density, the pores are closed, thereby eliminating continuous paths from the compact interior to the surface. Despite the closure of the pores, significant dehydroxylation continues increasing the internal vapour pressure. This pressure exceeds the mechanical strength of the solid and the result is the formation of blowholes. Above 1350°C, the same mechanism occurs but on a much larger scale and results in a larger decrease in strength [33].

The exact composition of the hydroxyapatite is an important parameter since for example, the biodegradation rate, depends on it [38]. The mechanical behaviour of hydroxyapatite also depends on the composition of the samples, as shown in Figure 1.13 [39].

The initial powder with Ca/P molar ratio > 1.667 usually contains hydroxyapatite and calcia (CaO) and Ca/P molar ratio < 1.667 contains hydroxyapatite and TCP ($Ca_3(PO_4)_2$). The presence of CaO blocks the densification of hydroxyapatite, whereas TCP delays the sintering process. However the transformation from β-TCP to α-TCP in HA+TCP

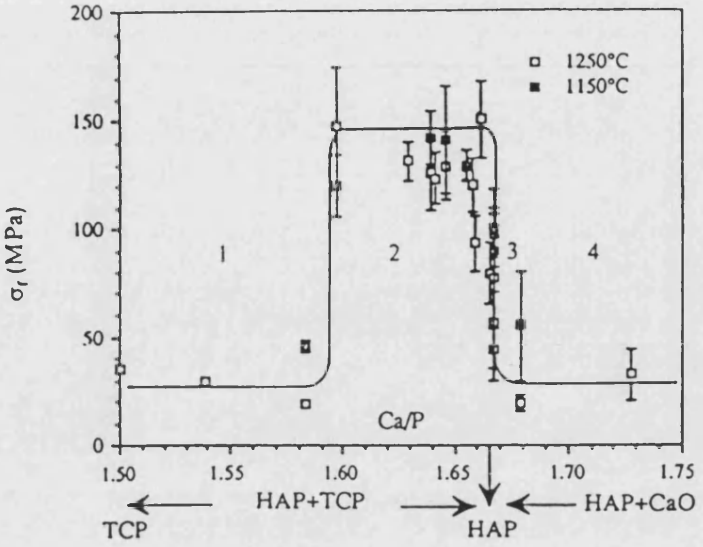

Figure 1.13: Influence of Ca/P ratio on the flexural strength: (□)1250°C and (■) 1150°C [39]

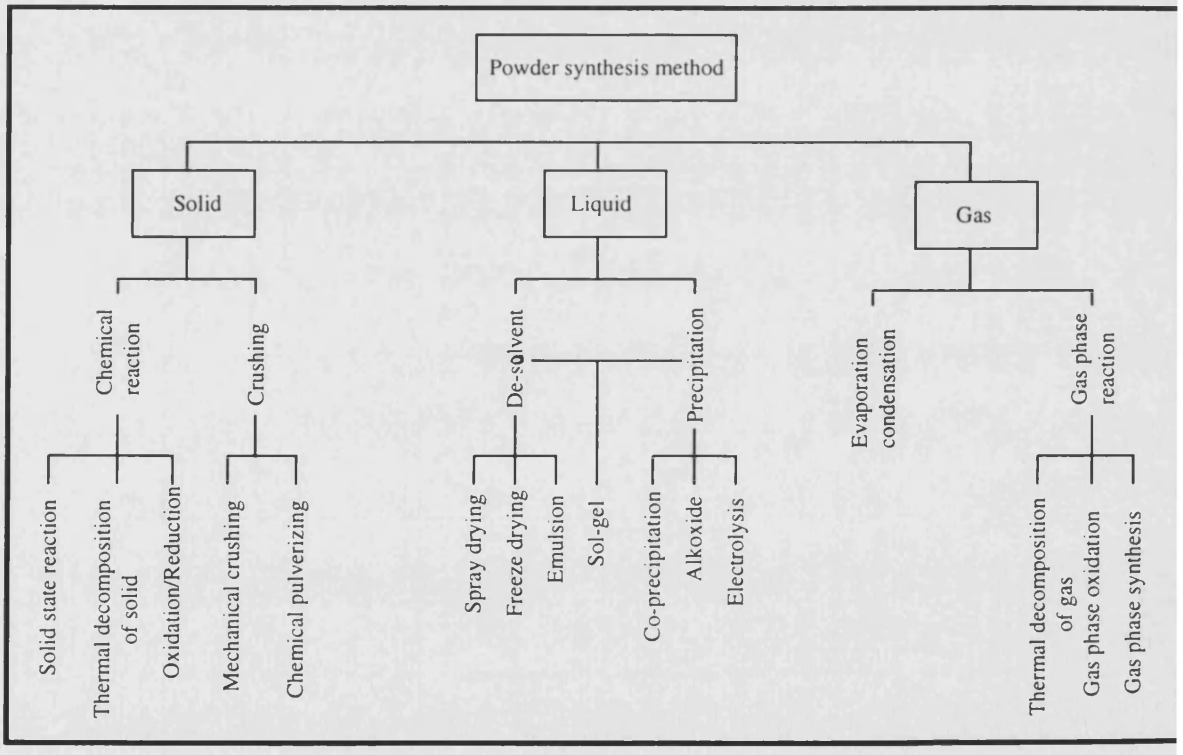

Figure 1.14: Powder synthesis method [79]

composite increases the volume and thus introduces compressive stress on the surface and therefore reduces the effect of critical flaws of any size located near the surface.

Powders with a Ca/P molar ratio <1.667 have a higher specific surface area and a smaller grain size after sintering compared to an initial powder with a Ca/P molar ratio >1.667. Powder with a high surface area and smaller mean particle size has a larger driving force for densification and leads to a higher density and hence higher mechanical strength [40]. Grain size does not increase until density is almost at its maximum and the strength increases when porosity effectively disappears.

During sintering at 1000°C and 1100°C, only a little densification occurs. Below this temperature, densification is limited to the first stage of sintering which corresponds to the formation of solid bridges between the grains. The density increases up to a sintering temperature of 1300°C. Only limited further progress is observed above 1300°C. This is due to the separation of the residual pores from the grain boundaries as a consequence of the increase of grain size. The grain size increases steadily on heating above 1300°C with exaggerated grain growth present at 1450°C. For the dense hydroxyapatite, the highest fracture toughness is obtained with the smallest grain sizes i.e. after sintering at 1300°C. However due to the decrease of the maximum flaw size with decreasing pore size, the hardness and compressive strength keeps increasing to an optimum value, for a sintering temperature of 1400°C [35].

1.2.3.4 Powder preparation of hydroxyapatite

Hydroxyapatite powder can be obtained via a number of ceramic processing routes, however, the resulting microstructure and properties vary considerably. To prepare a fine and sinter reactive powder, several wet chemistry-based techniques have been adopted, including the precipitation and hydrolysis method, and the solid-state reaction or hydrothermal reaction [25].

In the precipitation route, one of the commonly used methods in commercial preparations of hydroxyapatite is drop-wise addition of phosphoric acid (H_3PO_4) to a stirred suspension of calcium hydroxide ($Ca(OH_2)$) [41] or calcium carbonate ($CaCO_3$) in water, as shown below:

$$10\ Ca(OH)_2 + 3H_3PO_4 \longrightarrow Ca_{10}(PO_4)_6(OH)_2$$

$$10\ CaCO_3 + H_3PO_4 \longrightarrow Ca_{10}(PO_4)_6(OH)_2 + 10\ CO_2$$

To ensure the formation of hydroxyapatite, ammonium hydroxide (NH_4OH) is added. This method would result in a gelatinous precipitate that would be aged, separated from the supernatant, washed and dried in the oven and finally crushed to reduce the particle size and remove large particle lumps. The as-dried precursor powder is in a hydroxyapatite crystallite form [42].

The reaction between calcium nitrate ($Ca(NO_3)_2$) and ammonium phosphate ($(NH_4)_2HPO_4$) with added NH_4OH can also produce hydroxyapatite [25]. Puajindanetr et al [43] found that materials precipitated at 25°C using a reactant concentration of 1M gave sintered compacts with the best mechanical properties.

$$10\ Ca(NO_3)_2 + 6\ (NH_4)_2HPO_4 + 2\ NH_4OH \longrightarrow Ca_{10}(PO_4)_6(OH)_2$$

The precipitation method usually results in calcium deficient apatite (i.e. Ca/P molar ratio < 1.67) which will cause the formation of β-TCP and HA when sintered. Under very basic conditions, the precipitate will contain carbonate which will make the Ca/P ratio > 1.67.

In the hydrolysis method, apatite can be prepared by the mixing of acid calcium phosphates in ammonium, sodium or potassium hydroxide. Examples of acid calcium phosphates are dicalcium phosphate dihydrate ($CaHPO_4.2H_2O$) and octacalcium

phosphate ($Ca_8H_2(PO_4)_6.5H_2O$). Both monetite ($CaHPO_4$) and brushite ($CaHPO_4.2H_2O$) are stable at pH below 4.8, but at under certain other pH conditions, these compounds can be converted to hydroxyapatite. When α-TCP is treated in boiling water, it could be converted to HA but β-TCP under the same condition could not. Tetracalcium phosphate (TTCP) could be hydrolysed to form HA and $Ca(OH)_2$ according to the reaction below [44].

$$3Ca_4P_2O_9 + 2H_2O \longrightarrow Ca_{10}(PO_4)_6(OH)_2 + 2Ca(OH)_2$$

Hydroxyapatite can be prepared in a solid state reaction by mixing calcium compounds, followed by compression and sintering above 950°C according to the reaction below:

$$6\ CaHPO_4 + 4\ Ca(OH)_2 \longrightarrow Ca_{10}(PO_4)_6(OH)_2 + 6H_2O$$
(monetite) (hydroxyapatite)

$$3Ca_3(PO_4)_2 + Ca(OH)_2 \longrightarrow Ca_{10}(PO_4)_6(OH)_2 + H_2O$$
(β-TCP) (hydroxyapatite)

Hydroxyapatite can also be produced hydrothermally. α-TCP (tricalcium phosphate; $Ca_3(PO_4)_2$), for instance, when treated in boiling water, can be converted to hydroxyapatite [45]. Monetite ($CaHPO_4$), when heated at 275°C and under steam pressure of 12 000 psi, can also be converted into hydroxyapatite. Tetracalcium phosphate, TTCP ($Ca_4P_2O_9$) can hydrolyse to form hydroxyapatite according to the reaction below [46]:

$$3Ca_4P_2O_9 + 2H_2O \longrightarrow Ca_{10}(PO_4)_6(OH)_2 + 2Ca(OH)_2$$
(TTCP)

Liu et al [47] used a pressurised cooking utensil for synthesising HA hydrothermally. Heating powders of $Ca(OH)_2$, $Ca(H_2PO_4)_2.H_2O$ and distilled water in a pressurised pot at 109°C for 1-3h results in the formation of a powder of crystallised hydroxyapatite in a

needle shape, 130-170nm in length and 15-25 nm in width with a specific surface area of 31-43 m^2/g and Ca/P ratio of 1.640-1.643. The material produced had good crystallinity and did not require calcination to increase the crystallinity.

Unfortunately, most of the processing routes involve calcining the chemistry-derived precursor at an intermediate temperature in order to develop the required ceramic phase and this often results in coarsening and agglomeration of the powder and lowers the surface area, thus lowering the driving force for sintering.

Calcination is a heat treatment process used to modify the raw powder to acquire various properties for subsequent processing. Calcination changes the particle size distribution from multi-modal to unimodal and increases the particle size of the powder without any phase transformation occurring if heated below the decomposition temperature (~700-1000°C). At a temperature of 700°C, calcination does not affect the sintering behaviour significantly, but at a temperature 800°C and above, the initiation of sintering is delayed and a higher sintering temperature is needed for shrinkage to occur and to decrease the probability of grain growth during sintering. Calcination at 1000°C is too high for the powder, making it too coarse which inhibits the sintering behaviour of the powder. This study by Juang and Hon also showed that sintered material (at 1250°C) that has been calcined at 900°C showed better mechanical properties in comparison to the sintered material using uncalcined powder because it has a finer grain size [48].

1.2.3.5 Porous hydroxyapatite

Hydroxyapatite can be prepared as a dense body or as a macroporous form. Micropores as described by De Groot [30] are pores having a diameter < 5μm, and the macropore as a pore with a diameter > 100μm. Dense hydroxyapatite has been described as having a maximum microporosity of 5% by volume with the micropores measuring about 1 μm in diameter .

Biomaterials scientists [50] first recognised the importance of porosity in the early 1970's. Studies showed that certain physical parameters of the porosity affected the tissue type and the rate of ingrowth. The degree of interconnectivity and the nominal pore size were the critical factors that determined the success of the implants. Maximum interconnectivity (the absence of 'dead ends') was found to facilitate ingrowth. Studies showed that a pore size less than 10μm prevents ingrowth of cells; a pore size of 15 to 50μm encouraged the fibrovascular ingrowth; a pore size of 50 to 150μm resulted in osteoid formation; and a pore size greater than 150μm facilitated the ingrowth of mineralised bone [49]. Several researchers [50,119] claimed that a minimum pore size of 80-100 μm is necessary for porous implant materials to function well. The large pore size is needed so that the capillaries can provide a blood supply to the ingrown connective tissues. Without blood and nutrition the bone will die [51]. A larger pore size, ~300μm, during implantation of HA, would initially exhibit better ingrowth of bone, but there was no significant difference in bone ingrowth with the smaller pore size, ~100μm after 16 weeks of implantation [52].

Macroporosity is conducive to osteoconduction but also has many effects on the mechanical behaviour of the HA. A study by Gauthier *et al* [53] showed that macroporosity percentage was a less important influence than the macropore size. For a similar pore size, there was no significant difference in newly formed bone for implants with 40% or 50% macroporosity. Implants with even as low as 30 vol% macroporosity were successful in promoting deep and abundant bone substitution. Therefore, an implant with a lower percentage of macroporosity, which would mean better mechanical strength, could be used without reducing the bone ingrowth. This result also corresponded with the study made by Ono *et al* [54, 55] which revealed that for a huge cranial plate implant, the minimum optimisation of the strength, 200N, was achieved when the implant has a porosity of about 40% and a thickness of about 8mm.

1.2.3.6 Fabrication of porous hydroxyapatite

Introduction of polymeric powder in the ceramic material is among the methods used to fabricate porous ceramic. The polymeric powder could be mixed with the hydroxyapatite powder followed by simple die pressing [59], or, a mixture of the polymeric powder with a slip containing fine ceramic powder followed by oven drying of the green body [69]. The polymeric particles are burnt out followed by subsequent heating, leaving within the fired hydroxyapatite solid voids of identical geometry to the starting polymer particles. The resulting pores affect both mechanical properties and biological behaviour, post implantation. Among the polymers used to produce such porosity are poly (vinyl butyral) [57, 58], naphthalene particles [59] and polyethylene glycol 4000 [60].

Porous hydroxyapatite can also be fabricated through the replamineform process (meaning replicated life forms). This is a technique for duplicating the microstructure of carbonate skeletal components in ceramics, metals or polymer materials. The special pore structure of marine invertebrate skeletal materials such as *Porites* and *Ganiopora* can be copied. Using this technique, prosthetic materials having a controlled pore microstructure for optimum strength and tissue ingrowth may be obtained [61]. Matsuda et al [62], instead of using life forms, have successfully replicated the interconnected structure employing porous glass. Other techniques which have been used successfully include hydrothermal hot pressing techniques and pre-treatment of the hydroxyapatite powder with hydrogen peroxide, H_2O_2, prior to sintering.

Recently, a pure mineral bone has been developed from bovine bone. All the organic components of the bovine bone were removed and a high temperature heat treatment were given to the bovine bone. The sintered cancellous bone maintained the spongy structure of the natural bone, which has an interconnecting porous structure and high porosity (~70 vol%). The phase composition is also similar to the natural bone, with ~93wt% hydroxyapatite and ~7wt% of β-tricalcium phosphate [56].

1.2.3.7 Mechanical properties of porous hydroxyapatite

The strength of a material depends on the portion of the total volume fraction of the material occupied by the various pores. Although many relationships have been developed, a useful equation relating the porosity to the strength of hydroxyapatite is given below [63]:

$$\sigma = \sigma_o \exp. (-bP)$$

where:

σ = strength of porous body

σ_o = strength of non porous body of the same material

p = porosity expressed as a fraction

b = the slope of the ln σ vs. P curve.

Other than the total porosity volume, the size of the pores also has an influence on the mechanical strength [64]. The strength of hydroxyapatite decreases as the pore gets larger [66]. This relationship is expressed by the Griffith equation as below [66]:

$$\sigma = \left[\frac{2E\gamma}{\pi c}\right]^{1/2} \approx \left[\frac{E\gamma}{c}\right]^{1/2}$$

where:

E = Young's modulus

γ = thermodynamic surface free energy

c = radius of fissure

Shaw [67], developed three routes for preparing porous hydroxyapatite ceramics, under-sintered, graphite burn-out and H_2O_2 methods. From these three methods, pore sizes of 0-2.5μm, 0-110μm and 0-2000μm were produced, respectively. From the micro hardness measurements performed on the under-sintered route, it appeared that microhardness

depended solely on the percentage density, rather than the morphology and grade of the starting powder or on the grain size of the sintered body. The biaxial flexure failure stress was found to be dependent on the porosity, with failure at 7.3-96MPa, 1.4-26MPa and 0.78-28MPa for under-sintering, graphite and H_2O_2 routes respectively. When all the three routes were taken together, the relationship between strength and porosity was:

$$\sigma = 80.6e^{-4.91P}$$

where σ is failure stress in MPa and P is fractional porosity. The elastic modulus of porous hydroxyapatite fell in the ranges of 22.8-83.1GPa, 0.72-31.3GPa and 0.52-31.7GPa for the under-sintering, graphite and H_2O_2 routes respectively. It is found to vary primarily with percentage density rather than the grain size or powder type. The behaviour of the three materials taken together could be described by the equation:

$$E = 89.5e^{-5.1P}$$

where E is the elastic modulus in GPa and P is the fractional porosity. The fracture toughness of the under-sintered hydroxyapatite suggested that both porosity and grain size played a role in determining the mechanical properties of the porous hydroxyapatite. The maximum fracture toughness achieved was $0.7MPam^{1/2}$.

Yamasaki et al [68] prepared porous hydroxyapatite using the hydrothermal hot-pressing method. The solidified hydroxyapatite prepared by this route at 300°C with a pressure of 30MPa for 2h produced hydroxyapatite with a porous structure. The porous hydroxyapatite developed had pore size between 100 and 500μm with a 40vol% of open porosity. The compressive strength of the solidified hydroxyapatite was ~15MPa but increased after sintering at 1050°C for 3 hours, to 150 ± 20MPa. The strength increased due to the extreme decrease of the micropores.

Liu [69], prepared porous hydroxyapatite via a slip-casting route by mixing a polymeric powder (poly (vinyl butyral), PVB) with a slip containing fine hydroxyapatite powder. The shrinkage of the specimen apparent to be independent of the size of the PVB particle size but was a strong function of the PVB content. The specimen shrinkage becomes less pronounced with the increase of PVB content from 24vol% up to 62vol%. The increase of

PVB content substantially inhibits the shrinkage of the green powder compact during sintering. The macropore size achieved was approximately 160-200μm, closely resembling the starting PVB powder (~188μm) and the micropores were in the size range 2-20μm. The total porosity obtained is in the range of 32-78 vol%. The porosity-flexural strength description for samples with 0.188 mm PVB particles is: σ_f = 115 exp (-4.5P) MPa and for 0.42mm PVB particles, σ_f= 48 exp (-3.5P) MPa. The porosity-Young's modulus behaviour of porous hydroxyapatite is E= 140exp (-4.2P)GPa.

Interpore-200, a commercial porous hydroxyapatite ceramic was developed by White and Shores [49] using the replamineform process of coral. This material has a three dimensional interconnected porosity with a pore diameter of 200μm, wall thickness ~150μm and pore volume of 60%. The biomechanical properties of Interpore-200 are presented in Table 1.4.

Table 1.4: Biomechanical Properties of HA200 [49]

Property	Test	Orientation	Mean	Range
Crush Strength (kPa)	Compression	Parallel Perpendicular	9260 4316	6874-11549 1772-6640
Ultimate Strength (Ncm^{-1})	Compression	Perpendicular	373	251-544
Stiffness (Ncm^{-1})	Compression	Perpendicular	8300	3310-11470
Energy Absorption (Ncm)	Compression	Perpendicular	9.9	4.5-13
Tensile strength ($gcm^{-2} \times 10^4$)	4-point bending	-	-	2.5-3.3
Young Modulus ($gcm^{-2} \times 10^4$)	4-point bending	-	-	5.2-6.0
Elastic modulus ($dynescm^{-2} \times 10^{10}$)	Resource Frequency	Parallel Perpendicular	4.8 2.6	3.6-5.8 1.9-3.2

1.2.3.8 Summary

1. Ceramics have been used as implant materials for about 20 years.
2. The ceramics used to repair and reconstruct the diseased, damaged or worn out body parts are referred to as bioceramics.
3. Bioceramics can be divided into four types of implants according to the tissue response; nearly inert, porous, resorbable and bioactive implants.
4. Pore sizes up to 80-100μm are efficient for bone ingrowth but for the first few months of implant, the optimum pore size is between 300-600μm. However, the smaller pore size (~100μm) is totally infiltrated by bone or bone marrow after four months whereas for larger-pored hydroxyapatite implants, tissue did not penetrate all the pores even after 6 months of implantation.
5. The total volume fraction of porosity required for osteoconduction is as low as 30 vol%.
6. The Ca/P molar ratio does not affect the development of the bone-porous ceramic interface but samples with Ca/P ratio >1.6 have a higher percentage of bone-porous ceramic contact.
7. The chemical formula of hydroxyapatite is $Ca_{10}(PO_4)_6(OH)_2$.
8. Hydroxyapatite belongs to the hexagonal system with a space group $P6_3/m$.
9. Theoretical density for pure hydroxyapatite is 3.156 gcm^{-3}.
10. Apatite can undergo an isomorphous substitution classified as iso-ionic and hetero-ionic, and this could occur as anion or cation substitution.
11. Variation of Ca/P molar ratio reflects the purity of the prepared apatite before sintering:
    - Ca/P molar ratio < 1.67, HA and TCP present
    - Ca/P molar ratio = 1.67, only pure HA present
    - Ca/P molar ratio > 1.67, HA and CaO present
12. Dissociation of hydroxyapatite can be influenced by the purity, composition and particle size of the starting powder, and also by the sintering atmosphere and temperature.

13. Hydroxyapatite can be prepared from reactions in aqueous systems (precipitation and hydrolysis method), solid state reaction or by hydrothermal reaction.
14. Porous hydroxyapatite can be fabricated by adding polymeric powder to the starting materials which is subsequently burnt out from the mixture; the replamineform process, a hot pressing technique or pre-treatment of the hydroxyapatite powder with H_2O_2 before sintering can also be used.
15. The strength of a porous material depends on the volume of total porosity, pore shape, maximum size of pore and percentage density.

1.3 Polymer

Polymers are large molecules made up of simple repeating units. The name is derived from the Greek, 'poly', meaning many, and 'mer', meaning part. Polymers are synthesised from simple molecules called monomers (single part) by a process called polymerisation [70].

Polymer additives such as binder, have been used in the ceramic industry for a long time. Without the use of such aids many processes would be very difficult and some are impossible to carry out. The additives used not only to aid the processing and forming of ceramic products but can also be used as porosifiers in attaining porosity to produce porous ceramics.

1.3.1 Polymer degradation

In depolymerisation (decomposition of macromolecules into a simpler compounds), the products of decomposition all have the same empirical formula as the original polymer,

and may consist of monomer, larger chain fragments or a mixture of both. If the temperature is raised high enough, no solid residue would remain [71].

For vinyl polymers, there are three types of thermal degradation, non-chain scission, random chain scission and depropagation. In non-chain scission, the reaction would involve the pendant group that does not break the polymer backbone, for instance, dehydrochlorination of poly vinyl chloride, PVC. The random chain reaction would follow after the non-chain reaction, which results from the homolytic bond-cleavage reaction at the weak points in the polymer chain, as the example below illustrates. Complex mixtures of degradation products are formed.

$$\sim CH_2CH_2CH_2CH_2\sim \longrightarrow \sim CH_2CH_2\bullet + \bullet CH_2CH_2\sim \longrightarrow \sim CH{=}CH_2 + CH_3CH_2\sim$$

Depropagation or depolymerisation occurs to give monomers with the amount formed varying with the temperature. It mainly occurs for polymers prepared from 1,1-disubstituted monomers. Initiation of depropagation can be at the end of the chain or at a random site along the backbone, and tertiary radicals are formed with each depropagation step as shown below [70].

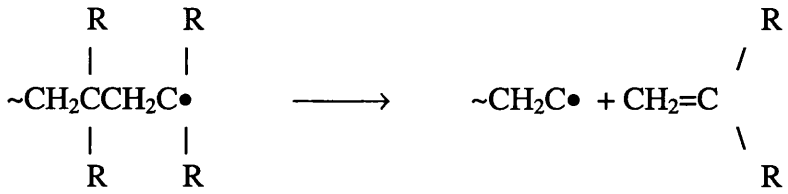

1.3.2 Poly (vinyl chloride)

PVC is thermally unstable at temperatures above 150°C, decomposing to hydrogen chloride and a polymeric product which is brown or black in colour depending on the extent of degradation [72]. The thermal degradation reaction can be represented as below:

Dehydrochlorination

-------CH2-CHCl-------- ⟶ -----CH=CH----- + HCl
(polymer
discolours)

Chain scission

---------- ⟶ ------- + -------

In air

OOH
|
------- + O2 ⟶ -------

At high temperatures

>300°C
---------- ⟶ aromatic and aliphatic hydrocarbons
(HCl evolved below 250°C)

During the dehydrochlorination reaction, at a temperature of around 200°C, PVC changes from colourless to a pale brown, darkens rapidly and finally becomes black. Simultaneously, with the change of the colour, HCl is released from the polymer. The elimination of the HCl from the polymer leads to it becoming unsaturated. Once one double bond has been formed in a polymer molecule, the bond strength of the hydrogen and chlorine atoms near to the double bond are lowered by allylic activation thus likely making the next HCl to be eliminated from the polymer molecule [72].

Materials balance through PVC pyrolysis in vacuum up to 500°C are HCl (53%), cold ring (tar) fraction (24.3%), liquid fraction (7%), gas fraction (apart from HCl) (6.6%) and char (9.5%). 10% of the Cl atoms remain in the polymer after HCl evolution ceases [73].

PVC shows two degradation stages. During the first stage, between 200 to 300°C, HCl and benzene are evolved but very little alkyl aromatic hydrocarbons (toluene, xylene isomers, ethylbenzene, etc.) or condensed ring aromatics (naphthalene, indene, indane

etc.). Through dehydrochlorination, ~15% double bonds are produced resulting in benzene formation; most are active in crosslinking. As a result, a crosslinked network is created which contains cyclohexene and cyclohexadiene rings embedded in an aliphatic matrix. In the second degradation stage (360-500°C), the aromatisation takes place with much scission [73].

1.3.3 Poly (vinyl alcohol)

PVA undergoes glass, structural and melting transitions upon heating and eventually decomposes at elevated temperatures [74]. The glass transition of amorphous PVA lies between 70 to 80°C. The melting temperature of the PVA generally follows the order syndiotactic (230-267°C) > atactic (228-240°C) > isotactic (212-235°C) with respect to tacticity. Tacticity refers to the side of the chain where an addition polymer, R group is placed.

In general, PVA when pyrolysed, undergoes dehydration and depolymerization. The stability of PVA is dependent on the method of its synthesis. Acid-hydrolysed products of polyvinyl esters begin to eliminate water below 200°C but similar polymer prepared by alkaline hydrolysis decomposes at temperatures above 180°C.

Under vacuum, decomposition of PVA proceeds in two stage. The first stage, which begins at 200°C, mainly involves loss of water, accompanied by the formation of some volatile products. In the second stage, the polyenes residues (produced from the water loss) are further degraded at 450°C to form aromatic hydrocarbons.

In the presence of air, thermal degradation of PVA can also be described by the two stage decomposition scheme, with one modification. Oxidation of the unsaturated polymeric residue from the dehydration reaction introduces ketone groups in the polymer chain. These groups then promote the dehydration of neighbouring vinyl alcohol units producing

a conjugated unsaturated ketone structure. The first stage degradation products is the same as when pyrolysed in vacuum. In the range 260-280°C, the second stage degradation is around 80 percent with a total weight loss of 40 percent.

1.3.4 Polymer Degradation in Ceramics

The thermal degradation of binders determines the quality of the ceramic substrate [75]. Incomplete binder burnout would retard densification rate and limit the final density achieved. The residual carbon left after thermal degradation affects the optical, electrical and mechanical properties of the substrate. An excess of 50 to 100 ppm of residual carbon would decrease the density and also affect many substrate properties such as flexural strength, breakdown voltage and dielectric constant.

Binder removal by heat treatment involves, (i) a chemical mechanism, where the organic compound thermally degrades into volatile species and, (ii) a physical mechanism, where the diffusion of the volatile species to the surface of the ceramic occurs. The binder distribution is controlled by diffusion and capillary migration, and it is important to design an efficient heating cycle to prevent stress and formation of cracks in the ceramic parts [76].

Capillary migration in the liquid phase, and diffusion in the gas phase are the two main mechanisms that control pyrolytic binder removal. These two mechanisms determine the path length of the molten binder and volatile species must migrate or diffuse. In the early stage of binder removal, due to the capillary forces, the molten binder would be segregated up to the smallest pores of the green body and this would create a stress gradient. The direction of the capillary force depends on the surface tension and the viscosity of the molten binder. At higher temperatures, if the generation of volatile species within the ceramic is more than diffusion and evaporation at the surface, and the solid is not strong enough to withstand the pressure generated, cracking would occur. Therefore, it is

important to obtain a balance between the rate of diffusion and evaporation at the surface. One way to do this is by controlling the heating rate. A study by Chartier et al [76] showed a heating rate of 1°C/min or lower for a 2 wt% of polystyrene and 12 wt% of paraffin oil in an alumina mixture is needed to ensure no defects or a reduction in the mechanical properties of the ceramic. Samples pyrolysed at a heating rate higher than 1°C/min exhibit macro-defects such as blistering, bloating, cracking and a consequent lowering of the mechanical properties.

Masia et al [36] reported that oxides have significant catalytic effects on both thermal and thermal-oxidative degradation of poly(vinyl butyral) (PVB). The oxides decrease the initial decomposition temperature of the PVB. Besides surface chemistry, the surface structure, number of hydroxyl groups, percentage of free water, amount of oxygen adsorbed on the oxide surface, and the surface impurities also affect the binder decomposition.

Analysis of the degradation products from the 6% poly (ethylene glycol) (PEG) and 0.5% poly (vinyl alcohol) (PVA) binder system used with alumina suggests that the two polymers degraded independently of each other. The products produced from the thermal degradation of PEG-alumina and PVA-alumina in air showed that the major degradation reactions are similar to those of pure polymer decomposed in nitrogen atmosphere which suggest that there is no major influence between alumina and the polymers during the polymer thermal degradation [77].

1.3.5 Summary

1. Polymers, such as poly (vinyl alcohol), poly (vinyl butyral) and poly (ethylene glycol) have been used as an additive to facilitate processing the ceramic green bodies.
2. Thermal degradation of the polymers produces volatile products and monomers and/or tars and waxes and at a high enough temperature, no solid remains.
3. There are three types of thermal degradation of vinyl polymer, non-chain scission, random chain scission and depropagation.
4. Decomposition of the PVA and PVC proceeds in two stages; dehydration/ dehydrochlorination, and depolymerisation.
5. Binder removal by heat treatment involves two mechanisms, chemical and physical, and the distribution of the binder is controlled by diffusion and capillary migration.
6. It is important to balance the rate of diffusion and evaporation at the surface of the ceramic to avoid cracking.
7. Decomposition of polymer in ceramics starts earlier compared to the polymer alone due to the catalytic effect of the ceramic.

1.4 Processing and Mechanical Behaviour of Ceramics

1.4.1 Ceramic processing technology

For the development of a good quality ceramic product, it is important to control the materials and the processing operation in order to minimise the microstructural defects. The basic steps in the processing of ceramics are materials preparation, forming or casting and thermal treatment by heating the ceramic shape to a high enough temperature to bond the particles together.

1.4.1.1 Powder synthesis method

There are three categories of powder synthesis, solid phase synthesis, liquid phase synthesis and gas phase synthesis (Figure 1.14). The product of liquid and gas phase synthesis is often used for the reaction in solid phase synthesis. Liquid and gas phase synthesis methods are more important methods in powder synthesis.

Liquid phase synthesis

In the de-solvent method, solvent is physically removed from the solution by means such as spray-drying, freeze-drying in vacuum or liquid drying where the solvent is absorbed by hygroscopic liquid to increase concentration and precipitate out the solute.

In the precipitation method, the solute is precipitated from solution and processes such as co-precipitation, homogenous precipitation, alkoxide hydrolysis and electrolysis are feasible. The precipitate may be powdered by filtration, washing and drying.

The sol-gel method belongs to both the de-solvent and precipitation method. A colloidal solution (sol) with its suspension of dispersed particles can be powdered by allowing it to become a gel. Next, the solvent may either be removed or the solute precipitated out.

Gas Phase Synthesis

Synthesis from the gaseous state can be achieved by precipitation of vapour deposition (PVD) or chemical vapour deposition (CVD). Small quantities of uniform, nearly monodispersed, very high purity powders of submicrometer particle size can be generated using these methods [79]. In the PVD method, the raw material is vaporised by an arc or plasma at high temperatures and is condensed to a fine powder by rapid cooling. In the

CVD method, synthesis is carried out through the chemical reaction of a vapour of a metallic compound for instance, synthesis of SiN_4 and SiC.

1.4.1.2 Forming Method

Forming changes the feed materials into a green product with a controlled shape, size and surface, and a particular density and microstructure. The shapes are kept to near net shape to keep the subsequent machining and surface finishing to a minimum. The size and green density are controlled to maintain a constant shrinkage factor between the formed and fired product. It is also beneficial to control the density and microstructure of the green product to obtain a product with a good performance because if large defects are introduced during forming, the defects are not eliminated during firing. Surface smoothness is usually desired in the product. The green product must also be strong enough for removal and subsequent handling.

During the forming cycle, pressure is gradually increased, creating strain on the compact which consists of solid brittle particles; cracks could form and cause the compact to fracture. To avoid this problem, a binder is added to enhance the lubrication of the powder. The type and quantity of the binder used varies according to the forming processes, powder used and product desired.

A binder system usually contains three components, binder, plasticiser and lubricant, each with a specific role. The binder (e.g. poly vinyl alcohol, PVA) improves cohesion between particles because its large molecules adsorb simultaneously on different particles and provide a network of entangled molecules after drying. The plasticiser (e.g. poly ethylene glycol, PEG) is used to lower the rigidity of the binder, because its molecules prevent functional groups of the binder from becoming linked. The presence of lubricants (e.g. stearic acid) lowers the friction coefficient of the powder.

The cohesion of the particle and binder system affect the mechanical behaviour of the product. The cohesion characteristics depend on the binder strength and binder/particle adhesion. The former is influenced by the molecular weight of the binder and the latter is influenced by the chemical nature of the binder. The binder strength is related to molecular entanglement, so, with the increase of molecular weight, it would increase the binder/particle adhesion and thus increase the particle and binder cohesion. As a result, a green product with a binder would have a higher strength compared to a product without a binder system. A higher molecular weight binder increases the adhesion between particles and walls, and results in less flow and re-arranging ability to the particles. In order to avoid this problem, industry usually uses a binder system with a high molecular weight, to increase the green product strength and a low molecular weight lubricant, to ensure fluidity of the particles.

There are five forming methods that are commonly used to produce green products; these are pressing, extrusion moulding, injection moulding, slip casting and tape casting.

In compact pressing, there are two types of processes, die pressing and isostatic pressing. Die pressing involves using a punch in hardened metal dies, with a surface relief in the pressing direction. The powder is mixed with an organic binder, filled into the die, and pressed into a strong solid product. This method is inexpensive and is used to make a product with a relatively simple shape. In isostatic pressing, the ceramic powder with an organic binder is pressed uniformly in a flexible rubber mould while immersed in a high pressure oil/water, and under hydrostatic pressure allows fabrications of complex shapes.

The extrusion method allows forming by forcing a plastic ceramic body through a forming die and then cutting the product to length. Most clay ceramic products such as brick, roof-tiles and ceramic honeycombs used for the automobile exhaust purification, are produced using this method.

For the injection moulding forming method, the ceramic is mixed with a thermoplastic resin and heated to provide the fluidity needed for the mixture to flow into the mould cavity. The resin is later burned off before firing. Sections as thin as 0.5mm and as thick as 8mm can be injection moulded and complex shapes with good dimensional accuracy can be rapidly produced.

Slip casting is another popular forming method. It involves suspending powdered raw materials in a liquid to form a slurry or slip that is poured into porous moulds, usually made of gypsum. The water is sucked from the contact area into the mould, leaving a layer of solid material on the mould surface. This method results in products shaped by the mould interior surface. For hollow components, the excess slip is removed after the desired shell thickness has formed. The products produced by this method are liable to shrinkage.

Paper-thin, flexible 'green' sheets of various ceramic composition are produced in high volumes using the continuous process of tape casting. The tape is produced first by mixing a concentrated slurry containing deflocculated powders with a relatively high concentration of binders and plasticisers. Then, the tape is formed by flowing the slurry beneath a blade, forming a film on a moving carrier substrate, which is then dried. Thin sheets of ceramics can also be formed by pouring the slurry onto a flat surface and moving a blade over the surface to form the film. The dried tape which is rubbery, flexible and with a smooth surface, is separated from the substrate and cut to size. Electronic conductors, resistors and capacitive materials are printed as film on the sectioned tape (substrate) to produce electronic packages. The substrate and electronic materials densify and bond together during firing to produce a monolithic electronic product. The ceramic tape can also be used as a mean to form a substrate for photovoltaic cells, electrical sensors, and solid electrolytes for batteries [80].

1.4.1.3 Sintering Processes

Material changes on heating prior to sintering include drying, decomposition of organic additions and the vaporisation of chemically combined water from the surface of particles [80]. In the presintering stage, stresses from the gases evolved or from the differential thermal expansion of a phase must not cause cracks or fracture to the product. Evolved gas must be eliminated while the surface permeability remains high.

Thermolysis or binder burnout is an important step prior to densification upon sintering. Incomplete burnout will introduce a new population of product defects and hence reduce the performance of the product. Binder burnout is dependent on the composition of the binder material, the composition and flow of the gas surrounding the product and on the morphology of the pores of the products. Binder burnout is the most time consuming process in the processing of the ceramic. The time required for thermolysis is controlled by the diffusion length of the vapour phase transport rather than the dimensions of the binder phase. The balance between the generation and the removal rate needs to be controlled. During the burnout, the volatile product diffuses towards the surface of the compact and evaporates. If the diffusion flux of the volatile product from the body centre towards the surface and evaporation out of the compact is not sufficiently fast, the concentration of the volatile degradation product would reach a limit, creating pressure within the compact itself and resulting in defects such as cracks or bubbles [81, 82].

The driving force for densification is the reduction of total surface area and total surface free energy by the elimination of solid-vapour interfaces. This usually takes place with the formation of a new but lower-energy solid-solid interface in the form of grain boundaries. Since grain boundary formation results in an increase in the free energy of the system, there is also a driving force for grain growth, which would result in the elimination of the grain boundary.

Table 1.5: Stages of microstructural characteristics during solid state sintering of powder compacts [80].

Stage	Observation
Initial	Surface smoothing of particles Grain boundaries form, neck growth Rounding of interconnected, open pores Porosity decreases <12%
Intermediate	Shrinkage of open pores intersecting grain boundaries Mean porosity decreases significantly Slow grain growth
Final (1)	Closed pores containing kiln gas form when density is ~ 92% (>85% in heterogeneous material) Closed pores intersect grain boundaries Pores shrink to a limited size or disappear Pores larger than grains shrink relatively slowly
Final (2)	Grains of much larger size appear rapidly Pores within larger grains shrink relatively slowly.

In solid state sintering, the microstructural characteristics change and can be observed in three stages as listed in Table 1.5. During the sintering process, the materials tend to move because of the difference in the surface curvature and vapour pressure. In the initial stage, also referred to as neck growth, the system tries to minimise its surface energy by causing a migration of atoms or ions via lattice vacancies that exist in the material. In a sintering system in which there is a difference in the concentration of lattice vacancies, material diffuses from the area of lower concentration to that of higher concentration. Depending on the curvature, the lattice vacancy density near the neck becomes greater, creating a concentration difference between it and that of the equilibrium area. Consequently, atoms migrate towards the neck area, increasing the interparticle contact, resulting in neck growth while the grain centres will move closer, resulting in an interparticle shrinkage of several percent and an increase of density. Since the vapour pressure also changes with respect to the curvature, it also gives rise to material transfer [78, 83]. The point when grain growth first occurs would terminate the initial sintering stage and allow the intermediate stage to begin. At this stage, the pore phase is interconnected and

continuous, and intersected by the grain boundaries. During this intermediate sintering stage, the pore would shrink. The final stage begins when the pore phase eventually becomes isolated and occupies the four-grain corners. The pores would shrink continuously, eventually disappearing and when all the pores are eliminated, the sintering process is considered complete. An alternate final stage of sintering could result when discontinuous grain growth occurs before all the porosity is removed. After the discontinuous growth of the grains, continued heating leads to the elimination of pores at the grain boundaries, but not those now situated within the grains [84].

1.4.2 Effect of porosity on the strength of the ceramics

The mechanical failure of ceramic materials occurs mainly from structural defects such as porosity and from the large grains produced during processing. Pores in brittle ceramic materials are regions where stress concentrates, and when the stress at a pore reaches a critical value, a crack is formed which can then propagate. Once a crack starts to propagate, it usually continues to grow until fracture occurs. Pores are also detrimental to the strength of ceramic materials because they decrease the cross-sectional area over which load is applied and hence lower the stress a material can support.

Porosity can reduced the strength of ceramic pieces very markedly and experimental results can often be shown to demonstrate an exponential dependence of the strength on porosity [85].

Pore size has no direct effect on strength when the pores are smaller than the grain size but otherwise can affect the strength [93]. When the grain size is smaller then the pore size and the specimens have the same volume of porosity, the specimens with larger pores show a lower strength than the specimen with a smaller pores. Biswas and Fulrath [59] explained that this behaviour is because the small pore specimens have a smaller effective flaw (critical flaw + pore diameter) than the large pore specimens, provided that the flaws

are identical in both cases. Le Huec *et al.*[87], have also confirmed the influence of pore size on the strength of a porous material.

The degree of strength degradation tends to decrease with the increased volume of the porosity. Even with a small porosity volume, the porosity has a significant damaging effect on the strength of a ceramic body, for example, a body with a 3% porosity, which is considered to be dense, is approximately 20% lower in strength than a completely dense body [63]. But at a relatively high level of porosity, e.g. 70%, the compressive strength appears to be insensitive to the total pore volume [65, 87].

Even though according to present theory, the highest strength is achieved in a pore-free material, small percentages of porosity may not have deleterious effect on strength, provided that the flaw size in the material is larger than the pore size. For example, for a polycrystalline alumina with coarse grains, of size ~30μm, no change of strength up to 6.5% pore volume fraction is found but for fine grains material, ~ 2μm, a significant decrease of strength with the same pore volume fraction is observed [88].

Liu [57] reported that the shape of the pores influenced the compressive strength of porous hydroxyapatite. Porous hydroxyapatite containing oblate pores shows lower strength than that containing either ellipsoid or spherical pores. However at a relatively high level of porosity, the load bearing capacity is similar regardless of the pore shape factor.

1.4.3 Effect of grain size on the mechanical properties of ceramics

For porosity free ceramics, the strength of a pure ceramic material is a function of its grain size, with finer grain size materials having smaller size flaws at their grain boundaries and thus being stronger than large grain size ceramics. [89, 90]. The relationship between grain size, D_g, and strength, σ_0, is well known as the Hall-Petch equation:

$$\sigma_0 = \sigma_s + BD_g^{-1/2}$$

where σ_s is the yield stress of a single crystal and B is a constant [91]. The effect of grain size on the strength is demonstrated for an engineering grade Si_3N_4 by a reduction of 50% in the strength between the finest grained and a coarsest grain material [92].

1.4.4 Summary

1. Ceramic powders can be synthesised by the solid phase, liquid phase and gas phase synthesis method.
2. There are five established methods available for forming green products; they are pressing, extrusion moulding, injection moulding, slip casting and tape casting.
3. The sintering process can be divided into three stages, initial (neck growth), intermediate (pore shrinkage and densification) and final stage (pore elimination complete and grain growth occurs).
4. The pore size, volume and shape, and grain size play important roles in influencing the strength of a ceramic material.

Chapter 2 Experimental Procedures

2.1 Fabrication and Processing Technique

2.1.1 Starting materials

Four main materials were used in the experiments, as shown in Table 2.1:

Table 2.1: Materials used in the study

	Materials		Supplier
1.	Hydroxyapatite (HA) powder	Captal R, a sintering grade powder	Plasma Biotal Limited
2.	Poly (vinyl chloride), PVC, powder	a. molecular weight of 200,000 (Product No.: 29784) b. molecular weight of 78,000 (Product No.:P9401)	a. BDH Inc b. Sigma Aldrich Co. Ltd.
3.	Poly (vinyl alcohol), PVA, powder	molecular weight of 115,000 (Product No.: B29791)	BDH Inc

2.1.2 Powder preparation

2.1.2.1 Sieving

The poly (vinyl chloride), PVC, received in particle size between 63μm and 180μm, was sieved using laboratory test brass sieves BS410 from Endecotts Ltd, London with

apertures of 180, 125 and 63μm to achieve powder size ranges of 63 to 125μm and 125 to 180μm required to act as a porosifier.

The poly (vinyl alcohol), PVA, was received as a powder with particle size > 250μm. The powder size was reduced using a Moulinex dry blender and sieved using laboratory test brass sieves with apertures of 180 and 125 μm. Powder with a size range between 125 and 180 μm was used in the experiment.

2.1.2.2 Mixing

The polymers were dry mixed with the HA powder in a dry plastic bottle in the volume percentage required in the experiments. Three zirconia balls with a diameter of 8 mm were used to make sure the components would mix homogenously. They were rolled for 30 minutes on a ball-mill.

2.1.3 Pellet formation

The pellets were formed mainly using uniaxial die pressing and cold isostatic pressing techniques.

2.1.3.1 Uniaxial die pressing

Mixtures of HA powder and polymer were prepared in different weight and size ratios according to the test as shown in Table 2.2. The mixtures were 25, 30, 35, 40, 45, 50, 53 and 60 volume % of polymer to the HA powder. For the tests undertaken at different temperature, only the samples with 53 volume % PVC were used.

The powder mixtures were fed individually into a 15mm diameter hardened steel die and pressed uniaxially with a punch to a pressure of 10 bar. The peak pressure was maintained

for 60 seconds for each compaction and then released. The samples were pressed at a low pressure, sufficient to allow them to be handled prior to cold isostatic pressing.

2.1.3.2 Cold isostatic pressing

The pre-pressed samples from the uniaxial pressing were placed inside a colostomy tube and vacuum sealed before immersing into the fluid (containing glycerine, hydraulic oil and water) of the pressure chamber of cold isostatic pressing machine (Stanstead Fluid Power Ltd., England). A pressure of 33 MPa was applied for 60 seconds. The pressurised liquid transmitted the pressure uniformly to the samples. The samples weights and sizes prepared for different experiments are shown in the Table 2.2 below.

Table 2.2: Sample size and weight used for different types of experiments

Test	**Weight (g)**	**Green body diameter (mm)**	**Green body thickness (mm)**
Dilatometer	2.0	8	19
Ca/P ratio measurement	1.0	15	6
Test	**Weight before sintering (g)**	**Sintered body diameter (mm)**	**Sintered body thickness (mm)**
XRD test	1.0	10	4
SEM	1.0	10	4
Porosity & density test	1.4	10	7
Compression test	1.4	10	7
Tensile test	1.0	10	4

2.1.4 Sample preparation

2.1.4.1 Sintering regime

The green bodies were sintered in air in two stages (as shown in Figure 2.1). In the first stage, the green bodies were heated at a ramp rate of 30°C from room temperature to 600°C with a holding time of 1 hour. This was to allow the polymer to degrade slowly and prevent the samples from cracking. In the second stage, the ramp rate was increased to 100°C/h and the final sintering temperature varied from 900°C to 1400°C with a holding time of 4 hours. The samples were later cool down to room temperature before characterisation. In Chapter 3, the sintering regime was changed to study the effect of sintering cycle on the samples (Table 2.3). An electric chamber furnace (Model RHF 1500, Carbolite, England) with silicon carbide heating elements was used for the firing.

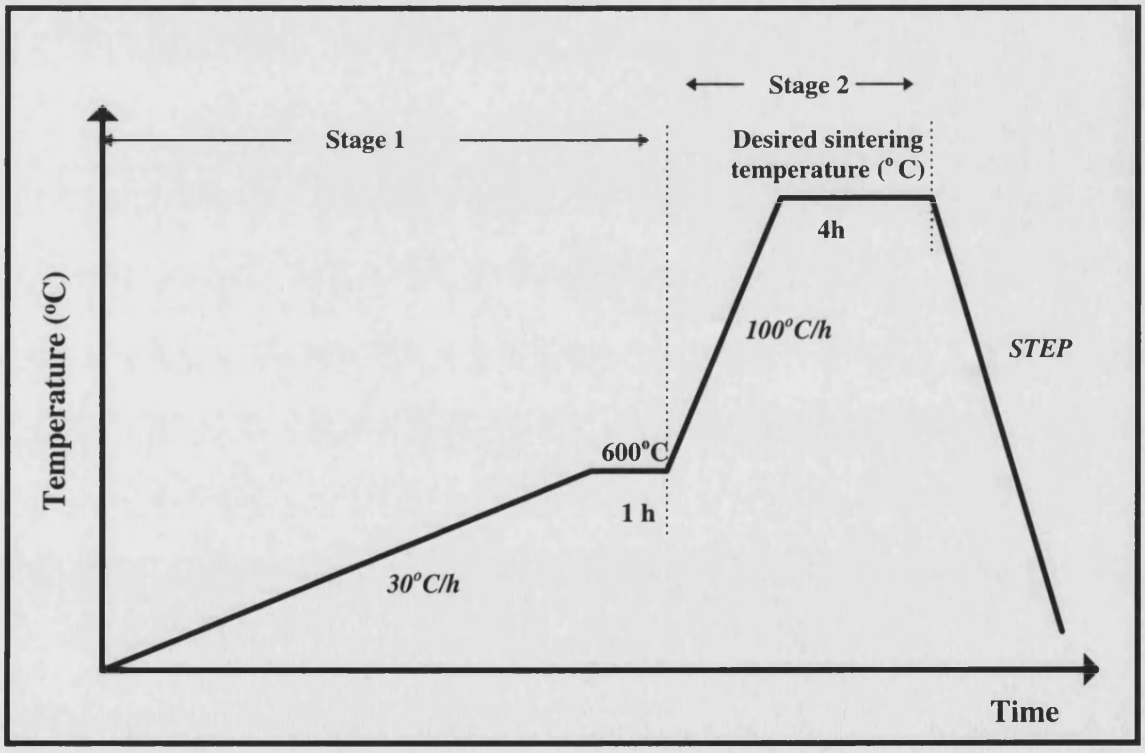

Figure 2.1: Stages of sintering of the green compacts.

Table 2.3: Sintering regime used to study the effect of sintering cycle on the HA

Stage	Ramp rate (°C/h)	Holding temperature (°C)	Holding time (h)
1	30 or 50	400 or 600	1
2	100	900 - 1400	1 - 36

2.1.4.2 Surface preparation

The sintered porous HA ceramics were mounted in an epoxide resin (Buehler UK Ltd, England) in order to support the samples during grinding and polishing. After it had hardened, the samples were ground and polished using a semi-automatic polishing machine Metapol 12, Buehler UK Ltd, England, according to the procedure in Table 2.4 below:

Table 2.4 : Surface preparation procedure for SEM samples

Stage	Surface	Particle Size	Wheel Speed (rpm)	Wheel Direction	Load lb/sample	Process Time (min)
Grinding	Paper	P320 grit SiC	200	comp.	6	Until Flat
Polishing	Perforated Texmet	9μm water based diamond suspension	200	comp.	6	8
	Texmet	3μm water based diamond suspension	200	comp.	6	8
	Mastertex	0.06μm colloidal silica	200	comp.	6	4

The surface of the porous HA ceramics was later chemically etched using 10% acetic acid glacial (BDH Chemicals Ltd., Poole, England) for approximately 4 minutes.

For SEM purposes, the samples were coated with a thin layer of gold to avoid static electric charging. For the Ca/P ratio analysis, the samples were coated with a thin layer of carbon to minimise the electric charging effects.

2.2 Characterisation Procedures

2.2.1 Powder characterisation

2.2.1.1 Sintering dilatometer

The apparatus consisted of a vertical tube furnace, molybdenum coil heating element, cooling water system and an alumina rod. It was used to measure the relative change in sample length during heating up to and cooling down from a temperature of 1550°C. A computer connected to the apparatus was used to set the temperature, ramp rate and store the reading of the displacement of the samples.

Sample preparation was described in section 2.1.3. In this experiment, two types of samples were prepared, pellets from HA powder only and, pellets from a mixture of 47 volume % of HA powder and 53 volume % of PVC powder. 2.0g of the powders were fed individually into a 15mm diameter hardened steel die and pressed uniaxially with a punch to a pressure of 10 bar. After 60 seconds, the pressure was released and the samples were taken out from the die and pressed further using cold isostatic press at the pressure of 33 MPa. The sample diameter were later reduced using P320 grit SiC paper to 8mm to fit the alumina rod in the dilatometer. The samples were sintered in air or argon up to a temperature of 1300°C with a ramp rate of 5°C/min.

2.2.1.2 Specific surface area

The surface area of the HA powder was analysed using a Gemini 2360 Analyzer, manufactured by Micromeritics. The powder was dried overnight under a nitrogen gas atmosphere at 120°C prior to testing.

The analyser contains a sample station and attached keypad and display. It uses a flowing-gas technique, in which helium and nitrogen gas flow into a tube containing the sample and into the balance tube at the same time. The internal volume and the temperature surrounding both tubes were maintained at identical conditions. The sample and balance tubes were immersed in a single liquid nitrogen bath which maintains isothermal condition for both tubes. The analysis gas is then delivered to the sample tube by a servo valve mechanism. The delivery rate of analysis gas flow into the balance tube is controlled by another servo valve connected to a differential pressure transducer which measures the pressure imbalance between the sample and balance tubes caused by the adsorption of the analysis gas in the tube, and the pressure would drop in the sample tube. The Gemini maintains a constant pressure of the analysis gas over the sample by admitting more gas into the sample tube through the servo valve (Gemini 2360 Micromeritics Operator Manual, 1996).

2.2.1.3 Particle size distribution

The particle size distribution of HA powder was investigated using a laser particle size analyser, Malvern Instruments System 3601. The HA powder received from Plasma Biotal Limited, was tested three times to ensure the consistency of the result. The powder was dispersed in distilled water using ultrasonic cell stirrers. The suspension was passed through a cell in the path of the laser and the data collected and analysed by Malvern Instruments computer software.

2.2.1.4 Measurement of calcium to phosphorus ratio

The ratio of calcium/phosphorus was measured and calculated using Electron Probe Analyser Model JXA 8600. The samples, as prepared in section 2.1.4, were analysed and compared with standards. The amount of calcium available in the sample was compared with $CaCO_3$ standard and the phophorus was compared with GaP standard. Six readings were taken from different points of the sample and these were averaged.

2.2.2 Microstructural characterisation

2.2.2.1 X-ray diffraction phase analysis

X-ray diffraction was used to identify the phases present in the raw materials and sintered samples. For powder samples, the samples were pressed onto an aluminium sample holder and for the sintered samples, the surfaces were polished before analysis.

The use of the x-ray diffraction method is of great importance in the analysis of ceramic materials. This technique is often used to (a) identify the crystalline phase and (b) compute the volume fraction present in ceramic materials by comparing the peaks obtained from the experimental samples with standard data.

Powder samples were prepared by compacting the powder onto an aluminium sample holder (standard Philips sample holder) and levelling it with the top surface of the holder. The sintered pellets samples were stuck on a double-layered glass sample holder using Blue-tac and were pressed to ensure the surface was level with the top surface of the sample holder. The sample holder was then positioned in the X-ray beam to obtain a maximum exposure of the sample.

In this experiment, the samples were scanned between 2θ values of 10° and 79.98° at a rate of 0.08° per minute, at intervals of 0.02° 2θ, using a Philips PW 1710 based diffractometer with a generator voltage of 40 kV and tube current of 25 mA. The X-ray source was CuKα.

2.2.2.2 Scanning electron microscopy

Powder samples were sprinkled on a conductive tape in a standard aluminium holder and an air duster was used to remove excess powder on the holder. Sintered compacted samples on the other hand, were mounted with an epoxy resin, ground, polished and chemically etched as described in section 2.1.4.2. Before examining the powders and the sintered samples, they were coated with gold to prevent charging in the SEM. The morphologies of the powder and sintered samples were examined using a JEOL 6300 scanning electron microscope with an accelerating voltage of 15kV.

2.2.2.3 Density and porosity

The density of the powders, HA, PVC and PVA were measured using a fully automatic gas displacement AccuPyc 1330 Pycnometer which determines density and volume by measuring the pressure change of helium in a calibrated volume.

The density and porosity of the sintered porous HA ceramics were measured using the Archimedes method as specified by the appropriate British Standard EN 623-2:1993 [114]. At least six samples with a diameter of 10mm and thickness of 7mm were prepared for each experiment and oven dried at 110°C to a constant mass before weighing the dry test piece. The mass thus determined is the mass of the dry weight, m_1. The dry pieces then were put in a beaker containing distilled water, placed in an airtight vessel and evacuated to a pressure of 1000 mbar to ensure complete penetration of the test piece by the distilled water. After a period of 1 hour, the pump was switched off and the vessel opened to ambient air pressure. The apparent mass of the test piece, m_2, was determined

by weighing it while completely immersed in distilled water. The mass of the soaked test piece, m_3, was determined by removing the test piece from the distilled water, removing excess water with a damp tissue and weighing it in air.

The bulk density, ρ_b, kgm^{-3}, defined by BS EN 623-2:1993 [114] as the ratio of the mass of the dry material of a porous body to its bulk volume, was calculated from the following equation:

$$\rho_b = \frac{m_1}{m_3 - m_2} x \rho_L \qquad \text{.....2.1}$$

The apparent porosity π_a, which is the total volume of the open pores in a porous body to its bulk volume, in percentage, was calculated from the following equation:

$$\pi_a = \frac{m_3 - m_1}{m_3 - m_2} x100 \qquad \text{.....2.2}$$

where:

m_1 = mass of test piece in grams
m_2 = the apparent mass of the immersed test piece in grams
m_3 = the mass of the soaked test piece in grams
ρ_L = the density of the distilled water in kgm^{-3}

2.2.2.4 Grain size measurement

The average grain size was measured as suggested by Mendelson [115]. The measurements were carried out using an SEM photomicrograph of sintered, polished and etched samples. The measurements were performed manually by drawing at least 8 straight lines in parallel across the photomicrograph. The length of each straight line (La)

and scale bar length (S) of the of the photomicrograph were measured. The real length of each line , (Lr), is

$$Lr = {La}/{S} \quad \text{..... 2.3}$$

The number of grains (n) on each line were counted. The apparent grain size, (Da),

$$Da = {Lr}/{n} \quad \text{..... 2.4}$$

The real grain size average, ($\overline{Dr}$) was calculated by multiplying the apparent grain size average, ($\overline{Da}$) with the proportionality constant as suggested by Mandelson [115],

$$\overline{Dr} = 1.558\overline{Da} \quad \text{..... 2.5}$$

2.2.2.5 Thermogravimetric and infrared spectroscopy analysis

System 2000 TG-IR, by Perkin-Elmer was used to study the physical and chemical reactions of the samples when heated. The experiments were carried out in SIRIM Berhad, Malaysia. As-received HA powder, PVC (molecular weight 200,000) powder, and the mixture of 43 vol% HA and 57 vol% PVC powder mixed as outlined in Section 2.1.2.2, weighing between 20-40 mg were heated up in two stages. Stage 1, samples were heated from room temperature at 20°C/min up to 400, 500 or 600°C, isothermally for ½ h and further heated to 900°C with a ramp rate of 20°C/min in Stage 2. The test were carried out using air or argon as a carrier gas. The results of the IR spectroscopy were analysed using the IR Mentor Pro Classes database from Perkin Elmer.

2.2.3 Mechanical properties evaluation

2.2.3.1 Compressive strength

The strength of the sintered materials was measured using a standard test method as specified by the American Society for Testing and Materials (ASTM C773 - 88) [116]. At least 10 specimens weighing 1.4g each with a diameter of 10mm and thickness of 7mm

were prepared for each experiment as described in section 2.1.3 and sintered according to the sintering regime, as described in section 2.1.4.1.

The samples were tested using an Instron 1195 with a crosshead speed of 0.5 mm/min and a chart speed of 50 mm/min. The compressive strength of each specimen were calculated as follows:

$$C = P/A \qquad \text{..... 2.6}$$

where: C = compressive strength of the specimen, MPa

P = total load on the specimen at failure, N

A = calculated area of the bearing surface of the specimen, mm^2

2.2.3.2 Tensile strength

The tensile strength of the samples was tested using a diametral compression (Brazilian disc) test [117; 118]. It was performed as shown in Figure 2.2 below:

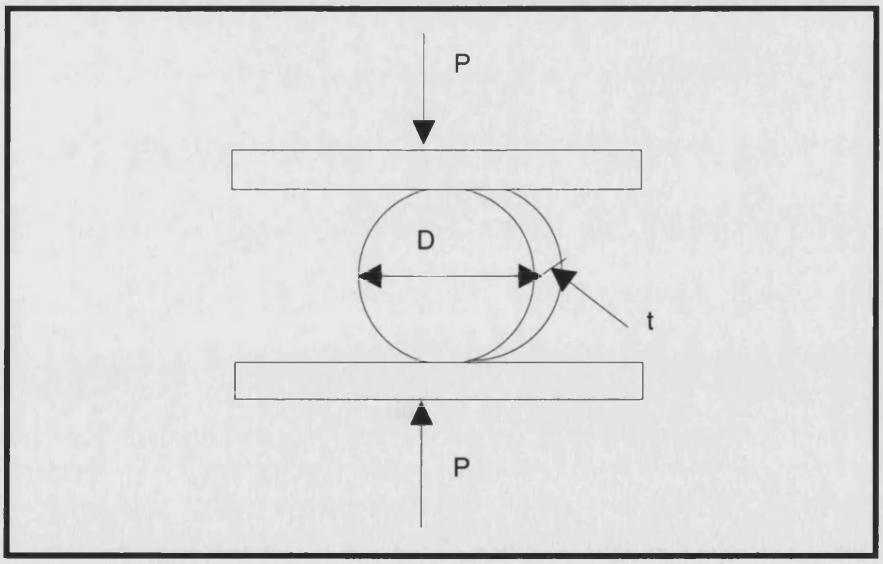

Figure 2.2: Schematic diagram of the diametral compression test.

This test involves compressing a flat disk diametrically between two flat platens. Fracture occurs along the loaded diameter as a result of tensile stress being generated across this diameter. The stress acts uniformly across the diameter and is given by the following equation:

$$\sigma = \frac{2P}{Dt\pi} \qquad \text{.....2.7}$$

where: P = applied load

D = specimen diameter

t = specimen thickness

At least 10 specimens weighing 1.0 g each were prepared for each experiment as described in section 2.1.3 and sintered according to the sintering regime as described in section 2.1.4. The samples with a diameter of 10mm and thickness of 4mm after sintering, were tested using an Instron 1122 with a crosshead speed of 0.5 mm/min and chart speed of 50 mm/min.

2.3 Sol-Gel Technique

2.3.1 Synthesis of calcium phosphate gel

The calcium phosphate (CP) gel was prepared by titrating 55 mls of 0.3M H_3PO_4 into a glass beaker containing 55mls of 0.5M $Ca(NO_3)_2$. Solution was mixed using a magnetic stirrer and the pH was kept between 10-12 by adding NH_4OH. The addition of NH_4OH was to ensure the development of a gelatinous suspension of CP.

$$10\ Ca(NO_3)_2 + 6\ H_3PO_4 + 2\ NH_4OH \xrightarrow[\text{room temperature}]{\text{pH 10-12}} Ca(PO_4)_6(OH)_2 + 20\ HNO_3 + 2\ NH_3\uparrow$$

The gelatinous suspension was aged between 0h and 48h at room temperature to obtain the correct Ca/P ratio and later filtered and washed with distilled water as shown in Figure

2.3. For the study of the effect of ageing to the ratio of Ca/P, the gel was dried in the oven at the temperature of 50°C for 1 week.

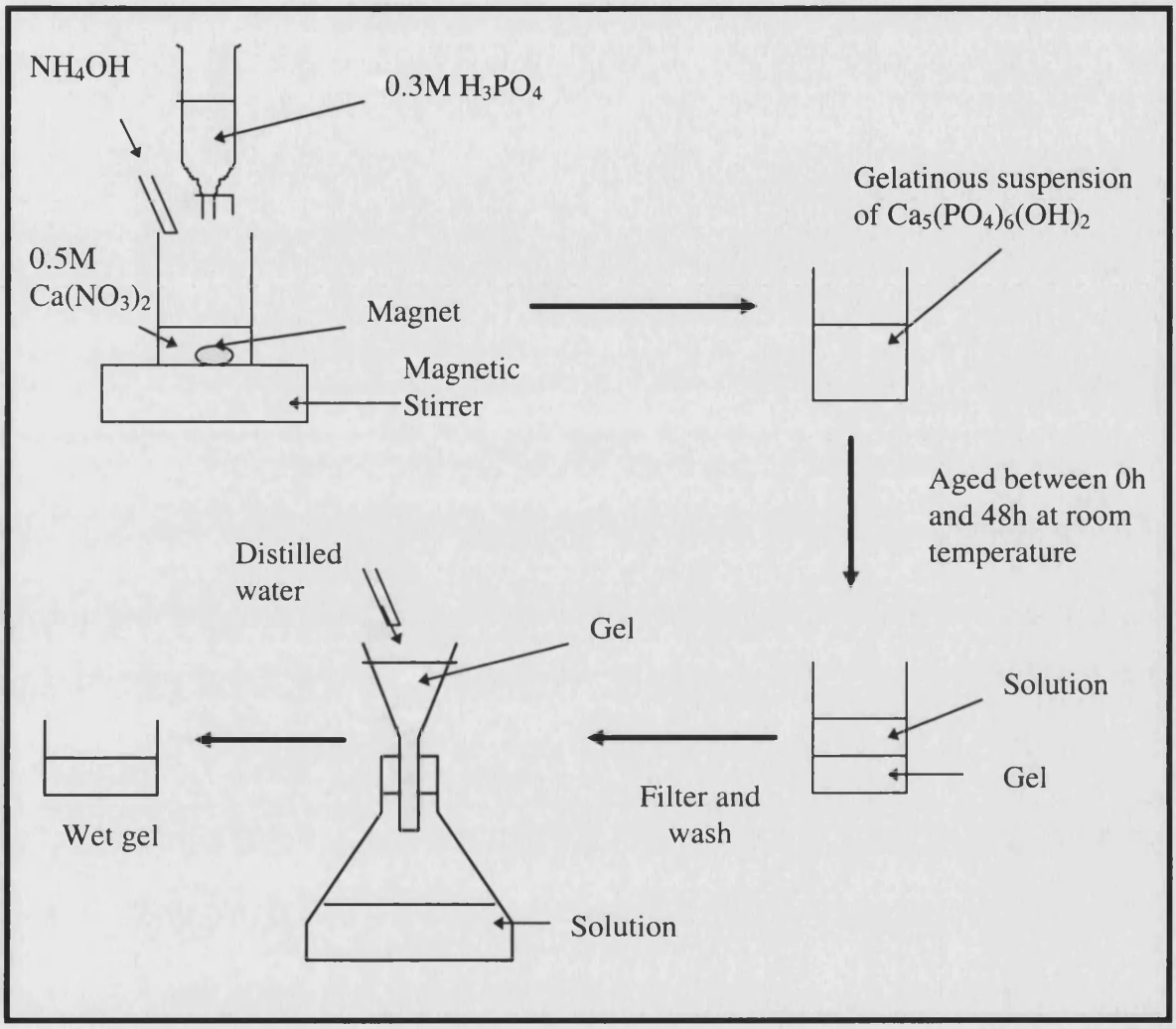

Figure 2.3: Schematic diagram showing the synthesis of calcium phosphate gel

2.3.2 Freeze casting

The wet gels as discussed in section 2.3.1 were mixed with filler, a commercial HA powder and/or SiO_2 with different weight ratios in a stainless steel container. The samples were then frozen in liquid nitrogen and maintained at a low temperature for 15 minutes. The samples were dried in one of two ways, either freeze drying or oven drying as shown in Figure 2.4.

Freeze drying was carried out using an Edwards - PearseTissue Dryer EPD3, England. The samples were put on the plate of the freeze dryer with phosphorus pentoxide to absorb water vapour and were capped with a glass jar. The freeze dryer was then evacuated to 10^{-1} torr and the temperature was lowered to - 60°C and left overnight. After all the ice was sublimed, the temperature was increased to room temperature and the samples were ready for characterisation and sintering.

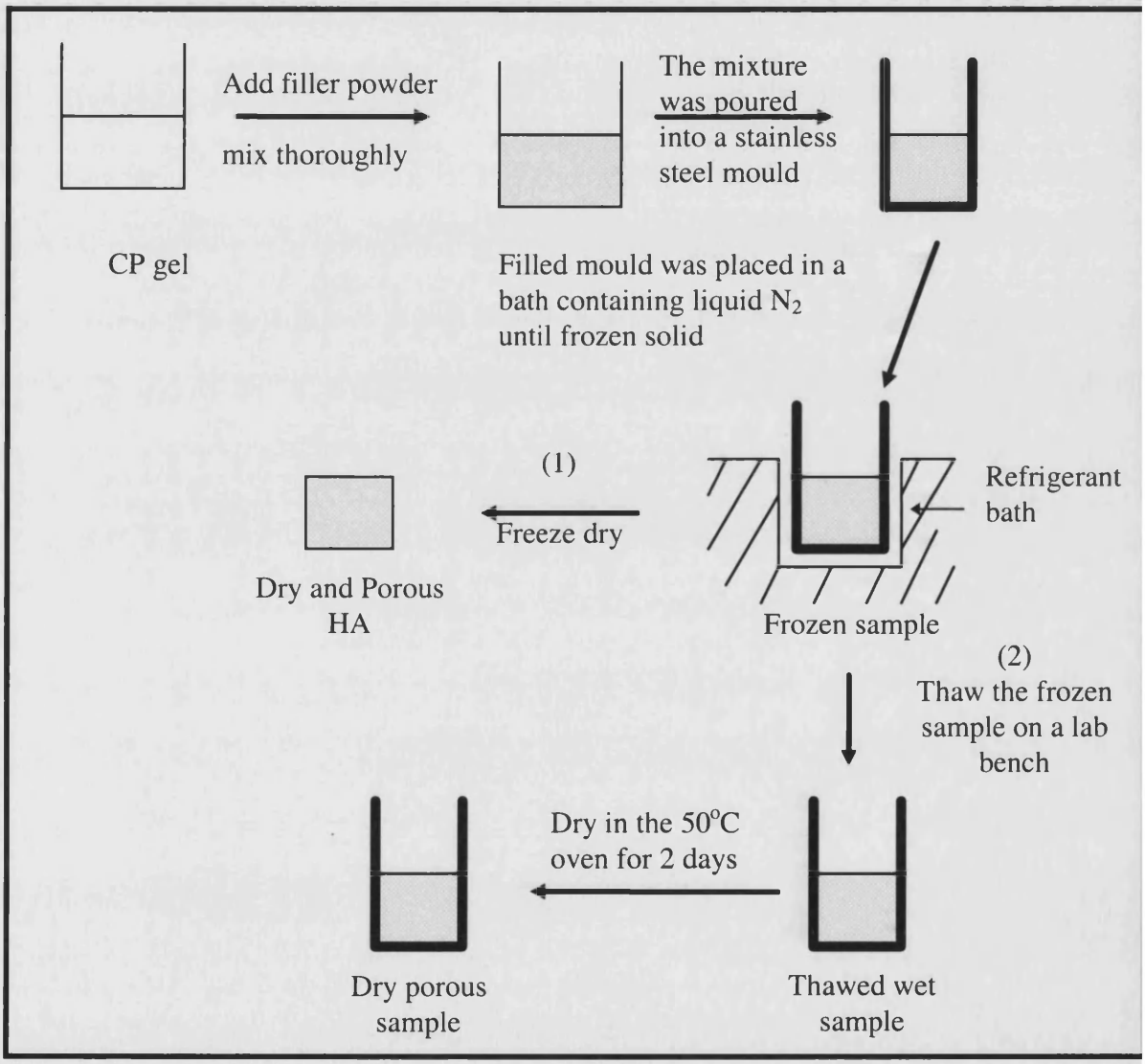

Figure 2.4: Schematic diagram of sample preparation by freeze casting

In order to dry using the oven method, the samples were slowly thawed on the laboratory bench, taken out from the stainless steel container. When the samples were completely thawed, they were dried in an oven for 2 days at a temperature of 50°C, prior to sintering to the desired temperature.

Chapter 3 Sintering and Decomposition of Hydroxyapatite

3.1 Introduction

The behaviour of hydroxyapatite has been widely investigated [1, 11, 24, 25, 30, 33, 35, 39, 41, 42]. The production of porous hydroxyapatite has also been studied by several researchers. Specific requirements have been defined in order to make the material useful for biological implantation. Among these requirements are porous hydroxyapatite with pores >80 μm with interconnection ≥ 20 μm for the human osteoblasts to penetrate into the pores [119], and sufficient strength to sustain in vivo loading when implanted in the body without mechanical failure.

Several studies have been made by researchers employing different techniques such as using foaming agent (e.g. H_2O_2), porous carrier body (e.g. sponge) or replamineform (e.g. coral). Although there have been studies using spherical polymer to produce porous bodies, the current study is the first that has attempted to use PVC or PVA to produce porosity and also preparing it using pressing technique. Both PVC and PVA were used due to their availibility. Many studies of the thermal decomposition behaviour the PVA and PVC have been made [74, 97, 98, 99, 100].

In this study, the effect of sintering cycle, sintering atmosphere and the effect of using different types of polymer, used to produce porosity on the microstructure and mechanical properties of the porous hydroxyapatite will be discussed.

3.2 Powder Characteristics

The results from an assessment of hydroxyapatite powder are listed in Table 3.1 below.

Table 3.1: The properties of the hydroxyapatite powder

Particle Size $D_{0.5}$ (Malvern Mastersizer)	3.24 μm
Particle Size $D_{0.1}$ (Malvern Mastersizer)	2.23 μm
Particle Size $D_{0.9}$ (Malvern Mastersizer)	4.29 μm
Specific surface area (BET method)	23.5123 m^2/g
XRD, FTIR	Hydroxyapatite and carbonate
Ca/P ratio (from Superprobe)	1.68 ± 0.01

The X-ray diffraction pattern in Figure 3.1 of the hydroxyapatite powder showed that the powder is highly crystalline and there are no other calcium phosphate phases present in the powder. EDAX analysis (Figure 3.2), also shows that no elements other than calcium and phosphorus are present in the powder. However, the Fourier transform infrared (FTIR) absorption spectra on the synthetic hydroxyapatite material showed that there was carbonate present in the powder (Figure 3.3). The presence of the carbonate was detected at wave numbers 1450 and 1388 cm^{-1}.

For this first study, the decomposition behaviour of hydroxyapatite (HA) and poly vinyl chloride (PVC) alone, and the combination of hydroxyapatite and poly vinyl chloride (HA+PVC) was investigated. The higher molecular weight poly vinyl chloride (HMWPVC) with a molecular weight of 200,000 was used, with a particle size range of between 125 μm and 150 μm. The structure of the poly vinyl chloride and the hydroxyapatite powder are shown in Figure 3.4.

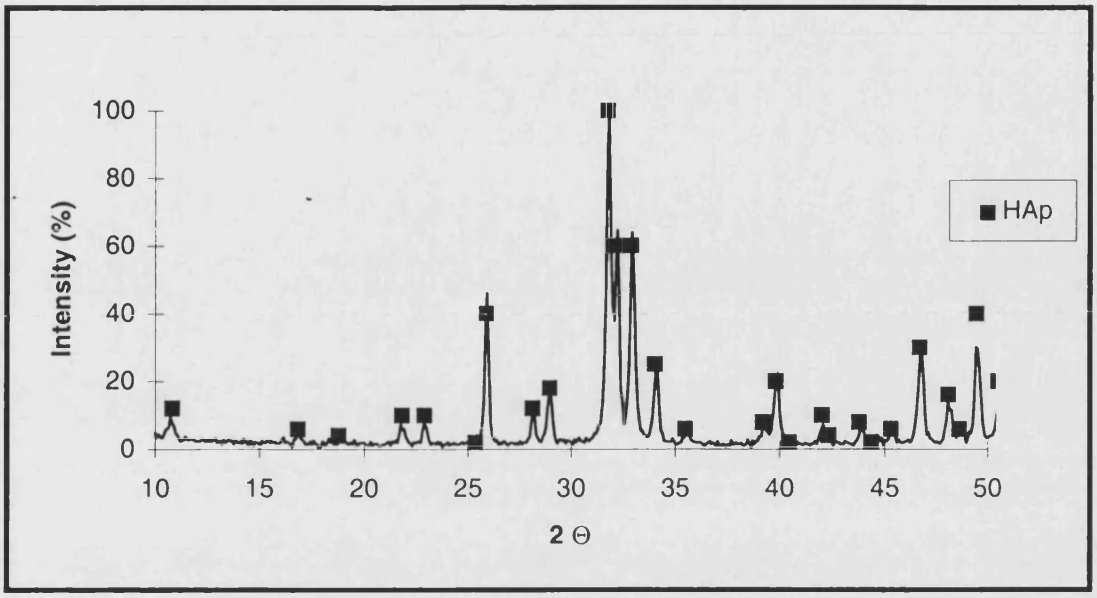

Figure 3.1: X-ray diffraction patterns of hydroxyapatite powder as received.

(■ = hydroxyapatite peak)

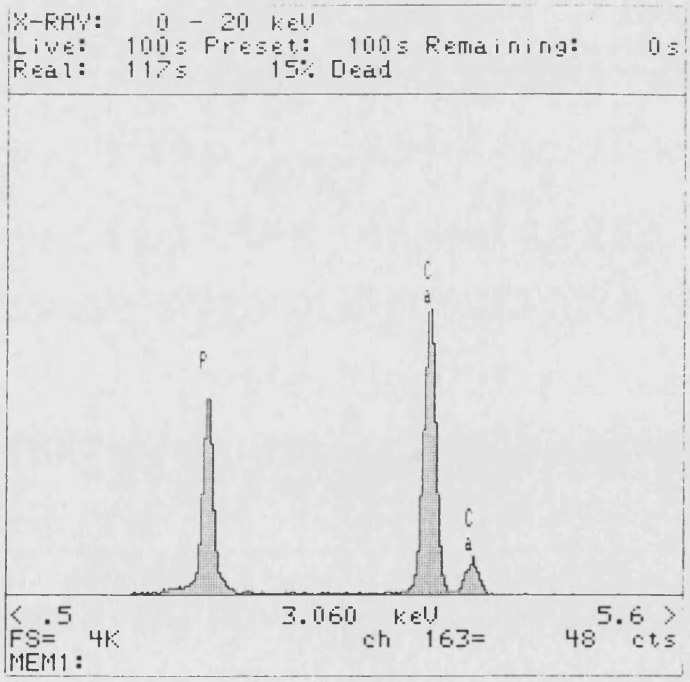

Figure 3.2: EDAX analysis of the hydroxyapatite powder as received

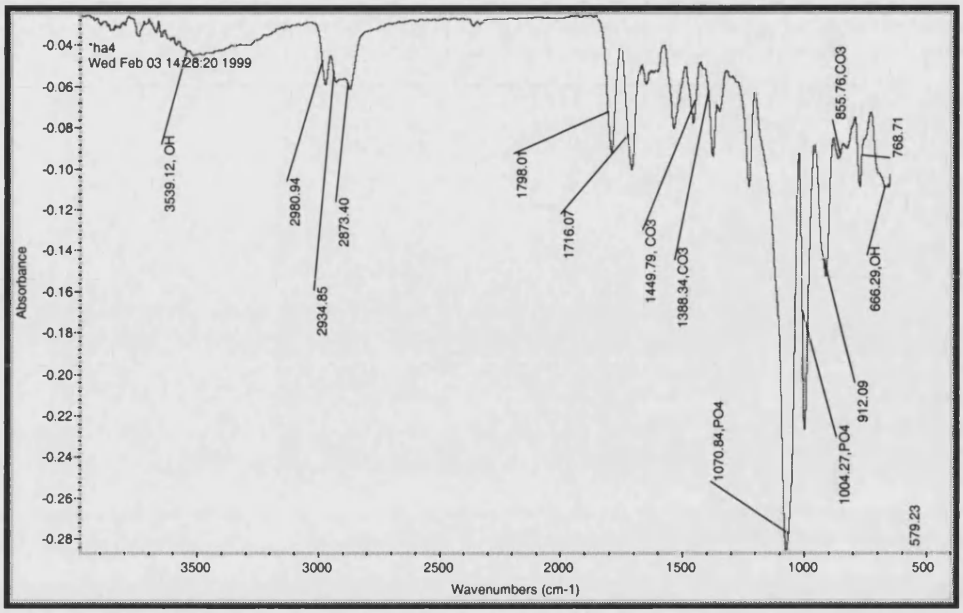

Figure 3.3: FTIR diagram of hydroxyapatite powder as received

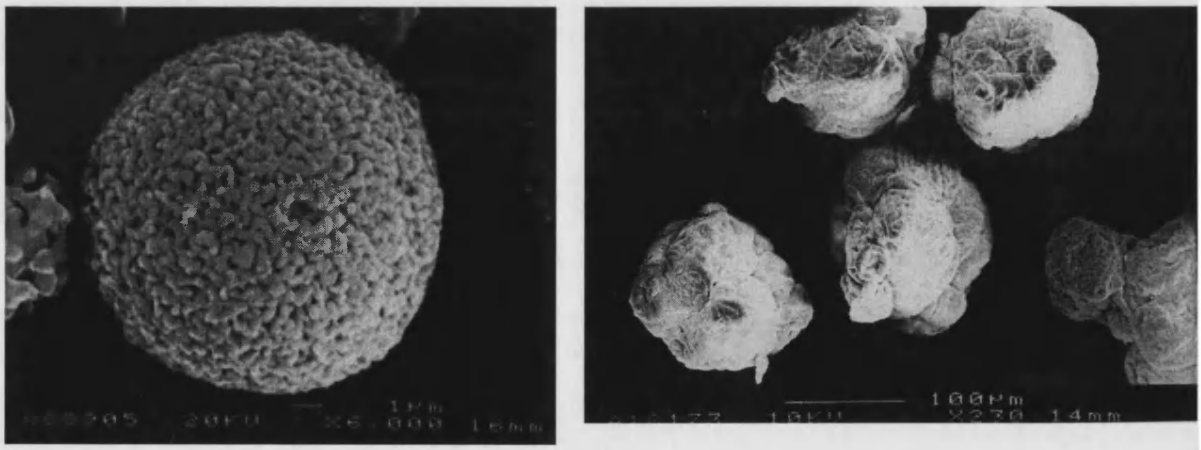

(a) (b)

Figure 3.4: SEM micrograph of (a) hydroxyapatite powder and, (b) poly (vinyl chloride) powder as received

3.3 The study of the hydroxyapatite and poly vinyl chloride and the mixture of both with temperature

3.3.1. Thermogravimetric analysis

The thermal gravimetric analysis of hydroxyapatite powder showed that when the hydroxyapatite powder was heated in air from room temperature to 900°C, there were two stages of weight loss. However, from Figure 3.5, three stages of weight loss can be observed. The separation between second and third weight loss in the graph was caused by holding the temperature at 500°C for 1h. The first slow weight loss was detected between room temperature and ~300°C; the rapid weight loss occurred below 393°C (6.2wt% loss). The second weight loss was detected between 393°C and 900°C (4.5wt% loss). The weight loss at both stages was considered to be due to the dehydroxylation of the hydroxyapatite powder.

When the PVC was heated from room temperature to 900°C in air, it showed three stages of decomposition (Figure 3.6), as suggested by Hassel [102]. The first stage was observed with a huge weight loss (63.89wt%) between 227°C and 400°C. Secondly, between 401°C and 500°C (22.3 wt% loss) and the third stage was from 500°C to 686°C (13.8 wt% loss). The first stage of weight loss was due to the dehydrochlorination of the poly vinyl chloride, where the HCl would be released from the polymer leaving polyene (an organic compound containing many double bonds). In the second stage, as the temperature increased, the low molecular weight of unsaturated hydrocarbon fragments (polyene) would turn into carbon ash and at the third stage, all the carbon residue would burn completely without leaving any ash.

When the hydroxyapatite was mixed with poly vinyl chloride (64wt% HA + 36 wt% PVC) it showed three decomposition stages as expected (Figure 3.7). In this study, the

holding temperature was 600°C for 30 minutes. The TGA and DTA results showed that the first stage of decomposition of the mixture was between ~278°C and 350°C where the weight loss was 23.169 wt%. The second weight loss was observed to occur between 350°C and 475°C (8.689 wt% loss) and the third weight loss was observed between 485°C and 900°C (4.368 wt%). In the first stage of weight loss, the decomposition of hydroxyapatite and poly vinyl chloride occurred. The weight loss occurred later than the poly vinyl chloride decomposition temperature but earlier than that of the decomposition of the hydroxyapatite powder itself. The decomposition temperature of the mixture in the first stage ended earlier than when hydroxyapatite was heated alone. The second stage also showed a similar result, where the decomposition of poly vinyl chloride and hydroxyapatite powders were shifted when they were fired together. This shows that the thermal behaviour of the individual components differs from that of the mixture.

3.3.2 Linear shrinkage

The results of the linear shrinkage experiment showed that the introduction of the polymer affects the thermal expansion of the porous hydroxyapatite. The thermal expansion of the material has to be studied carefully to know how the material behaves when heat is introduced as the sample needs to be fired to burn out the polymer in order to produce a porous hydroxyapatite.

The shrinkage or expansion of the hydroxyapatite compact and hydroxyapatite mixed with poly vinyl chloride does not have the same pattern for the first 400°C as seen in Figure 3.8.

Hydroxyapatite compacted and sintered in air at a heating rate of 5°C/min, showed a steady expansion with increase of temperature from room temperature to 750°C, with an overall expansion of ~7%. As the temperature increased, it started to shrink rapidly until it reached ~1100°C. The shrinkage from the starting volume was ~92%.

When the poly vinyl chloride was mixed with the hydroxyapatite, the compact behaved differently to the hydroxyapatite alone. When the compact was heated from the room temperature, it started to expand until it reached ~125°C (11%), it then shrunk ~7% when it reached ~175°C. The compact size then stayed unchanged until ~290°C when a sudden shrinkage (4%) occurred until ~285°C. As the temperature increased further, only a slight expansion of the compact occurred until it reached ~1020°C, when rapid shrinkage was observed. The shrinkage stopped at ~1175°C with ~18% reduction in volume. The expansion and shrinkage of the compact in the early stage of sintering was caused by the burning out of poly vinyl chloride in the compact.

By comparing the two results above, it is observed that although the pattern of shrinkage is almost similar for both hydroxyapatite compacts, with or without poly vinyl chloride, the temperature when the compact started to shrink was different. The presence of poly vinyl chloride was observed to delay the shrinkage, which was the starting of the densification process and also delayed the temperature when the shrinkage stopped where the densification could not go further. The shrinkage stopped due to the completion of sintering. The total of shrinkage for the mixture was also observed to be less than that of the compact without poly vinyl chloride.

3.3.3 Porosity and density

The porosity of the dense hydroxyapatite and porous hydroxyapatite fabricated using 53vol% of PVC and 47vol% of hydroxyapatite is shown in Figure 3.9. It was observed that the dense and the porous hydroxyapatite showed a decrease of volume fraction of porosity as the temperature increase. The dense hydroxyapatite showed an almost complete pore elimination at 1200°C and above. This showed that the final sintering occurred at 1200°C. The porous hydroxyapatite showed a rapid decrease of volume fraction of porosity as the temperature was increased up to 1250°C, and above that

temperature, only a slight volume fraction of porosity decrease observed. This result showed that the final sintering occurs at a lower temperature for dense hydroxyapatite than porous hydroxyapatite with 53 vol% of PVC present.

When a different percentage of polymer was introduced into the hydroxyapatite compact (Figure 3.10), it was observed that the porosity remained fairly constant at a stable volume fraction, up to 33 vol% of PVC content. A rapid increase in porosity was observed as the polymer content was increased. This graph shows that at all temperatures, from 900°C until 1400°C, the interconnectivity of the pores (macropores) starts after 33 vol% of polymer has been introduced.

The density of the non porous hydroxyapatite increased at a lower temperature than that of the porous hydroxyapatite (Figure 3.11). The non porous hydroxyapatite was observed to be fully densified at 1200°C. The porous hydroxyapatite showed a rapid increase in density up to 1300°C. The density continued to increase slightly above this temperature.

3.3.4 X-ray diffraction

The hydroxyapatite powder was fired at a heating rate of 300°C/h in two stages. The first stage was to burn out any presence of polymer that was introduced during mixing as the bottle used was made of plastic. The second stage was to sinter the hydroxyapatite powder and study when the decomposition of the powder started.

The sintering temperatures used were from 900°C until 1300°C with a holding time at the second stage of 4h. From Figure 3.12, it was observed that traces of β-TCP could be detected at a temperature of as low as 900°C and at 1300°C a further decomposition occurred to α-TCP and TTCP.

A study of the holding time (Figure 3.13) also showed that it does influence the decomposition of the hydroxyapatite powder. Even at 1h of holding time at 1150°C, the sample began to show decomposition of the powder. Holding at 10h or longer, would further decompose the material to α-TCP.

3.3.5 Scanning electron microscope

The porous hydroxyapatite developed from this technique showed interconnected channels between the pores as shown in Figure 3.14. The interconnectivity of the pores was proven by impregnating the pores with resin which was observed to fill the pores even in the internal part of the porous hydroxyapatite. The porous hydroxyapatite was prepared using 53 vol% of PVC and sintered at 1200°C for 4h.

3.3.6 Discussion

The presence of other material, such as polymer does have an effect on the way the hydroxyapatite behaved with temperature. It is very important to study the behaviour of the hydroxyapatite powder and its reaction in the presence of poly vinyl chloride. In this study, the objective was to obtain a ceramic with a small grain size for strength purpose, porous, with interconnected porosity and with a sintering cycle that does not cause decomposition at low temperatures.

It was observed that the poly vinyl chloride with or without hydroxyapatite would decompose in three stages. First, dehydrochlorination which would lead to the unsaturation of the polymer, then further decomposition of the polymer into carbon ash and with the presence of oxygen in air, the carbon ash would turn to carbon dioxide and water which would escape through the pores during the sintering [101, 102].

The hydroxyapatite, at temperatures below sintering (<800°C), would only release the absorbed water and strongly bound water. At higher temperatures (>800°C), the accelerated reversible dehydroxylation occurred. Some literature reports that the decomposition and dehydroxylation starts between 1300°C and 1400°C [46, 58, 103, 104] but this would depend on a lot of factors, including the sintering cycle parameter used.

The initial burnout of the PVC was observed to be delayed in the presence of hydroxyapatite. When the hydroxyapatite was compacted with poly vinyl chloride and fired, it was observed that a carbon residue was formed whereas when the poly vinyl chloride was burnt alone in air, no residue was left. Masia et al [36] suggested that the residue, which was a minor side-reaction to the main oxidation, was the effect of the presence of the ceramic, which increased the dehydration and dehydrogenation reaction, which in turn resulted in an increase of the unsaturation, crosslinking and and formation of polynuclear aromatic compounds. No further details on the changes were available to help fully understand this complex issue.

As the compact mixture was fired, the shrinkage of the mixture was less than that of the pure hydroxyapatite. One of the reasons for this behaviour was the presence of a high percentage of porosity. This porosity was developed after the burn out of the polymers during the first stage of firing. Slamovich & Lange [105], suggested that the driving potential for mass transport is inversely related to the pore size. Since the pores are too large and too close to each other, there was not enough mass to be transported to close the pores during sintering. So, the shrinkage of the material would be less than that of the dense compact. Jonghe & Rahaman [106], in their report, suggested that a densifying compact that contains a bimodal distribution of large and small pores would first show a partial or total shrinkage of the small pores, then followed by the same for the larger pores. This was observed in the current study.

The sintering behaviour of hydroxyapatite was observed to be different with and without polymer. The presence of polymer in the compact not only delayed the sintering of the

hydroxyapatite but also increased the decomposition temperature. It was also observed that the presence of poly vinyl chloride during the early stage of firing meant that the hydroxyapatite could withstand a longer duration of firing without decomposing into β-TCP, thereby allowing increased flexibility in sintering regimes.

3.3.7 Summary

1. The presence of the poly vinyl chloride in the hydroxyapatite compact delayed the densification, decomposition and reduced the shrinkage of the hydroxyapatite.
2. The porous hydroxyapatite obtained by the present experimental methods has interconnected porosity.
3. When the pores are too large and too close to each other, the macropores could not shrink and close completely because there was insufficient mass available to be transported to close the pores during sintering.
4. The poly vinyl chloride mixed with hydroxyapatite showed the presence of carbon residue after firing at 900°C but no residue was present when the poly vinyl chloride was burnt alone.

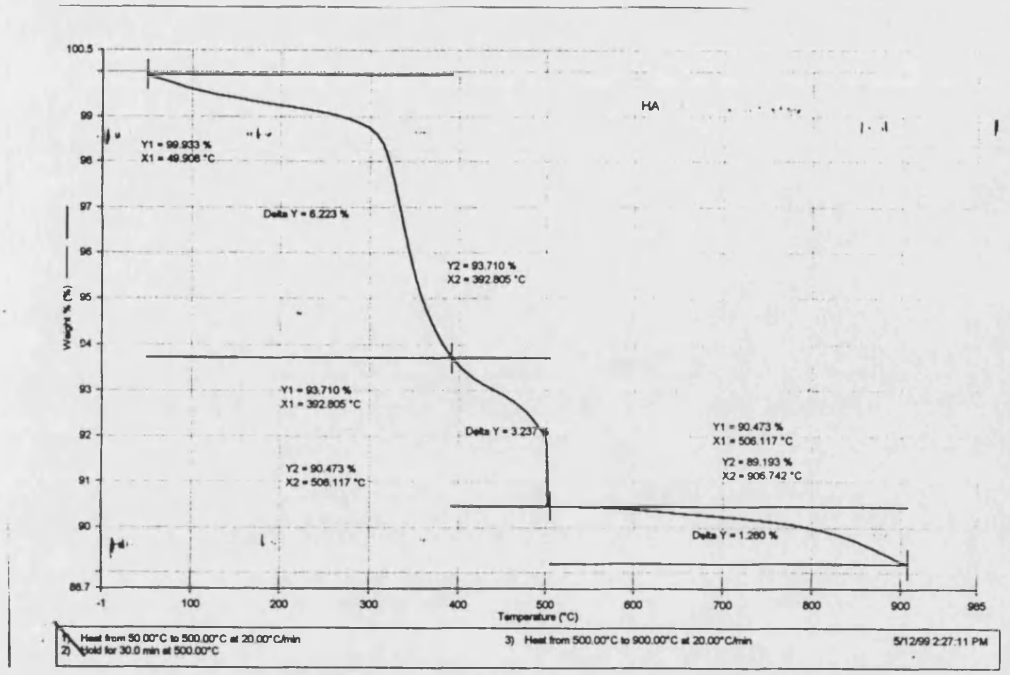

Figure 3.5: TGA plot of hydroxyapatite powder heated in air at 20°C/min with a holding temperature at 500°C for 1/2h

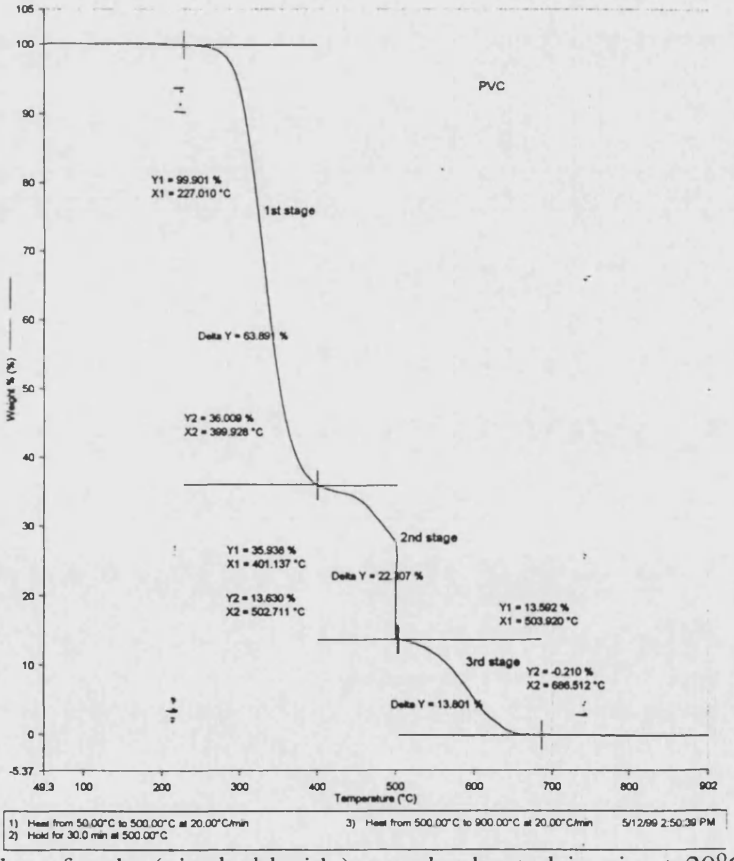

Figure 3.6: TGA plot of poly (vinyl chloride) powder heated in air at 20°C/min with a holding temperature at 500°C for 1/2h

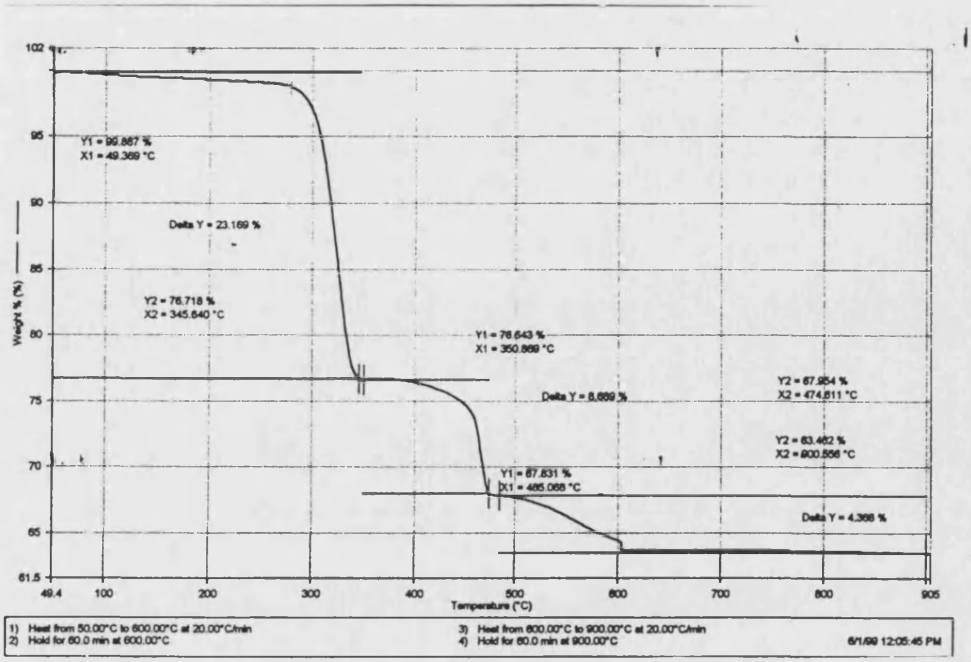

Figure 3.7: TGA plot of 64wt% of hydroxyapatite mixed with 36 wt% of poly (vinyl chloride) compact, heated in air at 20°C/min with a holding temperature at 600°C for 1h.

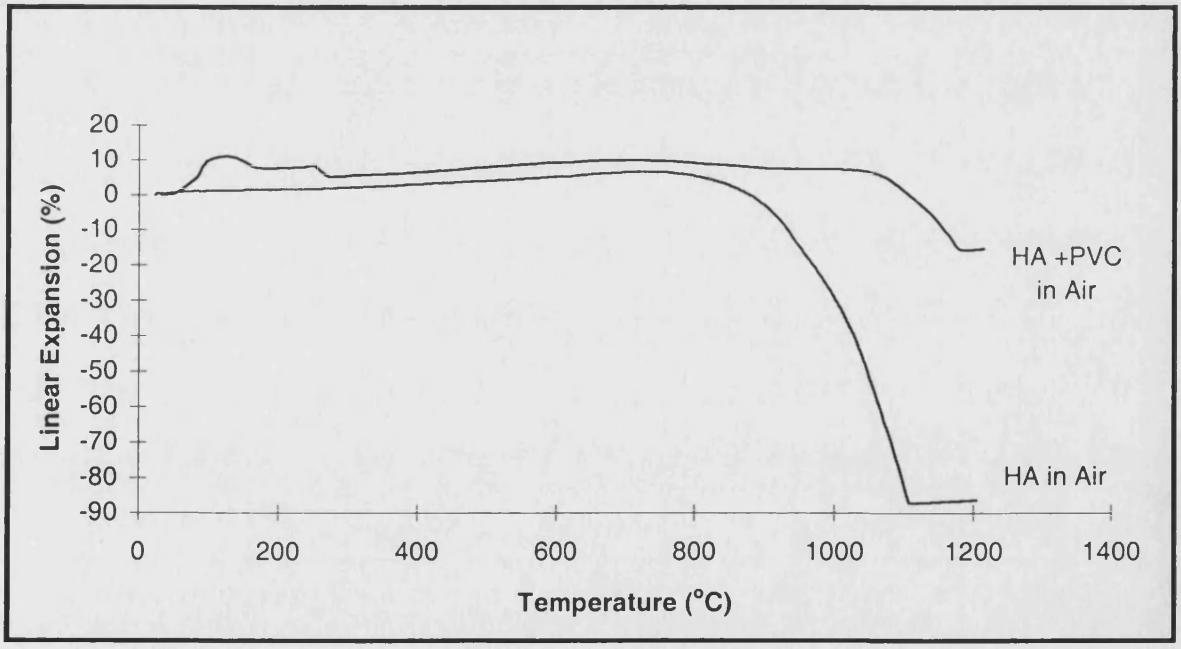

Figure 3.8: Linear shrinkage plot of HA and HA+PVC compact heated at 5°C/min

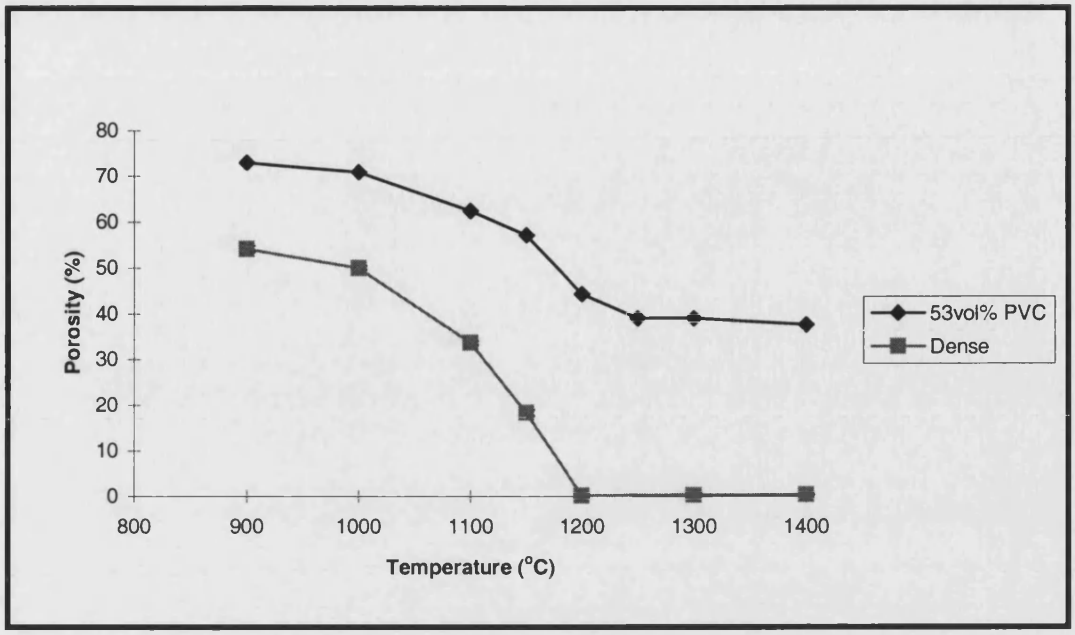

Figure 3.9: Porosity of dense and porous hydroxyapatite

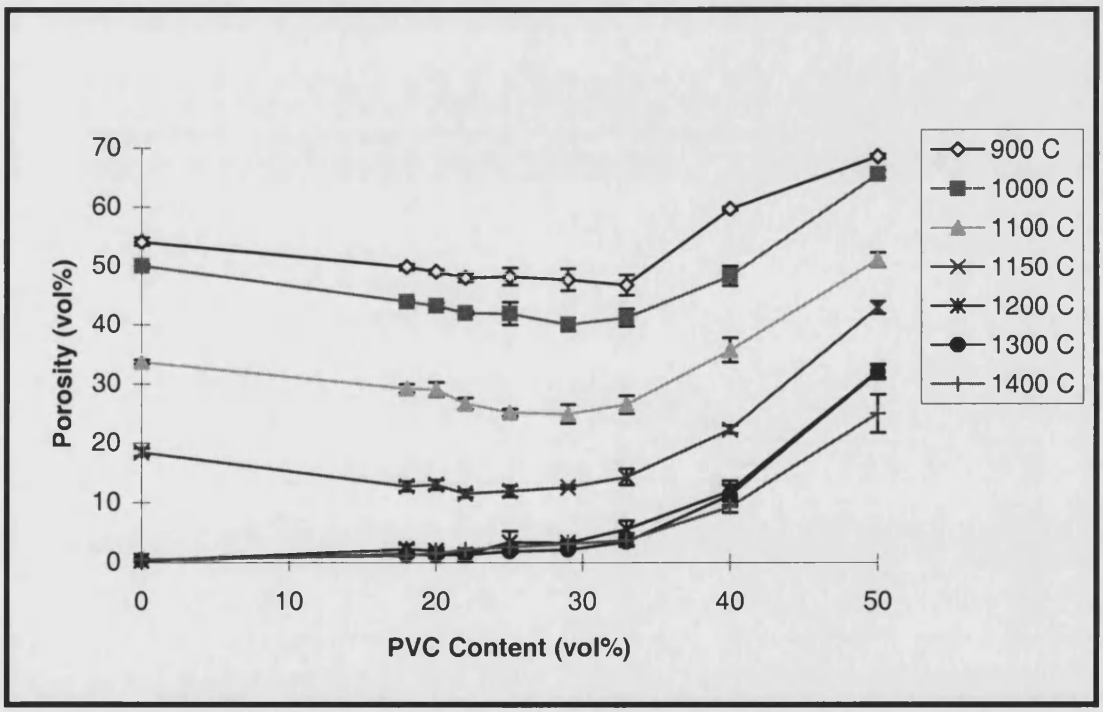

Figure 3.10: Porosity of porous hydroxyapatite at different poly (vinyl chloride) content sintered at different temperatures

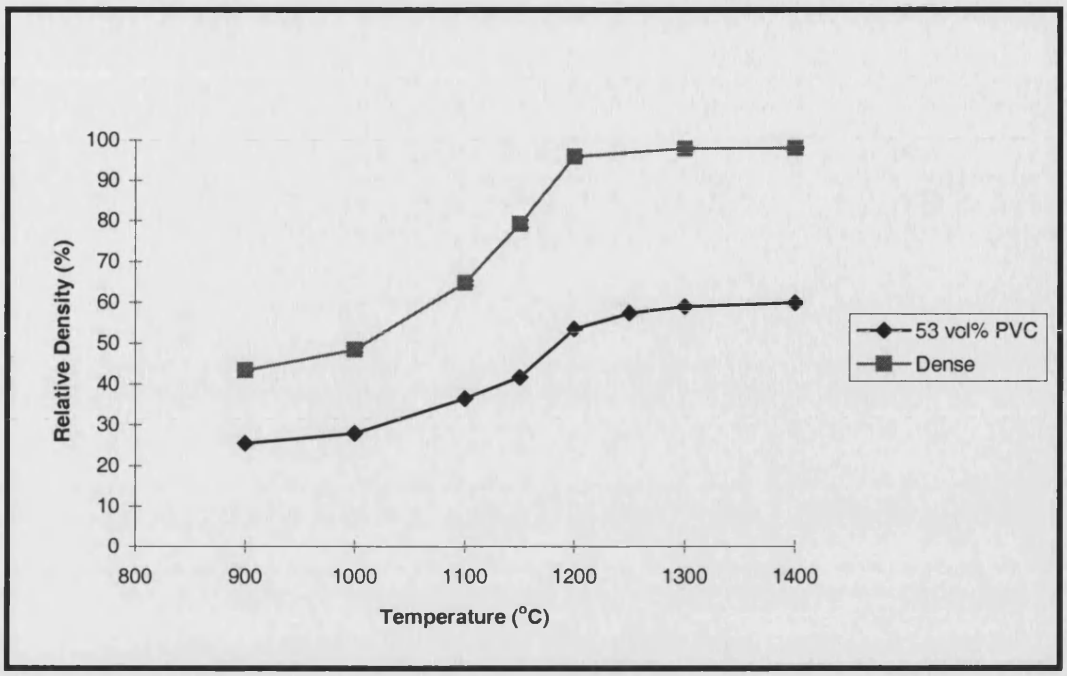

Figure 3.11: Density of porous hydroxyapatite achieved after sintering at 1200°C for 1h.

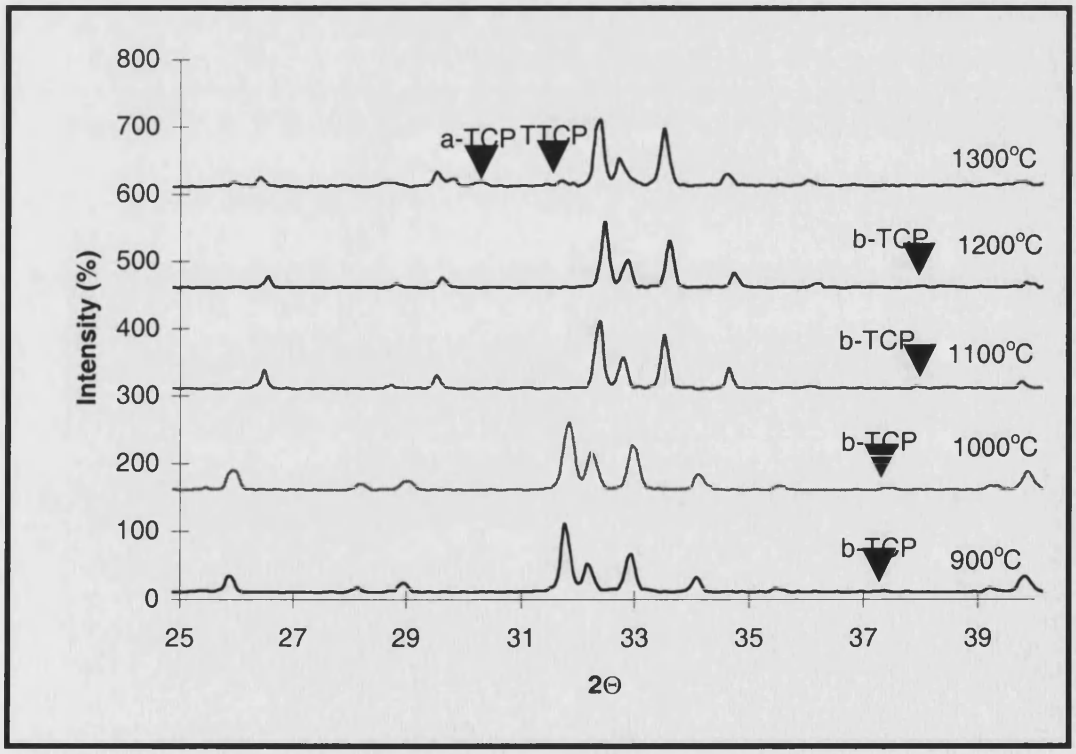

Figure 3.12: XRD result of HA powder after sintering at different temperature for 4h

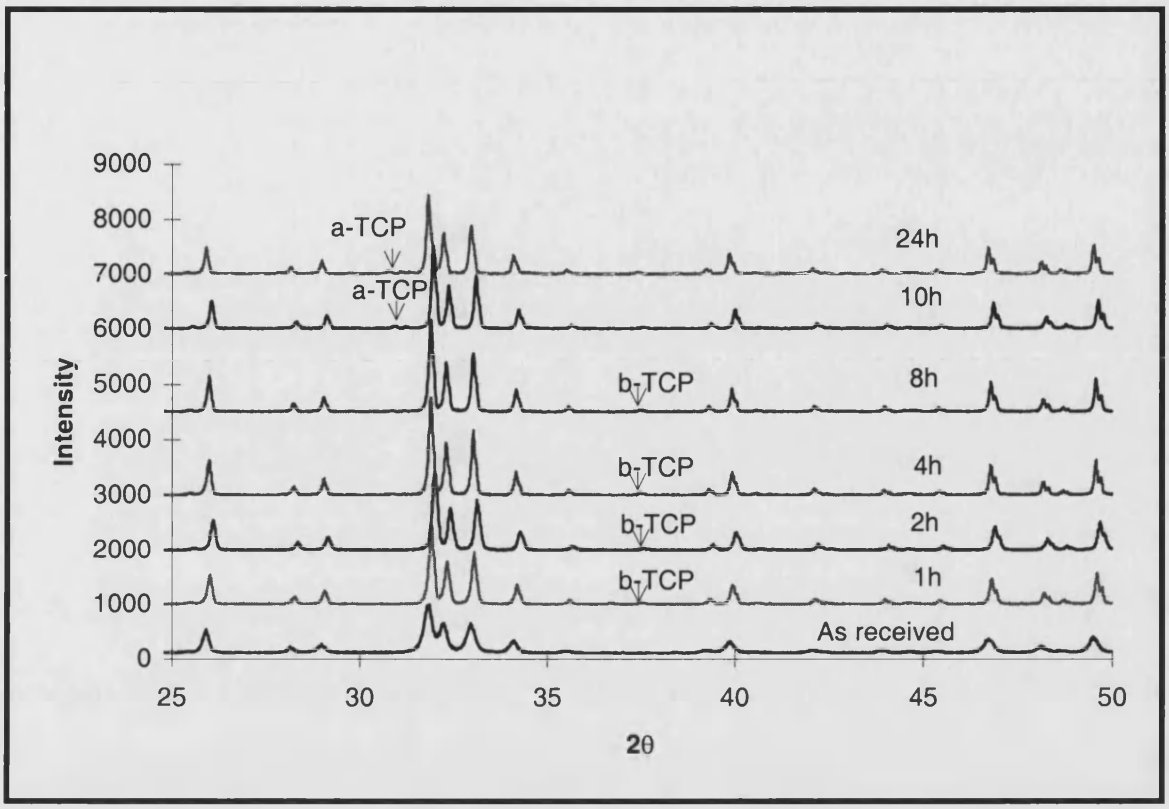

Figure 3.13: XRD result of HA powder sintered at 1150°C at different holding time

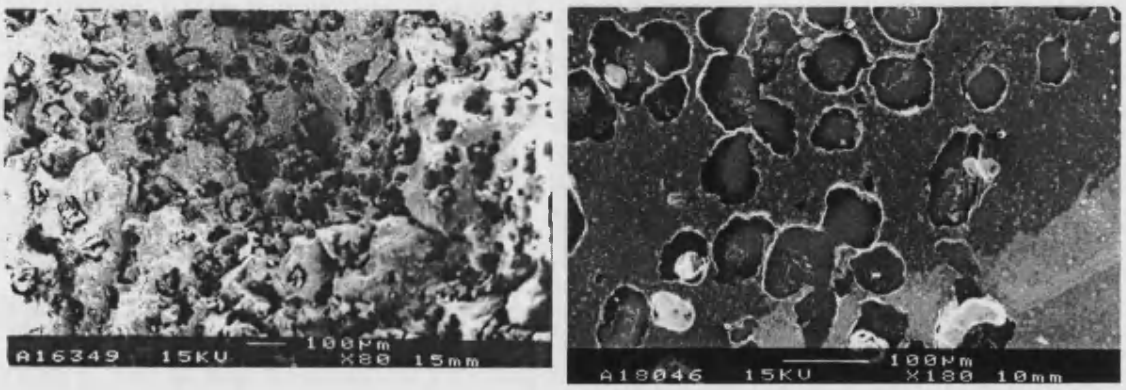

(a) (b)

Figure 3.14: SEM micrographs of porous hydroxyapatite with interconnected porosity (a) broken pieces of porous hydroxyapatite (b) porous hydroxyapatite impregnated with resin

3.4 Effect of sintering cycle on the porous hydroxyapatite behaviour

In the optimisation of a ceramic processing technique, other than the forming method, the removal of the organic additives is particularly important when a high percentage of polymer has been used. In this study, poly vinyl chloride has been chosen as the polymer to create the porous characteristic in the hydroxyapatite material. The effects of sintering cycle on the behaviour of the porous hydroxyapatite were studied.

3.4.1 Heating rate

The heating rate study generates important results for samples that use a high volume fraction of polymer in the compact mixture. Without controlling the heating rate, the sample would produce cracks or bloating as the thermal expansion of the polymer and ceramic differ. As a result, the strength of the sample would be lower than expected.

In a polymer burn-out process, only low heating rates were used as high heating rates would make the polymer expand too quickly and the pressure created internally in the compact due to the decomposition of the polymer would be too high for the ceramic solid to withstand. The inability to purge out the volatile product during the polymer burn-out from the internal compact would result in a sample with low mechanical properties.

3.4.1.1 Optical microscope photographs

The microstructures of porous hydroxyapatites formed at different heating temperatures were studied. Two heating rates (30°C/h and 50°C/h) were examined, with compacts of hydroxyapatite alone and a mixture of hydroxyapatite and poly vinyl chloride, 50 vol.% each. The results in Figure 3.15 showed that at both heating rates, the samples with the mixture of hydroxyapatite and poly vinyl chloride do not crack at all. When only hydroxyapatite was used, the compact showed large cracks. It is presumed that this is the

result of the ability of the volatile product of the degrading polymer to travel through the structure of the porous ceramic as the temperature increased, allowing escape to the atmosphere without the build up of internal pressure.

3.4.1.2 Porosity, density and grain size

The porosity and density of the samples sintered at different heating rates were observed to be similar (Figure 3.16 and Figure 3.17). The density increases as the temperature increases and no further densification was observed above 1300°C. The relative density achieved at 1300°C was ~53%.

The level of porosity in the porous hydroxyapatite was observed to decrease as the sintering temperature increased. Samples were sintered at 30°C/h and 50°C/h from room temperature up to 400°C and underwent a further heating to 1400°C with a heating rate of 100°C/h. The results were observed to be similar for both heating rates.

The grain size of the of the porous hydroxyapatite sintered at different heating rates showed almost similar grain sizes as the temperature increased (Figure 3.18). There was only a slight increase of grain size at 1400°C when the sample was heated at 30°C/h in comparison to 50°C/h.

3.4.1.3 X-ray diffraction

The results of the XRD taken when the samples were heated at a different heating rates can be seen in Figure 3.19. It was observed from these results that the heating rate has little effect on the decomposition temperature. The samples, heated at both 30°C/h and 50°C/h showed traces of decomposition of hydroxyapatite to β- tricalcium phosphate (β-TCP) at temperatures of 1200°C and above, and decomposition to α-tricalcium phosphate (α-TCP) and tetracalcium phosphate (TTCP) at 1400°C.

3.4.2 Holding time

In this study, two stages of holding temperature were performed. The first stage is the polymer burnout stage, which is up to 600°C and the second stage is the densification of the ceramic stage, from 900°C until 1400°C. In these two stages of sintering, only the results from second stage of sintering will be discussed.

3.4.2.1 Porosity, density and grain size

The porosity can be seen to decrease with the increase of temperature (Figure 3.20). At 1100°C, the porosity is still high, with at least 54 vol% present after 36h of temperature hold. There is then a rapid decrease in porosity between 1100°C and 1200°C. The compact can not reach zero porosity, or be expected to, due to the introduction of 53 vol% of poly vinyl chloride. The porosity of compacts with holding times of 12h and 36 hours could be seen to stop decreasing at lower temperatures (1200°C) than the 1h and 4h (1250°C) compacts. The volume fraction of porosity was observed to stay stable at ~38 volume percent after 1250°C for holding temperature >4h. However, the compacts sintered with a holding time of 1h showed an increase of volume fraction of porosity at ≥1300°C.

The density (Figure 3.21) of the compacts also increase with the increase of temperature regardless of the duration of holding time. However, the compacts held for 36h showed the highest density at a temperature of 1200°C followed by 12h, 4h and 1h respectively. At the temperature ≥1250°C, the density attained is almost the same except for the sample held for 1h, which has a lower density.

From Figure 3.22, it can be seen that as the sintering temperature increases the grain size also increases. At 1200°C, the grain size of the compacts at a holding time of 1h, 4h, 12h

and 36h were 1.01 ± 0.15 μm, 1.41 ± 0.17 μm, 1.72 ± 0.16 μm and 5.92 ± 1.02 μm respectively. As the temperature of sintering increased, the grain size increased exponentially.

3.4.2.2 Scanning electron microscope

The microstructures of the porous hydroxyapatite at different holding times in stage 2 is shown in Figure 3.23 (a-d). As can be seen in the SEM micrographs, the compact sintered at 1100°C for 1h (Figure 3.23a) showed an interconnected and incomplete closure of the pores which indicated that the temperature is not sufficiently high enough for complete sintering to occur. As the temperature increased, the pores were observed to significantly decrease in size. At 1200°C, the formation of the grain boundaries was still not complete and some of the neck growth can still be observed. The grain boundaries were observed to be completely formed at a temperature 1250°C. Most of the pores, which are typically ~ 1 μm disappeared on sintering at 1400°C and grain growth was also observed to occur at this temperature.

When the holding time was increased to 4 hours, it was apparent that the completion of the grain boundary formation was taking place at a lower temperature than 1200°C and 1h, and that less porosity (~ 1 μm) was present. As the holding time was increase to 12h, the necks were observed to disappear at a lower temperature, 1150°C and the pores (< 1 μm) were observed in smaller numbers than in the 4 hours holding time samples. After holding the temperature at 1200°C for 12 hours, fewer pores were present and grain growth was taking place. After 36 hours, the pores were observed to be eliminated almost completely and a significant degree of grain growth had occurred.

3.4.2.3 X-ray diffraction

In the second stage holding temperature, it was observed that the duration of holding time affected the decomposition temperature (Figure 3.24). The longer the holding time, the

lower the decomposition temperature started. In the compacts sintered at a holding time of 1h, decomposition of hydroxyapatite to β-TCP started at 1200°C but when the temperature was held for 4 hours or longer, the decomposition started at 1100°C or lower. Further decomposition to α-TCP and TTCP for compacts held for 1 hour only started at 1400°C but after 36 hours, the decomposition reaction could be detected at 1300°C and no hydroxyapatite was observed after heating above 1400°C.

3.4.3 Discussion

An examination of the thermal expansion of the compact containing the mixture of hydroxyapatite and poly vinyl chloride showed a high expansion during the initial burn out of the polymer, however, the sample did not show any cracks due to the ability of the volatile product of the decomposed poly vinyl chloride to escape through the porosity. This was created as the poly vinyl chloride structure started to collapse creating interconnectivity between the pores within the main body of the porous hydroxyapatite. The volatile product was able to escape through both the macropores and the micropores between the powder particles before the densification of the material started. This prevented pressure from building up within the compact, reducing the pressure below the level that would result in fracture of the hydroxyapatite. Thus control of the microstructure and nature of the porosity allows the fabrication of a suitable ceramic.

Varying the heating rate of the material did not result in any difference in volume fraction of porosity, density, grain size or decomposition temperature of the hydroxyapatite. This demonstrates that the control of the heating rate does not have an important effect on the behaviour of the porous hydroxyapatite.

However, the holding time did have an important effect on the porous hydroxyapatite. The longer the holding time, the earlier the final stage of sintering was reached. The pore volume fraction would reach a stable level at a lower temperature and the highest density

would also be achieved at a lower temperature. The grain size increased and decomposition temperature decreased as the duration of holding time increased.

The aim of the present part of the study was to achieve the best combination of properties in terms of density, grain size, etc. in order to optimise the mechanical properties. As suggested by other researchers, the mechanical properties could be maximised by optimising the microstructure of the material, taking into account factors such as having a small grain size [96], a high density and well distributed pores [110, 111]. The ability to control the purity of the material without decomposition at any given temperature and also to achieve interconnected porosity at the same time is not an easy task.

From the experiments in the current study, optimal results were obtained in the samples sintered at 1200°C for 4h. At this temperature region, although the porous hydroxyapatite had not achieved the maximum densification, the grain size showed an increase of ~ 50% (from 1.41 μm at 1200°C to 3.36 μm at 1250°C), a feature which would possibly lower the mechanical strength. As the XRD results also showed decomposition to have started at 1150°C, to β-TCP, an alternative sintering cycle was used. The only change was the holding temperature during the first stage, where the burning-out stage was changed from 400°C for 1 hour to 600°C for 1 hour. This resulted in a higher temperature (1400°C) necessary to decompose the hydroxyapatite (Figure 3.25). The new sintering cycle was used for the next set of experiments as it met the requirement of optimising the microstructure of the porous hydroxyapatite.

3.4.4 Summary

1. Heating rates of 30°C/h or 50°C/h do not result in significant difference in the density, porosity, grain size, and decomposition temperature of the porous hydroxyapatite.
2. For a given temperature, the longer the holding time during sintering, the porous hydroxyapatite achieves a higher density, lower porosity and a larger grain size.

3. The decomposition of the hydroxyapatite would initiate at a lower temperature for increased holding time.
4. The decomposition of the hydroxyapatite was influenced by the holding temperature during the polymer burnout stage.

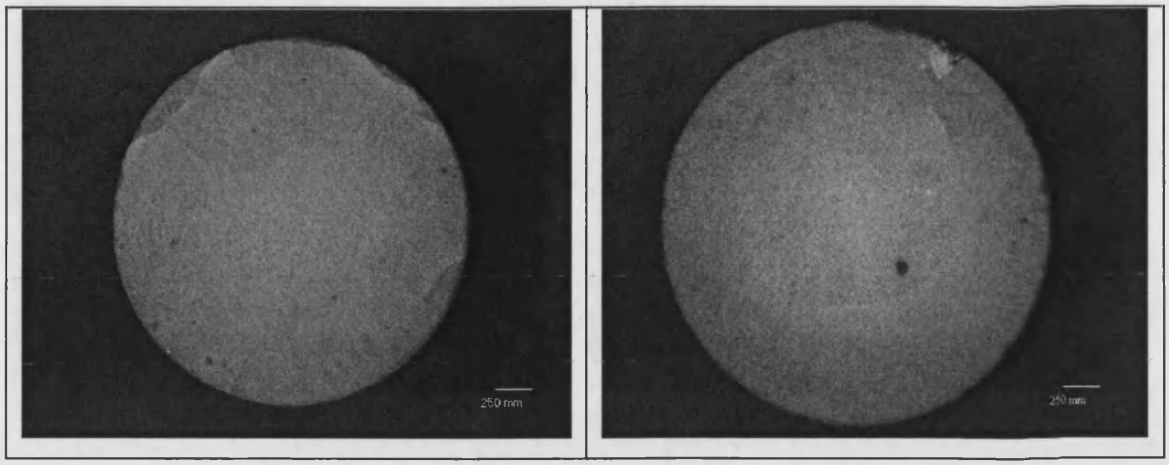

1 (a) 1 (b)

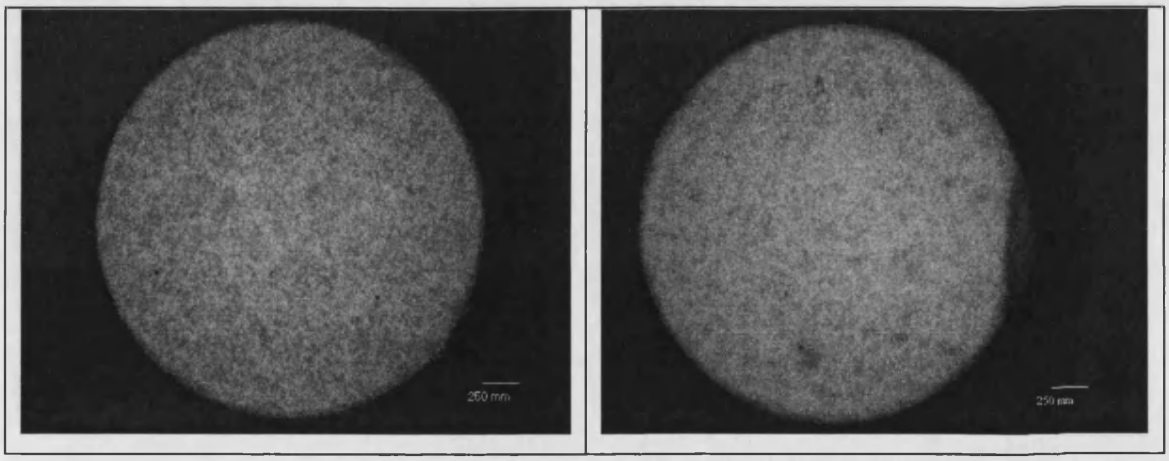

2 (a) 2 (b)

Figure 3.15: Optical micrograph of dense hydroxyapatite and porous hydroxyapatite sintered at a different first stage heating rate. (1). Dense hydroxyapatite at heating rate of (a) 30°C/h and (b) 50°C/h; (2). Porous hydroxyapatite at heating rate of (a) 30°C/h and (b) 50°C/h

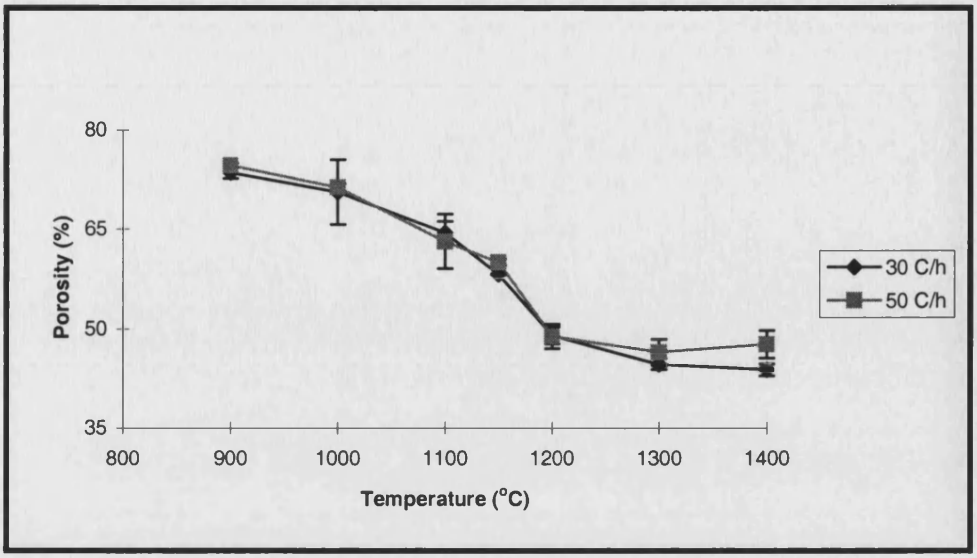

Figure 3.16: Volume fraction of porosity of porous hydroxyapatite sintered at a different temperature with a different first stage heating rate

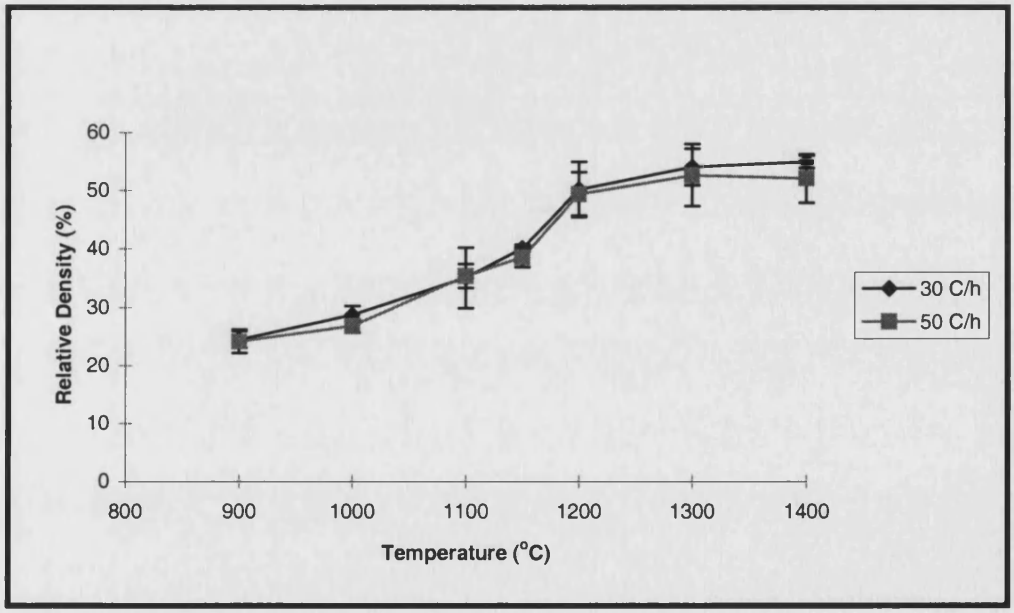

Figure 3.17: Relative density of porous hydroxyapatite sintered at a different temperature with a different first stage heating rate

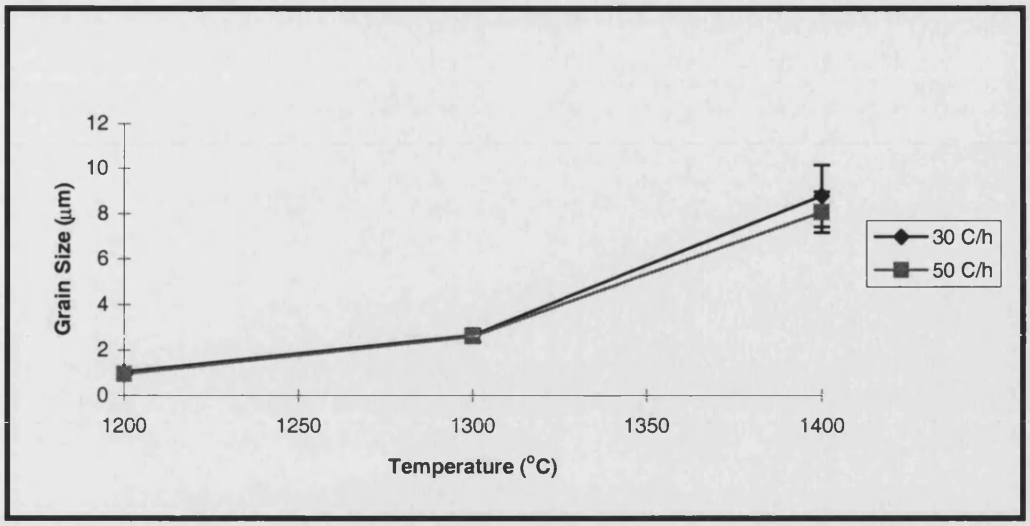

Figure 3.18: Grain size of porous hydroxyapatite sintered at a different temperature with a different first stage heating rate

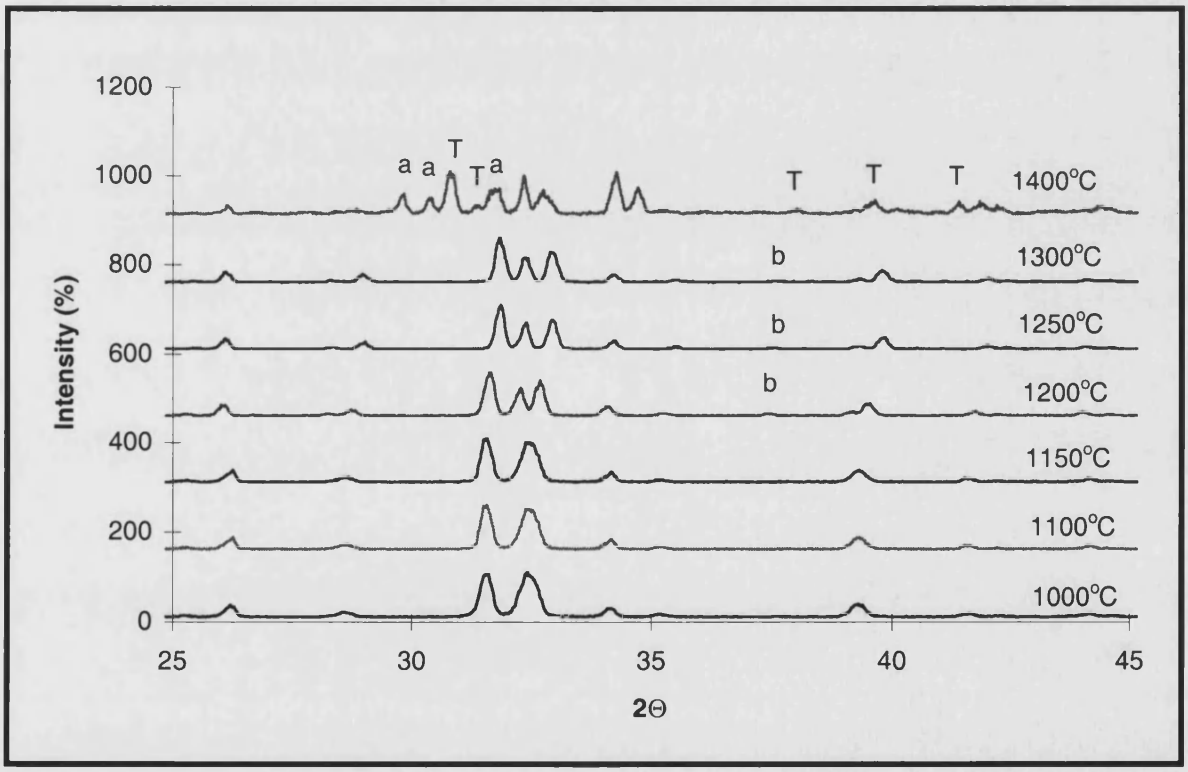

Figure 3.19(a): The XRD result of porous hydroxyapatite sintered at a different temperature with a heating rate of 30°C/h. a = α-TCP, b = β-TCP and T = TTCP.

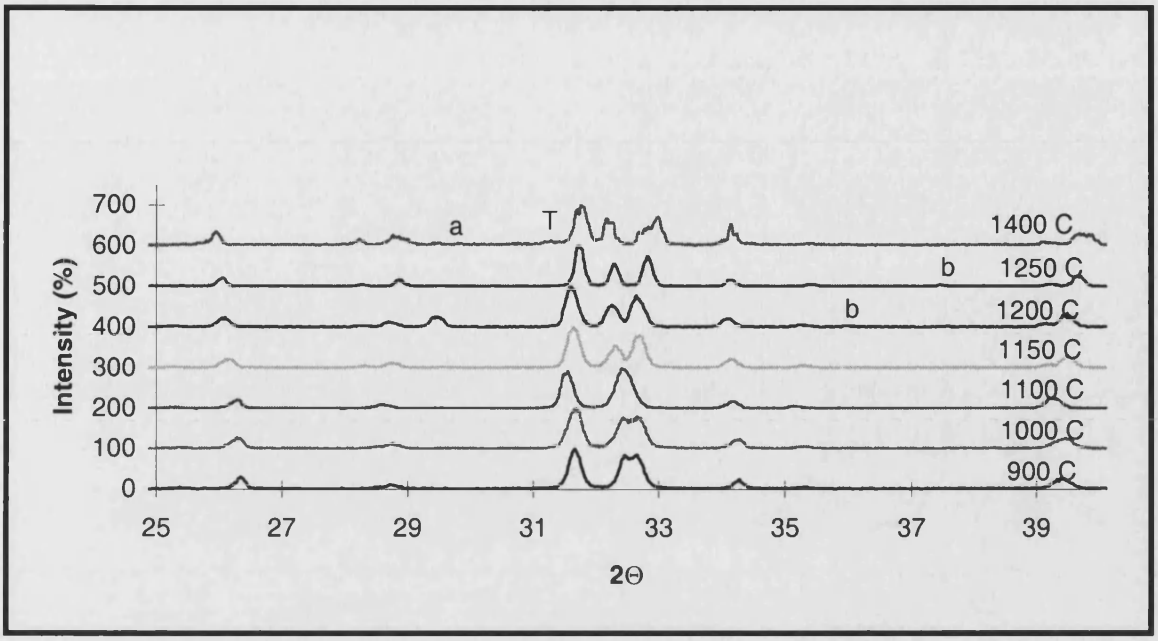

Figure 3.19(b): The XRD result of porous hydroxyapatite sintered at a different temperature with a heating rate of 50°C/h. a = α-TCP, b = β-TCP and T = TTCP.

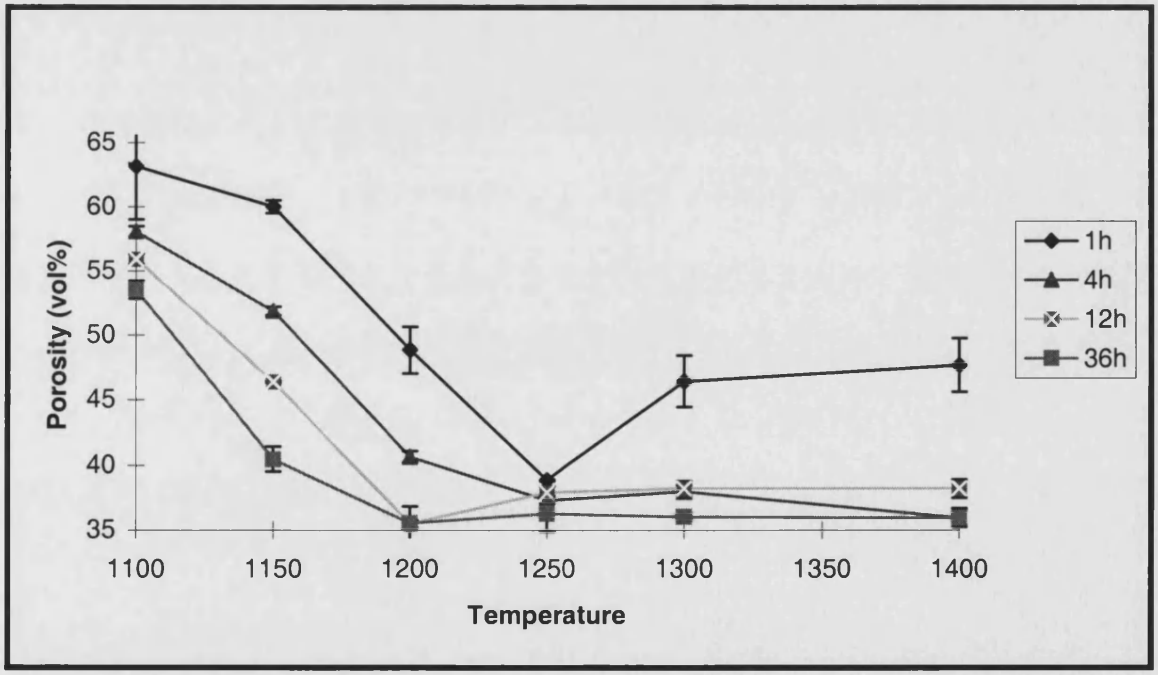

Figure 3.20: The volume fraction of porosity of the porous hydroxyapatite at a different holding time.

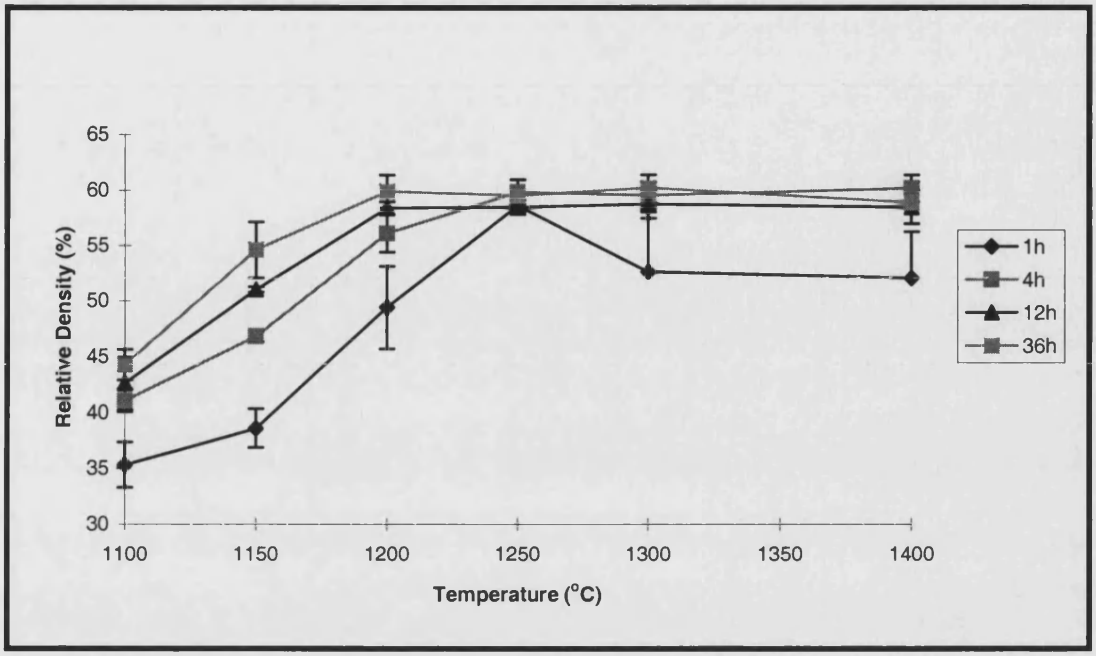

Figure 3.21: The relative density of the porous hydroxyapatite at a different holding time.

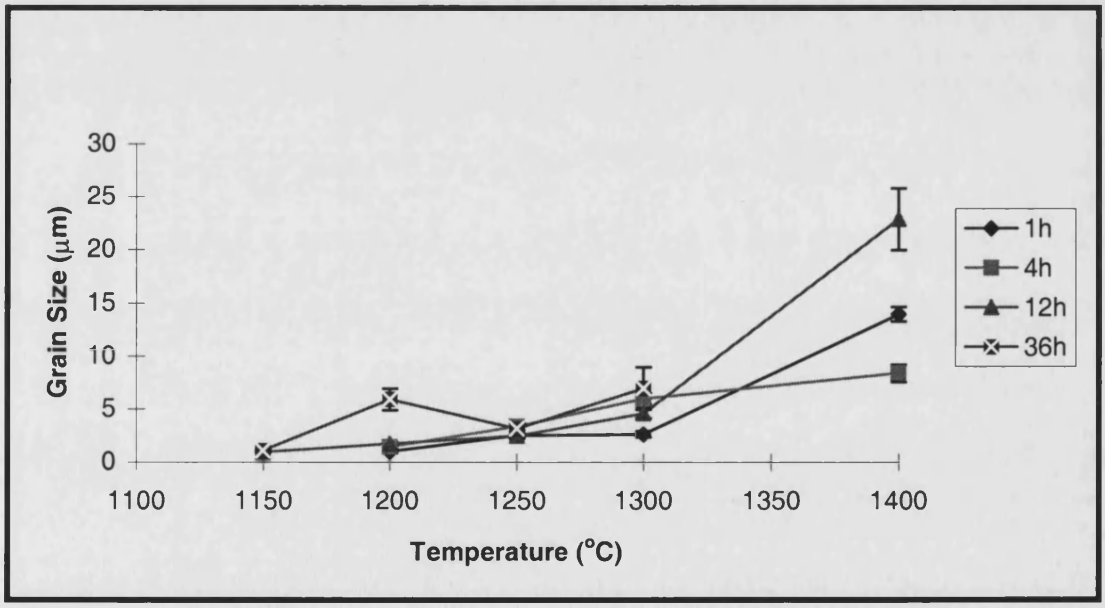

Figure 3.22: The grain size of the porous hydroxyapatite at a different holding time.

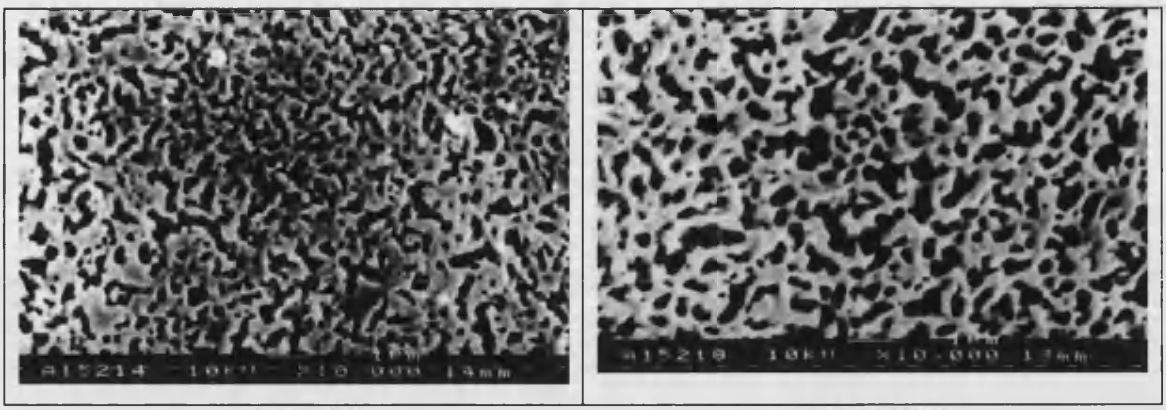

(i) 1100°C (ii) 1150°C

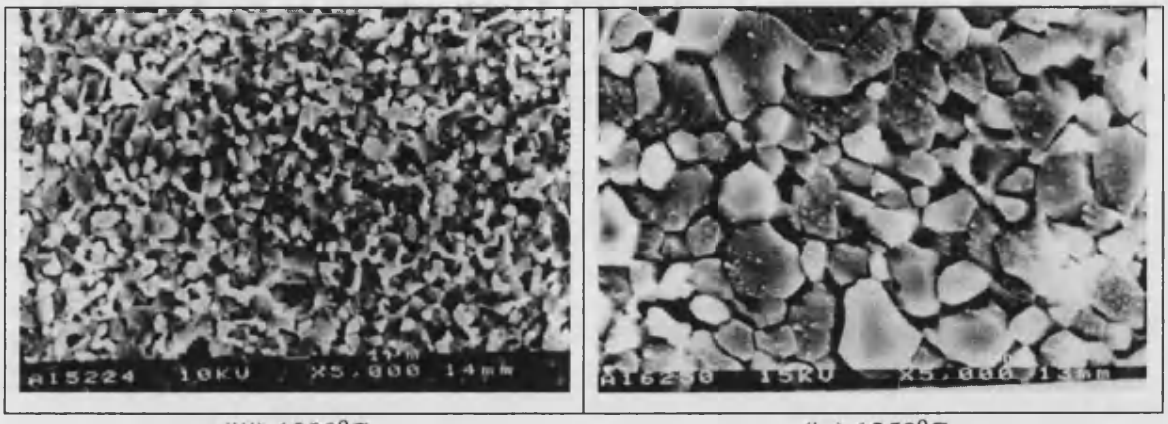

(iii) 1200°C (iv) 1250°C

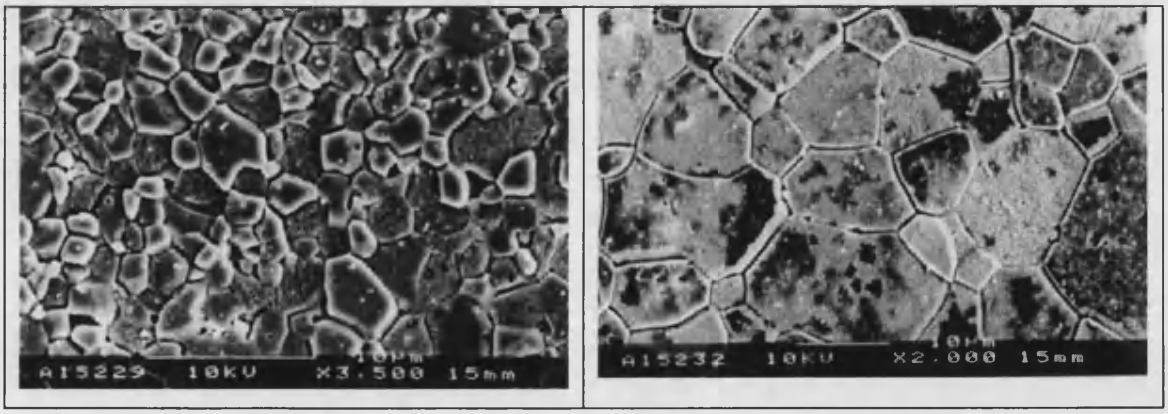

(v) 1300°C (vi) 1400

Figure 3.23 (a): The microstructure of porous hydroxyapatite sintered at different temperatures and holding time of 1h.

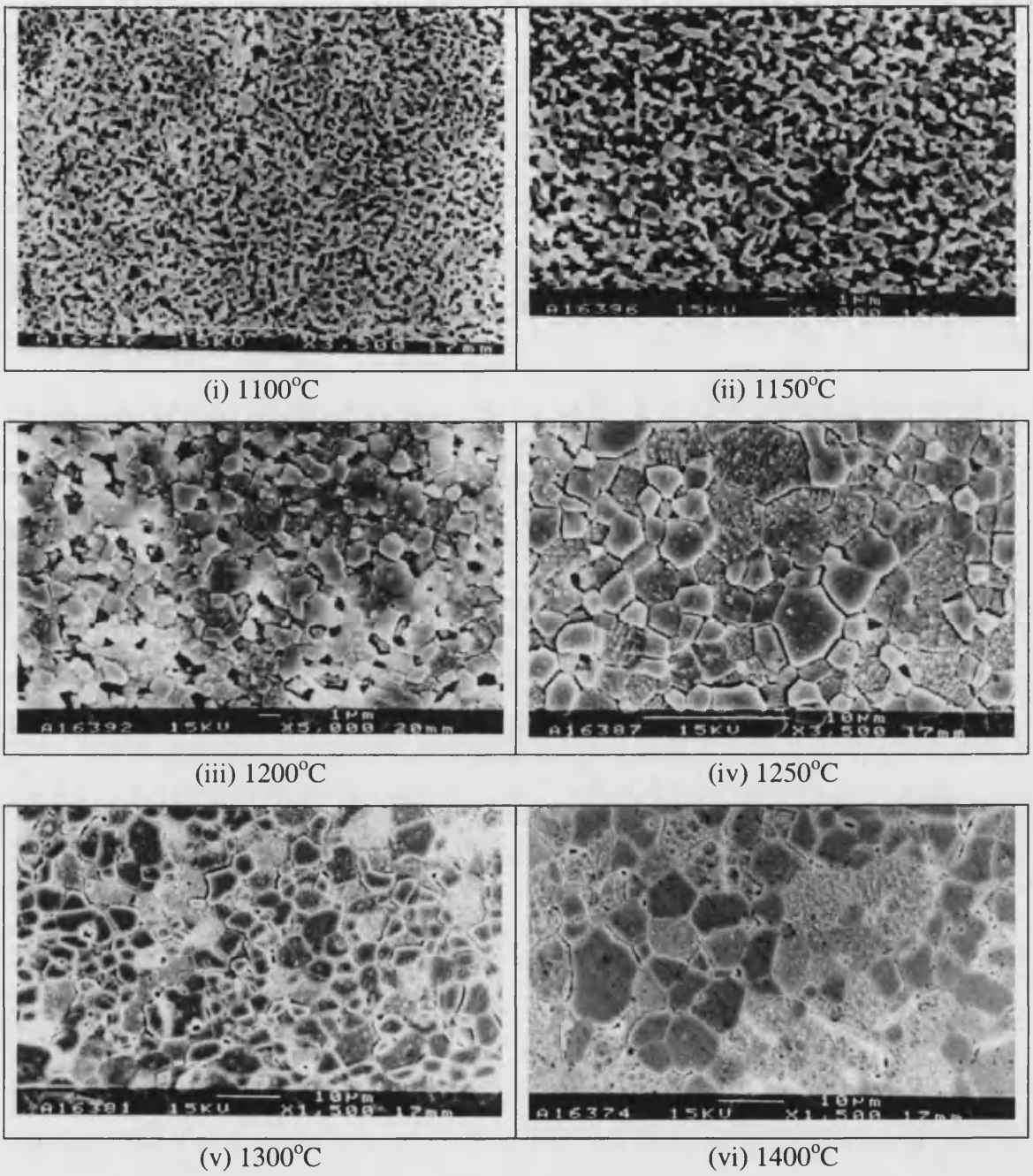

(i) 1100°C (ii) 1150°C

(iii) 1200°C (iv) 1250°C

(v) 1300°C (vi) 1400°C

Figure 3.23 (b): The microstructure of porous hydroxyapatite sintered at different temperatures and holding time of 4h

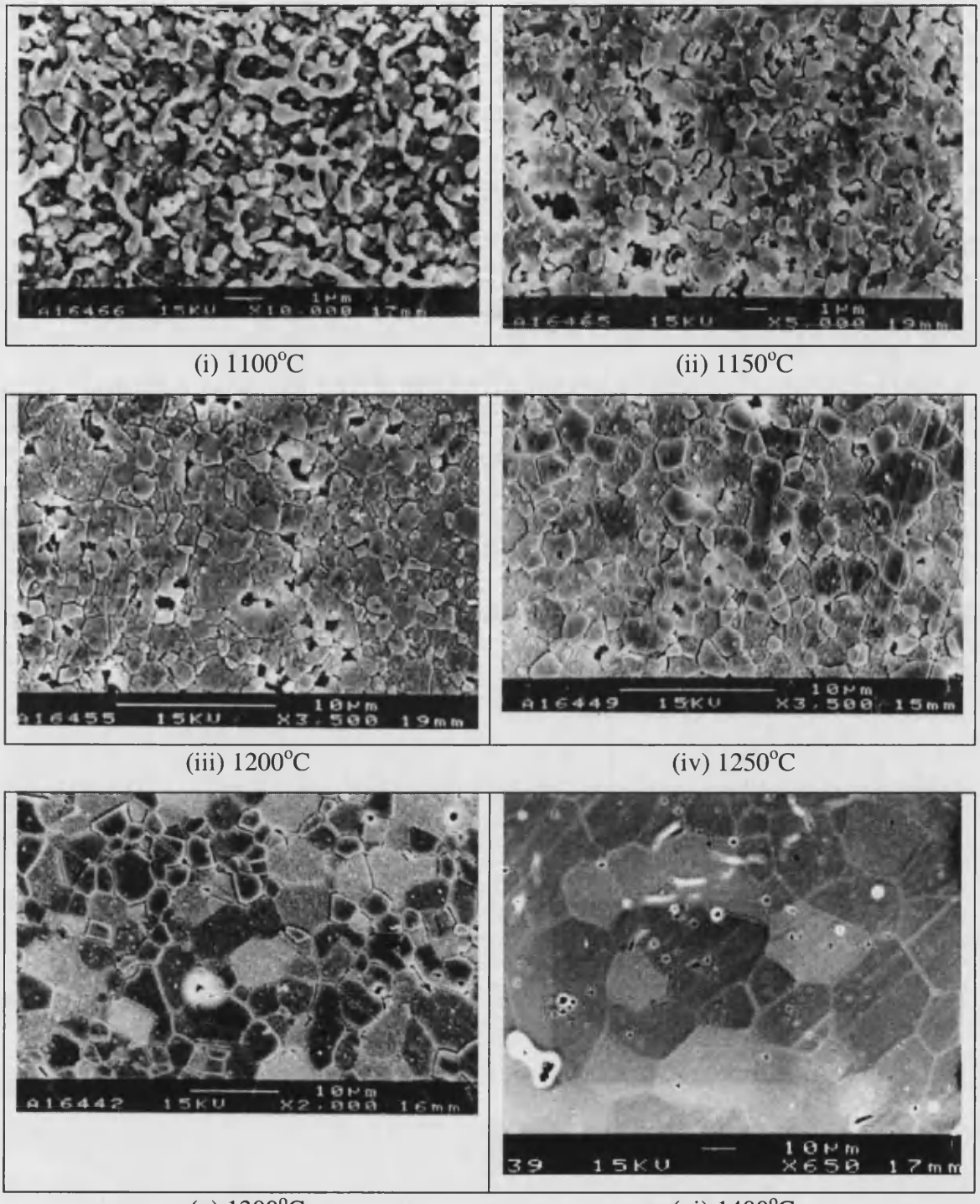

(i) 1100°C (ii) 1150°C

(iii) 1200°C (iv) 1250°C

(v) 1300°C (vi) 1400°C

Figure 3.23 (c): The microstructure of porous hydroxyapatite sintered at different temperatures and holding time of 12h

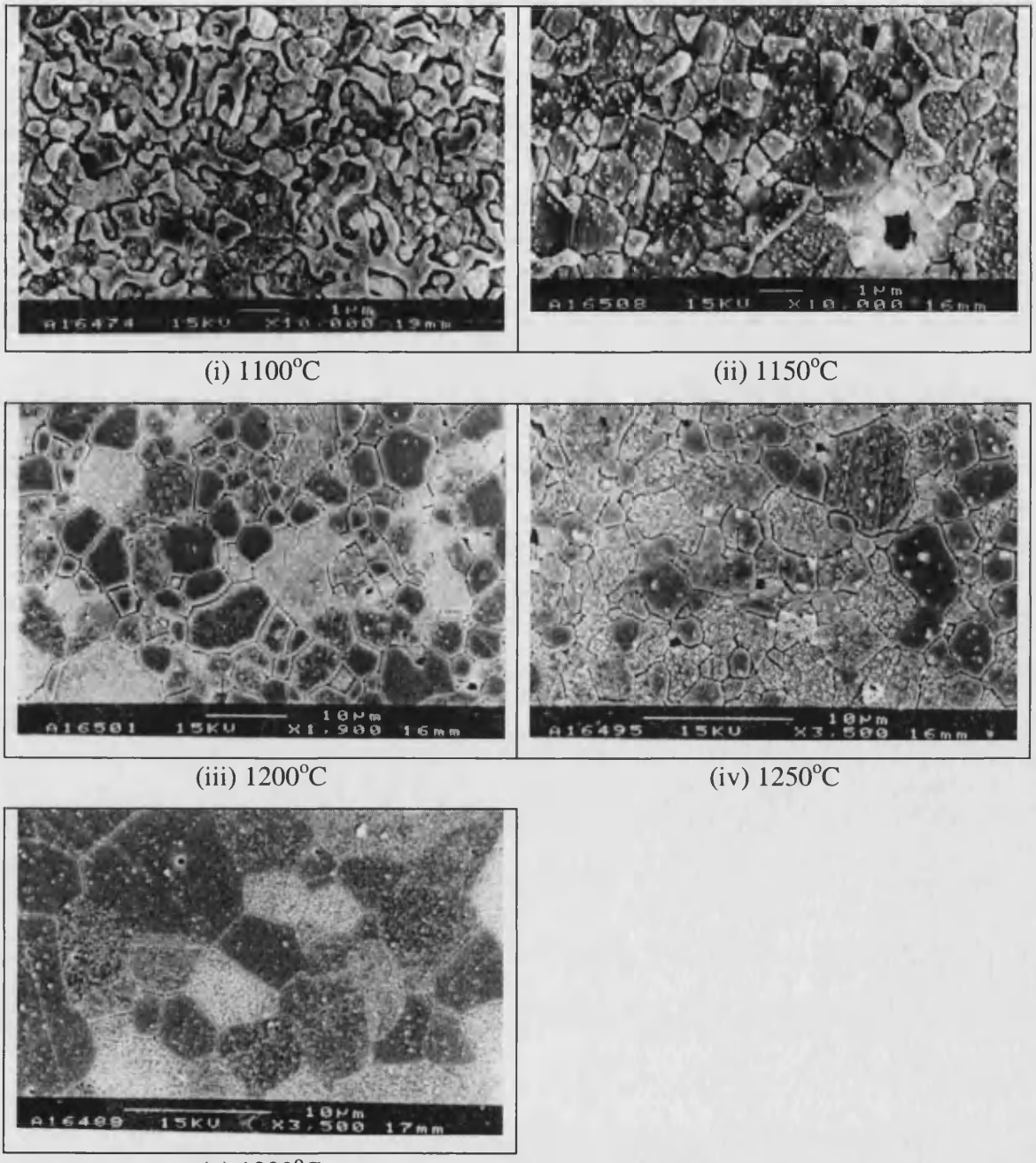

(i) 1100°C (ii) 1150°C

(iii) 1200°C (iv) 1250°C

(v) 1300°C

Figure 3.23 (d): The microstructure of porous hydroxyapatite sintered at different temperatures and holding time of 36h

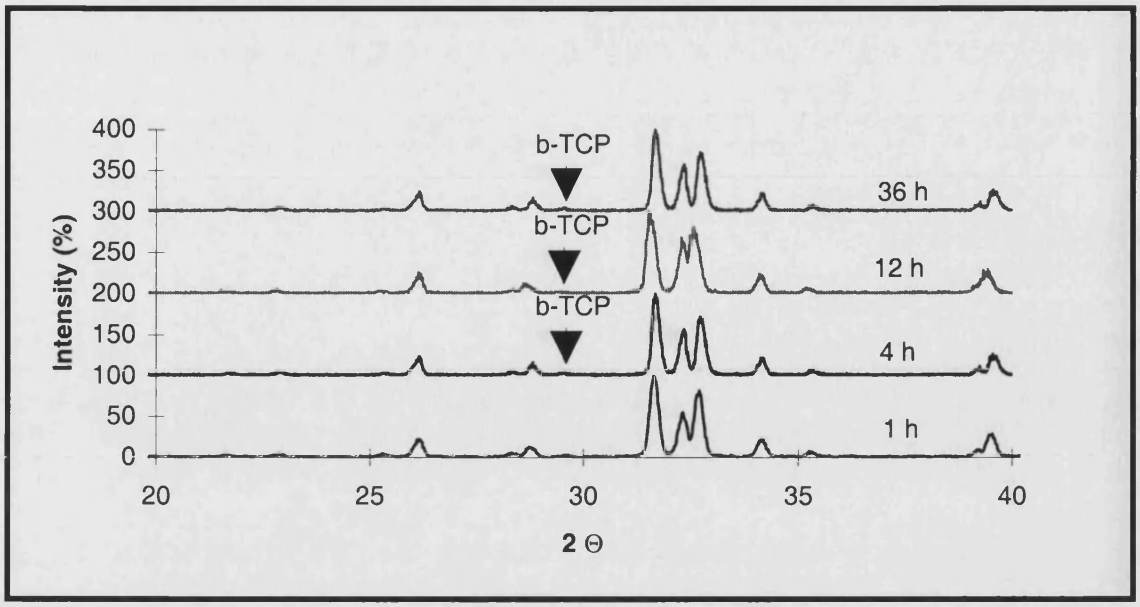

Figure 3.24: The XRD plot of porous hydroxyapatite sintered in the first stage at a heating rate of 50°C/h, holding temperature of 400°C for 1h and a second stage of holding temperature at 1150°C with a different holding time.

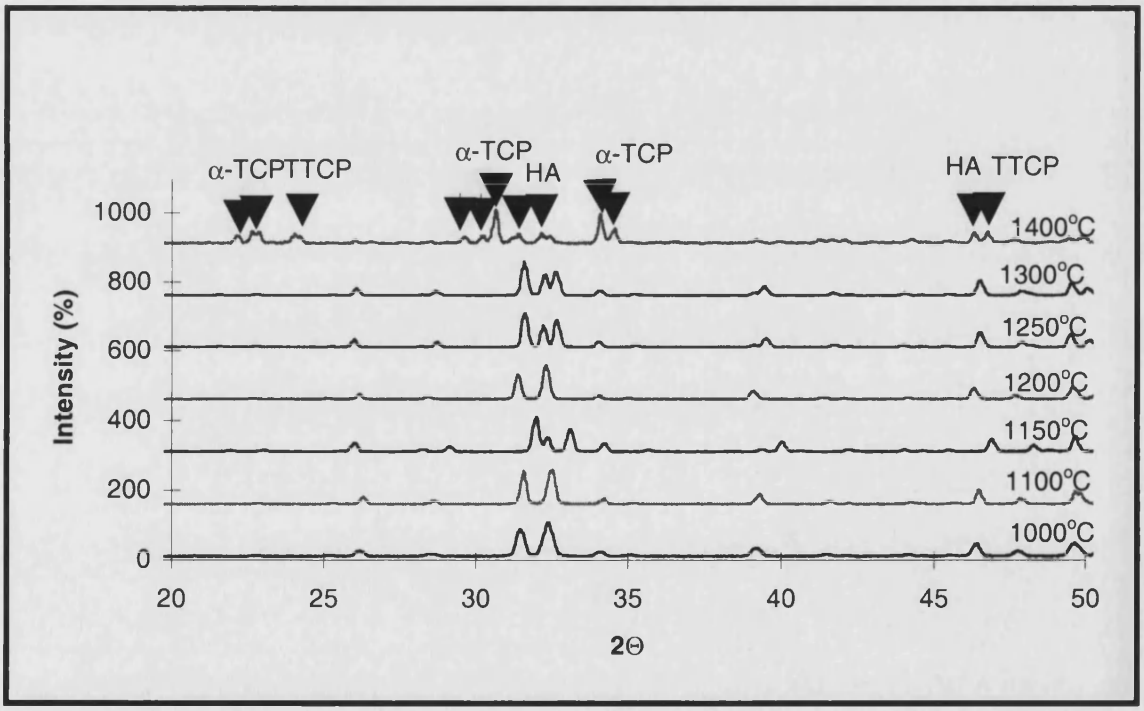

Figure 3.25: The XRD plot of porous hydroxyapatite sintered in the first stage of sintering at a heating rate of 30°C/h, holding temperature of 600°C for 1h and a second stage of sintering with different temperatures and holding time of 4h.

3.5 Effect Of Sintering Atmosphere

There have been studies on the sintering of hydroxyapatite in different atmospheres. The studies mostly used hydroxyapatite alone and analysed the decomposition behaviour of the material [103]. This study was important in generating an understanding of the behaviour of the material, how it is to be fabricated and the effect of the sintering atmosphere on the mechanical strength of the material.

3.5.1 Microstructural analysis

3.5.1.1 Linear shrinkage

In most solid materials, a controlled increase in temperature would result in a controlled increase in volume, the relationship often being linear. The thermal expansion coefficient of a polymeric material is generally greater than that of metals and ceramics. This is a direct result of the nature of temperature and sensitivity of the bonds that hold these atoms and molecules together to form the materials. In general, strong bonds are associated with relatively low coefficients of expansion and weak bonds with relatively high ones [107].

A study of thermal expansion behaviour is especially important for material that has components having different thermal expansions coefficients. When the temperature is raised and the heating rate is not controlled properly, a difference in thermal expansion can result in the development of cracks and/or bloating. The presence of these features severely reduce the mechanical properties of the ceramic.

In this study, the effect of different sintering atmospheres on thermal expansion was analysed using the dilatometer. The samples were prepared using 25 volume percent of poly vinyl chloride and 75 volume percent of hydroxyapatite. The preparation of the samples was explained in Section 2.2.1.1.

From Figure 3.26, the pattern of the expansion and shrinkage was observed to be almost the same for samples fired in both air and argon atmosphere. An initial expansion was observed when the temperature increased from room temperature to ~125°C. At this stage, the expansion was considered to be a result of the large thermal expansion coefficient of the polymer, without much polymer loss occurring during heating. As the temperature increased (>125°C), a rapid shrinkage began to occur. At this higher temperature, the polymer began to degrade and the volume of material expelled from the system was greater than the volume increase due to the thermal expansion. Thus the shrinkage was the result of the evaporation of the complex species resulting from the polymer degradation.

The shrinkage rate decreased when a temperature of ~180°C was reached and above this temperature there was a gradual expansion up to ~250°C. At these temperatures, the thermal expansion, degradation of the polymer and the evaporation of the evolving gaseous species from the thermal degradation of the poly vinyl chloride are occurring at rates which result in close to the change in dimensions. A sudden shrinkage occurred at ~250°C and continued up to ~275°C. In this temperature range, decomposition of the unsaturated hydrocarbon fragments occurred and the materials were leaving the system at a faster rate than the thermal expansion of the system can compensate thus resulting in shrinkage. As the temperature continued to increase, the system started to expand again until 700°C and 800°C for sintering in air and argon atmosphere respectively. The expansion in this temperature range was due to the expansion of the hydroxyapatite itself. Shrinkage than started to occur at 700°C (air) and 800°C (argon) due to the higher release of water from the dehydroxylation of the hydroxyapatite than could be compensated for by the expansion itself. At 1000°C (air) and 1060°C (argon), a rapid shrinkage occurred

as the densification of the ceramic particles took place. This stopped at ~1180°C when the densification process was effectively complete.

It is clearly apparent that the percentage expansion of the samples fired in air and argon differs. When heated from room temperature to 125°C in air, the samples showed an expansion of ~11%, in argon the expansion was 6.5%. As the temperature increased, the difference in thermal expansion was still high, 7.6 % and 4.5% for air and argon respectively at 180°C. At the second stage of shrinkage, at 250°C, the sample fired in air showed a higher percentage shrinkage (3.2%) than the samples heated in argon (0.8%). The samples heated in air continued to show a higher thermal expansion than in argon with a difference of ~1% up to 800°C. At higher temperatures still the sample in air shrank faster than the one in argon. At 1070°C, a rapid shrinkage occurred until the temperature reached 1180°C with a total shrinkage of 20%. The rapid shrinkage in argon started at 1065°C, and continued until it stopped at 1186°C with a total shrinkage of 13%.

3.5.1.2 Thermal gravimetric analysis

The TGA analysis of poly vinyl chloride shown in Figure 3.27 indicates that the thermal decomposition of poly vinyl chloride in argon at 20°C/min is incomplete. From the graph, it was calculated that 5.74 wt% of carbon residue was left unburned. This result is consistent with the findings of Hassel [102]. When the hydroxyapatite compact was tested in the TGA experiment (Figure 3.28), it was observed that the weight loss was 13.96 wt%. When the mixed sample (64 wt% HA + 36 wt% PVC) was examined using TGA (Figure 3.29), the weight loss found was 31.52 wt%. When calculated at 64 wt% of HA and 36 wt% of PVC, the weight loss was predicted to be 42.86 wt% (8.93 wt% HA + 33.93 wt% PVC). The 11.34 wt% difference between the predicted and experimental result was assumed to be the source of carbon residue which could not burn out completely and was probably trapped in the isolated pores.

When the poly vinyl chloride was fired in air (Figure 3.30), it was observed that a complete burnout of the poly vinyl chloride occurred, leaving no residue. The hydroxyapatite itself (Figure 3.31) showed some weight loss (10.7 wt%) due to dehydroxylation [31, 35, 58]. When both hydroxyapatite and poly vinyl chloride were mixed (64 wt% HA + 36 wt% PVC) and fired, a different result than that predicted was attained (Figure 3.32). The weight loss was observed to be 35.9 wt% while the expected result was 42.8 wt% (36 wt% PVC + 6.8wt% HA). The difference of weight loss calculated from the practical and theoretical was 6.9 wt%. This was also due to the incomplete burning of the poly vinyl chloride. The results showed that the polymer acts differently when it was burnt alone compared with when it was mixed with hydroxyapatite and then burned.

3.5.1.3 Porosity and density

There is no difference in volume of porosity and density when porous hydroxyapatite is sintered in air or inert atmosphere (argon) as showed in Figure 3.33 and Figure 3.34. The volume of porosity decreased as the sintering temperature increased and at 1250°C, the volume of porosity stabilised at ~38 volume %.

The relative density also showed a similar pattern in both air and argon as the sintering temperature increased. The relative density increased significantly (~60%) from 1000°C until the temperature reached 1250°C. No further densification occurred when the temperature was increased above 1250°C.

3.5.1.4 Grain size

The porous hydroxyapatite sintered using argon showed a lower grain size than the sample prepared in an air atmosphere (Figure 3.35). From this observation, it can be assumed that sintering in an inert atmosphere could slow down the grain growth of the porous hydroxyapatite without having any effect on the density and volume fraction of

porosity of the porous hydroxyapatite. This could be a consequence of the shrinkage or densification of the samples in argon starting at a later stage than in air.

3.5.1.5 Scanning electron microscope

The microstructure of the porous hydroxyapatite can be seen in Figures 3.36 and 3.37. It was observed that at 1100°C, the sintering temperature was still not high enough for the hydroxyapatite to be fully sintered as it is still at the intermediate stage, where the neck growth and interconnected pores can still be observed. At 1200°C the neck growth and interconnected pores were observed to have disappeared. Micropores (~1μm) could be observed at some of the junctions of the grain boundaries of the ceramic. At 1250°C, a smaller number of micropores were observed and grain growth had occurred. There was little difference in the microstructures of the porous hydroxyapatite sintered in air and argon atmospheres. As the sintering temperature increased, a difference in grain size could be seen.

3.5.1.6 X-ray diffraction

The XRD results of the hydroxyapatite mixed with poly vinyl chloride are shown in Figure 3.38. The porous hydroxyapatite sintered in air was observed to decompose at a higher temperature (1400°C) than the sample sintered in argon (1300°C). The samples decomposed from hydroxyapatite to α-TCP and to TTCP.

3.5.2 Mechanical property analysis

The strength of the porous hydroxyapatite prepared by sintering using different atmospheres can be seen in Figures 3.39 and 3.40. The samples' strength increased due to the decrease of the volume fraction of porosity fraction. For the sample prepared in an air atmosphere, the compressive strength could be seen to become almost stable after

sintering at 1250°C or above. For samples sintered in argon, it could be seen that the strength decreased after reaching a peak at a 1250°C sintering temperature. This was due to the decomposition of the hydroxyapatite taking place at ≥1300°C.

It was observed that overall, the samples prepared in air had a higher strength than the samples fired in argon. Since the samples prepared using both methods had the same volume fraction of porosity, pore size and density, then grain size could play an important role in determining the strength [66, 93, 96]. But in this case, the impurity level could have a major role in lowering the strength of the material. In both cases carbon residue was detected. However, in an argon atmosphere, a higher level of impurity in the form of carbon residue was found compared to samples prepared in air. This deleteriously affected the strength (compressive and tensile strength) of the porous hydroxyapatite material. As in Figure 3.39, the difference in compressive strength between air and argon was ~8 MPa. For some materials 8 MPa does not appear to be a large difference, but in the case of hydroxyapatite which was known to be brittle and also, in this case, porous, small changes in strength can be significant.

3.5.3 Discussion

Sintering hydroxyapatite mixed with poly vinyl chloride in different sintering atmospheres (air and argon) resulted in different thermal expansion behaviour. In air, at a low temperature (<300°C), samples had a higher expansion than in argon. This result must be considered carefully in relation to the sintering since an uncontrollable expansion would result in cracks and bloating which ultimately would reduce the mechanical properties of the porous material. In this study it was observed that cracking and bloating had not occurred in the samples prepared using either atmospheres. This could be due to the interconnected porosity of the porous material which resulted in less internal pressure being built up in the ceramic during the decomposition of the polymeric material.

The porous hydroxyapatite sintered in air showed a higher expansion than in argon due to the larger percentage weight loss during the first stage. This is considered due to the oxygen in air increasing the dehydrochlorination rate of the PVC [108]. Such a deduction can be supported by the results of the TGA investigation when the PVC was burnt alone, when, it was observed ~66 wt% loss could be measured in comparison to only ~46wt% loss in argon. This result was again repeated when the ceramic compact (mixture of PVC and HA) was heated, giving a higher weight loss in air of 22 wt%, and of 17wt% in argon. The volatile product produced by the decomposition would expand the ceramic compact due to the pressure built up in the ceramic during the PVC decomposition. As soon as the volatile product of the decomposition could escape from the compact, shrinkage of the compact could be observed as long as the diffusion of the volatile product is higher than the expansion of the compact. The ceramic decomposed at a higher rate in air than in argon.

When the polymer was heated on its own, it was observed that in air it decomposed completely without leaving any residue, but in argon there was ~6wt% of the residue left unburned. In the production of ceramic products, the presence of impurities is a factor that should be avoided as they are known to affect the strength of the material. When the PVC was mixed with the hydroxyapatite powder, formed and sintered, it was observed that in both atmospheres there was carbon residue present. In air, the presence of the residue was assumed to be caused by the inability of the oxygen to travel through the pores to reach the inner part of the compact, due to the difference of the partial pressure of oxygen between inside and outside the sample. The oxygen being consumed preferentially in the outer layer of the ceramic. This would create an inert condition in the internal part of the ceramic and the decomposition of the PVC would be incomplete, leaving residue in the pores. Even when the higher temperature was reached, the carbon residue would not be able to decompose. The carbon residue would be trapped in the pores as the densification of the hydroxyapatite progressed and would thus remain as an impurity in the porous hydroxyapatite.

Although there were remnant impurities in both porous hydroxyapatite sintered in air and argon, it was observed that the amount of the impurities also played an important part in determining the strength of the porous hydroxyapatite. It was observed that as the carbon residue in the porous hydroxyapatite increased, the strength would also decrease. In air, the carbon residue was ~6.95 wt% and in argon ~11.34wt%. With the difference of ~4.39 wt%, the strength was reduced by as much as 10 MPa after sintering at 1200°C.

The samples sintered using argon developed a smaller grain size than those produced in air. However, the results showed that the samples produced in an argon atmosphere did not have a higher strength than the samples prepared in air. As shown in other studies [66], samples with a smaller grain size have a higher strength than samples with a larger grain size. As the samples sintered in both atmospheres showed a similar volume fraction of porosity and density, it is clear that the grain size difference in this study was not sufficient to affect the strength significantly in comparison to the effect of the impurities and other variables.

The strength of the porous hydroxyapatite sintered in argon decreased as the sintering temperature increased above 1300°C due to the decomposition of the hydroxyapatite to α-TCP and TTCP.

3.5.4 Summary

1. Porous hydroxyapatite sintered in argon showed a lower rate of thermal expansion compared to the same sample sintered in air.
2. Samples sintered in air showed a higher shrinkage than in argon.
3. More carbon residue was left in the ceramic when sintered in argon than in air.
4. The presence of carbon residue has a significant impact on the strength of the porous hydroxyapatite.

5. The samples sintered in argon decomposed at a lower temperature (1300°C) than in air (1400°C).
6. The difference in grain size of the samples prepared in both atmospheres did not significantly affect the strength of the porous hydroxyapatite.

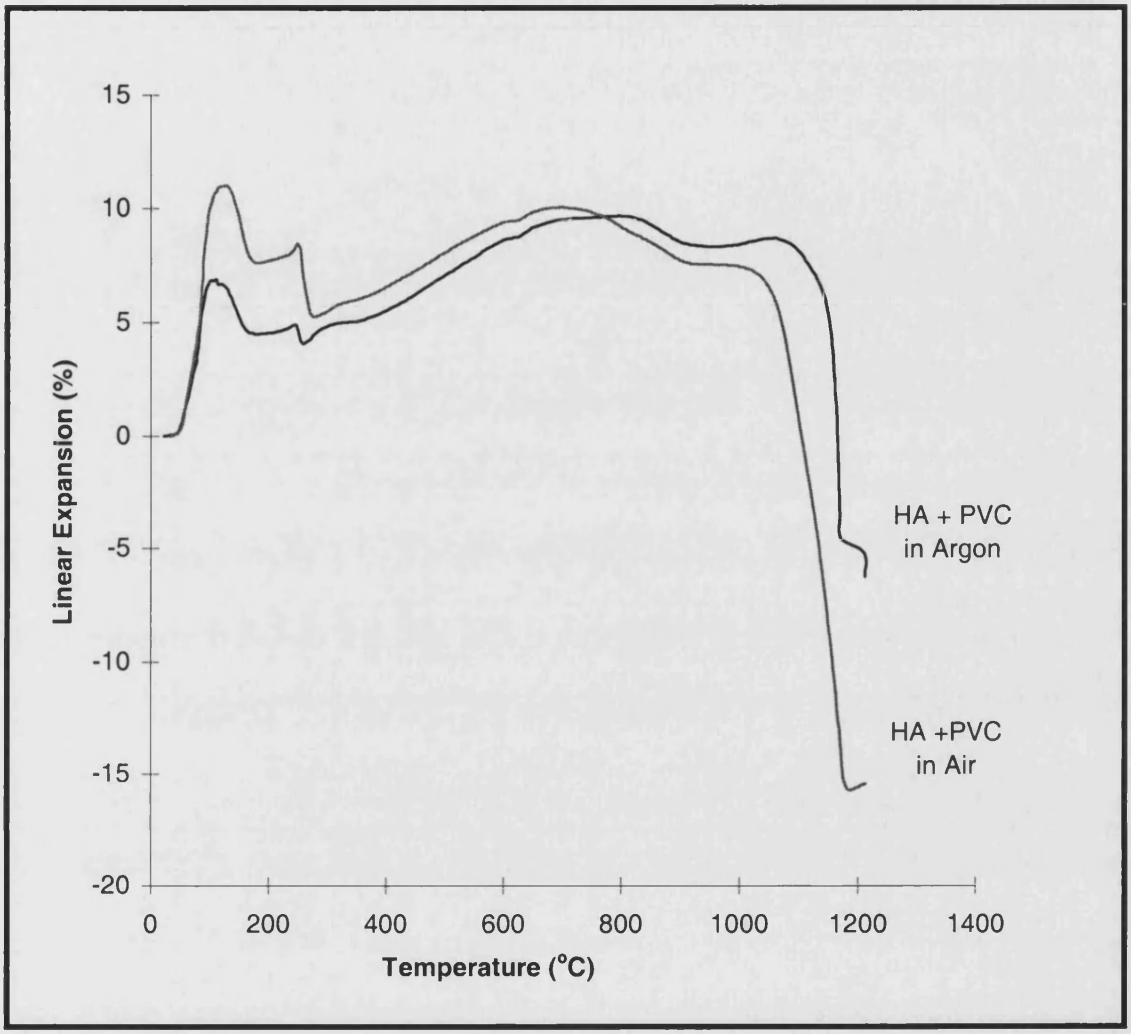

Figure 3.26: Linear shrinkage of hydroxyapatite and poly (vinyl chloride) mixture compact sintered in different environment, air and argon.

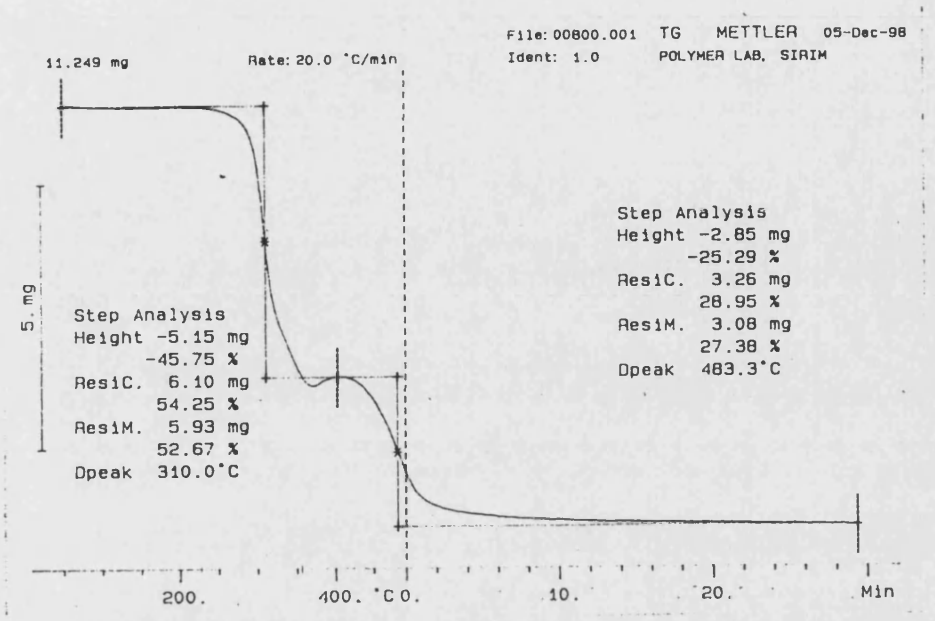

(a)

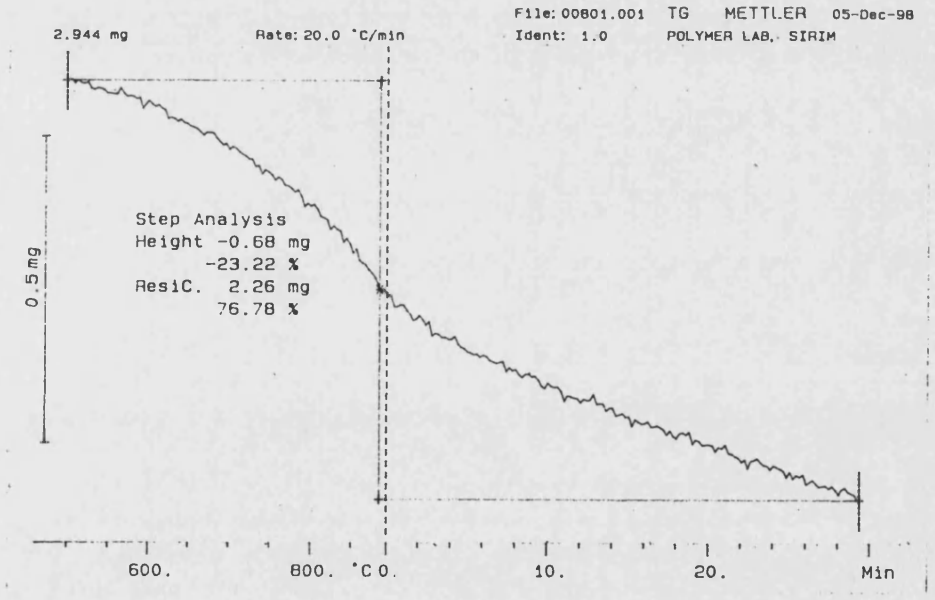

(b)

Figure 3.27: TGA result of PVC fired in argon at 20°C/min, (a) from 50°C to 500°C and (b) 500°C to 900°C.

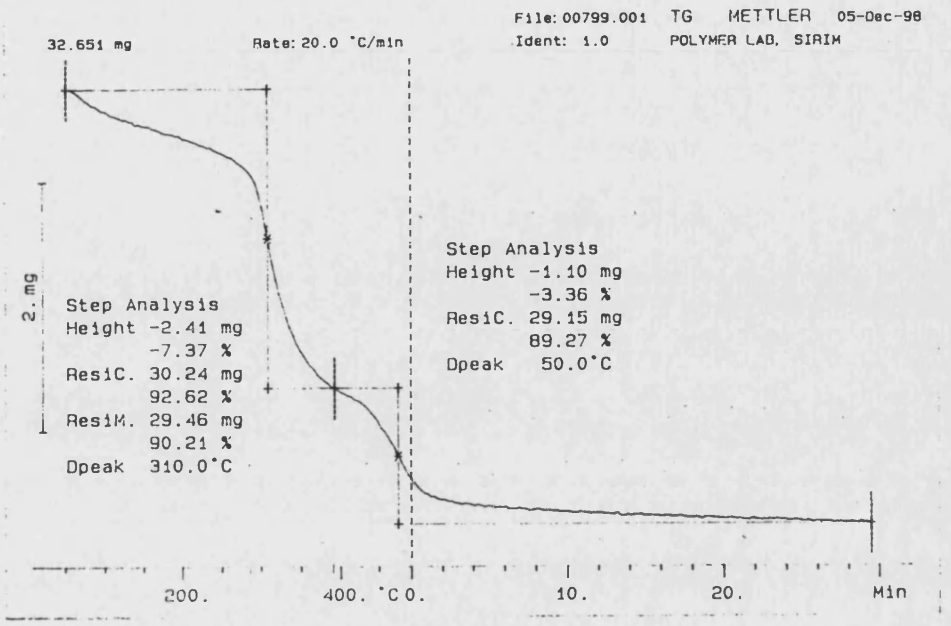

(a)

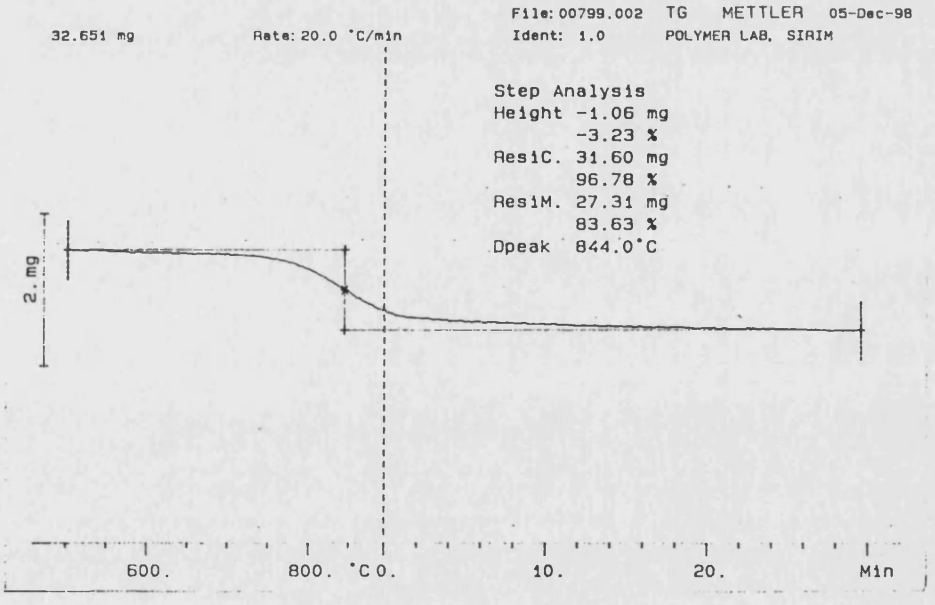

(b)

Figure 3.28: TGA result of hydroxyapatite fired in argon at 20°C/min, (a) from 50°C to 500°C and (b) 500°C to 900°C.

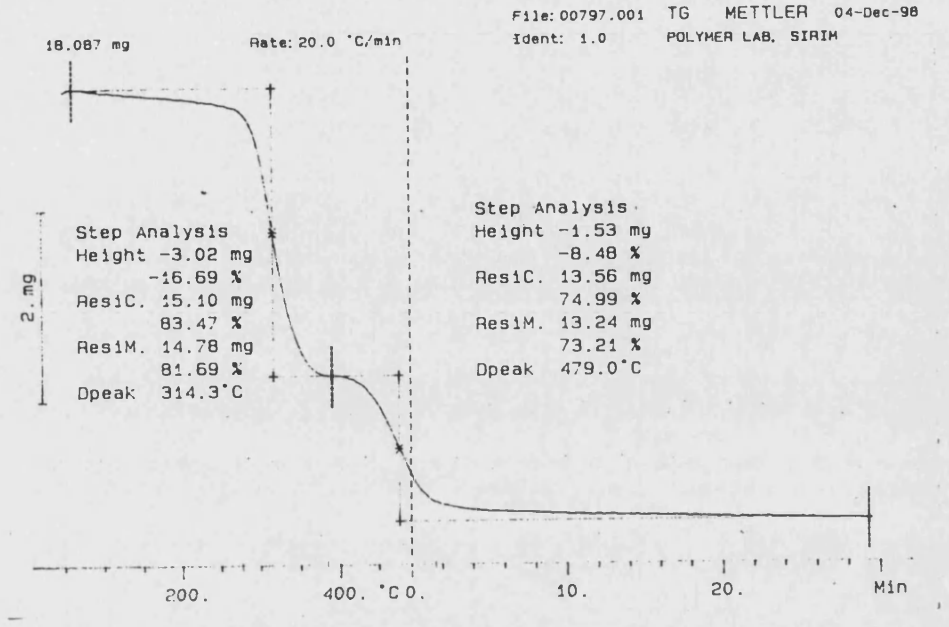

(a)

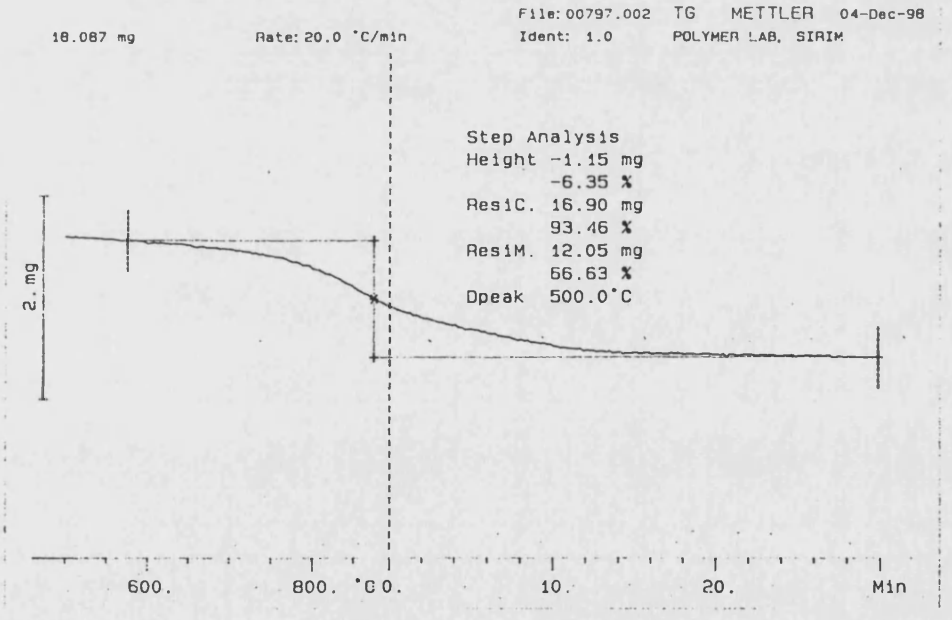

(b)

Figure 3.29: TGA result of hydroxyapatite (64wt%) mixed with PVC (36 wt%) fired in argon at 20°C/min, (a) from 50°C to 500°C, and (b) 500°C to 900°C.

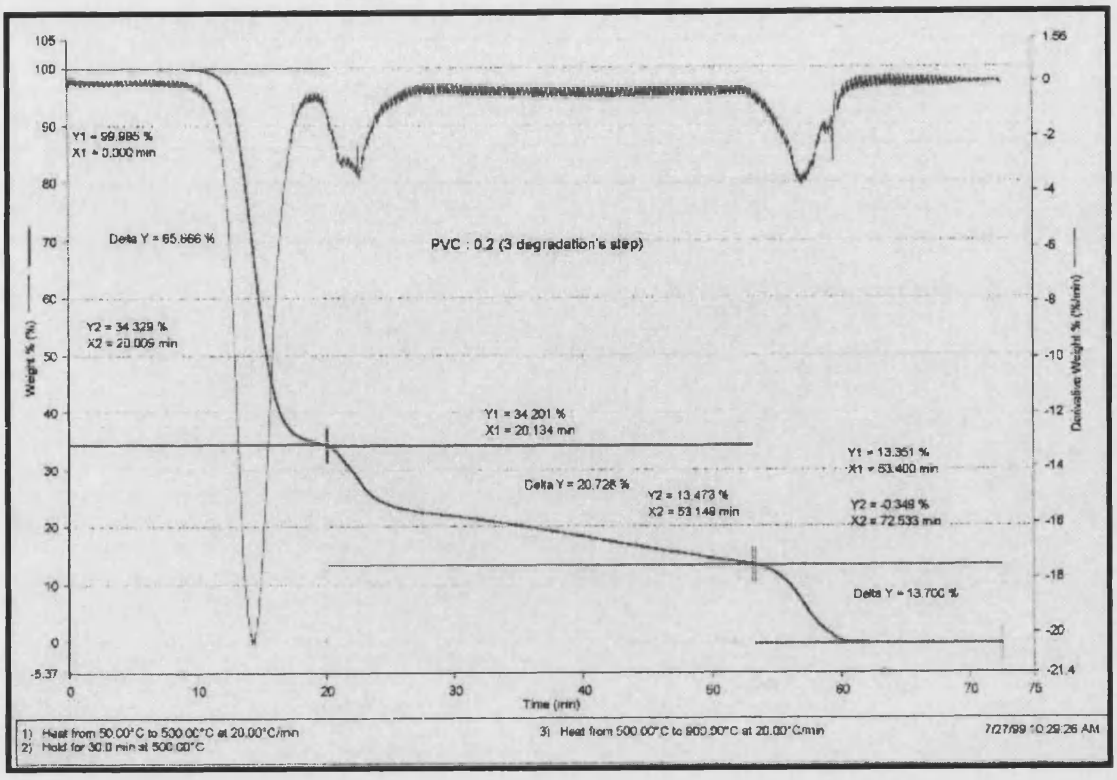

Figure 3.30: TGA and DTA result of PVC fired in air at 20°C/min

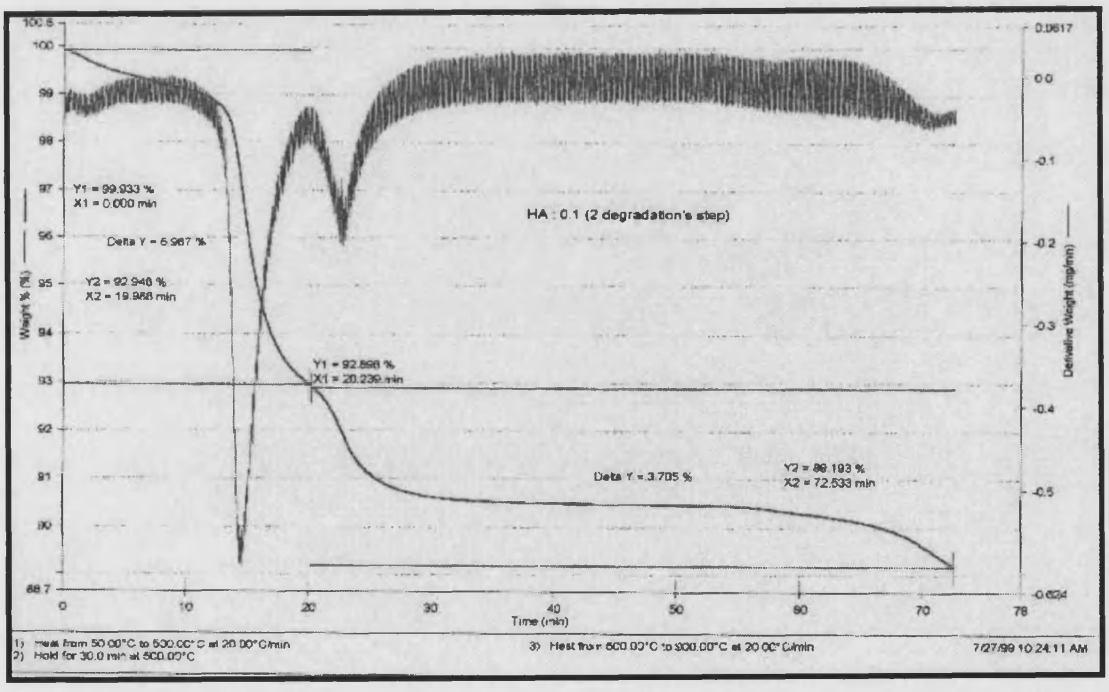

Figure 3.31: TGA and DTA result of hydroxyapatite fired in air at 20°C/min

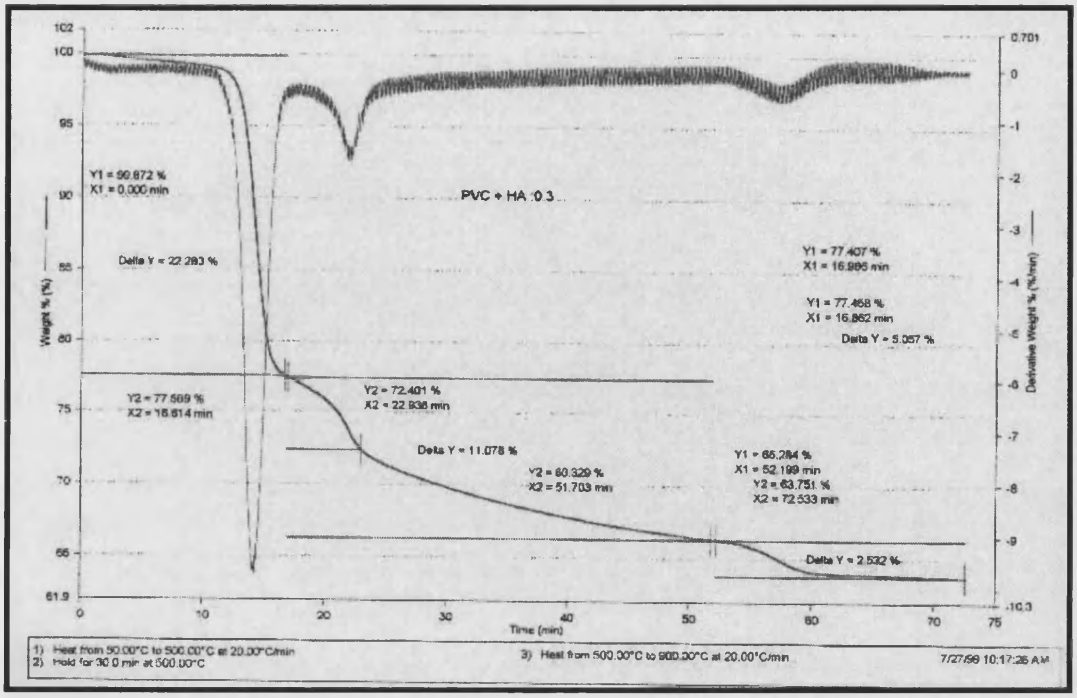

Figure 3.32: TGA and DTA result of hydroxyapatite (64wt%) mixed with PVC (36wt%) fired in air at 20°C/min

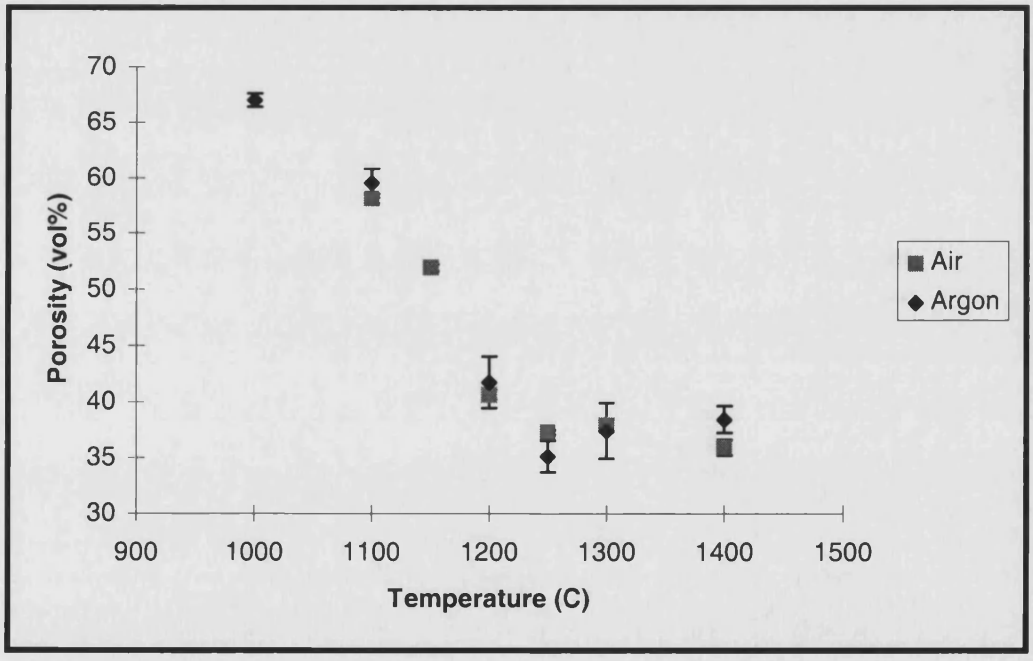

Figure 3.33: Volume fraction of porosity of porous hydroxyapatite sintered in air and argon

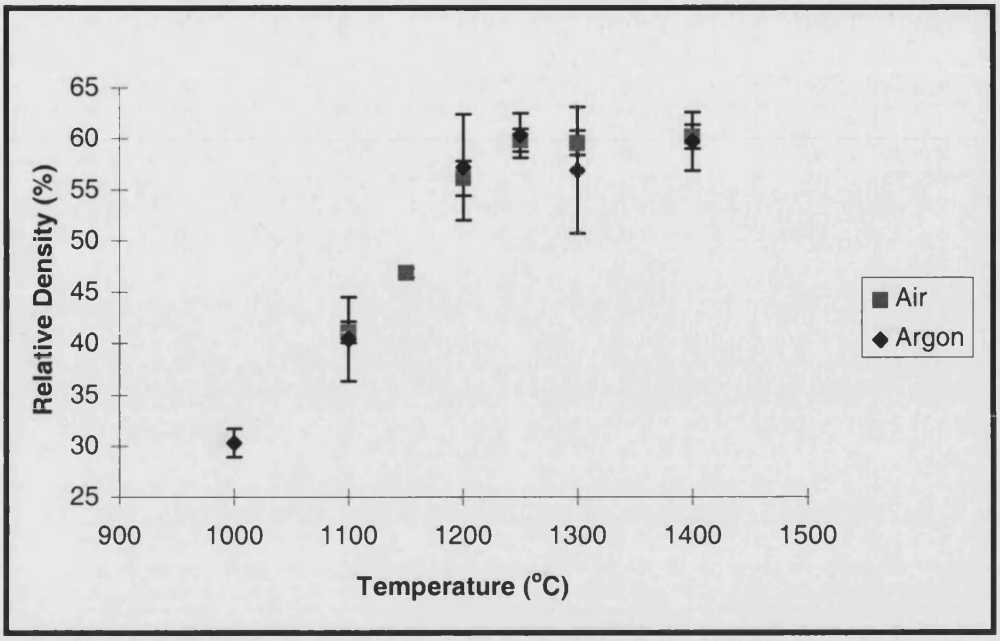

Figure 3.34: Density of porous hydroxyapatite sintered in air and argon

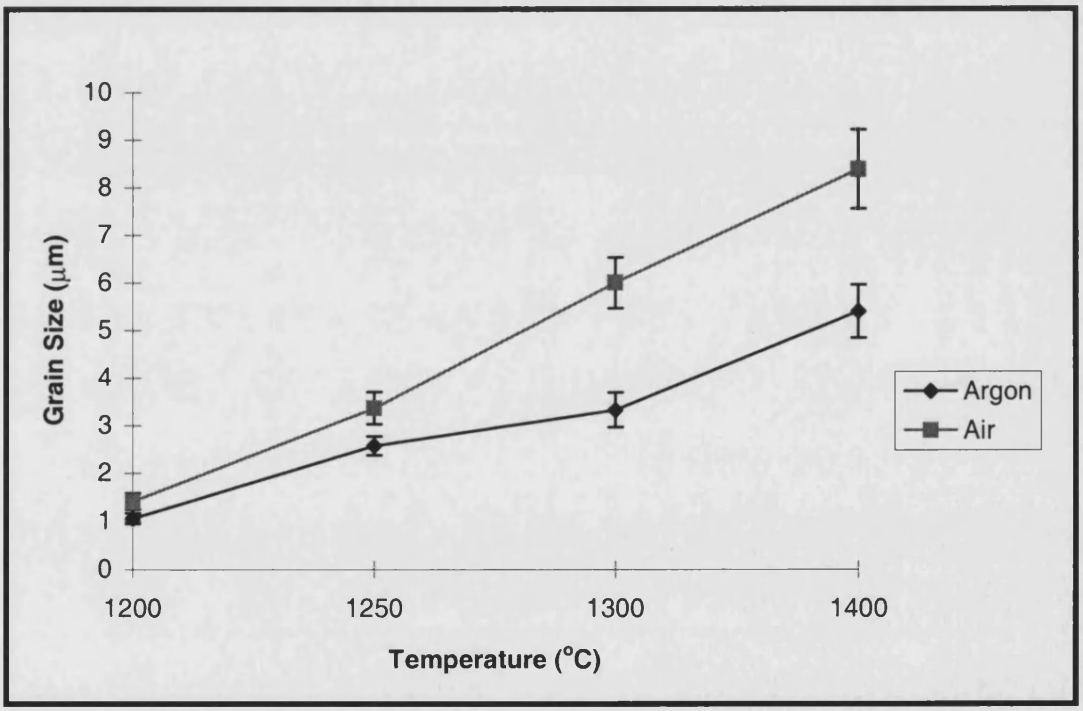

Figure 3.35: Grain size of porous hydroxyapatite sintered in air and argon

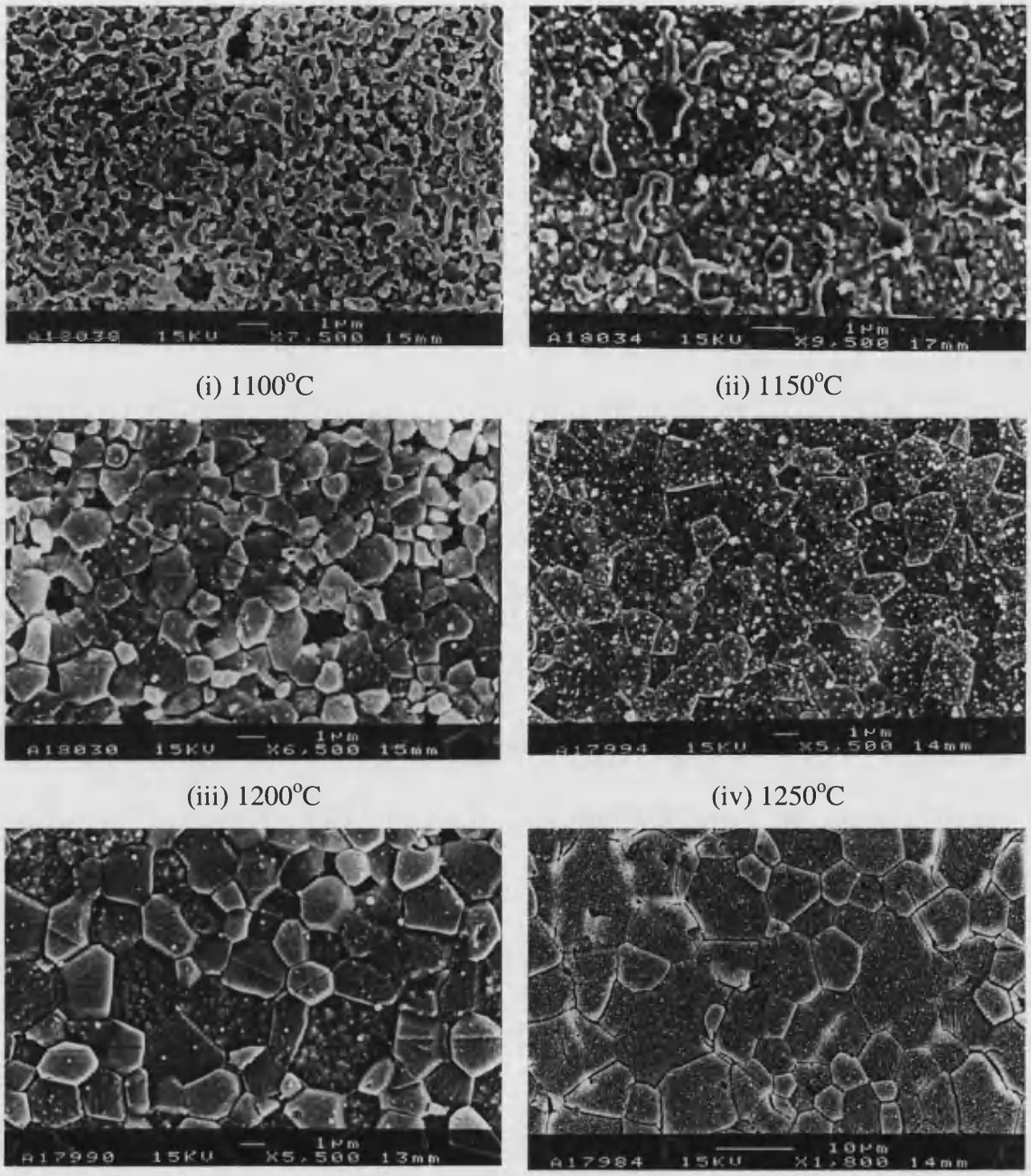

(i) 1100°C (ii) 1150°C

(iii) 1200°C (iv) 1250°C

(v) 1300°C (vi) 1400°C

Figure 3.36: SEM micrographs of porous hydroxyapatite sintered in air for 4h

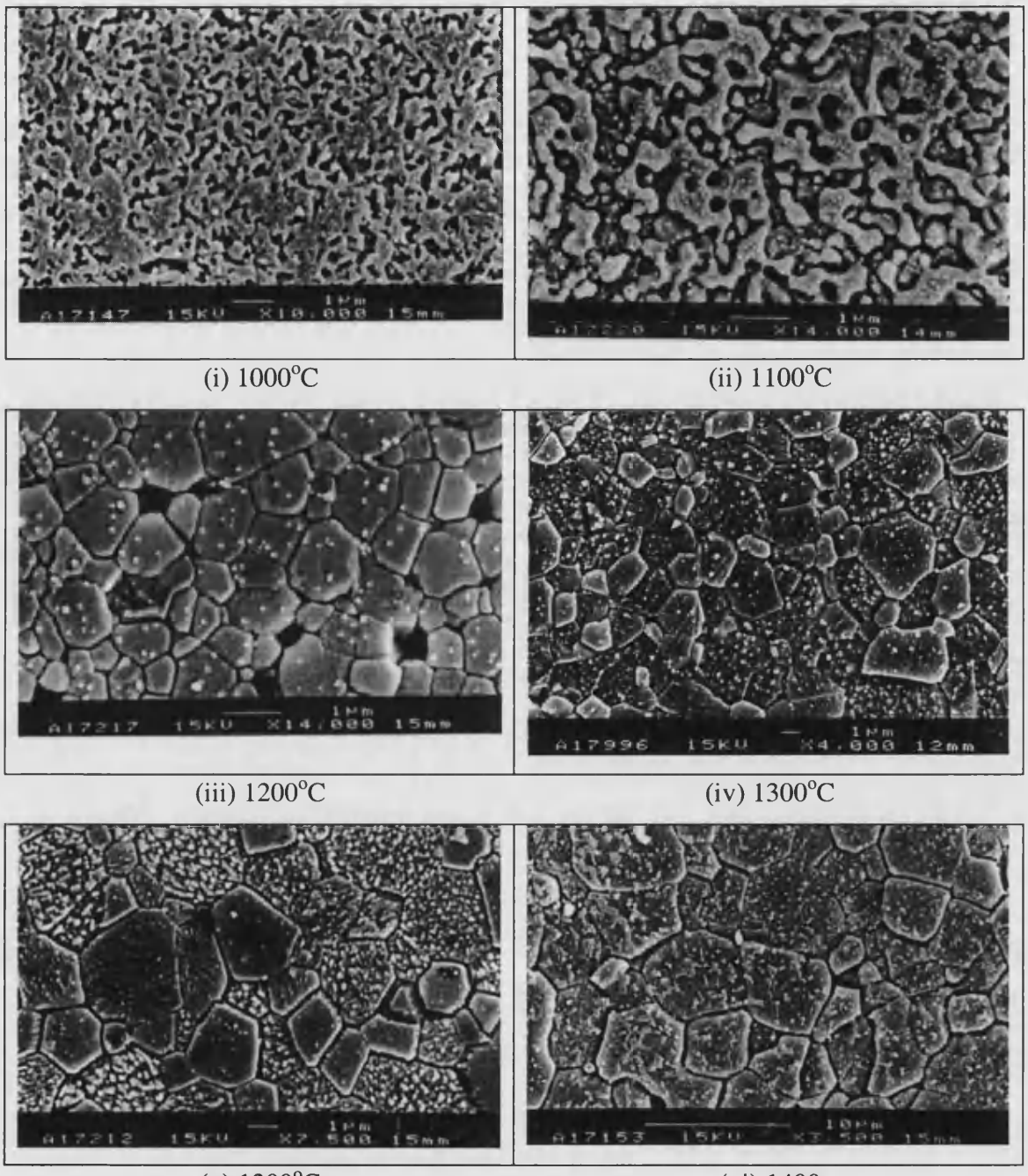

(i) 1000°C (ii) 1100°C

(iii) 1200°C (iv) 1300°C

(v) 1300°C (vi) 1400

Figure 3.37: SEM micrographs of porous hydroxyapatite sintered in argon at different temperatures for 4h.

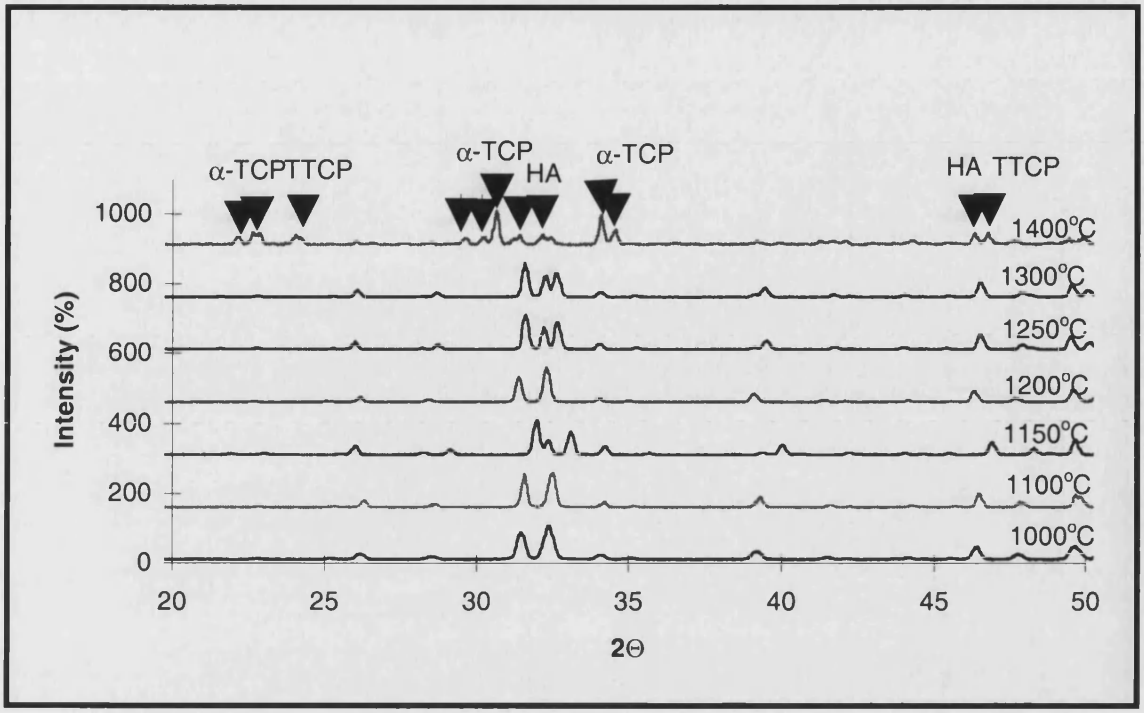

(a)

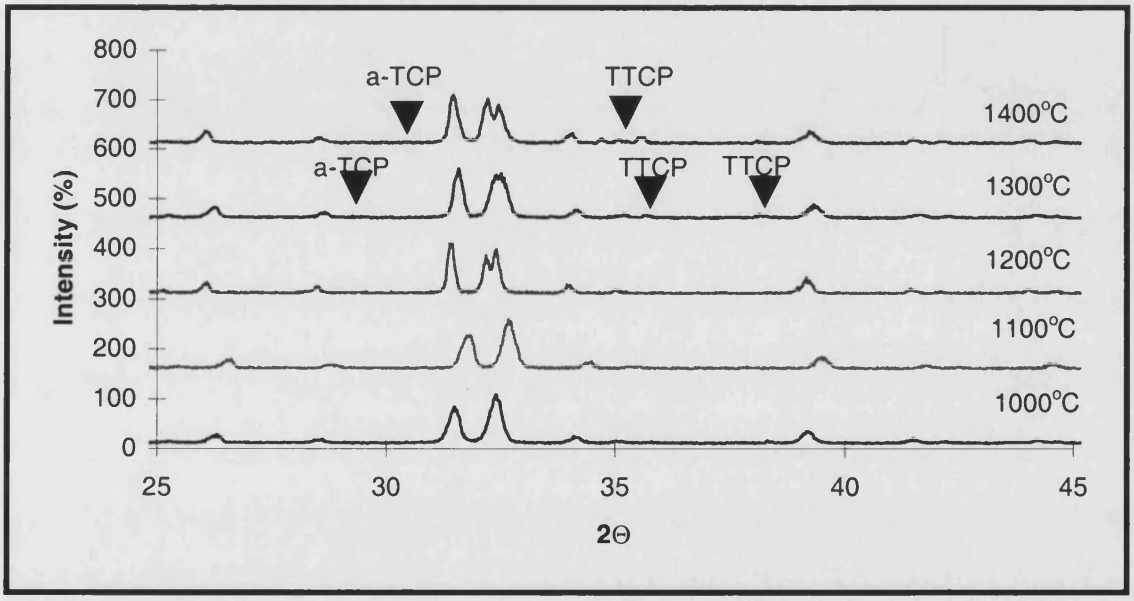

(b)

Figure 3.38: XRD pattern of porous hydroxyapatite ceramic sintered at different temperature with 53 vol% of poly (vinyl chloride) in (a) air (b) argon.

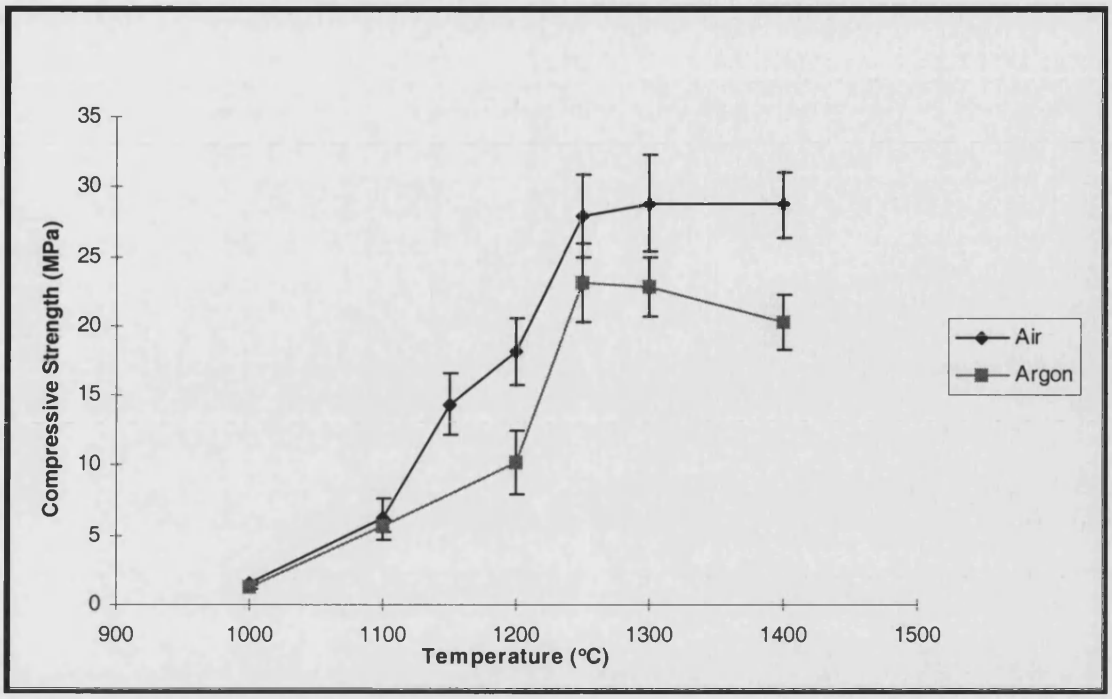

Figure 3.39: Compressive strength of porous hydroxyapatite ceramics sintered for 4h in air and argon.

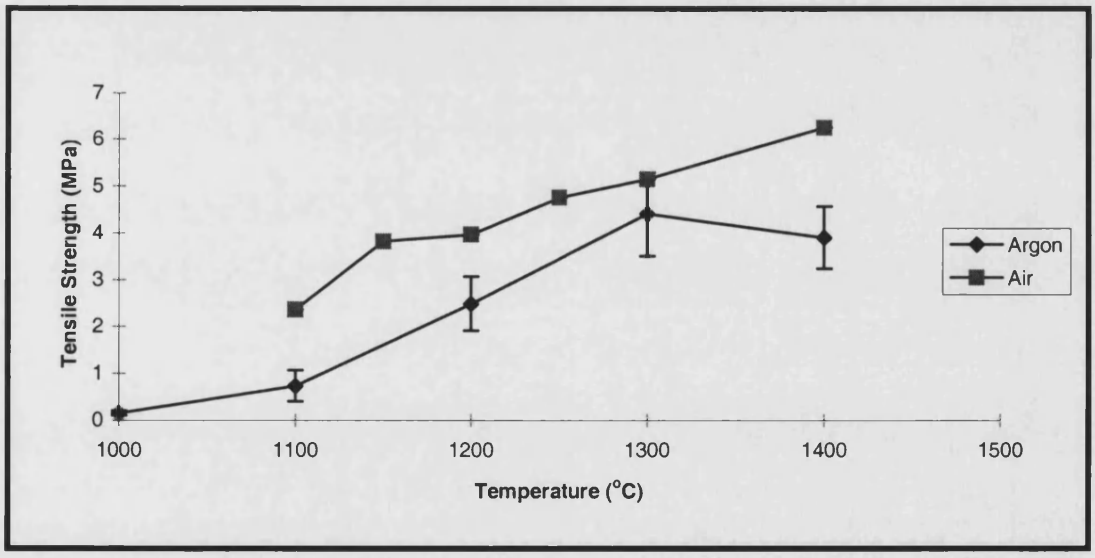

Figure 3.40: Tensile strength of porous hydroxyapatite ceramics sintered in air and argon for 4h.

3.6 Study of the Effect of Different Types Of Polymer

The effect of three types of spherical polymer on the strength of the porous hydroxyapatite was studied. Two grades of poly vinyl chloride with different average molecular weights were used, 200,000 and 78,000 and a poly (vinyl alcohol) (molecular weight: 115,000). The poly vinyl chloride with molecular weight of 200,000 is referred to as high molecular weight PVC (HMWPVC) and the poly vinyl chloride with molecular weight of 78,000 is referred to as low molecular weight PVC (LMWPVC). All the polymers studied had the same particle size (125μm - 150μm) and were almost spherical in shape (Figure 3.41).

The two grades of poly vinyl chloride with different molecular weight were used to study the effect of molecular weight on the end product of the porous hydroxyapatite ceramic. The literature [109] reports that molecular weight does not significantly influence the thermal behaviour. It only changes the physical properties of the polymer such as rigidity. PVA was used to observe the effect of using a different spherical polymer other than poly vinyl chloride, as a porosifier, on the properties of the porous hydroxyapatite.

3.6.1 Effect of different polymer content

3.6.1.1 Microstructural analysis

3.6.1.1.1 Porosity

The porosity of the hydroxyapatite prepared using the three different polymers can be seen in Figure 3.42. The HMWPVC showed a capability of being packed up to 60 vol.% of polymer to produce a green body of hydroxyapatite, but only to 55 vol.% for PVA and

50 vol.% of LMWPVC. After sintering, the porous hydroxyapatite, prepared using LMWPVC was observed to have a higher volume fraction of porosity with the increase of polymer volume than the other polymers. However at 50 vol. % of polymer content, the volume fraction of porosity was the same as the sample prepared using PVA (40 vol.%) but HMWPVC showed a lower volume fraction of porosity (38 vol.%). Only at 53 volume percent of polymer content, HMWPVC could achieve 40 vol.% porosity. At a lower level of polymer content (~25 volume %), both HMWPVC and LMWPVC were observed to have a very low volume fraction of porosity (~1-2 volume %) but for PVA, after sintering for 4h at 1200°C, 10 vol.% of porosity could be detected. The sudden increase of volume fraction of porosity with the increase of the polymer content showed that the pores began to open and became interconnected. The sudden increase in the volume fraction of porosity of LMWPVC, PVA and HMWPVC as observed from the graph occurred at polymer contents of 35, 40 and 45 volume percent respectively.

3.6.1.1.2 Density

The density (Figure 3.43) of the samples prepared using all the three types of polymers showed a similar result. The samples were sintered for 4h at 1200°C. The relative density decreased with the increase in polymer content.

3.6.1.2 Mechanical property analysis

The strength of the porous hydroxyapatite prepared using the three polymers as porosifiers is shown in Figure 3.44. The strength decreases as the porosity increases. At a lower volume fraction of porosity, it was observed that the samples prepared using HMWPVC had the highest strength. As the volume fraction of porosity increases, their strength became lower than samples prepared using LMWPVC and PVA. All the samples were sintered in air at 1200°C for 4h. The porous hydroxyapatite prepared using PVA showed the higher strength in comparison with the two PVCs as the volume fraction of porosity increases. The sample prepared using LMWPVC showed the second highest

compressive strength above that of the HMWPVC. If the graphs were extrapolated, it could be seen that at a higher porosity levels still, the porous hydroxyapatite would possess a similar strength irrespective of which polymer had been used as a porosifier.

The porosity-strength behaviour of the porous hydroxyapatite can be described as;
for LMWPVC,

$$\sigma = 153 \exp. (-0.069P); r^2 = 0.99$$

for PVA,

$$\sigma = 176 \exp. (0.065P); r^2 = 0.95$$

for HMWPVC;

$$\sigma = 191 \exp. (0.098P); r^2 = 0.90$$

The strength of the porous hydroxyapatite was studied in relation to the polymer content (Figure 3.45). Where the macropores are supposed to be present in the same volume, it was observed that samples prepared using HMWPVC showed the highest strength followed by LMWPVC and PVA. However, the strength of the porous hydroxyapatite using PVA seemed to be higher than LMWPVC when $\geq$ 40 vol.% of polymer was introduced. This phenomenon occurred due to the volume of porosity developed in the porous sample. The volume fraction of porosity of the porous hydroxyapatite developed using HMWPVC was always the lowest, thus resulting in the highest compressive strength. The higher the volume fraction of porosity, the lower the strength, especially at a low volume fraction of porosity. As for PVA and LMWPVC, at a low polymer content, the volume fraction of porosity of the samples prepared using LMWPVC were always lower than the PVA until it reached 40 vol.% of polymer content, where both samples showed a similar volume fraction of porosity (~18 vol.%). Above 40 vol.% of polymer content, the volume fraction of porosity of samples prepared using LMWPVC was higher than using PVA, thus resulting in a lower compressive strength.

3.6.2 Effect of different sintering temperatures

3.6.2.1 Microstructural analysis

3.6.2.1.1 Porosity

With the results obtained from Figure 3.42 above, further samples were prepared using the three polymers but with the same volume fraction of porosity. The amount of polymer used to obtain similar volume fraction of porosity was, 50 vol.% for LMWPVC, 53 vol.% for HMWPVC and 55 vol.% of PVA. From Figure 3.46, it was observed that the volume fraction of porosity of the LMWPVC and HMWPVC were almost the same but this was not the case for PVA. Porosity for samples prepared using HMWPVC and LMWPVC was high (~65 vol.%) at 1000°C and decreased drastically (35 vol.%) as the temperature increased to 1200°C. The volume fraction of porosity reached equilibrium at 1250°C with a volume fraction of porosity of ~35%. Only slight changes of volume fraction of porosity occurred as the temperature increased above 1250°C. Samples prepared using PVA showed a higher volume fraction of porosity than samples prepared using PVC. At 1100°C, the volume fraction of porosity for PVA was 65 % whereas for PVC it was ~57 %. The difference in volume fraction of porosity between samples prepared using PVA and PVC remained ~7-8 % as the temperature increased. At ≥1250°C, the volume fraction of porosity of the samples prepared using PVA showed an almost stable volume fraction of porosity (~39 %) of the porous HA after the rapid decrease of the volume fraction of porosity from 1100°C. There was no significant decrease of volume fraction of porosity as the temperature increased above 1250°C. The volume fraction of porosity of this sample at the temperature ≥1250°C was ~5 volume % higher than samples prepared using PVC.

From Figure 3.47, it was observed that the size of the macropores of the porous hydroxyapatite reduced as the temperature increased. The polymers had a starting size of between 125 μm and 150 μm and were sintered for 4 hours at different temperatures.

Samples prepared using PVA showed less shrinkage of the pores as the temperature increased and the pore size remained high in comparison to the samples prepared using PVC. At 1200°C, the pore size of samples prepared using PVA was ~120μm but for LMWPVC and HMWPVC was only ~85 and 88μm respectively. The difference of size between PVA and PVC was >30 μm. No explanation could be given for this. The pores in samples prepared using HMWPVC and LMWPVC showed little difference in size.

3.6.2.1.2 Density

The relative density of the porous hydroxyapatite (Figure 3.48) increased as the temperature increased. At 1100°C, samples prepared using LMWPVC and HMWPVC have the same relative density (~41%) but PVA showed a lower relative density (~33%). The density increased rapidly as the temperature increased and reached equilibrium at ~1250°C where the sample prepared using LMWPVC showed the highest density (~62 %) followed by HMWPVC (60%) and PVA (58 %). No significant increase in density was observed above 1250°C.

3.6.2.1.3 Grain size

The grain size for samples sintered using both HMWPVC and LMWPVC, shown in Figure 3.49, showed a similar grain growth as the temperature increased. In comparison, the samples sintered using PVA as a porosifier, showed a higher grain size as the temperature increased. For example, at 1300°C, the samples prepared using both types of PVC showed a grain size of ~3 μm, but the PVA has a grain size ~9 μm, which is three times greater. From the EDAX result (Figure 3.50), it was detected that samples prepared using PVC, at both molecular weights, had chlorine present as an impurity. The quantity could not be calculated as there was no standard available.

The chlorine was not reacting with the hydroxyapatite as from the TEM and EDAX result (Figure 3.51) there were no traces of chlorine found in the grains. The presence of

chlorine was suspected to be at the grain boundary, but due to the difficulty of preparation, a detailed study could not be made.

The porous hydroxyapatite prepared using PVA (Figure 3.52) did not show any presence of impurities. From this result, it could be asserted that the presence of chlorine retards the grain growth of the porous hydroxyapatite.

3.6.2.1.4 SEM micrographs

The microstructure of the porous hydroxyapatite prepared using LMWPVC and PVA is seen in Figures 3.53 and 3.54. From the micrographs, the increase of the grain size of the porous hydroxyapatite as the temperature increases and the difference of grain size between samples prepared using PVC and PVA could be observed.

As seen in Figure 3.55, the samples prepared using PVA as porosifier have three sizes of pores, large (~120μm), medium (~10μm) which is almost the same size of the grain itself and small (~1 μm). The large pores originate from the PVA introduced and the small pores are the residual pores from sintering. Both types of pores as mentioned above could also be found in samples prepared using PVC (Figure 3.56). The medium pores were only present from the preparation using PVA. As the study using pure hydroxyapatite sintered using the same sintering cycle did not produce the medium pore size, it is assumed that the pores originate from the decomposition of the PVA.

3.6.2.1.5 X-ray diffraction

Porous hydroxyapatite prepared using either PVA or PVC was observed to decompose at a high temperature, 1400°C (Figure 3.57 and Figure 3.58). The hydroxyapatite decomposed to α-TCP and TTCP from hydroxyapatite. No decomposition was detected using XRD at a temperature lower than 1400°C.

3.6.2.2 Mechanical property analysis

The strength of the porous hydroxyapatites showed different results for all the polymers used as a porosifiers (Figures 3.59 and 3.60). It was observed that the samples prepared using PVC had a higher strength than samples prepared using PVA. This was due to the higher volume fraction of porosity of the samples prepared using PVA. The strength of the porous hydroxyapatite prepared using different molecular weight PVCs differed. It was observed that the samples prepared using HMWPVC had higher tensile and compressive strengths.

3.6.3 Discussion

The effect of introducing different types of polymer into hydroxyapatite powder to act as porosifier was examined in this study. Three polymers were used to create a porous hydroxyapatite. The effect of the polymer content and temperature on the microstructure and mechanical properties was studied.

From the results of the experiments, it was observed that the polymers produced different volumes of porosity depending on the amount of polymer introduced. Even when the same volume of polymer was introduced e.g. 45vol.%, the levels of porosity that resulted were ~11 vol% (HMWPVC), 25 vol% (PVA) and 32 vol% (LMWPVC). Among the influencing factors was the amount of macro and microporosity developed after sintering. The amount of macroporosity should be the same due to the amount of polymer introduced but the volume fraction of the microporosity was different. Although the results could not be shown quantitatively, these findings could be observed qualitatively from the SEM results in Figure 3.61. Using this observation, the result of the porosity levels in relation to strength of the porous hydroxyapatite utilising different polymers could be explained. The strength of samples prepared using PVA showed a higher

strength in comparison to the HMWPVC and LMWPVC. This was due to the total porosity which was the total volume of macro and microporosity. As known from results in Chapter 4, the greater the pore size, the lower the mechanical strength would be. Since samples prepared using PVA had a greater volume fraction of microporosity but a lower volume fraction of macroporosity than LMWPVC and HMWPVC to make the total volume, at the same total porosity level, PVA would show a greater strength than the other two.

When the studied was continued at different temperatures, it was found that the samples prepared using HMWPVC and LMWPVC showed almost similar results in term of their microstructures, but this was not the case for PVA. The samples prepared using PVA showed a bigger macropore size and grain size , which also resulted in a lower strength. The retardation of grain growth of the porous hydroxyapatite when using PVC was thought to be due to the effect of chlorine impurities present after the sintering. The chlorine was assumed to originate from the decomposition of the PVC. The decomposition of PVA does not produce chlorine; the main product loss during decomposition is water [97].

LMWPVC and HMWPVC as polymer powders do not show a significant difference in properties other than that LMWPVC is slightly softer than HMWPVC. When sintered at different temperatures with hydroxyapatite, the porous ceramic obtained showed a lower strength for porous hydroxyapatite fabricated using LMWPVC. From Figure 3.62, it was observed that samples prepared using LMWPVC showed an agglomeration of pores due to the agglomeration of the polymer powder during packing of the powder prior to pressing. This would result in larger voids in the porous ceramic which would result in a weaker specimen. Samples prepared using HMWPVC showed a more even dispersion of pores in the porous ceramic.

3.6.4 Summary

1. The maximum amount of polymer that could be mixed with the hydroxyapatite powder, formed and sintered without breaking was found to be highest using HMWPVC powder, followed by PVA and LMWPVC.
2. With a higher polymer packing capability, a higher volume fraction of porosity could be achieved.
3. The three polymers used as porosifiers showed similar relative densities after sintering for 4h at 1200°C with different polymer content.
4. Although using PVA as a porosifier would seem to result in a higher compressive strength, it was observed that this was influenced by the total porosity which included both the micro- and macroporosity. The higher the volume of macroporosity, the lower the strength of the porous ceramic.
5. When the compressive strength was studied in relation to the polymer content, it showed that the sample using HMWPVC had the highest strength of the three.
6. The grain size of samples prepared using PVA was bigger than those produced using PVC due to the effect of chlorine impurities.
7. Samples prepared using PVA had three sizes of pores after sintering, macro (~120μm), medium (10μm) and micro (1μm). Using PVC resulted in two sizes of pores, macro (~90μm) and micro (~1μm).
8. Samples produced using PVA showed a larger final size of macropores.
9. The porous hydroxyapatite produced using all the three polymers as a porosifier started to decompose at 1400°C.
10. Porous hydroxyapatite prepared using HMWPVC showed the highest compressive and tensile strength in comparison to samples produced using LMWPVC and PVA.

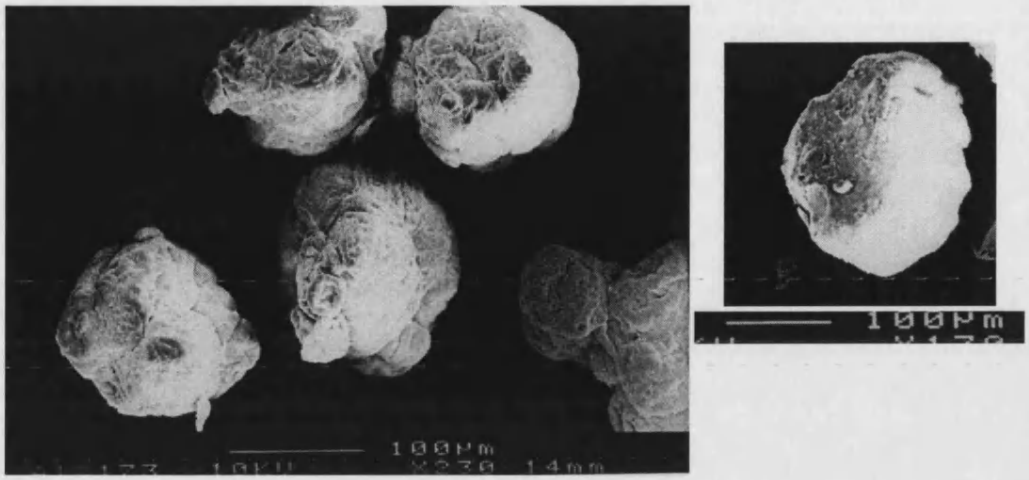

(a) (b)

Figure 3.41: Scanning electron micrographs of polymers powder used as a porosifier in producing porous hydroxyapatite ceramic: (a) poly (vinyl chloride) and (b) poly (vinyl alcohol).

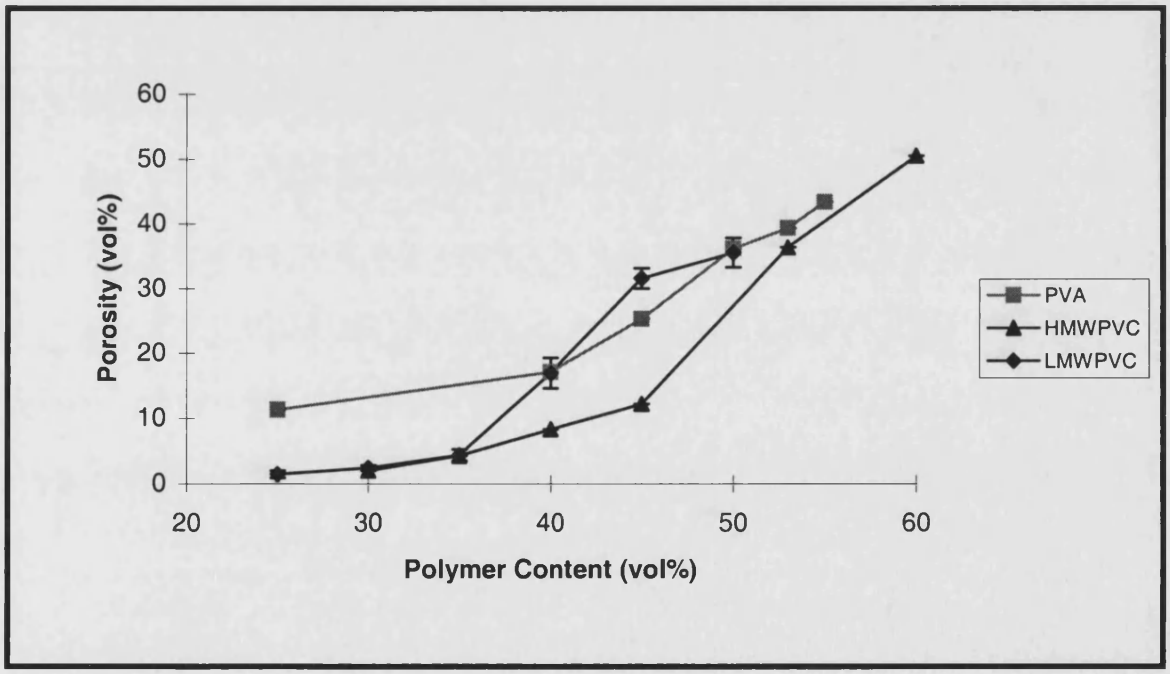

Figure 3.42: Volume fraction of porosity of porous hydroxyapatite after sintering for 4h at 1200°C at different percentage of polymer content.

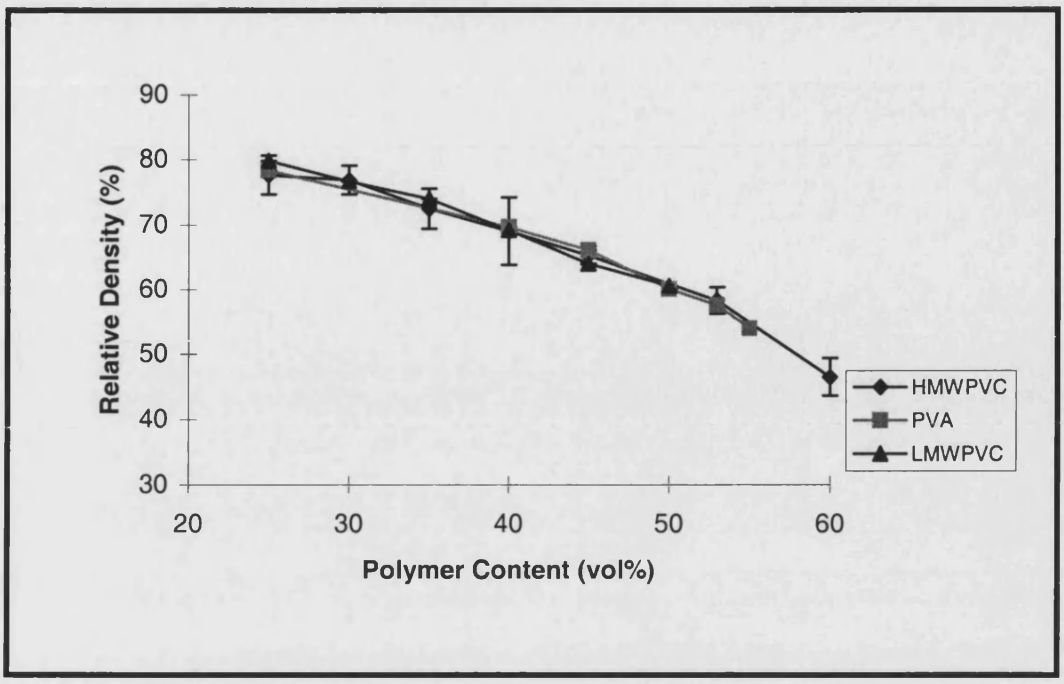

Figure 3.43: Density of porous hydroxyapatite at different polymer content after sintering at 1200°C for 4h.

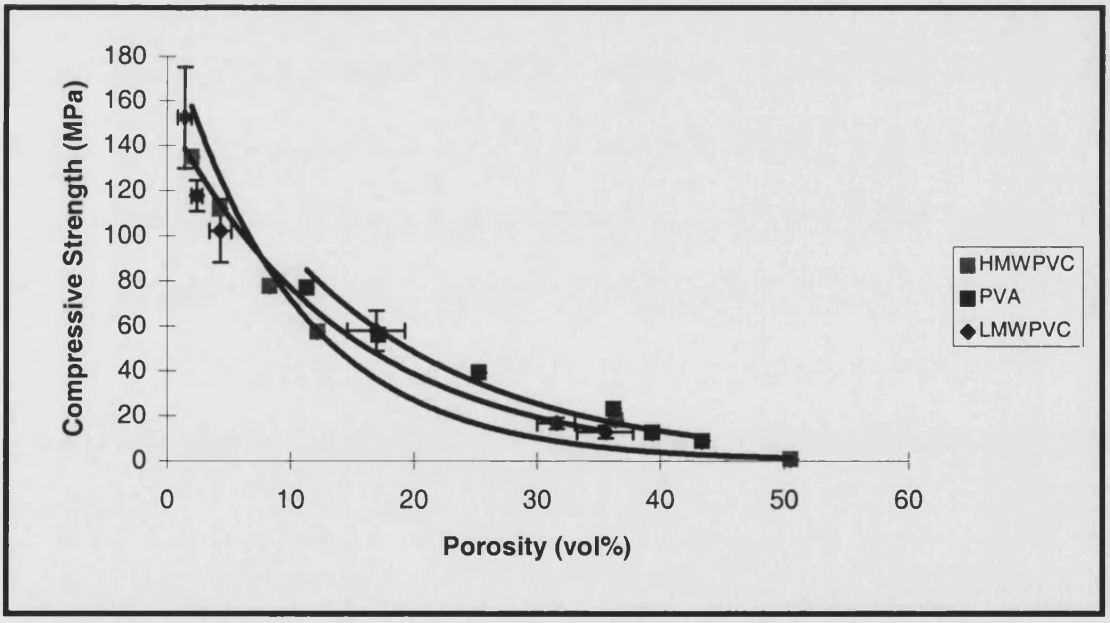

Figure 3.44: Compressive strength of porous hydroxyapatite after sintering for 4h at 1200°C using three types of polymer as a porosifier; HMWPVC, LMWPVC and PVA.

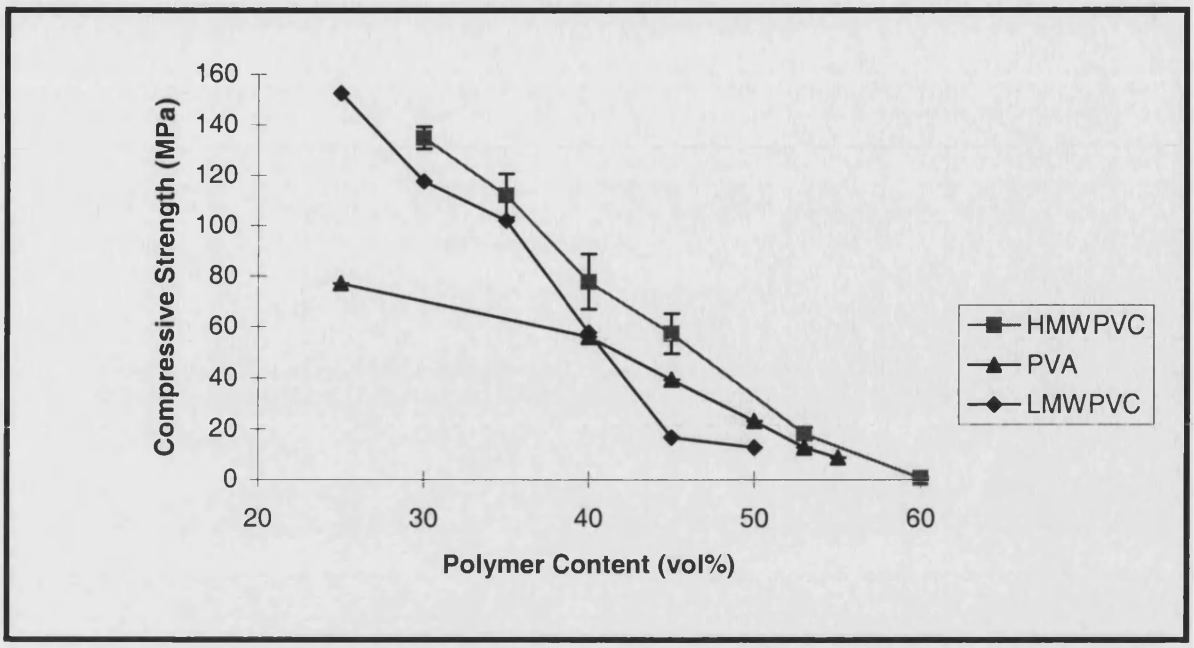

Figure 3.45: Compressive strength of porous hydroxyapatite sintered for 4h using different volume % of polymer content.

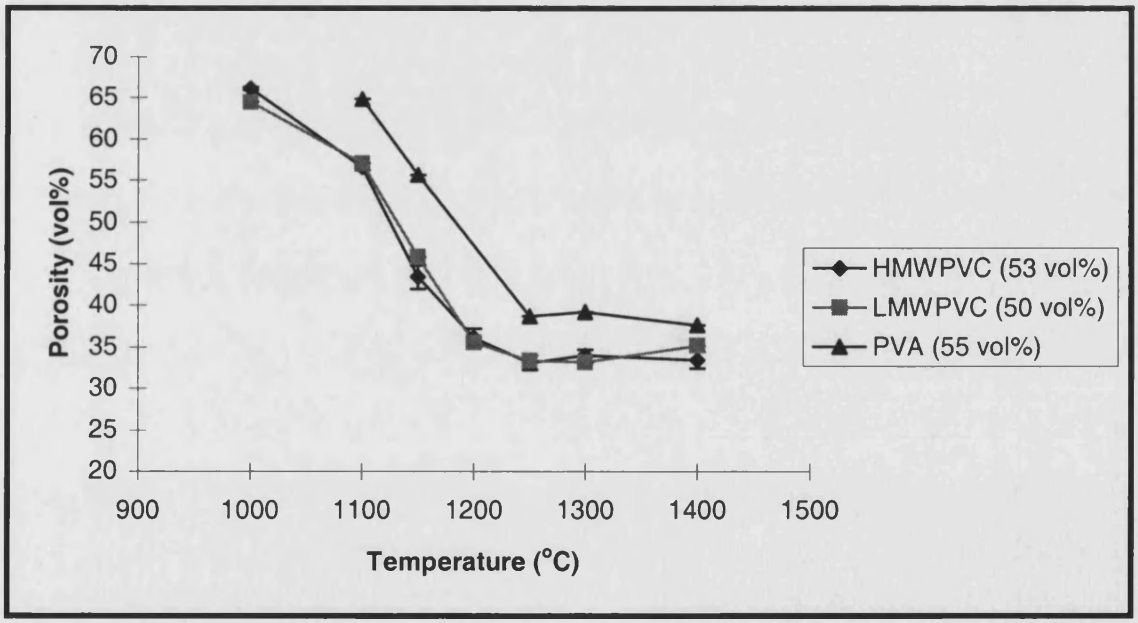

Figure 3.46: Volume fraction of porosity of the porous hydroxyapatite after sintering at different temperatures

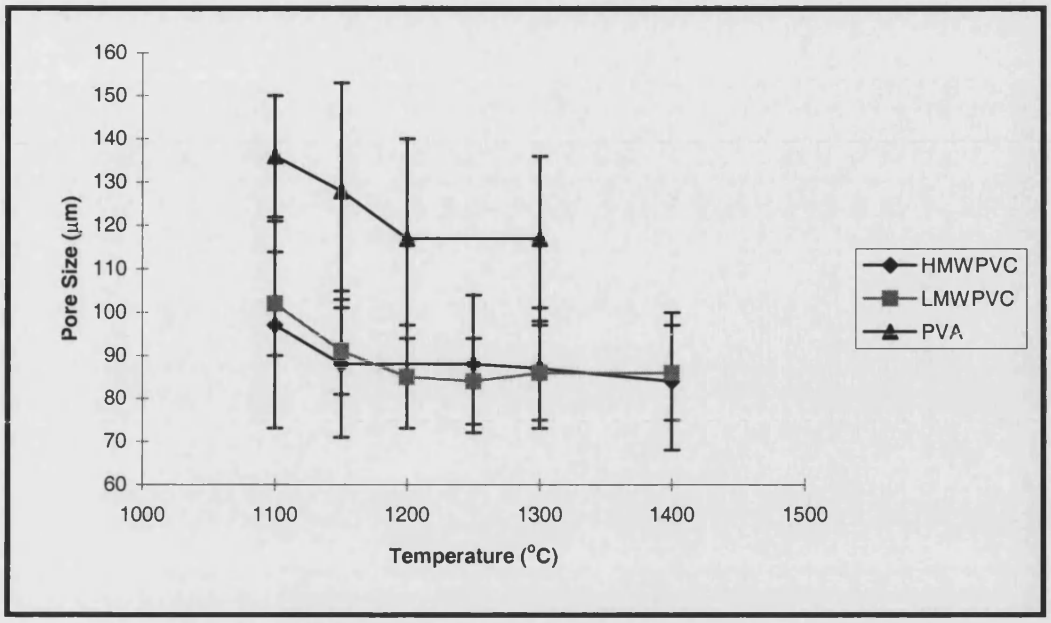

Figure 3.47: Size of macropores after sintering at different temperatures for 4h using different types of polymers with a starting size of 125μm - 180μm.

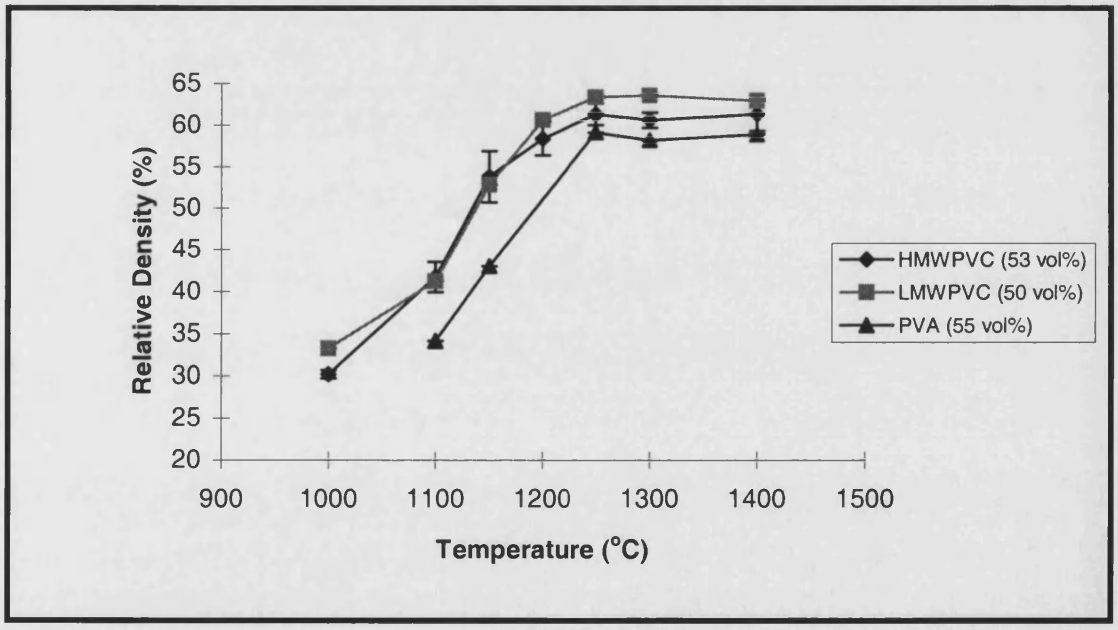

Figure 3.48. Relative density of porous hydroxyapatite using different types of polymers at different sintering temperatures.

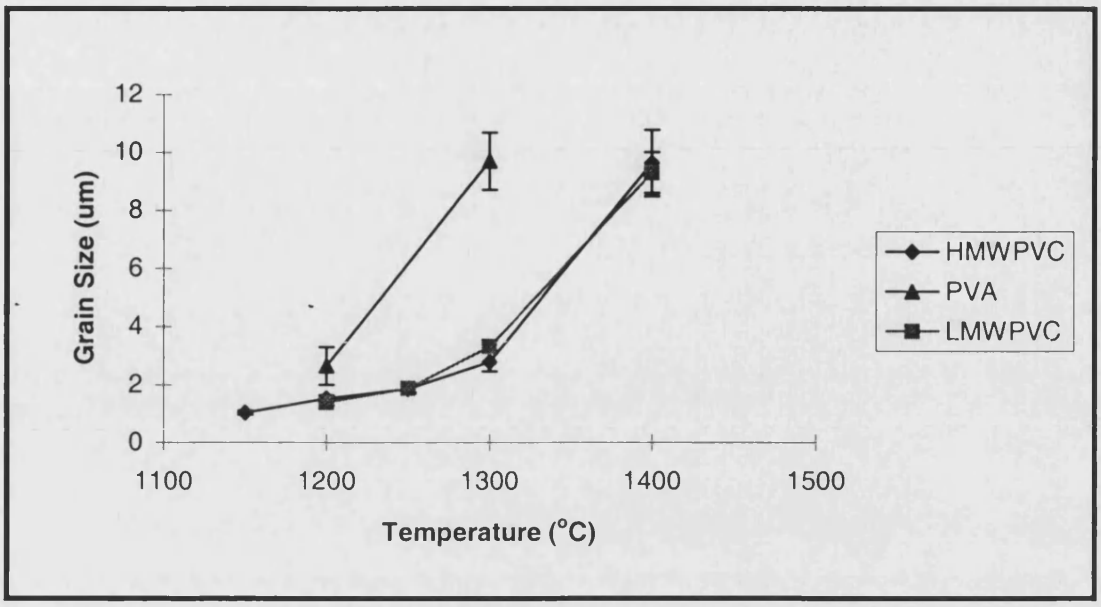

Figure 3.49: Grain size of porous hydroxyapatite sintered for 4h at different temperatures using different polymers.

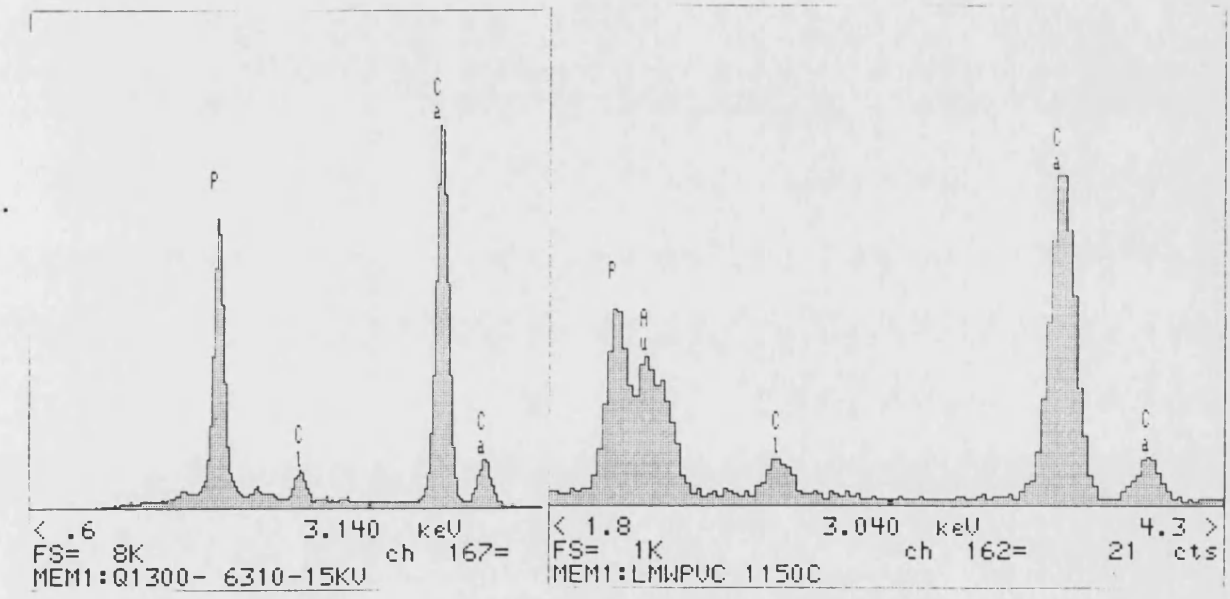

(a) (b)

Figure 3.50: EDAX result of samples prepared using (a) HMWPVC and (b) LMWPVC, as a porosifier.

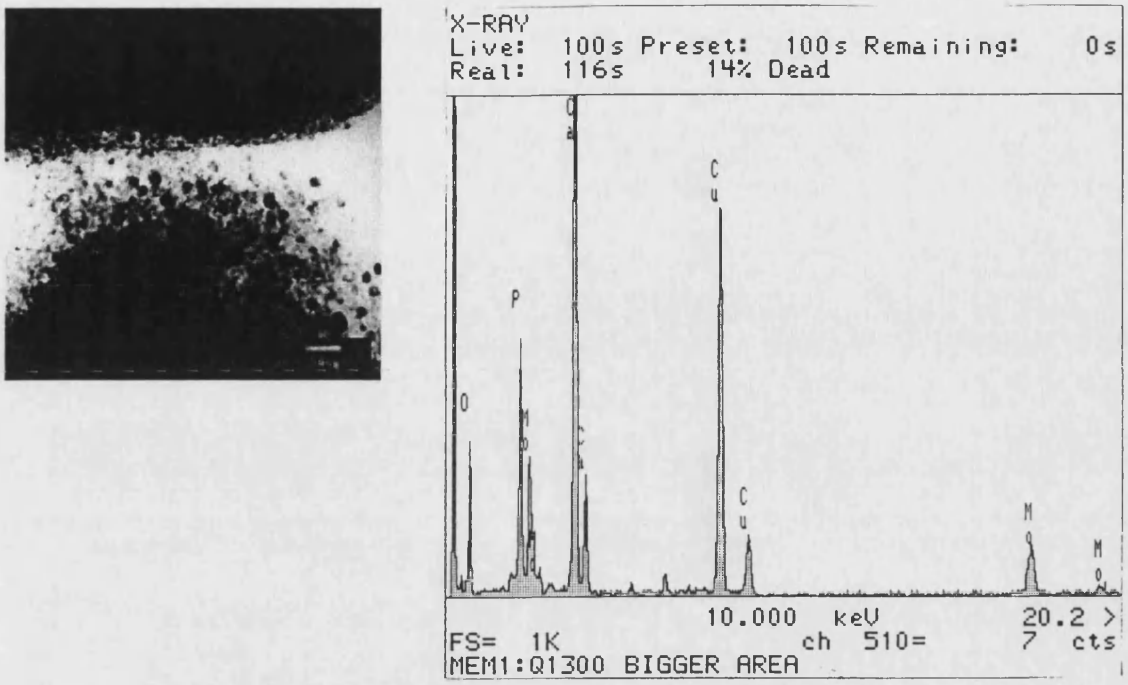

(a) (b)

Figure 3.51: (a) TEM micrograph and (b) EDAX result from porous hydroxyapatite prepared using PVC as a porosifier.

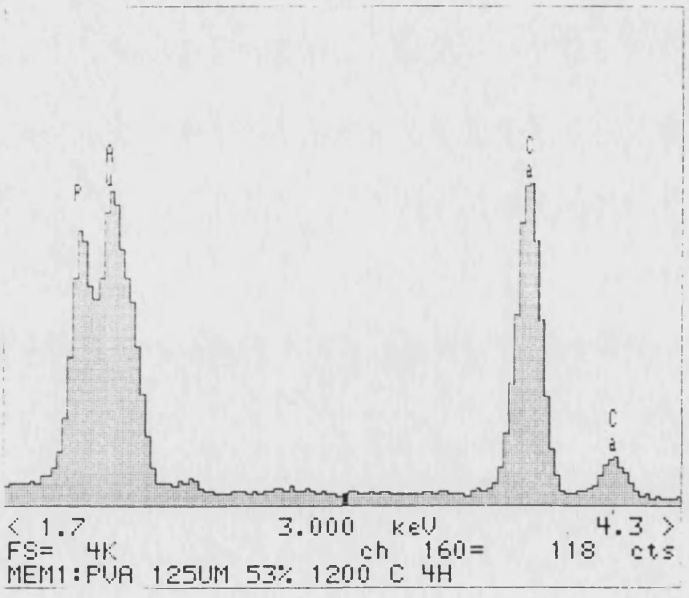

Figure 3.52: EDAX result of porous hydroxyapatite prepared using PVA as a porosifier.

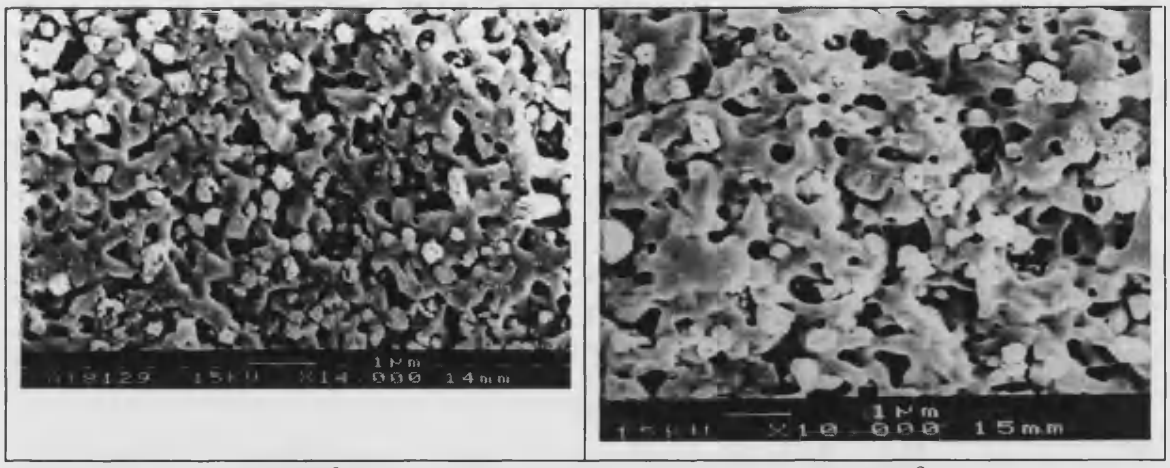

(i) 1000°C (ii) 1100°C

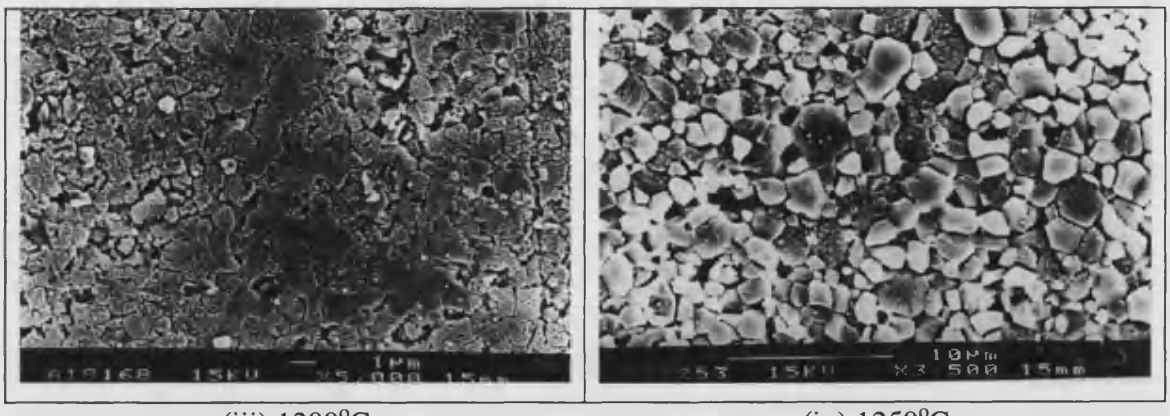

(iii) 1200°C (iv) 1250°C

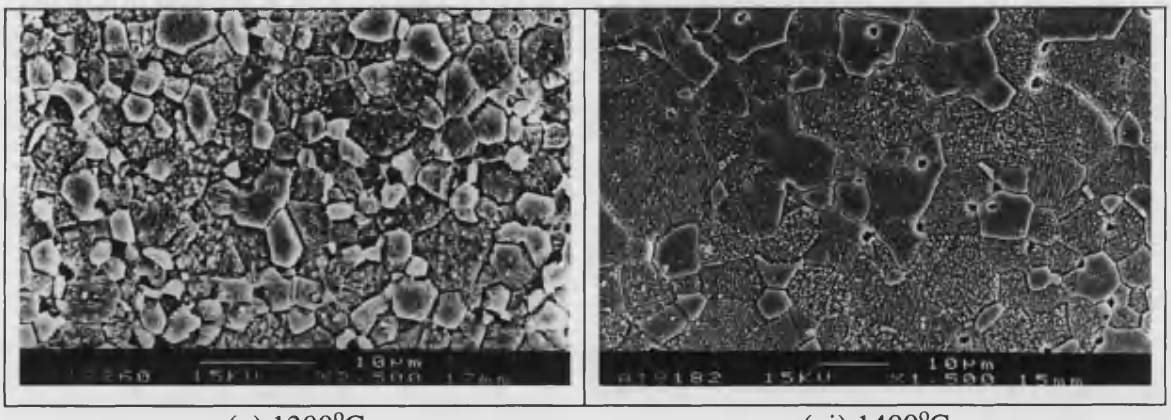

(v) 1300°C (vi) 1400°C

Figure 3.53: SEM micrographs of porous hydroxyapatite prepared using LMWPVC as a porosifier at different sintering temperatures.

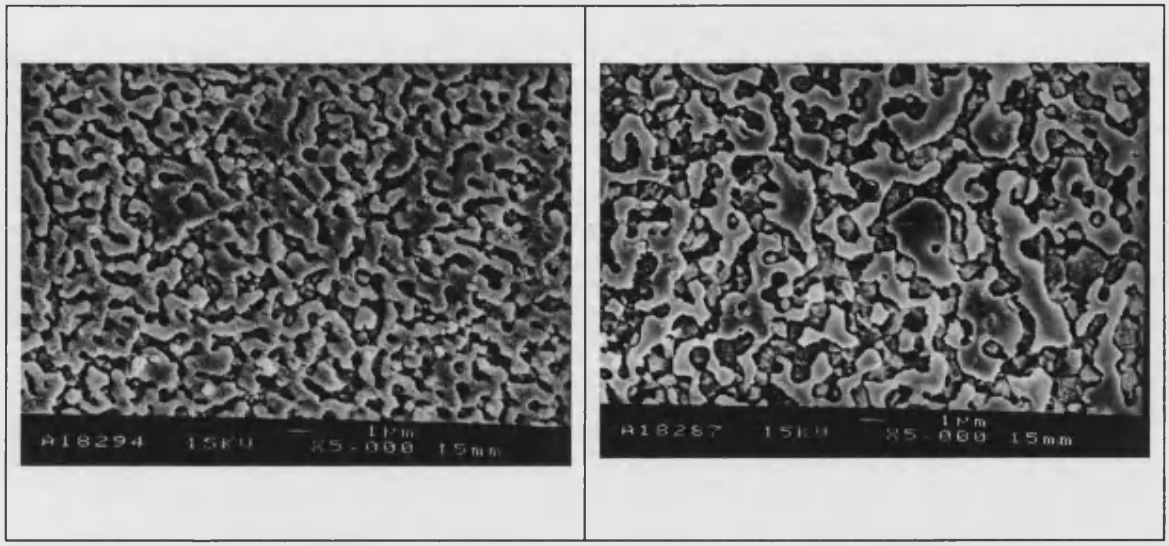

(i) 1100°C (ii) 1150°C

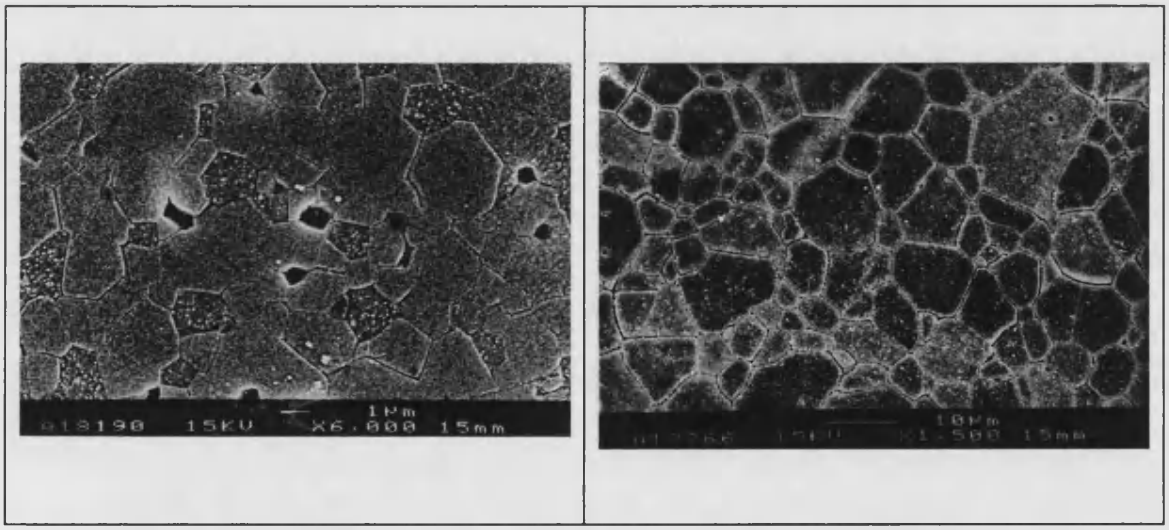

(iii) 1200°C (iv) 1300°C

Figure 3.54: SEM micrographs of porous hydroxyapatite prepared using PVA as a porosifier at different sintering temperatures.

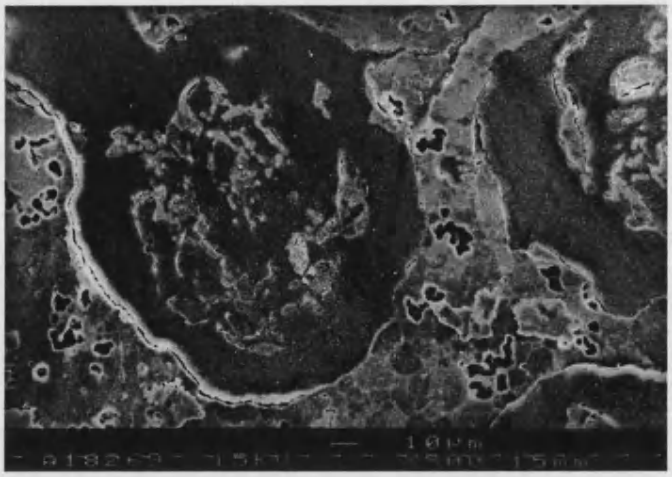

(a)

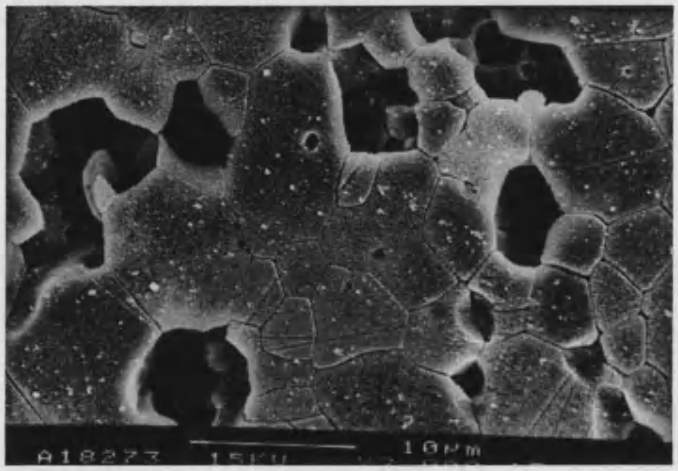

(b)

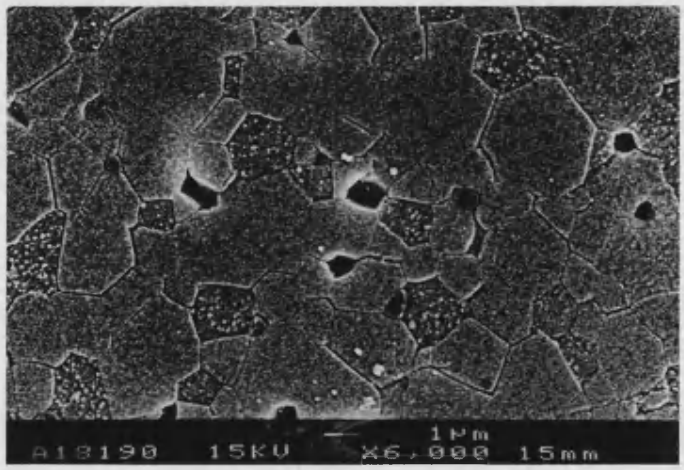

(c)

Figure 3.55: SEM micrographs of porous hydroxyapatite prepared using PVA as porosifier. (a) macropores (~120µm), (b) medium pores (~10µm) and (c) micropores (~1µm).

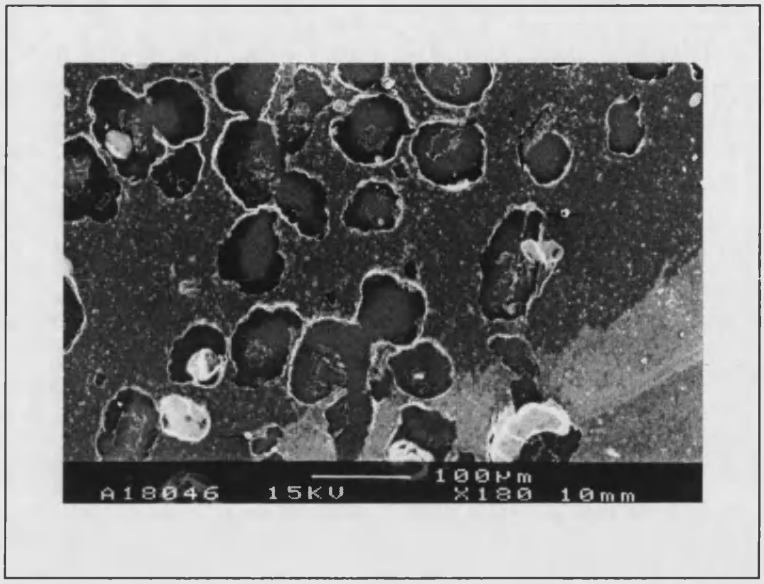

(a)

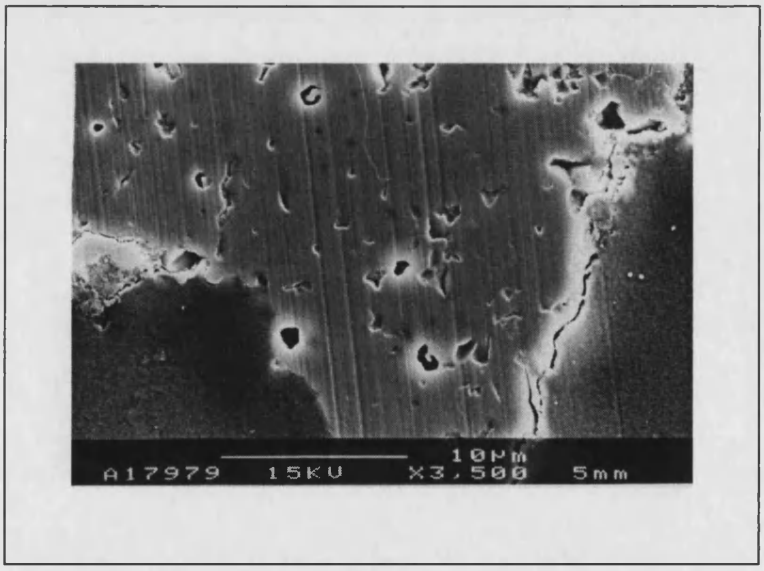

(b)

Figure 3.56: SEM micrographs of porous hydroxyapatite prepared using PVC as porosifier. (a) macropores (~90µm) and (b) micropores (~1µm).

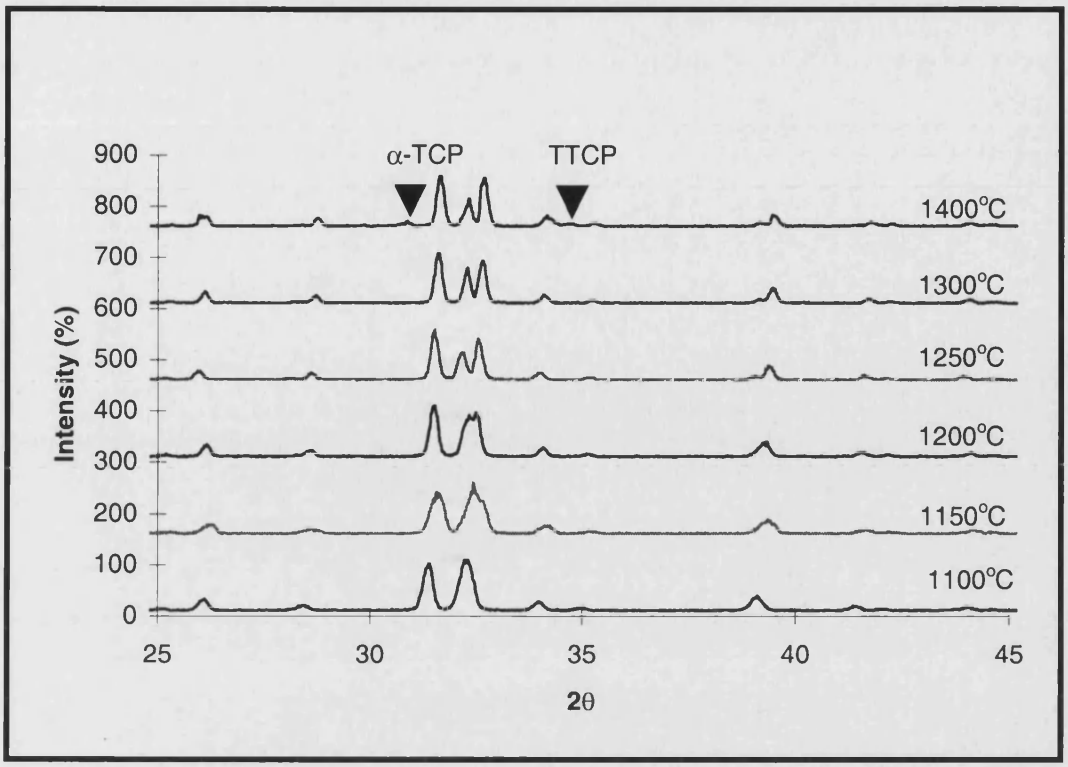

Figure 3.57: XRD result of porous hydroxyapatite after sintering for 4 hours using LMWPVC as a porosifier

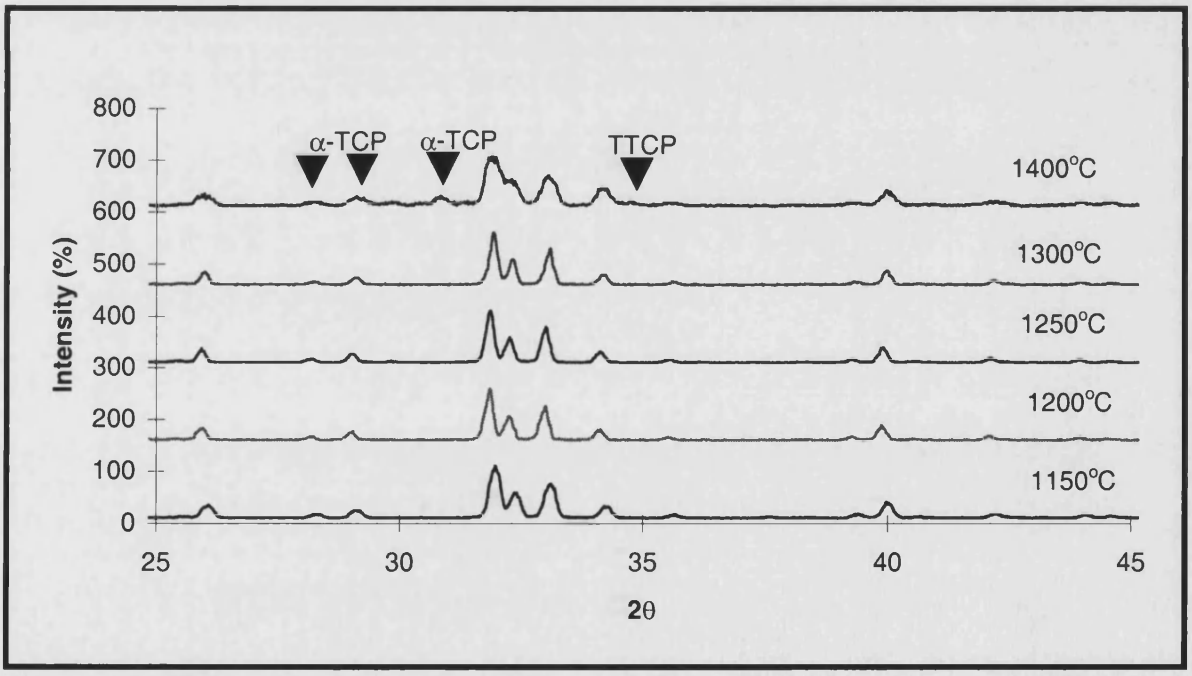

Figure 3.58: XRD result of porous hydroxyapatite after sintering for 4 hours using PVA as a porosifier

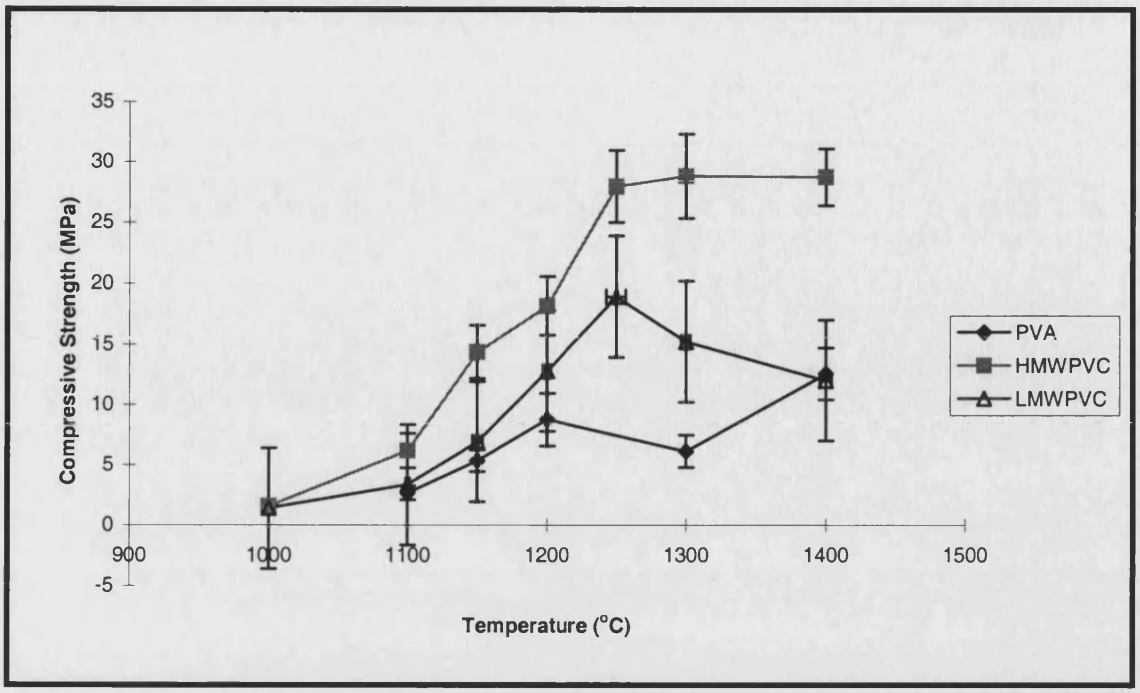

Figure 3.59: Compressive strength of porous hydroxyapatite sintered for 4h using three different polymers at different sintering temperatures.

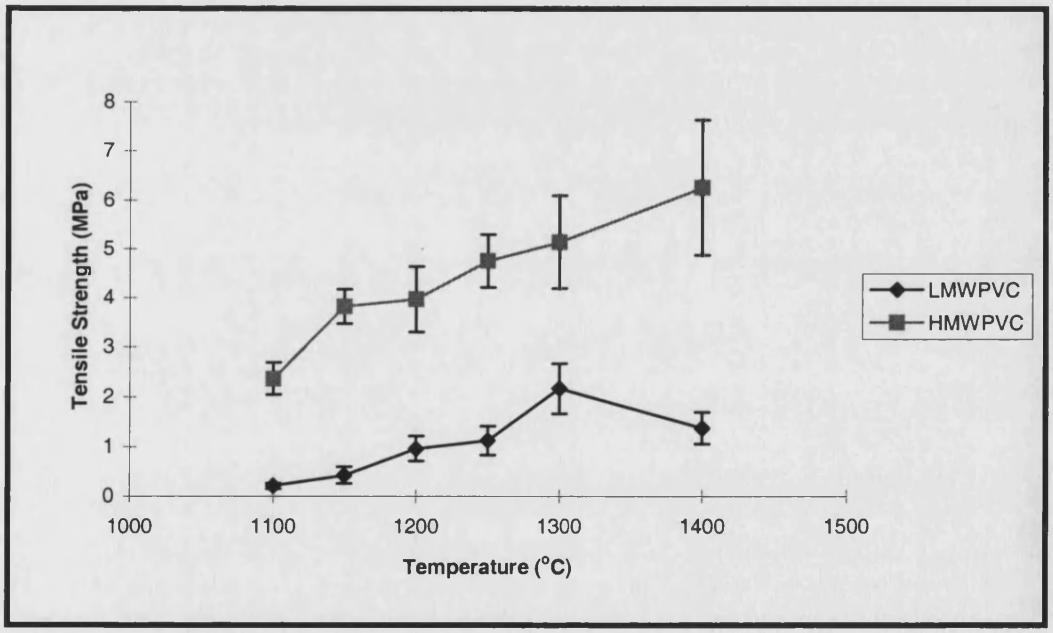

Figure 3.60: Tensile strength of porous hydroxyapatite sintered for 4h using two different polymers at different sintering temperatures.

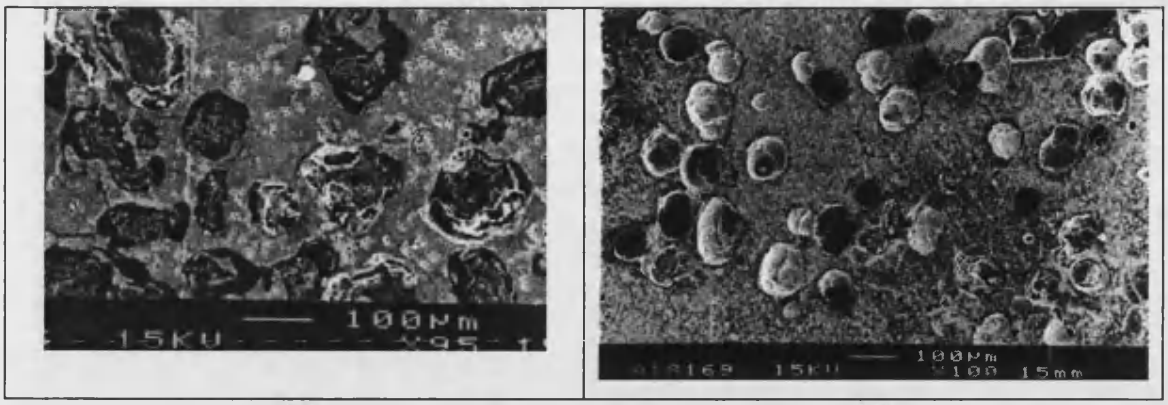

(a) (b)

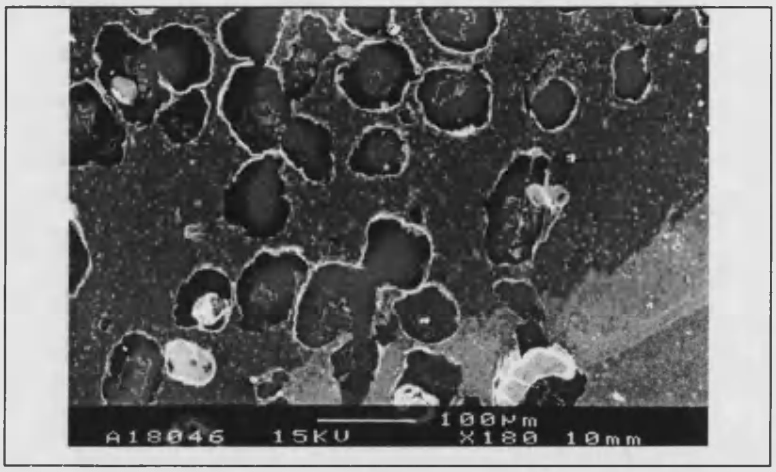

(c)

Figure 3.61: SEM micrographs of porous hydroxyapatite using different types of polymers: (a) PVA (55vol%) (b) LMWPVC (50 vol%) and (c) HMWPVC (53 vol%)

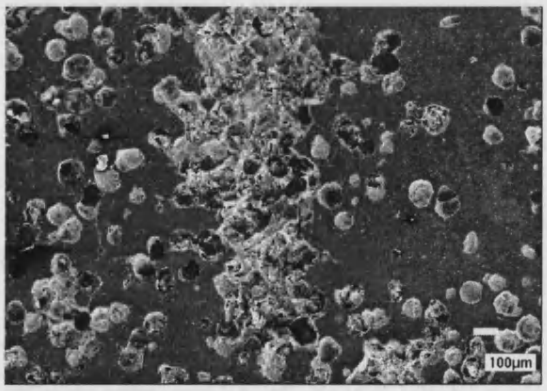

Figure 3.62: SEM micrographs of pore agglomeration occurred in porous hydroxyapatite prepared using LMWPVC

Chapter 4 Study on the Optimisation of Porosity

4.1 Introduction

A bone implant requires biocompatibility, mechanical strength and porosity to promote the interaction between the biomaterial and the host tissue without undesirable reactions. The creation of porous structure with an appropriate pore size, shape and volume is one of the most challenging problems in biomaterials engineering. The objective of this research is to fabricate a hydroxyapatite with the highest strength by studying the influence of forming techniques, pore shape, size and porosity volume on the strength.

4.2 Effect of using different forming techniques on porosity

The strength of the hydroxyapatite powder was studied by using compaction density, plotted in the density - log pressure diagram as shown in Figure 4.1. In this experiment, two stages of compaction behaviour can be identified. In stage 1, the pressure applied to the compact was increasing but the density of the compact remained constant. During this stage, the powder granules would be rearranging their relative positions, resulting in a very slight densification. In Stage 2, as the pressure of the punch increases, the density of the compact would start to increase immediately. The critical point, when the density gradient started to increase, was at 33 MPa. Above this critical point, at stage 2, the powder agglomerates begin to fracture and deform and major densification occurred. Although high density is more favoured in preparing ceramic compacts, in this research, it is important to retain the shape of the hydroxyapatite granules to obtain intergranular pores for interconnected porosity.

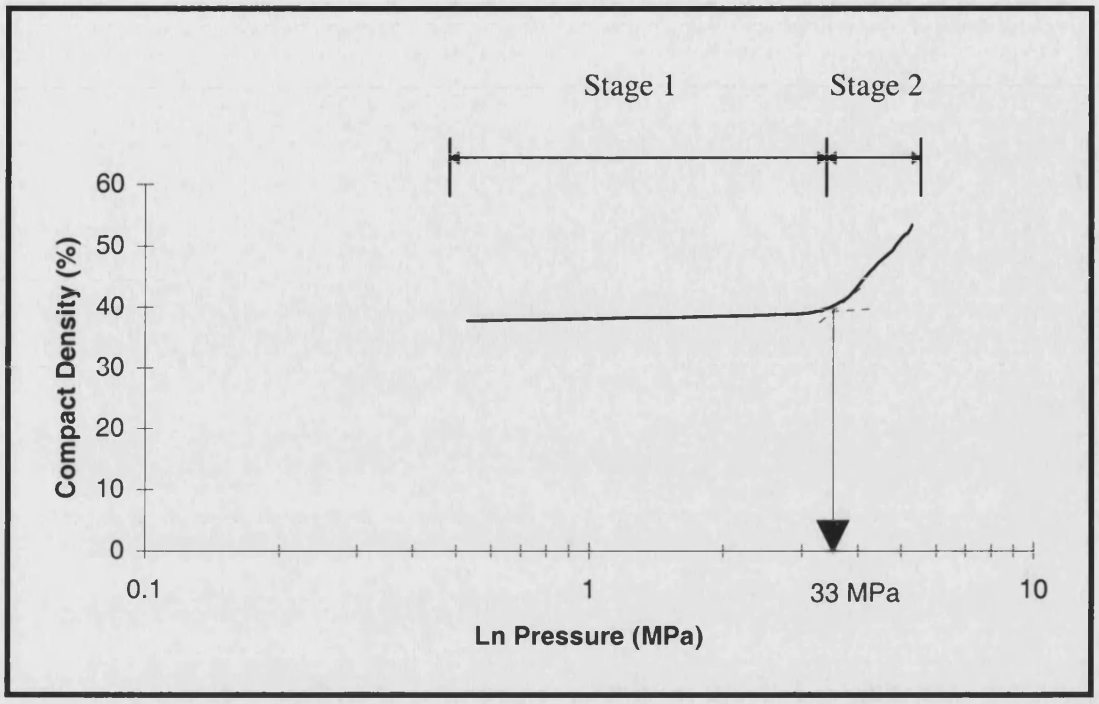

Figure 4.1: Compaction behaviour of hydroxyapatite powder at different pressure using the isostatic pressing technique.

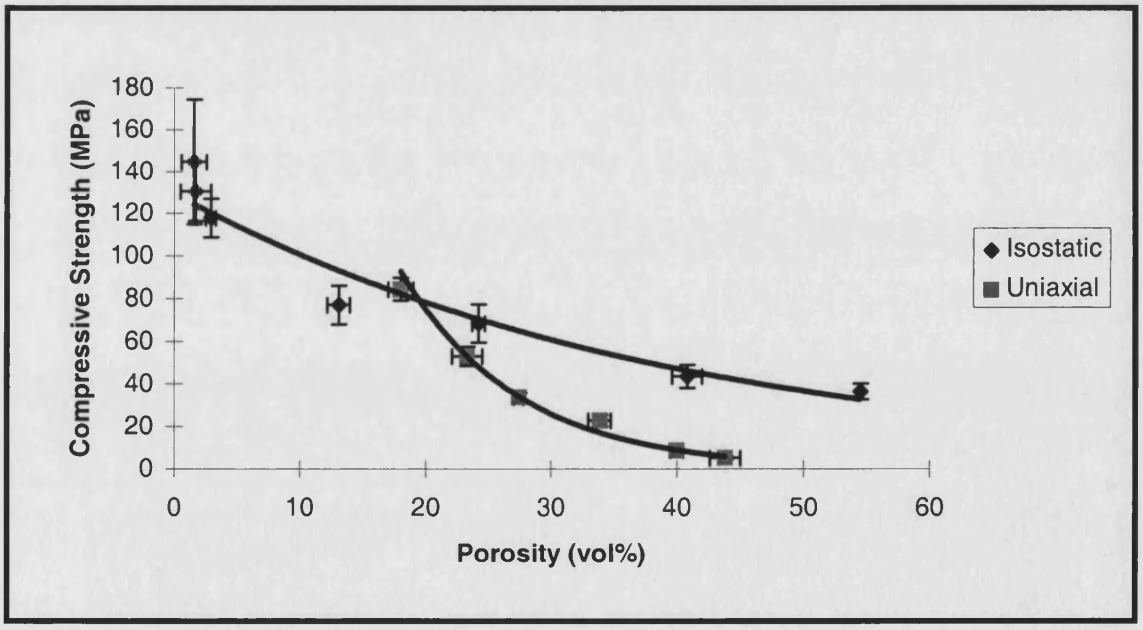

Figure 4.2: Compressive strength of porous hydroxyapatite using different forming techniques; (■) uniaxial and (◆) isostatic pressing technique.

Two dry pressing techniques, uniaxial and isostatic were compared to obtain a porous ceramic compact with the highest strength at a high volume of porosity. The hydroxyapatite powder was pressed with between 10 - 53 volume percent of poly (vinyl chloride) powder using the uniaxial and isostatic pressing techniques at a pressure of 50 MPa. The compressive strengths of the compacts were tested after sintering at 1200°C for 4h.

The porosity-strength behaviour of the porous hydroxyapatite ceramics can be described by the solid curves shown in Figure 4.2 and the equation below, with a corresponding correlation factor (r);
for isostatic pressing technique,

$$\sigma = 129.41 \exp(-0.0252P), r^2 = 0.96$$

for uniaxial pressing technique,

$$\sigma = 627.56 \exp(-0.1062P), r^2 = 0.98$$

The compressive strength of compacts decreases with the increase in the porosity volume in the compacts. At a porosity volumes less than 20 vol%, the strengths of the compacts prepared using the isostatic technique are less than those prepared using uniaxial technique. However, at a higher porosity volume, the compacts prepared using the isostatic technique have a higher strength when composed to those prepared using than the uniaxial technique.

As shown in Figure 4.3, the reduction of the pore strength for the porous compact prepared using uniaxial pressing technique in comparison to the isostatic pressing technique resulted from the presence of cracks. The cracks were observed to originate from the pores and extended to the adjacent pores. The length of the cracks were similar to the pore diameter. When a load was applied, the crack would continue to propagate until fracture occurred. The porous compact without a crack, as produced by the isostatic

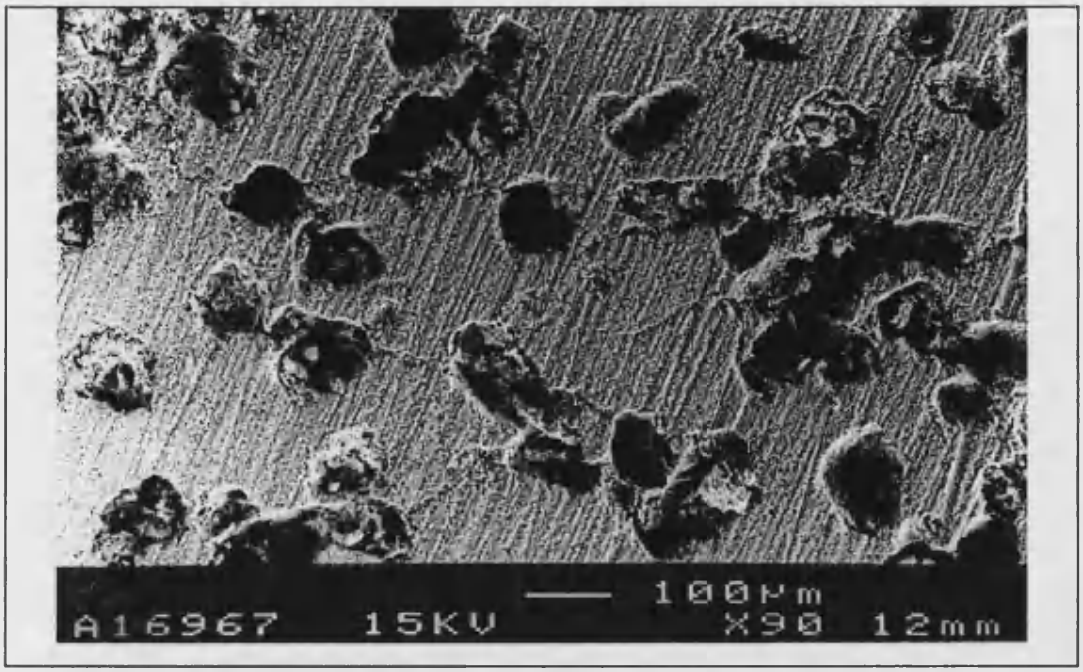

(a)

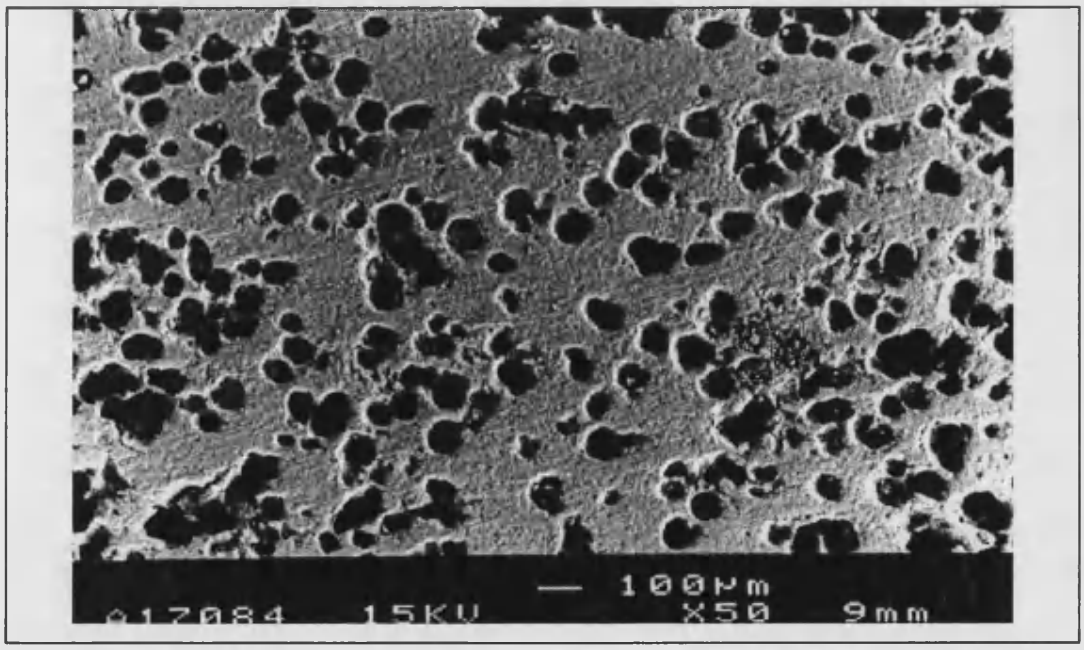

(b)

Figure 4.3: Scanning electron micrographs (SEM) of porous hydroxyapatite formed using (a) uniaxial and (b) isostatic pressing techniques.

pressing technique, takes a higher load to fracture because it is necessary to initiate cracks before continuing to failure according to the Griffith equation,

$$\sigma = \sqrt{\frac{2E\gamma}{\pi c}}$$

where σ is the strength of the ceramic, E is the Young's modulus, γ is the surface free energy and c is the radius of fissure.

4.3 Effect of pore size on strength

Porous hydroxyapatite was prepared using poly (vinyl chloride) particles with the size of 63μm and 125μm. The porosity of the porous hydroxyapatite produced ranged between 3 vol. % and 48 vol. % and the macropores were nearly spherical in shape (Figure 4.4).

The porosity-strength behaviour of the porous hydroxyapatite can be described as;
for 63μm particles,

$\sigma = 141 \exp. (-0.034P)$; $r^2 = 0.95$

for 125μm particles,

$\sigma = 120 \exp. (-0.055P)$; $r^2 = 0.98$

The high value of the correlation coefficient (r) in these expressions indicate that the porosity-strength behaviour of the porous hydroxyapatite can be well described by the exponent function but is restricted to the porosity level of 3-47 vol. %.

As the porosity increased, the compressive strength was observed to decrease. This can be related to the decrease in the volume of solid material available in the specimen to sustain the load, which would result in a weaker specimen as the porosity increased.

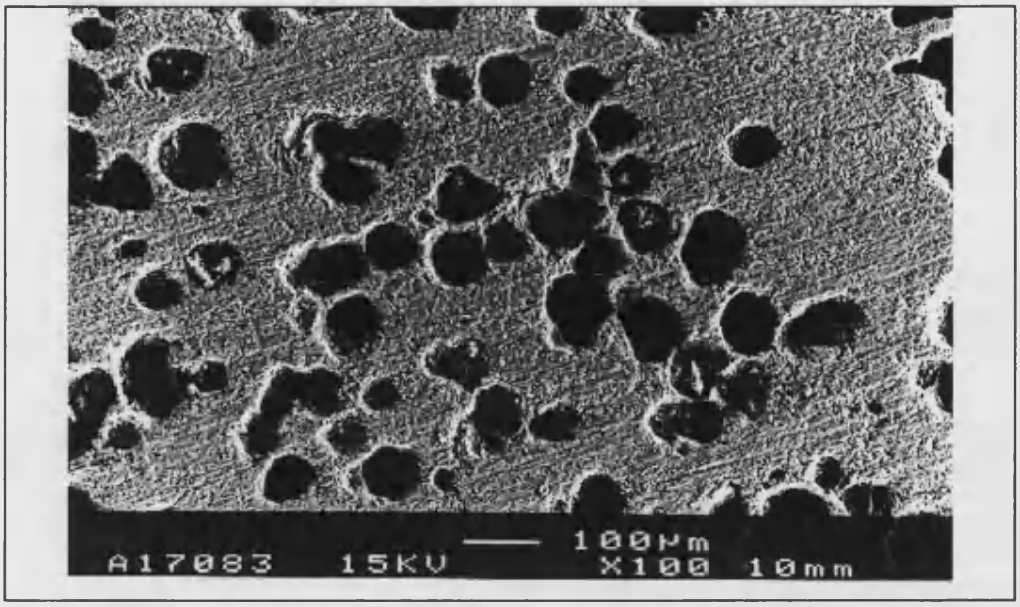

Figure 4.4: Scanning electron micrograph (SEM) of porous hydroxyapatite using poly (vinyl chloride) with a particle size of 125 µm.

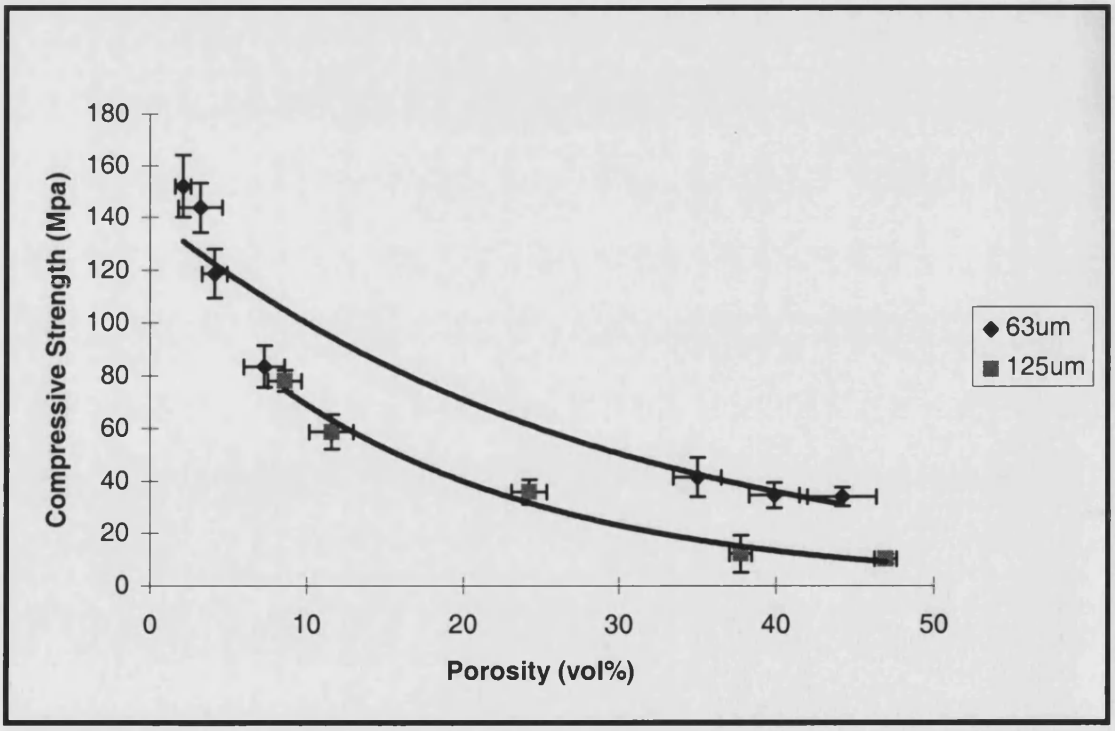

Figure 4.5: The compressive strength-porosity behaviour of the porous hydroxyapatite in terms of different sizes of starting poly (vinyl chloride) particles.

When the compressive strength of a porous compact with a smaller macropore size was compared with a bigger macropore size (Figure 4.5), it was observed that the porous compact with a smaller porosity had a higher strength. This is consistent with the finding of Liu [87] and Krstic [88] who indicated the significance of macropore size in relation to the compressive strength of porous materials.

The general expression used to describe the porosity-strength value as proposed by Ryshkewitch [63] is:

$$\sigma = \sigma_0 \exp(-bP)$$

where σ_0 is zero-porosity strength, σ is the strength at pore volume fraction P, and b is a constant. The b value for the porous hydroxyapatite of both macropore sizes was observed to be quite small (<0.1). This could be related directly to the pore characteristics such as size and shape. Rice [96] suggested that a lower strength-porosity dependence occurred for porous compacts that have more uniformly shaped and spaced pores. The porous materials that have a substantial inhomogeneity of spatial distribution and shape of pores would lead to a very high value of the exponent b.

4.4 Effect of pore geometry on strength

In this experiment, the pore geometry influence on the strength was studied by preparing the samples using a uniaxial pressing technique. The compacts were prepared by pressing at different pressures, between 30 MPa and 135 MPa. As the pressure increased, the introduced polymers were expected to deformed plastically in response to the applied pressure. Figure 4.6 shows the structure of the compact which was cut into half, vertically relative to the direction of the punch. At 76 MPa, the pore shape could be seen to have an ellipsoid shape which indicates that plastic deformation is occurring in the polymer when pressure is applied.

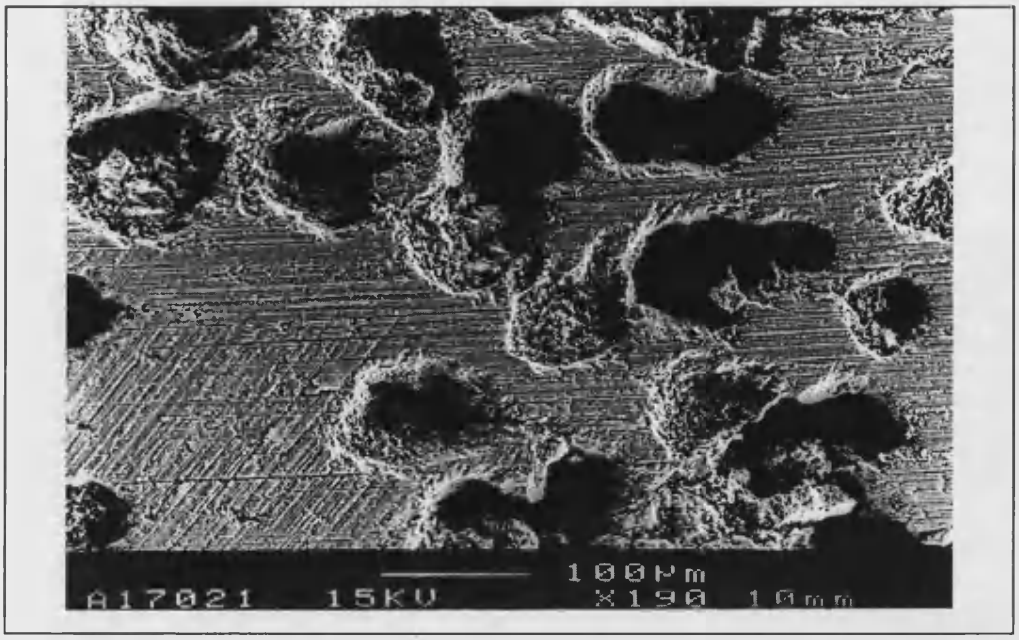

Figure 4.6: Scanning electron micrograph (SEM) of porous hydroxyapatite prepared at 80 MPa showing ellipsoid shape.

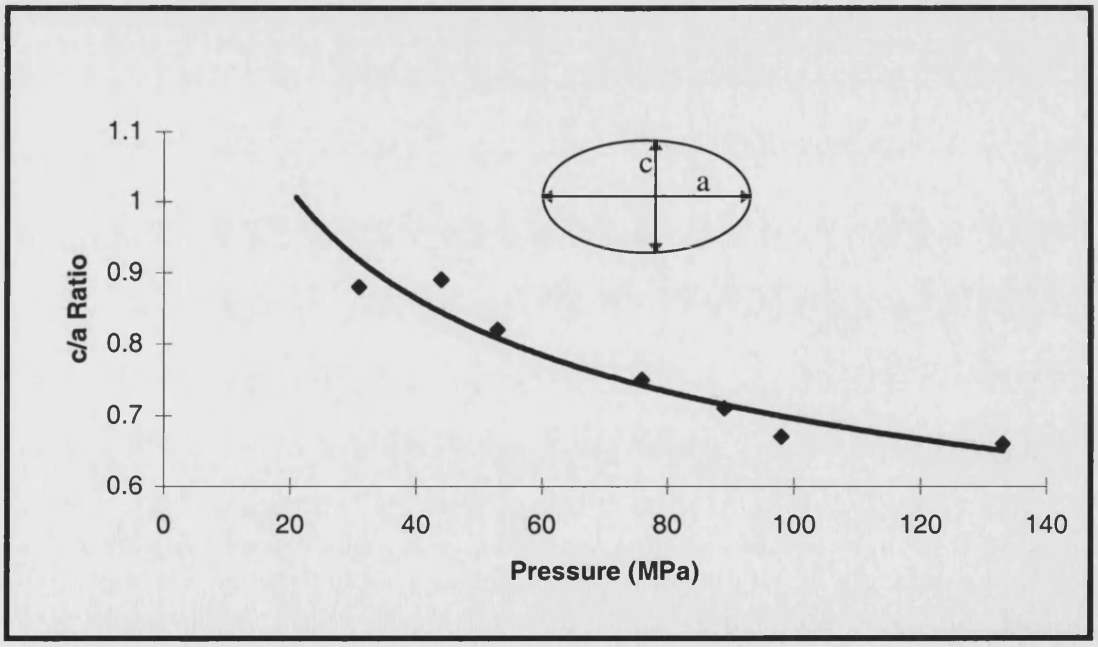

Figure 4.7: The pore geometry (pore axis ratio c/a) plotted against the effect of punch pressure.

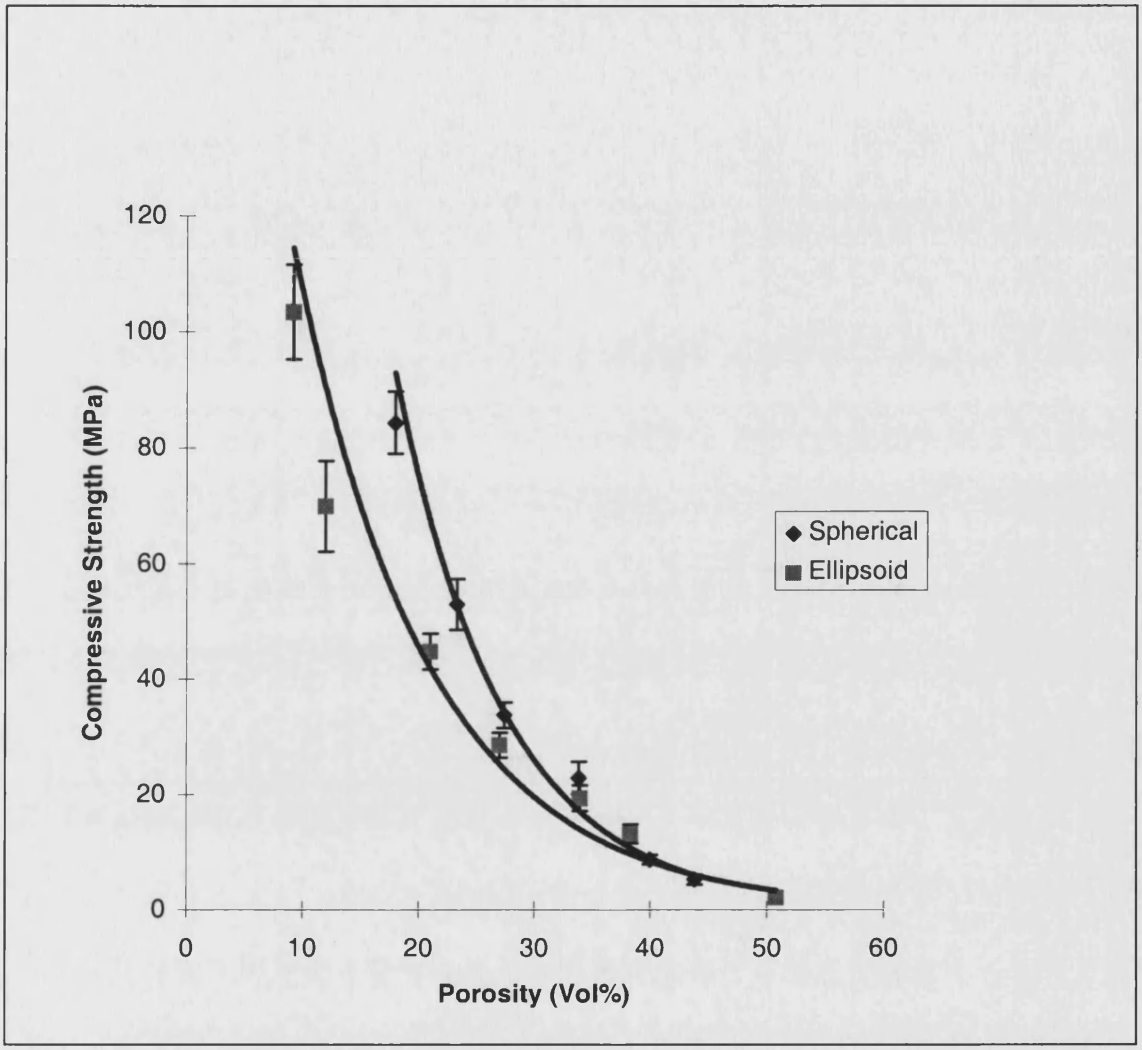

Figure 4.8: The compressive strength-porosity behaviour of porous hydroxyapatite plotted against different types of pore geometry: (◆) sphere and (■) ellipsoid.

The influence of pressure on the pore shape was quantified by calculating the pore geometry (in terms of the ratio of the breadth of the pore, c, to the length of the pore horizontally, a) as can be seen in Figure 4.7. A decrease in the c/a ratio can be seen between 40 MPa and 100 MPa which suggests a strong plastic deformation of the poly (vinyl chloride) particles. Above 100MPa, the plastic deformation can almost be seen to approach an equilibrium. This may be due to the hydroxyapatite powder being highly dense at high punch pressures which consequently restricts the poly (vinyl chloride) from further deformation.

The compressive strength-porosity behaviour of the porous hydroxyapatite ceramic with different pore geometries, prepared by using different forming pressures, is shown in Figure 4.8. The 'ellipsoid' geometry pore has a lower strength than the pore with a 'spherical' geometry. The results can be expressed as below:

$$\sigma_{ellipsoid} = 250 \exp. (-0.085P) \text{ MPa}$$

$$\sigma_{sphere} = 628 \exp. (-0.1062P) \text{ MPa}$$

The difference in the results can be explained by considering the solid area between the pores. As pressure was imposed on the poly (vinyl chloride) during the pressing, the polymer would deform in response to the direction in which the pressure has been applied. When the polymer was subsequently burnt out, the pores created would be the same shape as the deformed poly (vinyl chloride). The spacing of the pores, and the solid area between the pores would be reduced as the geometry of the pores changed from spherical to ellipsoidal. This would result in the solid area having less ability to bear a high load as the geometry changes from spherical to ellipsoidal.

However, at high porosity levels (Figure 4.8), ~40 vol%, the load bearing capacity appears to be similar regardless of the pore shape factor. This shows that at a high porosity level, porosity volume has a more significant effect on strength than the pore

shape. From these results, it appears that forming pressure plays an important role in determining the mechanical strength as it influences the pore shape of the porous ceramic produced.

4.5 Summary

1. This study showed the importance of choosing the right forming technique and pore characteristics in order to optimise the strength of a porous material.
2. The specimens prepared using isostatic pressing technique showed a better mechanical strength at a high porosity level than specimens prepared using the uniaxial pressing technique. This could be related to the observed cracking of the compact when using the uniaxial technique.
3. Both pore size and pore shape also play an important role in determining the strength of the porous ceramic material. The specimens with small macropores showed a higher strength than those with large macropores and also the specimens having pores with a spherical shape have a higher strength in comparison to the specimens with ellipsoidal shape.
4. From these results it may be possible to optimise the pore characteristics to produce a synthetic bone structure with appropriate porosity combined with adequate strength.

Chapter 5 Sol-Gel Technique

5.1 Introduction

This chapter was written to give a brief description of earlier research into the fabrication of porous hydroxyapatite using the freeze casting method. However, this route was not successful due to the problem encountered in producing a green product with sufficient strength and controlled porosity size.

5.2 Synthesis of calcium phosphate gel

There have been many studies into the preparation of calcium phosphate powder using solution-precipitation methods [42, 43, 52, 112]. The production of a porous calcium phosphate ceramic by drying the calcium phosphate gel obtained by the sol-gel method had never been attempted before.

5.2.1 Ageing effect on the Ca/P ratio

The first stage of the study was to produce a calcium phosphate gel with the correct Ca/P ratio. To produce hydroxyapatite, the molar ratio of the Ca/P must be at 1.67, as calculated from the formula of hydroxyapatite, $Ca_{10}(PO_4)_6(OH)_2$.

The hydroxyapatite was produced from the reaction between $Ca(NO_3)_2$ and H_3PO_4, with NH_4OH used to control the pH at a value in the region of 10-12. The technique has been discussed in some detail in Section 2.3. The Ca/P ratio of the hydroxyapatite produced was analysed using the Electron Probe Analyser and the results are shown in Table 5.1.

It was observed that ageing affected the ratio of the Ca/P. Initially, the ratio was 1.62 but as the ageing time increased, the ratio decreased. After 12h, the ratio increased again and reached the correct ratio for hydroxyapatite at 48h. The x-ray diffraction results of the calcium phosphate powder after ageing for 48h (Figure 5.1) indicate that the phase present is indeed hydroxyapatite.

5.2.2 Freeze drying and freeze casting

Two methods were used to obtain a porous calcium phosphate ceramic, firstly, using a freeze drying method and secondly, oven drying after the samples were frozen in the liquid nitrogen refrigerant. In the first case, the gel obtained from the method mentioned above, after ageing 48h, was placed in a stainless steel mould and frozen quickly in a bath containing liquid nitrogen. After it was completely frozen, the sample was then freeze dried. The idea was to obtain a porous hydroxyapatite by removing all the water using the freeze dryer while maintaining the porous structure. The green body of porous hydroxyapatite would later be fired in the furnace at a suitable sintering temperature. The porosity obtained using this method would be expected to be interconnected due to the evaporation of the water from the gel during freeze drying, leaving only the solids in a 3-D network. This idea could not be put into practice due to the problems in obtaining a green product with sufficient strength to be gripped and transferred into the furnace. Most of the samples were too friable and broke during handling because the bonding forces holding each particle together were insufficient. Although some attempt was made to increase the green strength of the porous calcium phosphate by adding a small weight percentage of silica, this too was unsuccessful.

The second method, freeze casting, thawing and oven drying the green product was investigated. In this method, the gel produced was not used but instead, the silica sol (X30 grade) was used with the commercial hydroxyapatite as the filler. The method performed by Laurie et al [113] was followed. Different wt% ratios of silica sol and filler were used to obtain a green product with a high enough strength to be held and

Table 5.1: Result of the ageing effect on the Ca/P ratio of the precipitated hydroxyapatite

Ageing Time (h)	Ca/P R.atio
0	1.62 ± 0.02
4	1.50 ± 0.02
8	1.44 ± 0.12
12	1.60 ± 0.01
17	1.62 ± 0.03
20	1.62 ± 0.01
48	1.67 ± 0.01

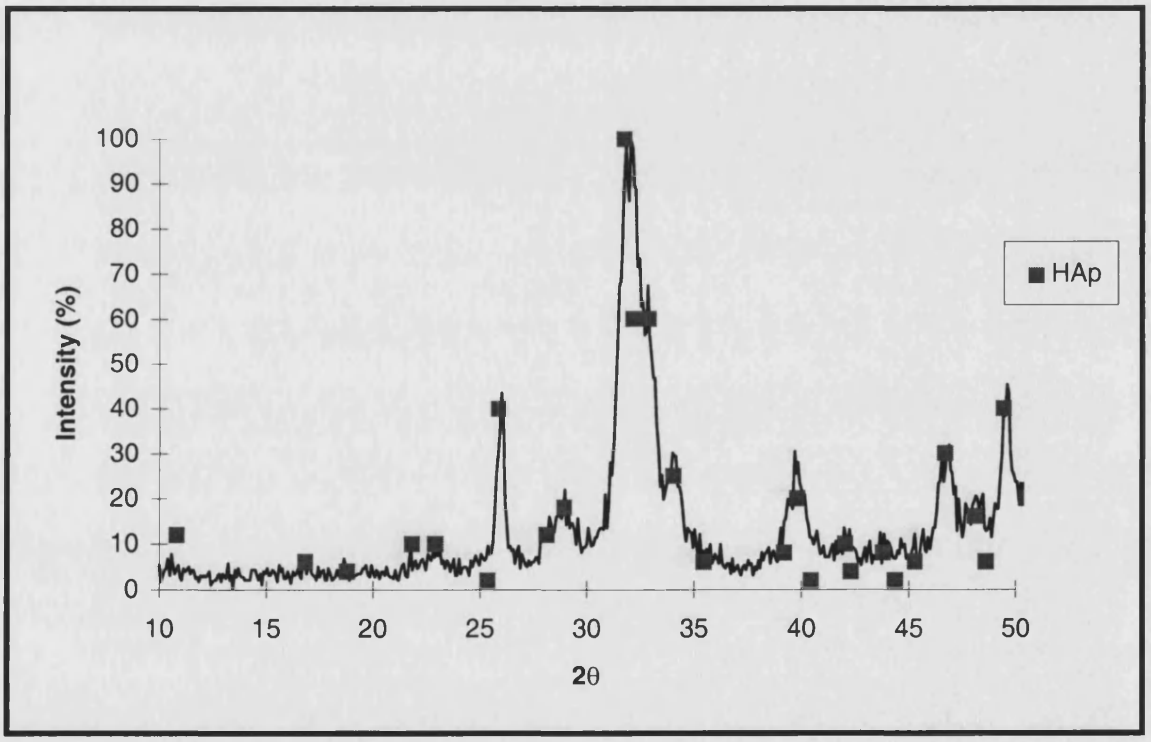

Figure 5.1: X-ray diffraction analysis of the hydroxyapatite powders produced after 48h. (Keynote: ■ = hydroxyapatite peaks).

transferred to the furnace and it was found that a weight ratio of 60wt% of silica sol and 40wt% of commercial hydroxyapatite was the right combination. The mixture was later placed in a stainless steel mould and frozen in the liquid N_2 refrigerant for 15 minutes. Different minimum temperatures were studied in the range -30°C until -90°C. After thawing at room temperature, the samples were taken out of the mould and dried in the oven. It was observed that all the samples produced a skin that peeled off after drying and was quite dense. Samples frozen at -90°C showed large cracks. This was not the case at -30°C and -60°C. This part of the project was later abandoned as it used too much commercial hydroxyapatite as a filler and was too costly to be continued. The concern over the usage of silica sol in the mixture with respect to the biocompatibility of the hydroxyapatite ceramic was also considered as being detrimental to the overall aims.

5.3 Summary

1. Calcium phosphate gel was obtained using $Ca(NO_3)_2$ and H_3PO_4 with NH_4OH to maintain the pH between 10-12.
2. The Ca/P molar ratio of 1.67 was obtained after the gel was aged for 48h.
3. The preparation of the porous calcium phosphate using the freeze drying method was not successful due to the lack of strength of the green body obtained after the freeze drying.
4. The preparation route using the freeze casting method was stopped due to the high cost of using commercial hydroxyapatite as a filler and concern that using the silica sol would affect the biocompatibility of the hydroxyapatite ceramic.

Chapter 6 General Discussion

6.1 General Discussion

This study was pursued with existing specifications and regulations in mind, in order that any material produced could be immediately useful for implant purposes. Among the specifications are:

a. the ASTM F1185-88 Standard [29] specified that composition of ceramic hydroxyapatite for surgical implants must contain a minimum of 95% hydroxyapatite;
b. the porosity of the porous material must be at least 80 μm in size in order for bone growth to occur [119];
c. the porosity must be interconnected with at least 20 μm channels for human osteoblasts to cross through the interconnections, spread and proliferate inside macropores [119].

The thermal behaviour of hydroxyapatite in the presence of the poly (vinyl chloride) was first studied. The presence of the polymer during sintering was observed not only to reduce the densification and decomposition temperature of the hydroxyapatite, but also to reduce the volume shrinkage of the porous hydroxyapatite due to the volume and size of the deliberately produced pores. Since the individual macropores were large, it was not possible to remove them by the normal sintering processes and they remained as a feature of the microstructure, their presence reducing the overall shrinkage.

The decomposition of the hydroxyapatite after sintering at a low temperature, $T < 900^{\circ}C$ involved the loss of adsorbed water and tightly bound water from the lattice.

At $T \geq 900^{\circ}C$,

$Ca_{10}(PO_4)_6(OH)_2 \longrightarrow Ca_3(PO_4)_2$

(HA) (β-TCP)

At T≥1300°C,

$Ca_{10}(PO_4)_6(OH)_2 \longrightarrow Ca_3(PO_4)_2 + Ca_4(PO_4)_2O$

(HA) (α-TCP) (TTCP)

The decomposition of the hydroxyapatite in the presence of poly (vinyl chloride) after sintering for 4h is as outlined below:

At T≥1200°C,

$Ca_{10}(PO_4)_6(OH)_2 \longrightarrow Ca_3(PO_4)_2$

(HA) (β-TCP)

At T≥1400°C,

$Ca_{10}(PO_4)_6(OH)_2 \longrightarrow Ca_3(PO_4)_2 + Ca_4(PO_4)_2O$

(HA) (α-TCP) (TTCP)

The study was continued to increase further the decomposition of the hydroxyapatite at an even higher temperature whilst studying the sintering cycle, yet maintaining the production of hydroxyapatite without cracks. First, a study on the effect of heating rate of the hydroxyapatite in the presence of polymer was made. Two heating rates were used, 30°C/h and 50°C/h, for the first stage of sintering (polymer burning out stage). No cracking was observed due to the ability of the volatile product to be released to the atmosphere through the interconnected pores which had been created. This indicated that heating during the first stage of sintering could be done at a higher rate without causing cracks. The heating rate does not appear to affect the decomposition temperature. The decomposition of hydroxyapatite into β-TCP initiated at 1200°C and further decomposition into α-TCP and TTCP started at 1400°C.

The effect of holding temperature and holding time during the second stage of sintering on the decomposition behaviour was also studied. It was observed, that the higher the temperature used and the longer the temperature held, the more likely the hydroxyapatite

was to decompose at a lower temperature. Traces of β-TCP were observed as low as 1100°C when held for 36h. The decomposition temperature was also found to be influenced by the holding temperature during the first stage. When the holding temperature in the first stage was changed (from 400°C to 600°C) and the holding time at the second stage was changed to 4h, it was observed that the hydroxyapatite could withstand a somewhat higher temperature without decomposing to TCP and TTCP (1400°C).

The sintering atmosphere was also observed to influence the decomposition conditions of the hydroxyapatite. Traces of α-TCP and TTCP were observed at a lower temperature (1300°C) in argon atmosphere in comparison to 1400°C when sintered in air. However, changing the type of polymer used to create the porosity did not appear to influence the decomposition temperature.

During the sintering process, densification occurs simultaneously with the changes in shape and size of both pores and grains. For non porous (very large pores absent) ceramic, firstly, when fired, the individual ceramic powder particles in contact would adhere and form necks. The necks would grow, the volume fraction of open porosity would decrease and the dimensions of individual pores would decrease. In the intermediate stage, the necks would become larger and the pores change their shape to become roughly spheroidal. Open pores would tend to disappear and an increased number of closed pores would become apparent. In the final stage of sintering, grain boundary migration occurs leaving spherical closed pores isolated within grains, away from grain boundary diffusion routes. For the porous hydroxyapatite made in this study, a similar sintering process was followed except that the elimination of the macropores which was introduced using the large polymer particles did not occur. A complete elimination of the micropores was achieved at 1200°C for non-porous hydroxyapatite. For porous hydroxyapatite, at the same temperature, a high volume of porosity was still observed, which consists of both micropores and macropores. As was planned in the

design of the microstructure, some of the macropores showed interconnected porosity while others were isolated.

Changing the heating rate during the first stage of sintering does not affect the volume fraction of porosity but the holding time produced a significant difference. The longer the temperature was held, the lower was the porosity level observed.

The sintering atmosphere appears not to change the sintering behaviour, as the density and volume fraction of porosity was observed to be the same after sintering in both air and argon atmosphere . However, the type of polymer used does influence the volume fraction of porosity produced. Samples prepared using PVA showed a higher volume fraction of porosity at the same polymer content compared to samples produced using PVC. Three types, defined by sizes of pore were observed using PVA, ~120 μm, ~10 μm and ~1 μm, but when using PVC, only two types of pore sizes were observed, ~90 μm and ~1 μm. The pore sizes of 120 μm and 90 μm observed in porous hydroxyapatite using PVA and PVC respectively, had originated from the introduction of the polymer spheres, and the pore size of 1 μm was presumed to result from the residual pores remaining after sintering. The pore size of 10 μm detected in the porous hydroxyapatite was assumed to have originated from the decomposition of the PVA.

The introduction of the polymer in the hydroxyapatite ceramic, changes the thermal behaviour of the hydroxyapatite. At low temperature, before the densification of the hydroxyapatite occurred, the presence of poly (vinyl chloride) was observed to catalyse the dissociation of the water molecule from the hydroxyapatite to a lower temperature. When the sintering temperature was reached, it was observed that densification started and finished at a higher temperature. The expansion and shrinkage of the porous hydroxyapatite ceramic was observed to be higher in air than in argon atmosphere.

The grain size of the hydroxyapatite was observed not to be significantly affected by the change of the heating rate but affected by the holding time and temperature. The growth rate of the grains was observed to increase rapidly above 1300°C.

The sintering atmosphere does have an effect on the grain growth of the hydroxyapatite. Sintering in air resulted in a bigger grain size than sintering in argon atmosphere. When different types of polymer were used to create the porosity, the grain size was also affected. For PVC, the main product released during burn-out was HCl and this product appeared to retard growth of the grains.

To obtain a porous hydroxyapatite with a high mechanical strength is a challenge. Porosity has been known to be the source of failure and a cause of the reduced strength of a material. The optimisation of the mechanical properties could be achieved by controlling the processing technique. The forming technique was the variable first studied. Two types of dry pressing techniques were used, uniaxial and isostatic. Samples prepared using uniaxial pressing technique were observed to produce cracks, thus resulting a poorer strength in comparison to samples prepared using isostatic pressing technique. When different types of polymer were used, it was observed that the mechanical strength of samples prepared using HMWPVC was observed to be the highest in comparison to LMWPVC and PVA.

Carbon residues which resulted from the incomplete burning of the polymer in the porous hydroxyapatite were observed when samples were sintered in both air and argon atmospheres. Sintering in air left less carbon residue, thus resulting in a porous hydroxyapatite with a better mechanical strength than those sintered in argon.

The size and shape of the pores influenced the mechanical strength of the porous hydroxyapatite. Samples with a bigger pore size were observed to have a lower mechanical strength than a smaller pore sized porous hydroxyapatite. Whereas the

samples with a spherical shape were observed to have a higher mechanical strength than samples with an ellipsoid shape.

The porous hydroxyapatite produced has medical importance as it has a similarity with bone structure. It has the same constitution as the crystalline phase of the inorganic substance of the bone, which is hydroxyapatite, and also pore size, channels and fraction volume of porosity required for the ingrowth of bone. The samples are easy to prepare and preparation time is short. However there is a limitation in size as the samples are prepared using a mould, therefore a larger size or complex shaped samples could not be prepared. The mechanical properties of the porous hydroxyapatite produced differ from those found in the bone, which is a sophisticated composite of hydroxyapatite and organic collegen fibres. The strength limitation of the porous hydroxyapatite however, could be overcome by the incorporation of a second phase such as alumina fibres. The fibres would stop the cracks from propagating further when force is applied and would fail at a higher force in comparison to the samples without the fibres. At this moment in time, the samples produced in this study are only suitable for small and non-major load bearing implants.

6.2 Summary

1. The decomposition temperature of the hydroxyapatite was influenced by the presence of polymer, holding time, holding temperature and sintering atmosphere but was not affected by the heating rate.
2. For non-porous hydroxyapatite, the elimination of pores was achieved at 1200°C but at the same temperature, large pores were still present in the porous hydroxyapatite. The porous hydroxyapatite showed interconnections between the pores.

3. Heating rate and sintering atmosphere did not affect the density and volume fraction of porosity of the porous hydroxyapatite but holding time and holding temperature showed a significant influence.
4. Using PVA as a porosifier resulted in three groups of pore sizes, 120 μm, 10 μm and 1 μm while PVC only produced two size groups, ~90 μm and 1 μm.
5. Grain size was not significantly affected by the change of heating rate but was affected by the sintering atmosphere, holding time and holding temperature.
6. Samples prepared using PVC showed a smaller grain size than samples prepared using PVA due to the effect of a chlorine residue that retarded the growth of the grain.
7. Samples formed using isostatic pressing showed a higher mechanical strength than samples prepared using uniaxial pressing.
8. Pore size and geometry affected the mechanical properties of the porous hydroxyapatite.
9. Samples sintered in air showed less carbon residue than samples sintered in argon, this resulted in a higher mechanical strength.
10. The porous hydroxyapatite prepared was structurally and chemically similar to bone and has potential for medical purposes.
11. The samples had the pore size, channels and volume fraction of porosity needed for implants and were easy to manufacture. However, there was a size and strength limitation, therefore the samples produced were only suitable for a small and non-major load bearing implants.

6.3 Conclusions

From this study, it can be concluded that there is an optimal combination of criteria for the formation of porous hydroxyapatite. It is recommended that an isostatic pressing technique (Figures 4.2 and 4.3), with a 53 vol. % (Figures 3.42 and 3.43) of HMWPVC (Figure 3.45) as the porosifier be used. The samples should be sintered in air (Figures

3.8, 3.32, 3.34, 3.36, 3.38 - 3.40), with a heating rate of 50°C/h (Figures 3.15 - 3.19) and held for 1h at 600°C (Figure 3.25) in the first stage. A subsequent heating rate of 100°C/h, held for 4h at between 1200 and 1250°C (Figures 3.9 - 3.11, 3.20 - 3.22, 3.23(b) and 3.25), with a spherical pore geometry (Figure 4.8) gave the best combination of properties. This resulted in an interconnected porous hydroxyapatite (Figures 3.10 and 3.14) with a pore size of ~90 μm (Figures 3.47 and 3.56), a volume fraction of porosity of ~35% (Figure 3.33) and a relative density of ~60% (Figure 3.43). Samples had a grain size of ~1.7-2μm (Figure 3.49), of compression strength of between 14-18 MPa (Figure 3.39) and a tensile strength of 4-5 MPa (Figure 3.40). The material was also chemically (Figure 3.38) and structurally (Figure 3.61) similar to bone.

6.4 Suggestions for Future Work

1. To study the biocompatibility of the porous hydroxyapatite prepared in this study, *in vivo* and *in vitro*.
2. Incorporate a second phase in the porous hydroxyapatite such as alumina fibres to further strengthen the porous hydroxyapatite.
3. To undertake a further quantitative study on the effect of sintering cycle on macro and microporosity, and the decomposition products of hydroxyapatite (β-TCP, α-TCP and TTCP) after sintering.
4. To use an alternative method of preparing porous hydroxyapatite, such as slip casting with a spherical polymer or with reticulated polymers to form the pore network.

References:

1. Hench, L.L. and Wilson, J., *An Introduction to Bioceramics*, World Scientific, Singapore, New Jersey, London, Hong Kong (1993)

2. Carola, R.; Harley, J.P. and Noback, C.R., *Human Anatomy & Physiology*, McGraw-Hill Publishing Company, USA, (1990)

3. Hinkle, C.Z., *Fundamentals of Anatomy and Movement - A Workbook and Guide*, Mosby-Year Book, Inc., Missouri (1997)

4. Marieb, E.N., *Human Anatomy & Physiology*, 4th ed., Addison Wesley Longman, Inc., (1998)

5. Van de Graaff, K.M. and Fox, S.I., *Concepts of Human Anatomy & Physiology*, 5th ed., WCB/McGraw-Hill, USA (1999)

6. Nordin, M. and Frankel, V.H., *Biomechanics of Bone*, in Kinesiology and Applied Anatomy, Rasch, P.J. (ed.), Lea & Febiger, Philadelphia, (1989) 3-29.

7. Solomon, E.P.; Schmidt, R.R. and Adragna, P.J., *Human Anatomy and Physiology*, 2nd ed., Saunders College Publishing, Florida (1990)

8. Narasaraju, T.S.B. and Phebe, D.E., *Review - Some Physico-Chemical Aspects of Hydroxylapatite*, Journal of Materials Science, **31** (1996) 1-21

9. Guyton, A.C., *Textbook of Medical Physiology*, 6th ed., W.B. Saunders Company, Philadelphia (1981)

10. Ben-Nissan, B.; Chai, C. and Evans, L., *Crystallographic and Spectroscopic Characterisation and Morphology of Biogenic and Synthetic Apatites*, Wise, D.L.; Trantolo, D.J.; Altobelli, D.E.; Yaszemski, M.J.; Gresser, J.D. and Schwartz, E.R. (eds.) in Encyclopaedic Handbook of Biomaterials and Bioengineering, Part B: Applications, Volume 1, Marcel Dekker, Inc., New York (1995)

11. Ravaglioli, A. and Krajewski, A. (eds.), *Bioceramics - Materials, Properties, Application*, Chapman & Hall, London (1992)

12. Hench, L.L. and Ethridge, E.C., *Biomaterials, An Interfacial Approach*, Academic Press, New York (1982) 137.

13. Kokubo, T., *Mechanical Properties of a New Type of Glass Ceramic for Prosthetic Application*, Tsuruta, T. and Nakajima, A., (eds.), Multiphase Biomedical Materials, VSP, Utrecht, Netherlands (1989).

14. Jarcho, M.; Bolen, C.H.; Thomas, M.B.; Boblck, J.; Kay, J.K. and Doremus, R.H., *Hydroxyapatite Synthesis and Characterisation in Dense Polycrystalline Form*, Journal of Materials Science **11** (1976) 2027-2035.

15. Jarcho, M.; Salsbury, R.L.; Thomas, M.B. and Doremus, R.H., *Synthesis and Fabrication of β-Tricalcium Phosphate (Whitlockite) Ceramics for Potential Prosthetic Applications*, Journal of Materials Science **14** (1979) 142-150.

16. Hulbert, S.F.; Bokros, J.F.; Hench, L.L.; Wilson, J. and Heimke, G., *High Tech Ceramics*, Vincenzini, P. (ed.), Elsevier Science Publication, Amsterdam (1987)

17. Hench, L.L., *Bioceramics*, Journal of American Ceramics Society, **81**, [7] (1998) 1705 - 1728

18. Klein, C.; de Groot, K.; Weiqun, C; Yubao, L. and Xingdong, Z., *Osseous Substance Formation Induced in Porous Calcium Phosphate Ceramics in Soft Tissues*, Biomaterials **15** (1994) 31-34

19. Daculsi, G. and Passuti, N., *Effect of the Macroporosity for Osseous Substitution of Calcium Phosphate Ceramics*, Biomaterials **11** (1990) 86-87

20. Ito, K. and Ooi, Y., *Osteogenic Activity of Synthetic Hydroxylapatite with Controlled Texture - on the Relationship of Osteogenic Quantity with Sintering Temperature and Pore Size*, Yamamuro, T.; Hench L.L. and Wilson, J. (eds.) CRC Handbook of Bioactive Ceramics, Vol. II - Calcium Phosphate and Hydroxylapatite Ceramics, CRC Press Inc., Boca Raton, Florida (1990) 39-44

21. Eggli, P.S.; Muller, W. and Schenk, R.K., *Porous Hydroxyapatite and Tricalcium Phosphate Cylinders with 2 Different Pore-Size Ranges Implanted in the Cancellous Bone of Rabbits - A Comparative Histomorphometric and Histologic-Study of Bony Ingrowth and Implant Substitution*, Clinical Orthopaedics And Related Research **232** (1988) 127-138

22. Frayssinet, P.; Trouillet, J.L.; Rouquet, N.; Azimus, E. and Autefage, A., *Osseointegration of Macroporous Calcium Phosphate Ceramics having a Different Chemical Composition*, Biomaterials **14** (1993) 423-429

23. Kitsugi, T.; Yamamuro, T.; Nakamura, T. and Oka, M., *Transmission Electron Microscopy Observations at the Interface of Bone and Four Types of Calcium Phosphate Ceramics with Different Calcium/Phosphorus Molar Ratios*, Biomaterials **16** (1995) 1101-1107

24. De Groot, K.; Klein, C.P.A.T.; Wolke, J.G.C. and Blieck-Hogervorst, J.M.A., *Chemistry of Calcium Phosphate Bioceramics,* Yamamuro, T.; Hench L.L. and Wilson, J. (eds.) CRC Handbook of Bioactive Ceramics, Vol. II - Calcium Phosphate and Hydroxylapatite Ceramics, CRC Press Inc., Boca Raton, Florida (1990) 3-16

25. LeGeros, R.Z. and LeGeros, J.P., *Dense Hydroxyapatite*, Hench, L.L. and Wilson, J. (eds.), in An Introduction to Bioceramics, World Scientific, Singapore (1993)

26. Young, R.A. and Elliot, J.C., *Scale Bases for Several Properties of Apatites*, Archs. Oral. Biol. **11** (1966) 699-707

27. LeGeros, R.Z., *Materials for Bone Repair , Augmentation and Implant Coatings,* in Proceedings of the International Seminar of Orthopaedic Research, Nagoya, Niwa, S. (ed.), (Springer-Verlag) (1990)

28. Denissen, H.; Mangano, C. and Cenini,G., *Hydroxyapatite Implants,* Piccin Nuova Libraria, S.P.A., India (1985)

29. American Society for Testing and Materials (ASTM) F1185-88, *Standard Specification for Composition of Ceramic Hydroxylapatite for Surgical Implants*, (1993) 473-474

30. De Groot, K., *Clinical Applications of Calcium Phosphate Biomaterials : A Review*, Ceramics International **19** (1993) 363-366

31. Wang, P.E. and Chaki, T.K., *Sintering Behaviour and Mechanical Properties of Hydroxyapatite and Dicalcium Phosphate*, Journal of Materials Science-Materials in Medicine **4** (1993) 150-158.

32. De Groot, K., *Ceramic of Calcium Phosphates: Preparation and Properties*, in Bioceramics of Calcium Phosphate, De Groot, K. (ed.), CRC Press, Boca Raton, Florida, (1983) 100-114

33. Ruys, A.J.; Zeigler, K.A.; Standard, O.C.; Brandwood, A.; Milthorpe, B.K. and Sorrell, C.C., *Hydroxyapatite Sintering Phenomena: Densification and Dehydration Behaviour.* In : Bannister, M.J. (ed.), Ceramics: Adding the Value, Volume 2. Proceedings of the International Ceramic Conference, Austceram 92. Melbourne: CSIRO, (1992) 605-610

34. Peelen, J.G.F., Rejda B.V. and De Groot, K., *Preparation and Properties of Sintered Hidroxyapatite,* Ceramicurgia Int. **4** (1978) 71-74

35. Van Landuyt, P.; Li, F.; Keustermans, J.P.; Streydio, J.M.; Delannay, F. and Munting, E., *The Influence of High Sintering Temperatures on the Mechanical Properties of Hydroxylapatite*, Journal of Materials Science: Materials in Medicine **6** (1995) 8-13

36. Masia, S.; Calvert, P.D.; Rhine, W.E. and Bowen, H.K., *Effect of Oxides on Binder Burnout During Ceramics Processing*, Journal of Materials Science **24** (1989) 1907-1912

37. Santos, J.D.; Morrey, S.; Hastings, G.W. and Monteiro, F.J., *The Production and Characterisation of a Hydroxyapatite Ceramic Material.* In Bioceramics, Bonfield, W.; Hastings, G.W. and Tanner, K.E. (eds.), Volume 4. Proceeding of the 4th International Symposium on Ceramics in Medicine, Butterworth-Heinemann, London (1991) 71-78

38. Ducheyne, P.; Radin, S. and King, L., *The Effect of Calcium Phosphate Ceramic Composition and Structure on In Vitro Behaviour. I. Dissolution*, Journal of Biomedical Materials Research **27** (1993) 25-34.

39. Royer, A.; Viguie, J.C.; Heughebaert, M. and Heughebaert, J.C., *Stoichiometry of Hydroxyapatite: Influence on the Flexural Strength*, Journal of Materials Science: Materials in Medicine **4** (1993) 76-82

40. Best, S. and Bonfield, W., *Processing Behaviour of Hydroxyapatite Powders with Contrasting Morphology*, Journal of Materials Science: Materials in Medicine **5** (1994) 516-521

41. Murray, M.G.S.; Wang, J.; Ponton, C.B. and Marquis, P.M., *An Improvement in Processing of Hydroxyapatite Ceramics*, Journal of Materials Science **30** (1995) 3061-3074

42. Yeong, K.C.B.; Wang, J. and S.C. Ng, *Fabricating Densified Hydroxyapatite Ceramics from a Precipated Precursor*, Materials Letter **38** (1999) 208-213

43. Puajindanetr, S; Best, S.M., and Bonfield, W, *Characterisation and Sintering of Precipitated Hydroxyapatite*, British Ceramic Transaction, **93** (1994) 97-99

44. Xie, L. and Monroe, E.A., *The Hydrolysis of Tetracalcium Phosphate and Other Calcium Orthophosphates*, Yamamuro, T., Hench, L.L. and Wilson, J. (eds.), CRC Handbook of Bioactive Ceramics Vol. 2, CRC Press Inc. Boca Raton, Florida (1990) 29-37

45. Monma, H. and Kanazawa, T., *The Hydration of Tricalcium Phosphate*, Yogyo Kyokai Shi, 84 (1976) 209

46. Corbridge, D.E.C., *Phosphorus: An Outline of Its Chemistry, Biochemistry and Technology*, 3rd ed., Elsevier, Amsterdam (1985) 138

47. Liu, H.S.; Chin, T.S.; Lai, L.S.; Chiu, S.Y.; Chung, K.H., Chang, C.S. and Lui, M.T., *Hydroxyapatite Synthesised by a Simplified Hydrothermal Method*, Ceramics International **23** (1997) 19-25

48. Juang, H.Y., and Hon, M.H., *Effect of Calcination on Sintering of Hydroxyapatite*, Biomaterials, **17** (1996) 2059-2064

49. White, E. and Shors, E.C., *Biomaterial Aspects of Interpore 200 Porous Hydroxyapatite,* Dental Clinics of North America, **30** [1] (1986) 49-67

50. Hulbert, S.F.; Young, F.A.; Mathews, R.S.; Klawitter, J.J.; Talbert, C.D. and Stelling, F.H., *Potential of Ceramic Materials as Permanently Implantable Skeletal Prostheses,* Journal of Biomedical Material Research **4** [3] (1970) 433-456

51. Hench, L.L. and Wilson, J. (eds.), An Introduction to Bioceramics , World Scientific (1993)

52. Zhou, P.; Hosonuma, M.; Kobayashi, T.; Mitsui H.; Akao, M. and Aoki, H., *Bone Ingrowth into Micropores of Hydroxyapatite Coated Titanium Plates*, Surface Engineering **13** (1997) 320-322

53. Gauthier, O.; Bouler, K.M.; Aguado, E., Pilet, P. and Daculsi, G., *Macroporous Biphasic Calcium Phosphate Ceramics: Influence of Macropore Diameter and Macroporosity Percentage on Bone Ingrowth*, Biomaterials, **19** (1998) 133-139

54. Ono, I.; Tateshita, T.; Nakajima, T. and Ogawa, T., *Determinations of Strength of Synthetic Hydroxyapatite Ceramic Implants*, Plastic and Reconstructive Surgery, **102** (1998) 807-813

55. Ono, I.; Tateshita, T. and Nakajima, T., *Porous Hydroxyapatite Ceramics and their Ability to be Fixed by Commercial Available Screws*, Biomaterials **20** (1999) 1595-1602

56. Lin, F.H.; Liao, C.J.; Chen, K.S. and Sun, J.S., *Preparation of a Biphasic Porous Bioceramic by Heating Bovine Cancellous Bone with* $Na_4P_2O_7 \bullet 10H_2O$ *Addition*, Biomaterials **20** (1999) 475-484

57. Liu, D.M., *Control of Pore Geometry on Influencing the Mechanical Property of Porous Hydroxyapatite Bioceramic*, Journal of Materials Science Letters **15** (1996) 419-421.

58. Liu, D.M., *Fabrication and Characterisation of Porous Hydroxyapatite Granules,* Biomaterials **17** (1996) 1955-1957

59. Shors, E.C. and Holmes, R.E., *Porous Hydroxyapatite*, Hench, L.L. and Wilson, J. (eds.) in An Introduction to Bioceramics, World Scientific, Singapore (1993).

60. Lin, F.H.; Lin, C.C.; Liu, H.C.; Huang, Y.Y.; Wang, C.Y. and Lu, C.M., *Sintered Porous DP-Bioactive Glass and Hydroxyapatite as Bone Substitute*, Biomaterials, **15** [13] (1994) 1087 - 1098

61. White, R.A.; Weber, J.N. and White, E.W., *Replamine: A New Process for Preparing Porous Ceramic, Metal and Polymer Prosthetic Materials*, Science, **176** (1972) 922-924

62. Matsuda, H.; Nishio, K. and Baba, N., *Preparation of Microporous Metal Membrane Using Two Step Replication of Interconnected Structure of Porous Glass,* Journal of Materials Science Letters **13** (1994) 338 - 340

63. Ryshkewitch, E., *Compression Strength of Porous Sintered Alumina and Zirconia*, Journal of the American Ceramic Society, **36** [2] (1953) 65-68

64. Le Huec, J.C.; Schaeverbeke, T.; Clement, D.; Faber, J. and Le Rebeller, A., *Influence of Porosity on the Mechanical Resistance of Hydroxyapatite Ceramics Under Compressive Stress*, Biomaterials **16** (1995) 113-118

65. Rice, R.W., *Comparison of Physical Property-Porosity Behaviour with Minimum Solid Area Models*, Journal of Materials Science **31** (1996) 1509-1528

66. Kingery, W.D.; Bowen, H.K. and Uhlmann, D.R., *Introduction to Ceramics*, 2nd ed., A. Wiley-Interscience Publication, New York (1976)

67. Shaw, J.H., *Preparation and Characterisation of Porous Hydroxyapatite*, PhD thesis, Queen Mary and Westfield College, University of London, London (1996)

68. Yamasaki, N.; Kai, T.; Nishioka, M.; Yanagisawa, K. and Ioku K., *Porous Hydroxyapatite Ceramics Prepared by Hydrothermal Hot-Pressing*, Journal of Materials Science Letters **9** (1990) 1150-1151

69. Liu, D.M., *Preparation and Characterisation of Porous Hydroxyapatite Bioceramic via a Slip-casting Route,* Ceramics International **24** (1998) 441-446

70. Stevens, M.P., *Polymer Chemistry - An Introduction*, 3rd ed., Oxford University Press, Oxford (1999)

71. McNeill, I.C., *Thermal Degradation Mechanisms of some Addition Polymers and Copolymers*, Journal of Analytical and Applied Pyrolysis, **40-41** (1997) 21-41

72. Pinner, S.H. (ed.), *Weathering and Degradation of Plastics*, Columbine Press (Publishers) Ltd. (1966)

73. McNeill, I.C.; Memetea, L. and Cole, W.J., *A Study of the Products of PVC Thermal Degradation*, Polymer Degradation and Stability **49** (1995) 181 - 191

74. Finch, C.A. (ed.), *Polyvinyl Alcohol - Properties and Applications*, A Wiley - Interscience Publication (1973)

75. Yang, T.C.K.; Chang, W.H. and Viswanath, D.S., *Thermal Degradation of Poly (Vinyl Butyral) in Alumina, Mullite and Silica Composites*, Journal of Thermal Analysis **47** (1996) 697-713

76. Chartier, T.; Ferrato, M. and Baumard J.F., *Influence of the Debinding Method on the Mechanical Properties of Plastic Formed Ceramics*, Journal of European Ceramic Society **15** (1995) 899-903

77. Voorhees, K.J.; Baugh, S.F. and Stevenson, D.N., *The Thermal Degradation of Poly (ethylene glycol)/ Poly(vinyl alcohol) Binder in Alumina Ceramics,* Thermochemica Acta **274** (1996) 187-207

78. Ichinose, N., *Introduction to Fine Ceramics - Applications in Engineering*, John Wiley & Son Ltd, Chichester (1987)

79. Cahn, R.W.; Haasen, P. and Kramer, E.J.(ed.), *Materials Science and Technology - A Comprehensive Treatment, Volume 17A- Processing of Ceramics*, Brook, R.J.(volume editor), VCH, Weinheim, New York (1996)

80. Reed, J.R., *Principles of Ceramics Processing,* 2nd ed., John-Wiley & Sons, Inc., New York (1995)

81. Trunec, M. and Cihlar, J., *Thermal Debinding of Injection Moulded Ceramics*, Journal of European Ceramic Society **17** (1997) 203-209

82. Tseng, W.J. and Hsu, C.K., *Cracking Defect and Porosity Evolution During Thermal Debinding in Ceramic Injection Moulding*, Ceramics International **25** (1999) 461-466

83. White, J., *Sintering of Oxides and Sulfides*, in Sintering and Related Phenomena, Proceedings of the International Conference in 1965 at the University of Notre Dame, Gordon and Breach, Science Publisher, New York (1967) 245-272

84. Coble, R.L., *Sintering Crystalline Solids. I. Intermediate and Final State Diffusion Models*, Journal of Applied Physics, **32** (1961) 787-792

85. Budworth, D.W., *An Introduction to Ceramic Science*, Pergamon Press, Oxford (1970)

86. Rice, R.W., *Comparison of Stress Concentration versus Minimum Solid Area Based Mechanical Property-Porosity Relations*, Journal of Materials Science **28** (1993) 2187-2190

87. Liu, D.M., *Influence of Porosity and Pore Size on the Compressive Strength of Porous Hydroxyapatite Ceramic*, Ceramic International **23** (1997) 135-139

88. Krstic, V.D., *Porosity Dependence of Strength in Brittle Solids*, Theoretical and Applied Fracture Mechanics **10** (1988) 241-247

89. Smith, W.F., *Principles of Materials Science and Engineering*, McGraw-Hill Book Company, Singapore (1986)

90. Yue, T.M.; Ha, H.U.; Musson, N.J., *Grain Size Effects on the Mechanical Properties of Some Squeeze Cast Light Alloys*, Journal of Materials Science **30** (1995) 2277-2283

91. Ohring, M., *Engineering Materials Science*, Academic Press, London (1995)

92. Li, C.W., Lui, S.C. and Goldacker, J., *Relation Between Strength, Microstructure, and Grain-Bridging Characteristics in Situ Reinforced Silicon Nitride*, Journal of the American Ceramic Society **78** (1995) 449-159

93. Rice, R.W., *Relation of Tensile Strength-Porosity Effects in Ceramics to Porosity Dependence of Young's Modulus and Fracture Energy, Porosity Character and Grain Size*, Materials Science and Engineering, **A112** (1989) 215-224

94. Albee, F.H., *Studies in Bone Growth. Triple Calcium Phosphate as a Stimulus to Osteogenesis*, Ann. Surg., **71** (1920) 32-36

95. Klawitter, J.J. and Hulbert, S.F., *Application of Porous Ceramics for the Attachment of Load Bearing Orthopedic Applications*, Journal of Biomedical Material Research Symposium **2** (1971) 161.

96. Rice, R.W., *Treatise on Materials Science and Technology*, Vol. 11, McCrone, R.K. (ed.), Academic Press, New York (1977) 199-380

97. Tsuchiya, Y. and Sumi, K., *Thermal Decomposition Products of Poly (vinyl alcohol)*, Journal of Polymer Science: Part A-1, **7** (1969) 3151-3158

98. Koleske, J.V. and Wartman, L.H., *Poly (vinyl chloride)*, MacDonald Technical & Scientific, London (1969)

99. Matthews, G., *PVC: Production, Properties and Uses*, The Institute of Materials, (1996)

100. Grassie, N., *Developments in Polymer Degradation - 3*, Applied Science Publishers, London (1981)

101. German, R.M. *Theory of Thermal Debinding*, The International Journal of Powder Metallurgy **23** (1987) 237-245

102. Hassel, R.L., *Analysis of Polymer Decomposition by a Combined Thermogravimetric - Mass Spectroscopy System*, Thermal Analysis - Application Brief (No. TA 45), Du Pont Company, Wilmington, USA

103. Liao, C.J.; Lin, F.H.; Chen, K.S. and Sun, J.S., *Thermal Decomposition and Reconstitution of Hydroxyapatite in Air Atmosphere*, Biomaterials **20** (1999) 1807-1813

104. Tampieri, A.; Celotti, G.; Szontagh, F. and Landi, E., *Sintering and Characterisation of HA and TCP Bioceramics with Control of their Strength and Phase Purity*, Journal of Materials Science: Materials in Medicine **8** (1997) 29-37

105. Slamovich, E.B. and Lange, F.E., *Densification of Large Pores : Driving Potentials and Kinetics*, Journal of American Ceramic Society **76** [6] (1993) 1581-1590

106. Jonghe, L.C. and Rahaman, M.L., *Pore Shrinkage and Sintering Stress*, Journal of American Ceramic Society **67** (1984) C214- C215

107. Moore, G.R. and Kline, D.E., *Properties and Processing of Polymers for Engineers*, Prentice-Hall International, Inc., London (1984)

108. Wypych, J., *Poly Vinyl Chloride Degradation*, Elsevier, Amsterdam (1985)

109. Rudnik, E. and Dobkowski, Z., *Thermal Degradation of UHMWPE*, Journal of Thermal Analysis **49** [1] (1997) 471-475

110. Zhao, J. and Harmer, M.P., *Effect of Pore Distribution on Microstructure Development: I, Matrix Pores,* Journal of American Ceramic Society **71** [2] (1988) 113-120

111. Zhao, J. and Harmer, M.P, *Effect of Pore Distribution on Microstructure Development: II, First and Second Generation Pores*, Journal of American Ceramic Society **71** [7] (1988) 530-539

112. Bako, Z. and Kotsis, I., *Composition of Precipitated Calcium Phosphate Ceramics,* Ceramics International **18** (1992) 373-378

113. Laurie, J.; Bagnall, C.M.; Harris, B. Jones, R.W.; Cooke., R.G.; Russell-Floyd, R.S.; Wang, T.H. and Hammett, F.W., *Colloidal Suspensions for the Preparation of Ceramics by Freeze Casting Route*, Journal of Non-Crystalline Solids **147&148** (1992) 320-325

114. BS EN 623-2:1993, Advanced Technical Ceramics - Monolithic Ceramics - General and Textural Properties - Part 2. Determination of Density and Porosity

115. Mendelson, M. I, *Average Grain Size in Polycrystalline Ceramics*, Journal of American Ceramics Society, **52**, [8] (1969) 443-446

116. ASTM C773 - 88, Standard Test Method for Compressive (Crushing) Strength of Fired Whiteware Materials

117. El Wakil, S.D., *Materials Science and Engineering Lab Manual*, PWS Publishing Company, Boston (1994)

118. Thomas, M.B.; Doremus, R.H.; Jarcho, M. and Salsbury R.L., *Dense Hydroxyapatite: Fatigue and Fracture Strength after Various Treatments, from Diametral Test,* Journal of Materials Science **15** (1980) 891 - 894.

119. Lu, J.X.; Flautre, B.; Anselme, K.; Hardouin, P.; Gallur, A.; Descamps, M. and Thierry, B., *Role of Interconnections in Porous Bioceramics on Bone Recolonization in vitro and in vivo*, Journal of Materials Science: Materials in Medicine **10** (1999) 111-120.